CANADIAN THESES

THÈSES CANADIENNES

NOTICE

The quality of this microfiche is heavily dependent upon the quality of the original thesis submitted for microfilming. Every effort has been made to ensure the highest quality of reproduction possible.

If pages are missing, contact the university which granted the degree.

Some pages may have indistinct print especially if the original pages were typed with a poor typewriter ribbon or if the university sent us an inferior photocopy.

Previously copyrighted materials (journal articles, published tests, etc.) are not filmed.

Reproduction in full or in part of this film is governed by the Canadian Copyright Act, R.S.C. 1970, c. C-30.

AVIS

La qualité de cette microfiche dépend grandement de la qualité de la thèse soumise au microfilmage. Nous avons tout fait pour assurer une qualité supérieure de reproduction.

S'il manque des pages, veuillez communiquer avec l'université qui a conféré le grade.

La qualité d'impression de certaines pages peut laisser à désirer, surtout si les pages originales ont été dactylographiées à l'aide d'un ruban usé ou si l'université nous a fait parvenir une photocopie de qualité inférieure.

Les documents qui font déjà l'objet d'un droit d'auteur (articles de revue, examens publiés, etc.) ne sont pas microfilmés.

La reproduction, même partielle, de ce microfilm est soumise à la Loi canadienne sur le droit d'auteur, SRC 1970, c. C-30.

THIS DISSERTATION HAS BEEN MICROFILMED EXACTLY AS RECEIVED

LA THÈSE A ÉTÉ MICROFILMÉE TELLE QUE NOUS L'AVONS REÇUE

Canada

Electrochemical, Photoelectrochemical and Transient Behaviour of Maleonitriledithiolate Complexes of Ni, Pd, Pt and Cu.

Lalchan Persaud

A Thesis

in

The Department

of

Chemistry

Presented in Partial Fulfilment of the Requirements
for the Degree of Doctor of Philosophy at
Concordia University
Montréal, Québec, Canada
August 1985

ISBN 0-315-30598-3

ABSTRACT

Electrochemical, Photoelectrochemical and Transient behaviour of Maleonitriledithiolate complexes of Ni, Pd, Pt and Cu.

Lalchan Persaud, Ph.D.
Concordia University, 1985

Electrochemical and photoelectrochemical behaviour of the above complexes were investigated in a homogeneous phase in acetonitrile at Pt and SnO_2 electrodes and in a heterogeneous phase on polymer modified electrodes of Pt and SnO_2.

Homogeneous reactions at Pt electrodes were controlled by diffusional mass transfer process. At SnO_2 electrodes the kinetics are limited by the electron transfer steps.

Solution photoelectrochemistry at transparent SnO_2 electrode suggested short lived excited states, the reactivity of which is determined by the type of charge transfer transition excited. In Ni and Pt the transition is dominated by $M \longrightarrow L\pi^*$. These are photoactive. In Pd and Cu the transition is $L\pi \longrightarrow M$. These are photoinactive. Energetics suggest reaction from the lowest

excited state. Picosecond pulse excited state spectra suggest direct excitation by 355 nm produces a short lived singlet excited state which via intersystem crossing produces a triplet. The latter with lifetimes approximating 7 ns ($Ni(mnt)_2^{2-}$) and > 10 ns ($Pt(mnt)_2^{2-}$) are important in the photoelectrochemistry. The triplets are quenched by O_2 and pyridine. The triplet of Pt is also quenched by water (acceptor) via electron transfer process.

The heterogeneous electrochemistry at anion exchange polymer modified electrodes suggests penetration of halide counterions from the electrolyte throughout the polymer film as the kinetically limiting process. Diffusion of counterions appears to be facilitated by methanol but not water. The D_{app} is of the order of 10^{-11} $cm^2 \cdot sec^{-1}$.

Photoelectrochemistry at modified electrodes incorporating $Ni(mnt)_2^{2-}$ is similar to the homogeneous phase. The larger photocurrent is attributed to the higher concentration of the complex near the SnO_2 surface. Modified electrodes of $Pt(mnt)_2^{2-}$ in contact with aqueous electrolyte undergoes photochemical oxidation at the polymer/electrolyte interface. At the SnO_2/polymer interface the reaction similar to the solution phase. The photo-oxidized $Pt(mnt)_2^{1-}$ appears to form aggregates which accummulated on the film and decrease the photoelectrochemical activity. The aggregates appear to be

associated with the electrocatalytic decomposition of water. Aggregates also form in aqueous/acetonitrile mixed solvent under continuous photolysis.

ACKNOWLEDGEMENTS

I would like to express my sincere appreciation and gratitude to Dr. C.H. Langford for his guidance and assistance in all forms throughout this project.

I also wish to acknowledge and thank Dr. D. Sharma for performing the pulse photolysis experiments and for his advice whenever it was sought.

Thanks also to Dr. B.A. Lombos for his assistance in the prolifometer measurements.

List of Contents

Chapter 1

INTRODUCTION

1.1 General Introduction

Photoelectrochemistry involves the combination of two traditional and separate disciplines of Chemistry; Photochemistry and Electrochemistry. Photoelectrochemical effects then are the results of a combined Photophysical, Photochemical and Electrochemical processes. The Photophysical processes involve electronic excitation and charge separation. The Photochemical processes involve reactions of the excited molecule. The electrochemical step includes electron transfer indirectly at the electrode / electrolyte interface. For any Photoelectrochemical effect the primary step of electronic excitation is a necessity. The electronic excitation can occur in molecules in the electrolyte solution or on the electrode surface. The consequences in both the homogeneous and heterogeneous phases are similar and stimulate electron transfer. The electrochemical step in which charge is transferred to or from the electrode is measurable in the form of a photocurrent or photovoltage. Figure 1-1 showed in a simplified picture how electronic excitation may influence electron transfer processes.

Electron tansfer occurs between an occupied and a vacant electronic energy state. Upon absorption of light the distribution of electrons over the available energy

levels changes. Electrons are promoted to higher energy

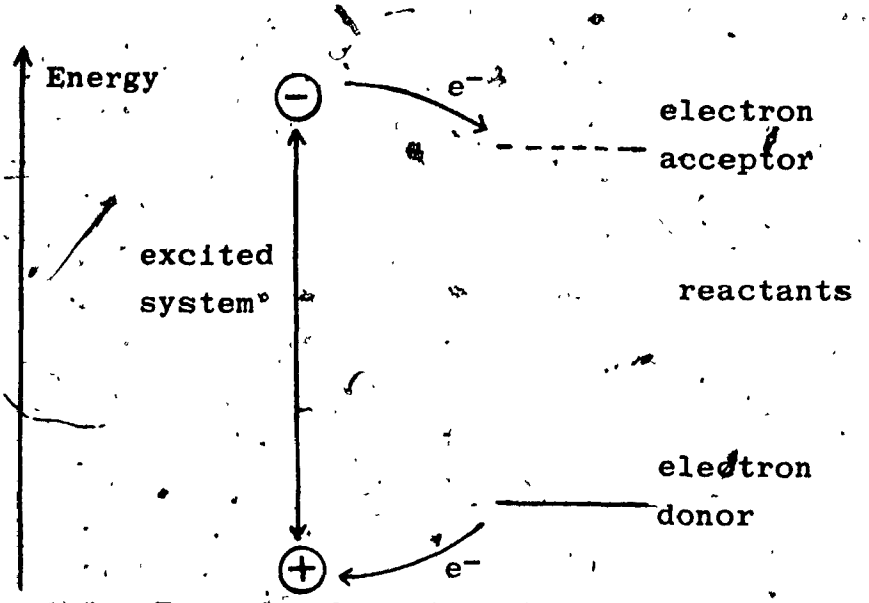

Figure 1-1. Energy scheme for electron transfer between excited system and electron donor acceptor.

level concurrently creating holes or vacant electronic states at lower energies. The holes can be filled with electrons by electron donors with slightly higher electronic energies. The promoted electron can be transferred to an electron acceptor at a lower energy level. In electrochemical terms the redox potential of the excited molecule has shifted in two directions. It has become a molecule with a greater reducing power (stronger reducing agent) as well as a higher oxidizing power (stronger oxidizing agent) resulting in enhanced cathodic and anodic reactions. These enhanced reactions at an electrode give rise to the photocurrents. The molecule in its excited state is either oxidized or

reduced, it undergoes only one type of redox reaction depending on the reaction partner it finds in the surroundings.

It is accordingly evident that not all materials can be used in photoelectrochemical or photochemical electron transfer studies. Candidates for this field of investigation must possess two basic properties. They must be excitable i.e. they must be a strong absorber of light in the radiation spectrum chosen for photochemical experiments. For the visible region they must be strongly coloured. Secondly, they must be stable and capable of existing in more then one oxidation state. It is important to realize that these two properties are those exhibited by the ground state molecule and do not give any indication about the behaviour of the molecule in the excited state. Successful photoinduced electron transfer depends on the probability of the excited state reaction and this can only be determined experimentally. Prospective candidates for this type of studies can only be identified by their ground state behaviour.

1.2 Review of Maleonitriledithiolate Complexes and U.V. Photochemistry.

The family of complexes containing as ligand the dianion of maleonitriledithiolate, abbreviated as mnt has been extensively studied and its chemical properties are well known (1). The limiting electronic structures of the ligand are shown in Figure 1-2 as the oxidized

dithioketone and the reduced ethylenedithiolate which has two additional electrons.

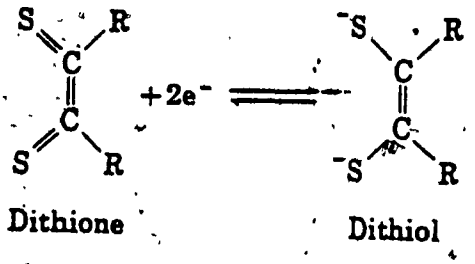

Dithione Dithiol

Figure 1-2. Limiting structures of Maleonitriledithiolate ligand.

This ligand forms four coordinated complexes with many metal ions including Ni, Pt, Pd, Cu. The complexes are represented by the general formula of Figure 1-3. They

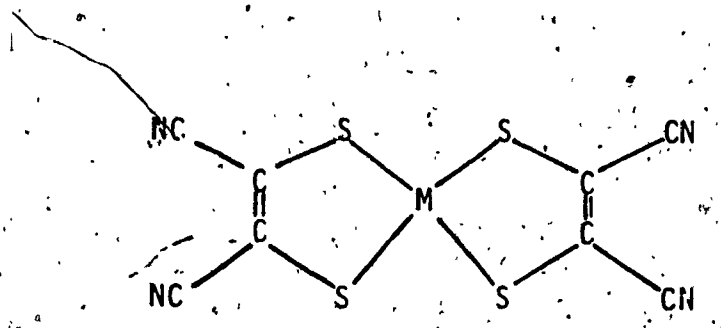

Figure 1-3. General structure (formula) for mnt complexes

are an extensive series of anions in which the net ionic charge n may take values from 0 to 3- for the same metal ion. The mono and dianions can be isolated without difficulty. The existance of the neutral and trianion was

established by electrochemical and spectral studies (3,4).

The growth of chemistry of these complexes is partly due to electrochemical studies which discovered that they undergo facile reversible electron transfer reactions. Most of the available electrochemical techniques have been used to investigate these reactions and it is concluded that the wide range of oxidation states available to these complexes is in part a result of the accessibility of a number of oxidation states of the ligand. The ligand itself exhibits two oxidation waves at +0.08 and +0.43V vs SCE in aqueous solution (1). The first and second oxidation waves of the complex dianion, $M(mnt)_2^{2-}$ were found to be practically independent of the identity of the metal and it is generally agreed that the dianion approximate a metal ion in the 2+ oxidation state in which the ligands each carry a charge of 2-. The reduction of the dianions was found to be significantly dependent on the metal ion (2,3). This qualitatively confirmed that an orbital of considerable metal character is involved in the generation of the trianions. The metal ion in the trianion species is regarded as in the uncommon 1+ oxidation state.

The structure of the mono and dianions (of the Ni complex) as analysed by x-ray diffraction techniques are square planar (6,7). Of particular interest is the insignificant distortion from planarity as the bond lengths vary with the change in the overall charge n. This

retention of structure over different oxidation states would suggest that electron transfer can occur with very little or no structural reorganization. In such a situation, the electron transfer can probably occur under Frank-Condon conditions. The structural investigation of the complexes $[Ni(S_4C_4(CN)_4)]^n$ and $[Ni(S_4C_4(Ph)_4)]^n$ for n=0, 1-, 2- allowed for a useful comparison of variation of bond lengths with charge (1,2,6,7). As the charge increases the ethylenic bond length decreases from 1.39 to 1.31A while the Ni--S and S--C bond distances increase from 2.00 to 2.17A and 1.67 to 1.75 A respectively. The contraction of S--C and expansion of C C bond lengths as n goes from 2- to 0 suggests that as the complex is progressively oxidized, the sulfur ligand gradually loses its dithiolate character and becomes more dithioketonic.

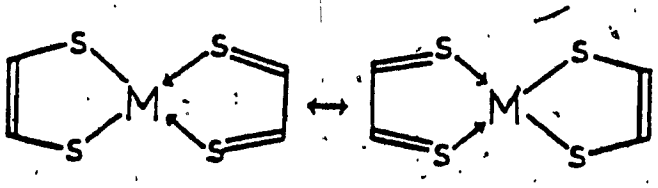

(a) (b)

(c)

Figure 1-4. Resonance structures of Maleonitriledithiolate complex.

The neutral species are then considered as a first approximation to be in an intermediate state between the dithioketonic and dithiolate character representably by resonance structures of the forms shown in Figure 1-4a and 4b or more usefully as π delocalized covalent derivatives of the metals in the 2+ oxidation state (Figure 1-4c shown above). Gray et al(8) agreed that stabilization of the square planar geometry involved extensive delocalization over the entire molecule. The redox processes which cover a wide potential range of approximately +1.0 to -2.7 Volts can then be represented according to the following equation:

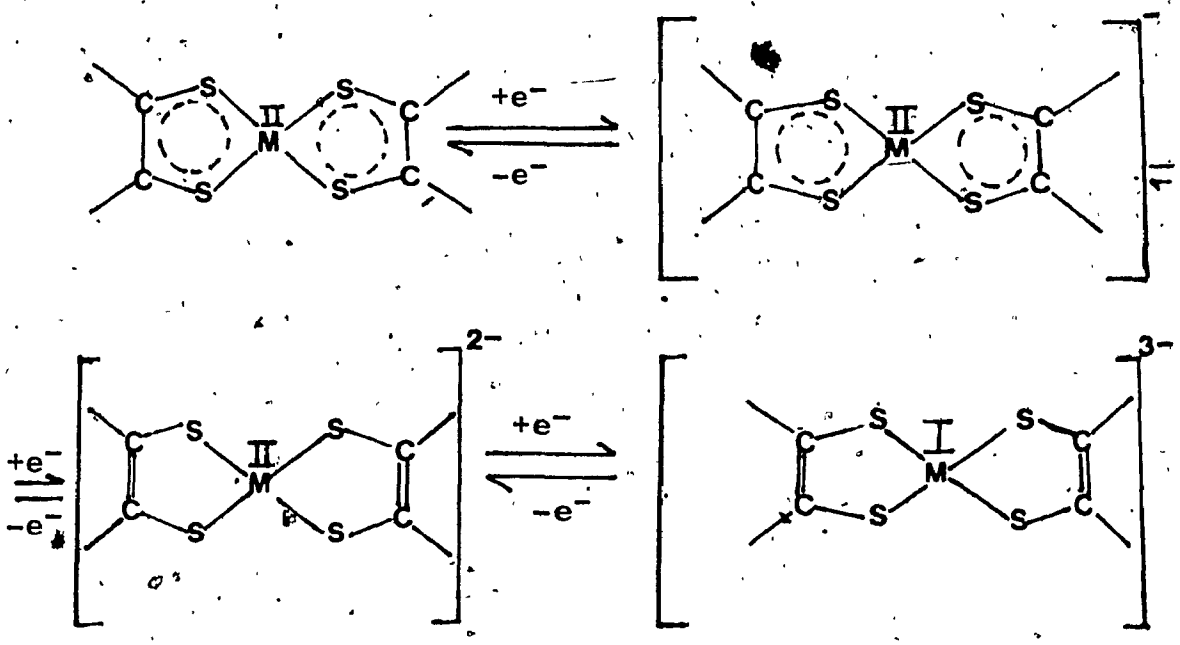

(1)

The ligands in the dianions have considerable dithiolate character and in the highly reduced member of the series the addition of another electron leads to a d^9

configuration for Nickel involving a predominately metal based orbital.

The ability of these complexes to take part in a series of one electron reduction or oxidation and the theoretically challenging bonding system prompted intensive investigation into the electronic structures. The intense absorptions exhibited by these complexes at low energy in the visible spectrum and the absorption in the near infra-red region allowed for the use of electronic absorption spectral studies to aid in the assignments of the electronic structures. Other techniques including ESR, photoelectron and more recently resonance Raman experiments have been employed in the electronic structural characterization (1,12,13,14). The major contribution came from the solution electronic absorption data and their interpretations based on molecular orbital calculations. Two independent approaches have been made. The assignments of Gray and his co-worker (8) were based on a modified Wolfsberg-Hemholtz molecular orbital calculations for the dianion $Ni(mnt)_2^{2-}$, while Schrauzer and Mayweg (15) assignments were derived from energy level diagram also obtained from the Wolfsberg-Hemholtz model for the neutral complex of $NiS_4C_4(C_6H_5)_4$.

The true electronic structure is difficult to assign. Bonding and electronic delocalization have wide and

varying effects on the results. The low lying high intensity charge transfer bands frequently masked the d--d transitions. These ligand field bands appeared as shoulders on the charge transfer transition in the visible and their observed intensities could be higher than the true intensity due to borrowing of intensity from the charge transfer bands. It is not uncommon then that there is not complete agreement between the two sets of electronic spectral assignments. According to Schrauzer and Mayweg the difference lies in the choice of the imput parameters. They disagreed with Gray's calculations on the grounds that treatment implied charge separation between the metal and the ligands and also pointed out an inconsistency between the calculations and the e.p.r. analysis of the monoanions (16). However, they conceded that theis calculation is not strictly applicable to the dianions since it does not account for the changes that occur in the ligand upon reduction. In addition Clark et al (14) also noted that the calculation by Schrauzer and Mayweg ignores conjugation of the CN group with the system of the ligand. X-Ray photoelectron spectroscopy showed that the metal-sulfur binding energies are essentially constant in the mono and dianions (12,13). This was taken as an indication that when the monoanion gains an electron the extra negative charge is delocalized over the cyanide groups. This conjugation effect was considered in Gray's treatment. Furthermore, in the same

photoelectron spectroscopic study it was deduced that the charge on the nickel atom was +0.25 compared to the +0.26 used by Gray. The Gray and Schrauzer assignments represent extreme descriptions of the system and both are seen as contributing significantly to the electronic characterization of these type of compounds. Recent investigations (14,17) of the $M(mnt)_2^{2-}$ M = Ni, Pd and Pt and $NiS_4C_4H_4$ would suggest that the differences between the Gray and Schrauzer assignments for $M(mnt)_2^{2-}$ and $MS_4C_4(C_6H_5)_4$ are real and these complexes are spectroscopically different . Calculations performed by the intermediate neglect of differential overlap (INDO) method (17) which includes configurational interaction (CI) determined that the electronic ground state and first few excited states of $NiS_4C_4H_4$ are in agreement with those of Schrauzer and Mayweg. On the other hand resonance Raman spectroscopy (14) of $M(mnt)_2^{2-}$ M = Ni, Pd and Pt supports the assignments of Gray. It could be that the degree of participation of the ligand and metal orbitals to the molecular orbital could vary with the type of ligand and each description is perhaps appropriate to the particular ligand system.

From the extensive ground state investigations of the metal dithiolates certain characteristic features have emerged. The remarkable series of facile one electron transfer reactions over a wide potential range; the

stability of the square planar matrix and insignificant structural change with the oxidation or reduction, and the strong absorbance in the ultra-violet, and visible along with the rich electronic spectra are the most interesting. These features are the essential ground state properties of materials for photochemical electron transfer reactions. The ground state properties of the metal dithiolate were known about a decade ago and despite possessing the prerequisites for photochemical studies their photochemistry was up to recently unexplored. Photoactivity in the U.V. region was reported and these reactions were of two kinds. Members of the family have been shown to initiate hydrogen evolution from a water/THF solvent mixture. Two reports by Kish et al (18,19) of catalytic hydrogen production from water by U.V. photolysis are known. The report of 1980 appears to be a preliminary study involving the neutral complex, $NiS_4C_4(C_6H_5)_4$. It was irradiated with wavelength, 290nm. and hydrogen detected by chromatographic technique. The cleavage of water by the complex under irradiation was verified by using a deuterated solvent mixture. The rate of hydrogen generation was found to increase with decreasing wavelength irradiation but the total production remained small. The reaction mixture at the end of photolysis contained the dianion as well as the monoanion and the authors were uncertain which excited specie promoted the hydrogen production. The second report in

1983 by Kish et al was a more extensive work and involved a variety of metal dithiolates, mixed diimine dithiolate and related M--S compounds. Their purpose was to identify the most catalytically active class of these complexes and investigate the influence of the nature of the central metal as well as the ligand. Their investigations revealed that the metal complexes of the type shown below

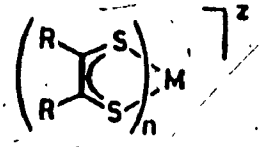

I

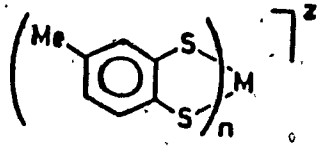

II

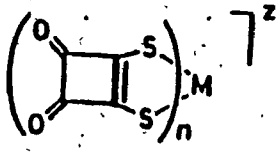

III

exhibited the highest hydrogen production rates and among these the ligand system of complex I was the most active. The substituent R on the ethylene dithiolene ligand was shown to have a significant effect. The turnover rate (moles of hydrogen per moles of complex per hr.) was

doubled when Cyano group was substituted for the phenyl ring. The zinc complex was determined, by compariaon between $Ni(mnt)_2^{2-}$ and $Zn(mnt)_2^{2-}$ to be the most active and suggests that the metal has a significant influence on the catalytic activity. There was also evidence of sensitizing effects. The presence of reducing agent increased hydrogen formation. The most effective donor was 2,5 dihydrofuran which when used in conjunction with $Zn(mnt)_2^{2-}$ greatly enhanced hydrogen production and the turn over rate. A very recent paper shows the $Zn(mnt)_2^{2-}$ complex photodecomposes to ZnS under U.V. irradiation and the catalyst in the hydrogen production is ZnS(20).

In the nearer U.V. region,366 to 313nm independent studies showed a one electron photooxidation of $M(mnt)_2^{2-}$ in halocarbon solvents (21,22). Progress of the oxidation was monitored by the electronic absorption spectra. The quantum yields decreased with increasing wavelength radiation and increased with the halogen content of the solvent in the order $CCl_4 > CH_2Cl_2 > CH_3Cl$. Volger and Kunkely (22) proposed that photooxidation occurs via a charge transfer to solvent state (CTTS). They pointed out that the energy of the CTTS state depends on both the redox potential of the complex and solvent. The photoactive wavelength would then be shifted to the red in accordinance with E^o for $CCl_4 > CHCl_3 > CH_2Cl_2$ and the quantum yield would paralled the redox potential.

Dooley and Patterson (21) proposed an alternate

mechanism. They observed that quantum yields did not correlate with $E_{\frac{1}{2}}$ values for the complex and the quantum yield decreased very much in acetonitrile. They attributed the decrease to excited state quenching by the solvent and suggested a bimolecular excited state electron transfer pathway as in equation 2:

$$M(mnt)_2^{2-} \underset{k_{-1}}{\overset{k_1(h\nu)}{\rightleftharpoons}} {}^*M(mnt)_2^{2-}$$

$${}^*M(mnt)_2^{2-} + CH_2Cl_2 \xrightarrow{k_q} M(mnt)_2^{1-}\text{---}CH_2Cl_2^- \qquad (2)$$

$$M(mnt)_2^{1-}\text{---}CH_2Cl_2^- \xrightarrow{k_5} M(mnt)_2^{1-} + .CH_2Cl + Cl^-$$

$$M(mnt)_2^{1-}\text{---}CH_2Cl_2^- \xrightarrow{k_4} M(mnt)_2^{2-} + CH_2Cl_2$$

1.3 Review of Chemically Modified Electrodes.

As mentioned earlier, molecules can be excited in a homogeneous solution phase or in a heterogeneous solid phase. The electrochemical as well as photoelectrochemical behaviour of molecules can also be studied in these phases. In the solution phase the molecules are dissolved in a suitable solvent containing an appropriate depolarizer and the homogeneous solution contacts an optical electrode as in conventional electrochemical studies. In the heterogenous phase the

molecules attached to an electrode to form a chemically modified electrode on which the electrochemistry and photoelectrochemistry can be studied.

Attachment of molecules to the electrode may not alter them chemically and they maybe therefore expected to display chemical, electrochemical, and photoelectrochemical reactions similar to the nonimmobilized solution species. In the solution phase high concentration usually lead to wastage of absorbed quanta by self quenching and competitive absorption. These reduce the photocurrents. Attaching the photoactive species to the electrode is an attempt to overcome this problem. Also molecules confined to the electrode surface do not have to diffuse to reach the surface to react so that specfes with lifetimes as short as the time for a diffusional step may react and the probability of excited molecules undergoing collisional quenching in the process of diffusing to the electrode is eliminated. Photoreaction of short lived excited states can therefore be observed at a modified electrode. In addition, the surface attachment confines high concentrations of molecules at the electrode surface favouring absorption in the reactive zone. The increase in concentration at the electrode interface and the stabilization of the excited state can lead to enhanced photoeffects. The photoelectrochemical behaviour of the $M(mnt)_2^{2-}$ complexes will therefore not be fully understood

without the information from the homogeneous solution phase as well as the heterogeneous phase on a chemically modified electrodes.

Chemically modified electrodes fall in that branch of surface chemistry which seeks to selectively modify the chemical and physical properties of surfaces or an interface in order to achieve some desirable behaviour. Chemically modified electrodes are sometimes referred to as derivatized, functionalized and polymer coated electrodes. They are distinguished form the traditional study of adsorption on the electrode surface. Adsorption on an electrode results in a monolayer or submonolayer deposit of uncharacterized ions or molecule on the electrode. All the adsorbed molecules are situated at the same distance from the electrode surface. Chemically modified electrodes are different. They are the result of a deliberate synthetic attempt to confine a well defined chemical species on the electrode surface. All the molecules are not at the same distance from the electrode surface when the electrode is coated with a polymer and the majority of the electroactive species are no longer in direct contact with the electrode

Premodified electrodes are not commercially available and studies on polymer modified electrodes necessitate their synthesis which includes preparation of the polymeric coating and the immobilization of the electroactive species on the polymer if it is not an

electroactive polymer. In general the synthetic chemistry of surfaces is in a developing stage particularly with respect to attachment of electroactive species on electrode. The conductive substrates are the typical electrode materials such as Pt, Au, Oxide layer films on glass, and semiconductor materials of silicone, germanium and GaAs surfaces. Some of the principal routes which were successful in immobilization of electroactive species on electrodes for electrochemical studies have involved both chemical and physcial methods of attachment. The chemical method uses the covalent linkage of an electroactive species to a preformed active site on electrode. This is a two step process in which the active site on the surface is first prepared and then coupled to the electroactive species by a reactive group. A typical example is the silanization of Pt or metal oxide (SnO_2) and subsequent reaction with on electroactive molecule containing a nucleophilic site as in the reaction on page 18, (see references 23,24,25,26).The physical methods of preparing polymer modified electrodes consider no specific requirements. The polymer adheres to the electrode surface by a poorly understood combination of adsorptive attraction and low solubility in the solvent contacting the electrode. This method mainly uses preformed polymer which can be either a redox polymer or a non electroactive one including ion exchange polymer. The redox polymer may

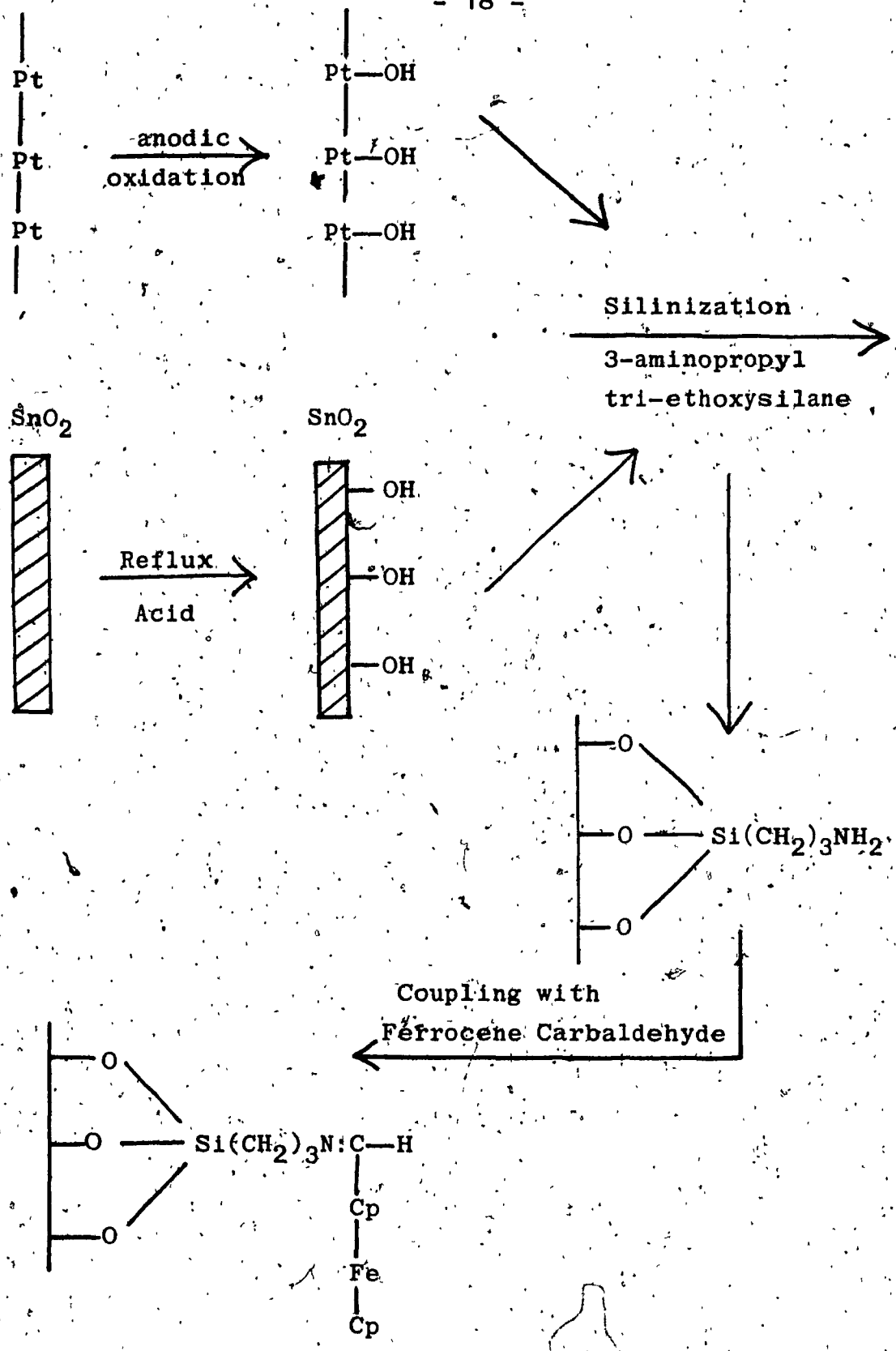

Preparation of Modified Electrode.

contain electroactive centers as part of the polymer chain or a pendant groups coupled to the polymer. The redox polymer is usually synthesized by polymerization of the electroactive monomers or by copolymerization of the electroactive and another monomer e.g. poly (xylylviologen) prepared by the polymerization of 4,4-bipyridine with p-xylene (27,28); a tetracyanoquinodimethane (TCNQ) polymer obtained from dioxydiethanol (TCNQ) polymer obtained from dioxydiethanol TCNQ monomer and adipolychloride (29). Pendant groups-attached to polymer have included the poly(pyridyl)-complexes of Ruthenium, Osmium and iron and PVP$[Fe(CN)_5]_n$ polymer obtained by reacting PVP with $Fe(CN)_5OH_2^{3-}$ (30).

The nonelectroactive or ion exchange polymers include Nafion, the polyviologens, sulfonated polystyrene, protonated PVP and quaternized PVP (31,32,33,34,35,36,37). These polymers usually incorporate the electroactive species by an ion exchange reaction. The electroactive species is partitioned usually by soaking the polymer coated electrode in a solution of the ion. After incorporation of the redox species the electrode is transferred to fresh electrolyte for electrochemical study. A recent review by Murray (38) provides detailed descriptions of both preformed redox and ion exchange polymers. A preformed polymer can be filmed on the electrode by various techniques. Dip coating is a simple procedure in which the electrode is dipped into a solution

of the polymer. The polymer adheres to the surface and forms a film. The polymer may already contain redox species or one can be subsequently coupled or incorporated into the polymer. Slow evaporation of the polymer solution onto smooth film. Spin coating the solution on the electrode surface was also used. This involves flooding the electrode surface with dilute solution of the polymer and by mechanically rotating the electrode the solution is spun off in all directions leaving a thin uniform film. This technique is usually favourable for disc type electrodes. Electrochemically initiated polymerization involves growing polymer at the electrode surface. This is an in situ technique in which the monomer must be electroactive and on reduction or oxidation polymerizes rapidly at the electrode to form a film. This technique can only form thin film unless the deposited film is itself electroactive and can catalyse the reduction or oxidation of fresh monomer or the monomer must be able to penetrate the film and react the electrode surface. If the situation is otherwise the electrode become passive, and the film growth is stopped. Radiofrequency plasma polymerization is also used. Radiofrequency plasma discharge in a reactor containing the monomer vapour causes polymerization of the monomer. In the presence of the electrode the polymer film can become attached to it.

The success of the attachment is usually determined by measuring electrochemical response. Known electrochemical techniques including cyclic voltammetry, differential pulse voltammetry, chronoamperometry and A.C. voltammetry can be employed. Differential pulse and A.C. voltammetry are not frequently used. These are sensitive techniques and since the immobilized species provide a large surface coverage sensitivity is not required. The most commonly used techniques are cyclic voltammetry, chronoamperometry and chronopotentiometry. In this study cyclic voltammetry and chronoamperometry were employed. The current potential representation of the cyclic linear sweep for a modified electrode is referred to as surface wave. It is analogous to the voltammogram of homogeneous solution electrochemistry. The surface wave measures the redox potential of the attached species. This potential can be the same or very close to that observed in a voltammograms in solution and is useful in ascertaining that the correct or intended species is attached to the electrode. The surface wave not only characterizes the immobilized species but its shape and position on the potential axis reveal valuable thermodynamic and kinetic information about the modified electrode. The analysis of a surface wave is not as simple as the voltammogram of a solution electrode process where mass transport by diffusion of the electroactive species is the principal process of charge transport. For a modified electrode the

charge transport mechanism is complex involving a combination of events all of which may influence the shape and position of the surface wave. The thermodynamics and kinetics of a modified electrode are therefore the consequence of a multistep process involving the oxidation or reduction of the attached species.

There are no major new electrochemical theories to exploit in the analysis of surface waves. The results of theoretical studies of solution voltammograms, monolayer adsorption peaks appearing in linear sweep voltammetry at bare electrodes and the Frunkin isotherm-like model of Brown and Anson (39) are useful in some cases in the

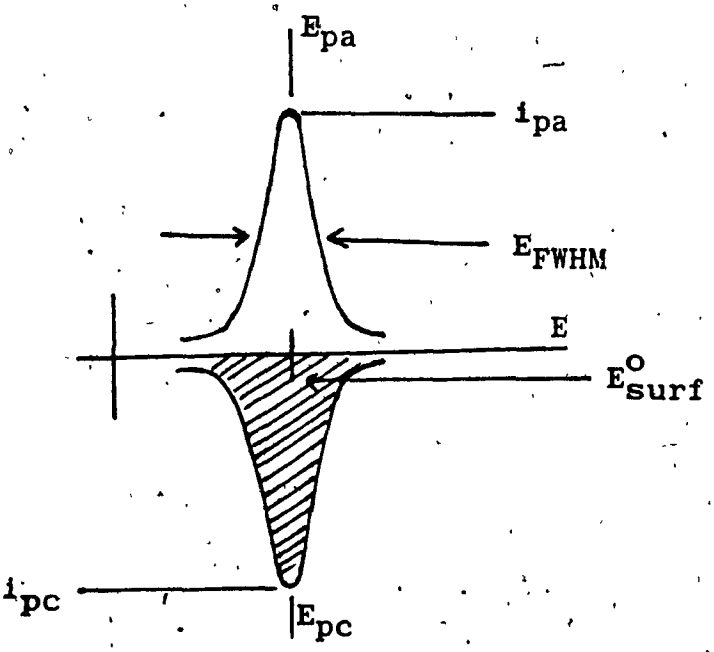

Figure 1-5. Schematic, reversible voltammetric surface waves for an adsorbed monolayer at an electrode.

analysis. The quantities of interest in a voltammetric surface wave are therefore the same as those for solution voltammograms and for voltammograms of an adsorbed monolayer. These quantities are depicted in an ideal wave shape in Figure 1-5 for a reversible process of an adsorbed monolayer at a bare electrode surface.

The thermodynamics are usually revealed through the formal potential E^o of the electrode and the activity. For a monolayer adsorbed on the electrode the ideal situation is where all the adsorption sites are equivalent and there is no interaction between the molecules adsorbed on the electrode surface. In such situation a Langmuir isotherm is obeyed and under these conditions the superficial concentration Γ_O and Γ_R can be replaced in the surface Nernst equation. The standard surface potential is then given as:

$$E^{o'} = E^o - (RT/nF)\ln b_O/b_R \qquad (3)$$

the peak potential can then be written as:

$$E_p = E^{o'} - (RT/nF)\ln b_O/b_R \qquad (4)$$

where b_O and b_R are the surface activities, under Langmuir conditions $E_{pa} = E_{pc}$, the anodic peak potential equals the cathodic peak potential, and the anodic and cathodic wave are mirror image of each other as in Figure 1-5. The total width at half height of either peak or the Full Width Half Maximum, E_{FWHM} is given as:

$$E_{p\frac{1}{2}} = 3.53\ (RT/nF) = (90.6/n)mV \qquad (5)$$

at 25°C. The location of E_p, the peak potential depends on the surface activity of the oxidized, O and the reduced, R forms of the species.

In most cases even when the waves shapes are symmetrical about the peak potential, the wave shapes and E_{FWHM} deviated from ideality. Brown and Anson (39) ascribed this to interaction between the adsorbed molecules and proposed a Frumkin isotherm like expression to connect activity and the interaction parameter of adsorption, g. The Frumkin isotherm is a logarithmic one and the activity coefficient is given as:

$$\beta_O = \exp - (g_O \tau_O + g_{OR} \tau_R) \qquad (6a)$$

$$\beta_R = \exp - (g_R \tau_R + g_{RO} \tau_R) \qquad (6b)$$

where g_O and g_{OR} are the interaction parameters between two oxidant molecules O, and between and oxidized and reduced molecule, O and R. g_R and g_{RO} are the analogous parameters for the reduced molecule. Using the expressions of equation 6a and b, equation 7 was derived for the peak potentials of the attached species:

$$E_{pa} = E_{pc} = E^{o'} - RT/2nF\ (g_O - g_R)\tau_T \qquad (7)$$

where τ_T is the total coverage of O + R. Equation 7 predicts that the two peak potentials are equal but well

shifted along the potential axis as a function of concentration of the attached species unless the interaction parameters are equal. In equation 7 $RTg_0\Gamma_0$ represent half of the energy which has to be spent during the oxidation or reduction because of the gradual disappearance or appearance of the interactive forces between molecules of O. If $g_0 > 0$ (attractive force between O) the peak becomes more negative for reduction because more electrical energy has to be spent to overcome the attractive force. If $g_0 < 0$, the peak potential is towards more positive potential. The term $RTg_R\Gamma_R$ is similarily interpreted. The wave shape according to Laviron (40) is a result of the net interaction between molecules of O, molecules of R and molecules of O and R and is defined by the quantity

$$G = (g_0 + g_R - 2g_{OR}) \qquad (8)$$

when G = O (the interaction between the oxidized and reduced sites are of the same type and magnitude) the shape and characteristics are ideal. When G < O i.e. the interaction between molecules of O or molecules of R are repulsive and the waves are broader, flatter, the peak currents are smaller. For G between zero and 2 (attractive forces prevail) the peak becomes narrower and sharper.

The theoretical treatment of the monolayer surface

wave and the surface activity parameters of Brown and Anson, and Laviron may be used as an empirical approach in the analysis of the surface waves for modified electrodes. A number of authors have transposed this theory to the situation of covalently modified electrodes but the relationship do not fit the entire voltammetric wave particularly when the peak broadens. It was suggested that other factors may influence broadening of the peak width (38,41,42). Broadening could occur if all the redox sites are not characterized by the same E^{o} . Two types of sites may be signalled by observation of shoulders on the wave. Unequal values in $E^{o'}$ may result from variation in polymer packing which may have a higher density at the surface then layers further from the surface. Inhomogenity in the polymer morphology, crosslinkage may lead to a nonuniform distribution of the electroactive species, solvent intrusion and extrusion with accompanying counter ions, molecular conformation are factors which may be asymmetric with the electrode reaction making $E^{o'}$ different in the two reaction directions. Regarding peak narrowing, the variation in R values cannot account for this and the attractive forces offer a useful explanation.

Since in modified electrodes the majority of the electroactive species are not in contact with the electrode surface but are distributed throughout the polymer matrix the reduction and oxidation reactions

require mechanisms for the transport of charge from the remote sites in the interior of the polymer to the interface. Kaufman et al (43) proposed an electron self-exchange reaction between neighbouring oxidized and reduced sites. This sequence of electron exchange rection was demonstrated by Murray et al, (44) by using polyosmium and ruthenium complexes by bipyridine. The transport process was also shown to occur by actual diffusion of the electroactive specie within the polymer film (38,44). This mode of conduction is accompanied by a concentration gradient of the oxidized and reduced forms. In some instances both the electron hopping and diffusion (45,46) of the electroactive species were shown to occur on the same electrode with the physical diffusion process the major contributor. The reduction or oxidation accomplishes an over change in oxidation state and this is accompanied by transport of charge compensating counter ion into/out of the polymer film. The charge transport process can be further complicated by other factors such as segmental motion of the polymer to permit collision of electroactive species and electron transfer as well as the influence of solvent and morphology of the polymer which can align redox site to aid electron transfer (47). Many studies have proposed the secondary process of counter ion diffusion or polymer motion as the rate limiting step in the charge transport process (38). The important quantity

in the charge transport process that reflects the kinetics of the electrode reaction is the apparent diffusion coefficient. It is represented by the same diffusion laws as the diffusion constant for solution electrode reactions but contains the contributions of all the processes involved in the charge propagation. There have been numerous determinations of D_{app} for various polymer modified electrodes but recently, studies of molecular events influencing the processes which control D_{app} has become the focus. Work by Bard et al (45) distinguished between electron exchange and physical diffusion of the redox ion in Nafion film. Buttry and Anson (48) showed that electron exchange and as wellas physical diffusion in a polymer film follow homogeneous theory and the counter ion effects discussed by Murray and Chambers (29,49) represent only some of the studies in this area. Understanding of the factors controlling D_{app} and the transport of charge in polymer film is therefore fundamental to the kinetics of a modified electrode in electrochemistry as well as photoelectrochemistry.

Since the apparent difussion coefficients follow the same diffusion phenomenology as in solution electrochemistry; solution electrochemical equations have been applied to extract the apparent diffusion coefficient from the response of polymer modified electrodes. In linear sweep voltammetry the peak currents in the waves at different scan rates are analysed by the Randles-Sevick

equation (49):

$$i_p/A = 0.452(nF)^{3/2}C(Dv/RT)^{1/2} \qquad (9)$$

where v is the scan rate, A is the area of the electrode in cm^2, n is the number of electrons, F is the Faraday, R is the gas constant and T is temperature. This equation is derived for a reversible electrode process under linear semi-infinite conditions. In potential sweep experiments of this kind for solutions at metal electrodes where the potential is always changing there is always a change in the potential across the electrode/solution interface. This results in a charging current i_c. The charging current is proportional to scan rate via the equation:

$$i_c = ACv \qquad (10)$$

while the faradic current i_p is proportional to the square root of scan rate $v^{1/2}$ (see equation 9). The charging current can become significant at high scan rates causing the cyclic wave to become distorted. Additionally if uncompensated cell resistance is large R_u becomes significant the sweep rate would not be truly linear and the electrode potential would lag the desired value from the potentiostat. This results in a shift in the peak potential with scan rate. The important parameters for solution voltammogram are the same as for a voltammetric

surface wave for an adsorbed monolayer i.e. the peak current and peak potential. However, in homogeneous solution the peak potentials are not equal but differs by a value of 59 mV at 25°C for a one electron transfer reaction in a reversible electrode process.

In a chronoamperometric experiment the unstirred solution of the electroactive species in the presence of the supporting electrolyte is electrolyzed at a constant potential where the electroactive species can undergo a redox reaction and the current variation with time is recorded. Mass transport is presumed to occur only by linear diffusion under the influence of a concentration gradient established by the consumption of the reactant in the electrode reaction. Transport under the influence of a gradient of electrical potential is eliminated because of the large excess of supporting electrolyte. Under semi-infinite linear diffusion condition the current is given by the Cotrell equation:

$$i_d = nFAD^{1/2}C/(\pi t)^{1/2} \qquad (11)$$

where i_d is the limiting current. In both the Randles-Sevick and Cotrell equations the difusion coefficient, D can be extracted since all the other parameters are known.

Polymer modified electrodes are open to the immobilization of any chemical species provided it can be successfully attached to the electrode. Since the attached

species is defined and the electrode is expected to display the main characteristic properties of the non-immobilized molecule, polymer modified electrode can be tailor made to exhibit any desired property. They can be therefore exploited in a number of ways depending on the properties of the immobilized species.

Modified electrodes on Pt, Au, or carbon as the conductive supports were shown to be analytically useful for preconcentrating molecules or ions from dilute solution for analysis. As an electron transfer agent or electron transfer mediator modified electrodes were found to be used in biological redox systems where the electrochemical redox system is sluggish. Modified electrodes are also useful for their electrocatalytic behaviour. Electrodes of this type can be viewed as a "giant surface molecule", [(electrode)---(complex)] where the electrode is one end of the molecule with an adjustable chemical potential. In such a situation the electron transfer at any potential can be seen as intramolecular.

Chemical derivization of semiconductor electrode is especially useful. In addition to their electron mediator and electrocatalytic properties they are interesting for their photochemical and photoelectrochemical behaviour. Semiconductor surface modified electrodes are prepared for three main purposes. These are photocorrosion protection

of the semiconductor, photosensitization and photoenhanced kinetics. In the protection of the semiconductor the strategy is to alter the interfacial energies to disfavor decomposition with respect to another redox reaction or promote rapid interfacial charge transfer to a redox species in solution. Photosensitization of large band gap semiconductors by a low energy light absorbing chromophore is an attractive technique to extend the absorptive range of the semiconductor and make it equivalent to a low band gap semiconductor for solar energy utilization. Enhanced photoreaction on semiconductor can be achieved by immobilizing the electroactives species to complete with electron hole recombination.

Chapter 2

EXPERIMENTAL

2.1 Materials

Commercially available materials were used as starting reagents in preparation and physical measurements. Table 2-1 presents a list of these reagents along with their respective supplier and their grade.

Table 2-1

Suppliers and grade of materials.

Compound	Supplier	Grade
Nickel(II)chloride-hexahydrate.	May & Baker	Analytical
Copper(II)chloride-dihydrate.	Mallinckrodt	Analytical.
Potassium tetra-chloroPlatinate(II)	Alfa	Reagent.
Palladium(II)di-chloride	Alfa	Reagent
Sodium Cyanide	BDH Chemicals	Reagent
Ferric Perchlorate-hexahydrate	Fredrick Chemicals	Reagent
Carbon disulphide	J.T. Barker	Reagent
Iodine	J.T. Baker	High purity
Anhydrous Sodium-Perchlorate	Anachemia	Purified
Tetraethylammonium-bromide	Aldrich	Reagent

Poly(4-vinyl-pyridine-10% co-styrene	Aldrich	Reagent
Benzyl Chloride	Fisher	Reagent
Dichlorodimethyl-silane	Petrarch Systems, Inc.	Reagent
Silver Nitrate	Fisher	Reagent
Sodium Nitrate	Fisher	Reagent
Dichlorofluorescein	BDH Chemicals	Analytical

Alkali metal salts of lithium, sodium and potassium chloride as well as sodium fluoride, chloride and bromide were all Fisher reagent grade and were recrystallized from water before use. Common solvents e.g. methanol, ethanol, chloroform dichloromethane, ether, dimethyl sulfoxide, N,N-dimethyl- formamide, sulfuric acid and nitric acid were all reagent grade obtained from Anachemia Spectrograde solvents e.g. acetonitrile, methanol, ethanol, toluene were obtained from A & C Chemicals and used as received. Water was dionized and distilled in glass before usage in the synthetic procedure as well as any physical measurements. In the course of the synthetic work deoxygenations were carried out by bubbling purified nitrogen gas. Filtrations were accomplished by the use of Buchner or sintered glass funnels connected to water aspirator. All product were vacuum dried in an oven at 50 to 60 °C unless other wise mentioned.

Microanalyses were performed by Galbraith

Laboratories. In the absence of microanalyses, the purity was established by comparison of the U.V.-Visible spectrum of the final product with the published spectrum.

2.2 Preparation of Ligand and Complexes

2.2.1 Preparation of Sodium Maleonitriledithiolate (Na_2mnt)

The maleonitriledithiolate dianion abbreviated as mnt was prepared as a sodium salt from sodium dicyanodithioformate by a modified procedure of Bahr and Schleitzer(51). 5 g of powered sodium cyanide was suspended in 60 ml of dimethylformamide to which was added 12 ml of CS_2. The mixture was stirred for 16 hrs until a red black crystal mass of sodium dithioformate was obtained. This was filtered and recrystallized from 1:1 ratio of isobutyl and isopropyl alcohol. The (mnt^{2-}) salt was then obtained by dimerization of the sodium dithioformate in $CHCL_3$ for 7 days by spontaneous desulfurization. Purification was effected by recrystallization from methanol/ethanol solution. The yellow product was vaecum dried and stored in the dark at about 5 C.

2.2.2 Preparation of $[(C_2H_5)_4N]_2Ni(mnt)_2$

The well known 2- oxidation level Ni complex of mnt (formally Ni(II) was prepared according to published procedure(52). 50 ml aqueous 1:1 methanol solution of

11.8 g of Na_2mnt was warmed on a hot plate. To this solution 7.5 g of $NiCl_2$ in 12 ml of water was added dropwise with stirring. The intense red solution was filtered and a saturated solution containing 8.0 g of $(C_2H_5)_4NBr$ was slowly added to the filtrate. The red precipitate which formed after cooling was filtered washed with water; purified by recrystallization several times in water-acetone solution and confirmed by comparison of the U.V.-Visible spectra with literature reports(8).

2.2.3 Preparation of $[(C_2H_5)_4N]_2Cu(mnt)_2$

The related Cu complex formally Cu(II), was prepared by a similar procedure. A deaerated alcohol solution of $CuCl_2$ was added dropwise to one of Na_2mnt with vigorous stirring. (It is important to use excess of the ligand inorder to avoid a thick sludge). Shiny dark red crystals separated on addition of a saturated aqueous alcoholic solution of $(C_2H_5)_4NBr$. They were filtered and recrystallized from acetonitrile/water solution. Anal. Calc'd. for $[(C_2H_5)_4N]_2CuS_4C_4(CN)_4$: C, 47.69; H, 6.67; N, 13.90; S, 21.22; Cu, 10.51. Found: C, 47.45; H, 6.82; N, 13.84; S, 21.06; Cu, 10.46.

2.2.4 Preparation of $[(C_2H_5)_4N)]_2Pd(mnt)_2$

This complex was synthesized by the mthod of Benson et al(53). 2.0.g of powdered $PdCl_2$ was suspended in 150

ml of deaerated water and 4.0 g of Na_2mnt was added. The mixture was stirred under nitrogen atmosphere for 3 days at room temperature. It was heated to about 75°C and treated with 4.5 g of $(C_2H_5)_2NBr$. A green solid separated and was collected by filtration and recrystallized from ethanol/water to form shiny platelets. The Pd complex was compared to the literature spectra (8).

2.2.5 Preparation of $[(C_2H_5)_4N]_2Pt(mnt)_2$

The method of Benson et al(53) was again adopted to prepare the Pt complex. 1.0 g of Potassium hexachloroplatinate(II) was dissolved in deaerated distilled water to which was added 1.0 g of Na_2mnt. The red solution was warmed and treated with 2.0 g of saturated alcoholic solution of $(C_2H_5)_4NBr$. The red precipiate was filtered and recrystallized from ethanol/water. The Pt complex was analysed. Calc'd for $[(C_2H_5)_4N)]_2Pt(mnt)_2$: C, 39.70; H, 5.48; N, 11.24; S, 17.43; Pt, 26.51; Found: C, 38.82; H, 5.27; N, 11.32; S, 17.69; Pt, 26.31.

2.2.6 Preparation of $[(C_2H_5)_4N]Ni(mnt)_2$

This complex was prepared by the oxidation of $[C_2H_5)_4N]_2Ni(mnt)_2$ with iodine by the precedure of Davison et al(54). 2.0 g of $[(C_2H_5)_4N]_2Ni(mnt)_2$ was dissolved in freshly distilled deaerated dimethyl-sulfoxide. Excess of iodine dissolved in the same solvent was added to this solution. The solution turned from red to black and on

addition of ethanol fine black needles crystallized from acetone/ethanol and vacuum dried. The product spectrum did not agree with some literature reports in that no 366 nm band was found. Investignation revealed that this band appears to have arisen from excess iodine remaining. Oxidation of the $[(C_2H_5)_4N]_2Ni(mnt)_2$ with 6.0 M H_2SO_4 did not show this 366 nm band but only a shoulder on the intense 311 nm band similar to the product spectrum obtained by iodine oxidation in this synthesis. Anal. Calc'd for $[(C_2H_5)_4N]Ni(mnt)_2$: C, 40.95; H, 4.30; N; 14.92; S; 27.32; Ni, 12.51. Found: C; 41.10; H, 4.33; N, 14.90; S, 27.29; Ni, 12.40.

2.2.7 Preparation of $[(C_2H_5)_4N]Pd(mnt)_2$

$[(C_2H_5)_4N]Pd(mnt)_2$ was prepared by published procedure (54) by iodine oxidation exactly analogous to that of the nickel compex expect that large excess of iodine was required. The product was found to be contaminated with iodine which was removed by sublimiation at 50 C. Recrystallization from dichloromethane gave dark brown crystals which was washed quickly with cold ethanol and then with water. Prolonged contact of the product with ethanol resulted in its reduction to the dianion. Anal. Calc'd: for $[(C_2H_5)_4N]Pd(mnt)_2$: C, 37.17; H, 3.90; N, 13.54; S, 24.81; Pd, 20.58. Found: C, 37.36; H, 4.03; N, 13.37; S, 24.[illegible], 20.38.

2.2.8 Preparation of $[(C_2H_5)_4N]Cu(mnt)_2$

Ferric perchlorate-hexahydrate, 4.0 g was dissolved in 20 ml of deaerated acetonitrile. This solution was added to a deaerated solution of 2.0 g of $[(C_2H_5)_4N]_2Cu(mnt)_2$ in acetonitrile. Addition of water caused precipitation of the product which was filtered and again copiously washed with water. The dark red crystals were dissolved in minimum hot dichloromethane and again filtered. This volume of the filtrate was reduced under pressure and recrystallized using dichloromethane/ethanol with cooling to -10 C. Anal. Calc'd: for $[(C_2H_5)_4N]Cu(mnt)_2$: C, 40.53; H, 4.25; N, 14.77; S, 27.05. Found: C, 40.35; H, 4.03; H, 14.17; S, 27.35.

2.3 Preparation of Quaternized PVP

2.3.1 Quaternization of Poly (4-vinylpyridine-10%-co-styrene)

Poly(4-vinylpyridine) containing 10% styrene content (PVP) was quaternized with benzyl chloride by the following procedure. 2.5 g of PVP estimated to contain approximately 0.02 mole of vinylpyridine units was dissolved in 150 ml of spectrograde methanol in a 3-necked flask fitted with a water condenser and gas bubbler. 12 ml (0.1 mol) of reagent grade benzyl chloride was added to the solution which was heated in a water bath to about 60° C. After the solution was equilibrated at this temperature, it was degassed with prepurified nitrogen.

The pressure in the flask was reduced to below atmospheric, the temperature decreased to 55°C and the solution maintained at this temperature for 60 hrs. Excess benzyl chloride and the reduced pressure appear to ensure maximum quaternization. The quaternized PVP (QPVP) was recovered from a reduced volume of the polymer solution with boiling ether. Purification was accomplished by dissolving the quaternized polymer several times in dry methanol and reprecipitating with dry ether. The product was vacuum dried at 50°C and stored in a dessicator.

2.3.2 Extent of Quaternization

The degree of quaternization was determined indirectly by an adsorption indicator titration technique. The QPVP is a cationic polymer with chloride as counter ions. The determination of the quantity of chloride ion would reveal the content of cationic groups. The chloride ions were titrated with standard $AgNO_3$ solution in the presence of the color indicator dichlorofluorescein to determine the end-point. Triplicate samples of QPVP were titrated. Samples were prepared by dissolving the polymer in 250 ml of warm 0.1 M $NaNO_3$ solution. The pH of this solution was previously adjusted to 4.2 with HNO_3. Indicator solution was prepared by dissolving 0.21 g of dichlorofluorescein in 100 ml of 70% methanol. $AgNO_3$ solution standardized against 0.1000 M NaCl solution by a known procedure(55). Concentration of the $AgNO_3$ solution

was found to be 0.1004 M and this was used to titrate the sample solution of QPVP using the same method as in the standardization of the $AgNO_3$ solution. From the volume of titrant used in the titration process the number of moles of Cl^- ions was calculated. This number reflected the number of quaternized pyridine groups in the poylmer. In determining the percentage quaternization the number of vinyl pyridine groups in the polymer was first estimated. The 10% styrene content was also considered. A molecular weight of 231.73 g/mole was taken for the quaternized vinylpyridine units and 104.12 g/mole for the styrene. All the pyridine groups were assumed to be quaternized and the molar ratio of the quaternized vinylpyridine to styrene was taken as 9:1. This gave a 95.24% by weight of quaternized vinylpyridine in a polmer which is 100% quaternized. From the total weight of the quaternized vinylpyridine groups the number of moles of pyridine was obtained. The percentage quaternization was the determined from the ratio of the moles of Cl^- ions to pyridine. The average of the three samples titrated revealed quaternizations of greater than 99%.

2.4 Modified Electrode: Preparations and Analysis

2.4.1 Preparations of Pt and SnO_2 modified electrodes

Pt plate electrodes were prepared by spot welding a square platinum plate of dimension 0.5 cm^2 and thickness

of 60 μm onto one end of a short piece of Pt wire, the other end of which was sealed into a 6 mm soft glass tubing. Contact to the external current was accomplished with the help of a Copper wire welded to the Pt wire in the glass tube.

The Pt plate and SnO_2 discs were the conductive substrate used to prepare the modified electrodes. The SnO_2 discs were from the same batch in the electrochemistry and photoelectrochemistry measurements. The Pt plate was boiled in concentrated H_2SO_4 for 1 hr, washed copiously with distilled water and absolute ethanol and dried in a vacuum oven for 1 hr at 50°C. An adherent coating of quaternized PVP, (QPVP) onto the Pt plate was produced by dipping the electrode base (plate) two or three times into a 2.5% methanol solution of the polymer. The electrode was kept between 35 to 40°C and the solvent allowed to evaporate slowly under a methanol atmosphere. The slow evaporation in a container nearly saturated with solvent vapor produced a topologically smooth film.

The SnO_2 discs were subjected to a more extensive pretreatment than the Pt plate. The discs were refluxed in concentrated sulfuric acid for 4 hrs, washed with distilled water and absolute ethanol and dried in vacuum at 50 C for 12 hrs. They were further refluxed under a nitrogen atmosphere in 5% dichlorodimethylsilane in spectrograde toluene for 3 hrs, after which they were washed thoroughly with dry toluene and dried in vacuum at

50°C. Coating of QPVP on the silanized SnO_2 and allowing the solvent to evaporate under the same conditions as the Pt electrode. The weights of the polymeric coating was determined by recording the weight of the disc before and after it was coated on a microbalance.

The silinization of the SnO_2 electrodes was found to be important in the preparation of stable and adherent film on the SnO_2 electrode. Polymer films with incorporated $Ni(mnt)_2^{2-}$ complex on bare SnO_2 surface (surface not subject to silinization) peeled off after prolonged soaking in water. The polymer film itself was not visibly swollen or soggy and was neither cracked or broken. Water appears to diffuse from the edge of the disc between the SnO_2 layer and the polymer film and lifted the polymer off from the SnO_2 surface. A very much more adhesive film was obtained when the SnO_2 surface was silinized. Prolonged soaking does not affect the film. It remains adherent, durable and robust.

The dichloromethylsilane is a non electroactive molecule and silinization produced a very thin layer (probably a monolayer since it cannot be measured on the profilometer) and is not expected to seriously inhibit electron transfer across the electrode/polymer surface. The silane groups are attached to the SnO_2 surface by silicate ether bonding. The acid treatment of the SnO_2 introduced hydroxyl groups on the surface. The dichlorodimethylsilane containing the hydrolytically

unstable Si--Cl bond reacted with the surface OH groups to form a silyl ether bond to the surface. The silinized surface is not believed to react and form a chemical bond with the QPVP since the QPVP can be easily removed in solvents such as DMSO, DMF and methanol. It probably acts as a water repellant at the peripheral edge of the SnO_2-QPVP electrode where the water could otherwise diffuse.

The $M(mnt)_2^{2-}$ complexes were loaded unto the polymer coatings on the electrode in two ways. The polymer coated electrode was refluxed in spectrograde acetonitrile containing 4×10^{-3} M of the complex or alternatively the polymer coated electrode was soaked in 0.1 M $NaClO_4$/acetonitrile solution for 5 mins before heating it in the solution of the complex. Loadings were mostly done by the first procedure. Those electrodes loaded by the second, or alternative, will be specified. Excess complex adhering on the surface coating was removed by rinsing in methanol.

The Pt and SnO_2 modified electrodes are abbreviated as Pt-QPVP-$M(mnt)_2^{n-}$ and SnO_2-QPVP-$M(mnt)_2^{n-}$ respectively where M = Pt or Ni. n designates the charge on the complex anion and does not refer to the overall charge on the modified electrode. The electrode is neutral.

2.4.2 Profilometer Measurements and Analysis

Thickness of polymer film loaded with the complex on the SnO_2 electrodes were determined from mechanical

surface profile measurements using a Talysurf Taylor-Hobson step profilometer. Measurements for films before and after the complex was loaded, gave approximately the same thickness.

The amount of QPVP deposited on SnO_2 electrodes were obtained from weight measurements. Using 231.74 g as the Molecular Weight for the quaternized vinylpyridine unit and the weight of the polymer film, the number of moles of these units was established. The amount of $M(mnt)_2^{2-}$ incorporated in the QPVP coating was estimated by a spectrophotometric technique. The polymer coating along with the incorporated complex was dissolved from the electrode in a known volume of DMSO and the concentration determined from absorbance measurements in the visible. In some instances the complex was removed from the polymer coating by equilibrating the modified electrode in a known volume of 1.0 M $NaClO_4/CH_3CN$ solution. This process involved in perchlorate ion exchange from the solution into the film for the complex. Absorbance of the acetonitrile solution gave the concentration from which the amount of the complex in the film was determined. From the concentration and the volume, the number of moles of $M(mnt)_2^{2-}$ was estimated and this reflected the quantity incorporated in the polymer.

The thickness of QPVP film on a Pt modified electrode cannot be measured by the surface profilometer technique. It was indirectly determined by relating the amount or

number of quaternized vinylpyridine units per square centimeter on the electrode to thickness as follows. Various film thickness on SnO_2 electrodes ranging from about 2 to 4 μm were prepared by transferring different volumes of methanol solution of the polymer to the discs and allowing the solvent to evaporate as described. The weight of the polymer coating on the SnO_2 electrode was determined and used to calculate the number of moles of QPVP units per square centimeter. The thickness of these films as per surface profilometer measurements was plotted as a function of cencentration (moles of QPVP units/cm^2). This plot is shown in Figure 2-1 and relates thickness to moles of QPVP/cm^2. The calibration curve of Figure 2-2 relates moles of QPVP/cm^2 or concentration to absorbance. These two plots together relates the thickness to absorbance of QPVP. The calibration curve was obtained by preparing different concentrations of the QPVP polymer in a methanol solution and recording the absorbance at 256 nm). The average extinction coefficient of 4000 was calculated from this curve for the QPVP polymer based on the molecular weight of 231.73 g/mole for the quanternized vinylpyridine unit.

The $M(mnt)_2^{2-}$ complex incorporated into the QPVP film of the Pt modified electrodes was first removed from the polymer by the ion exchange method described previously. The adhering polymer on the Pt electrode was then removed

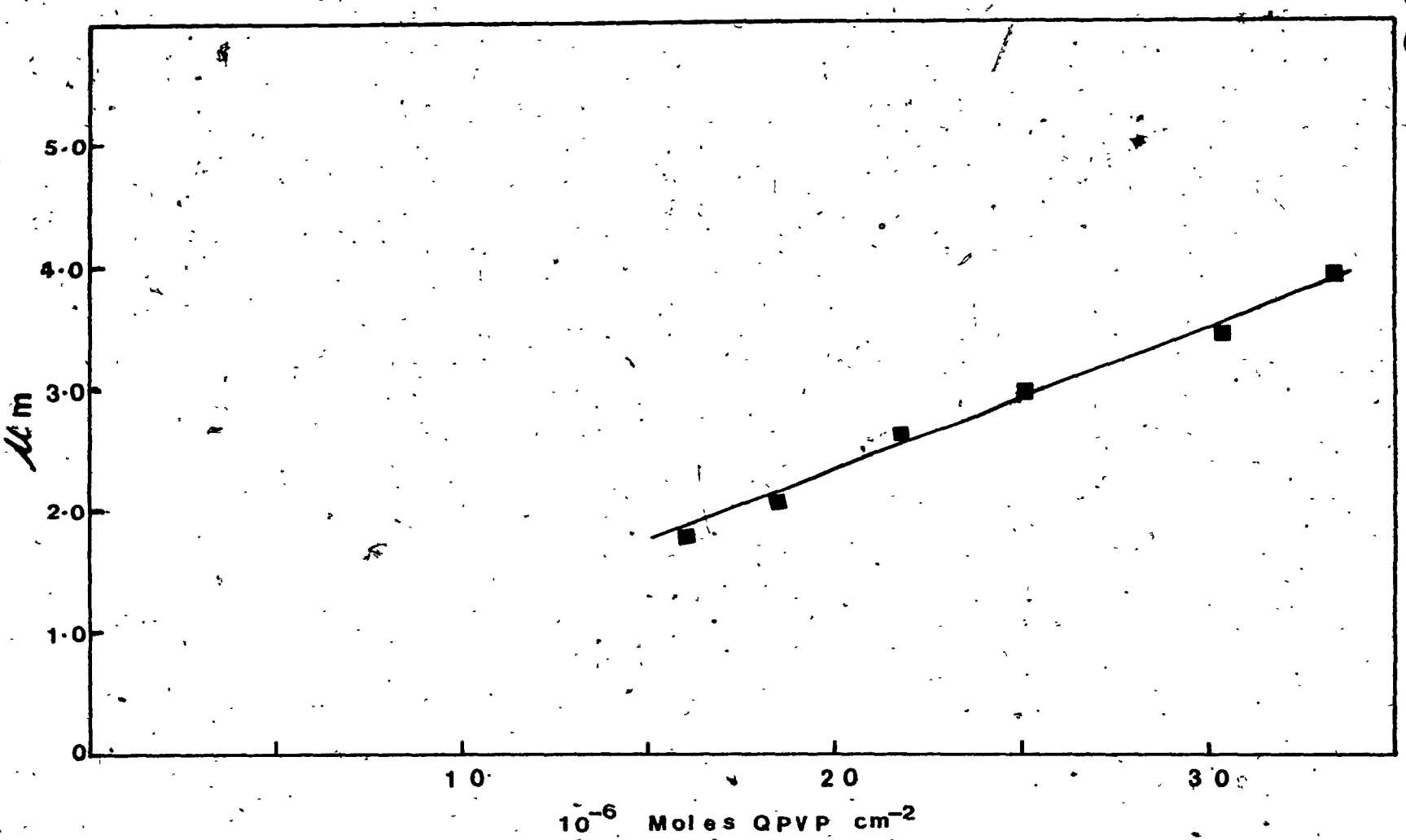

Figure 2-1. Plot of thickness of QPVP film on SnO_2 electrode as a function of concentration in Moles (based on vinylpyridine unit) per cm^2.

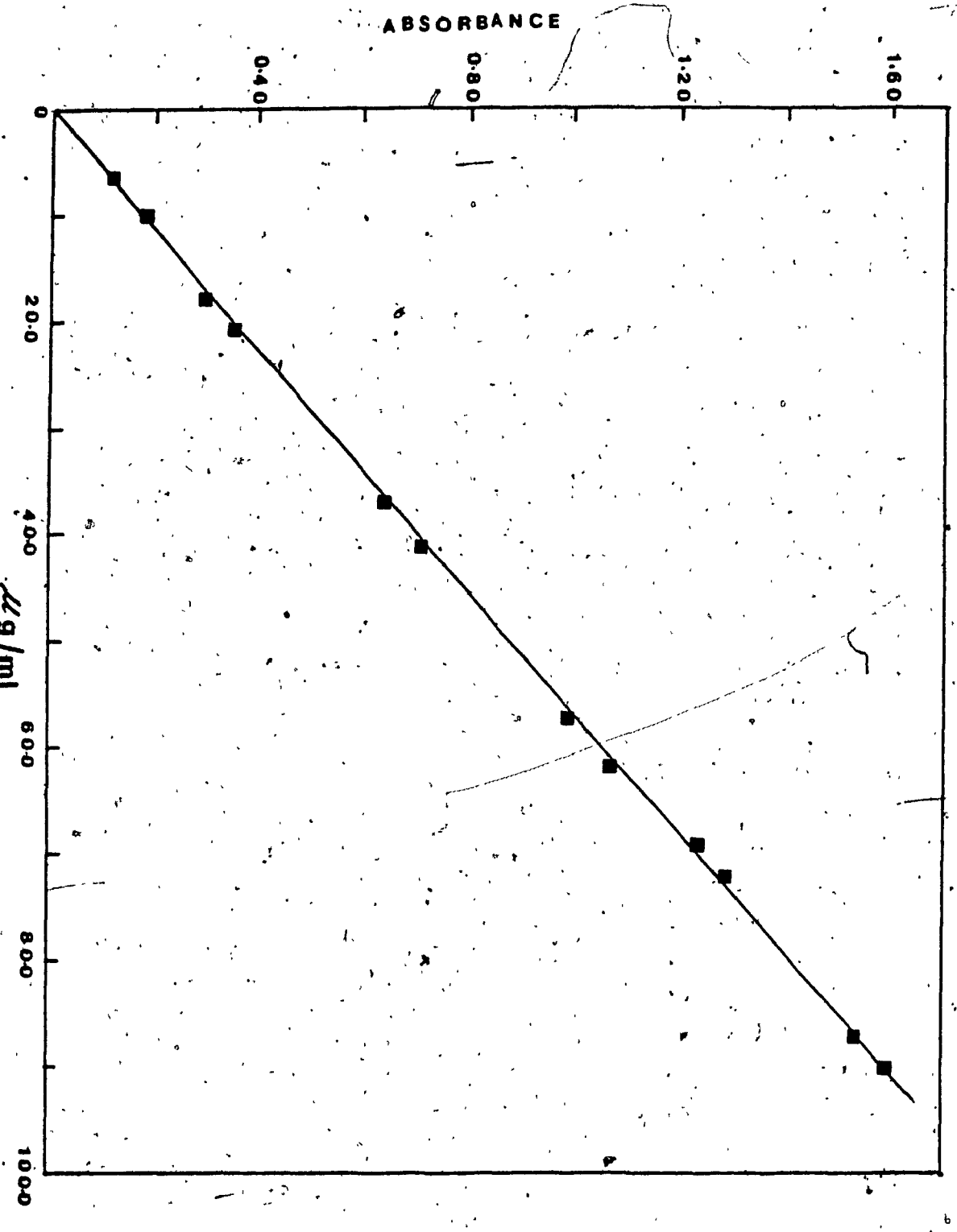

Figure 2-2. Plot of absorbance of QPVP at 256 nm as a function of concentration in methanol.

by dissolving it off the electrode in hot methanol solution and the absorbance at 256 nm taken and compared to the calibration curve. This solution was usually made dilute so that the absorbance did not exceed 1.6. From the absorbance measurement the concentration of the polymer was calculated and used to determine the number of moles of quaternized vinylpyridine units per cm^2 on the electrode. This value was then related to a thickness value in Figure 2-1 which was taken as the thickness of the film on the Pt modified electrode.

2.5 Electrochemical and Photoelectrochemical Techniques

2.5.1 Electrochemical Techniques

Solution or homogeneous electrochemical experiments were performed using a PAR 363 Potentiostat in conjunction with a locally constructed triangular pulse generator on a design in the literature (56). The electrode response was recorded on a X-Y and a strip chart recorder. Measurements were made at a Pt wire electrode in a conventional polarographic cell and also at SnO_2 working electrode in a teflon cell. The SnO_2 electrodes were the same type used for photoelectrochemical measurements and were subjected to the same treatment prior to usage. Reference electrodes either Ag/AgCl (Sat. KCl) separated from the voltammetric cell by a glass frit tube containing the appropriate depolarizer solution or Ag/Ag^+ (0.1 M $AgNO_3$) in CH_3CN a redox couple which was found to be +0.27

V vs Ag/AgCl (Sat. KCl). A Pt wire auxilliary electrode was used. Measurements were performed in spectrograde acetonitrile (American Chemicals) with 0.1 M anhydrous sodium perchlorate (Anachemia) as inert electrolyte unless otherwise noted. The solvent was transferred to the electrochemical cell by the technique described in section 2.5.2. Reactants were dissolved directly inside the cell and the sample solutions were degassed by bubbling prepurified N_2 through the solutions.

Thin film heterogeneous electrochemical measurements were performed using the same equipment as the solution studies. Reference and auxillary electrodes were Ag/AgCl (Sat. KCl) and Pt wire respectively while the supporting electrolyte consisted of a halide salt of either lithium, sodium or potassium as will be specified. Water deionized and doubly distilled from glass were used in the preparation of all electrolytic solutions. Measurements were made on Pt plate (0.5 cm^2) modified electrode in a conventional glass electrochemical cell equipped with a dispersion tube for deoxygenation and on SnO_2 modified electrode in the teflon flow cell used for photoelectrochemical measurements. The polymeric coating on the outer periphery of the SnO_2 modified electrode was neatly removed by a sharpedged blade industrial cutting knife to provide an electrical contact between the brass ring and the SnO_2 layer.

2.5.2 Photoelectrochemical Techniques

All solution or homogeneous experiments were performed at optically transparent electrodes with a usable window of 360 to 600 nm. These electrodes were frabricated as discs 2.5 cm in diameter from SnO_2 coated "NESA" glass obtained from O.H. Johns Glass Division and marketed as I.R. reflective conducting glass. Typical resistances are less than 50 Ohms. The electrodes were prepared for use by soaking in absolute ethanol at 70 C for six hours, and then washed several times with hot absolute ethanol and dried acetonitrile. They were stored in vacuum at 160 to 180 C prior to use. Heating was for at least 12 hours. Measurements were conducted in a teflon flow cell equipped with a Pt coil counter electrode and an Ag/Ag^+ (0.1 M $AgNO_3$ in CH_3CN) reference electrode. The optically transparent electrode was tightly pressed against a silicone rubber "O" ring and a thin brass ring in the wall of the cell. It was held securely in this position from the outside by means of screws and a brass plate that permitted an optical window of 0.78 cm^2. The "O" ring served as a seal and prevented electrolytic solution from coming into contact with the brass ring on the outer periphery electrode. The brass ring provided the electrical connection between the SnO_2 layer (working electrode) and the potentiostat. The cell along with all unsheilded connecting ends of the potentiostat was kept in

a Faraday cage to reduce the electrical noise.

Spectrograde acetonitrile (American Chemicals) was kept in an inert atomsphere. Anhydrous sodium perchlorate (Anachemia) was stored under vacuum at 200°C. Solutions for photoelectrochemical measurements were made by pumping the acetonitrile solvent directly into a reservoir containing sodium perchlorate which served as inert electrolyte (0.1 M) and the maleonitriledithiolate complex. The solution was circulated at the rate of 45 mls/min from the closed reservoir using a Masterflex peristaltic pump and silicone tubing. The reservoir was equipped for deaeration of the solution by means of a glass frit dispersion tube. Deoxygenation was persumed to be accomplished after continuous passage of a stream of purified nitrogen gas for two hours.

A supply of dry oxygen free nitrogen was obtained by passing prepurified nitrogen through columns of 4 A° molecular sieves and a supported copper catalyst a system described in the literature (57). The catalyst was prepared by the method of Meyer and Ronge (58) on a diatomite support.

The solution was irradiated through the SnO_2 electrode using either an argon ion laser (nominally 6 W) from Coherent Radiation or 200 W Xenon lamp filtered by 6 cm of water and a 420 nm filter to cut off IR and U.V. radiation respectively. The light beam was interrupted at a frequency of 13 Hz by a Model CA chopper from Hurst

Manufacturing Corp. The output level of the chopped beam was monitored at the front face of the SnO_2 electrode by Coherent Radiation power meter which has been calibrated by reineckate chemical actinometry (59). A small portion of the beam was deflected by a beam splitter to a photodiode which serve as a reference channel signal for PAR model 128 Lock-in Amplifier. The Lock-in Amplifier received its input from the current channel of the potentiostat and its output was recorded on a strip chart recorder. The phase relation between the output of the Lock-in Amplifier and the irradiation beam was determined using an input signal from a photodetector positioned in the place of the photoelectrochemical cell.

The experimental arrangement in these investigations was introduced by Phillips et al (60, 61). It requires irradiation of the solution through the optical electrode to generate excited states in the solution but close to the electrode so that these species can diffuse and react at the electrode within their excited state relaxation time. The continuous circulation of the electrolytic solution through the cell suppressed thermally induced current resulting from light absorption, replenished the electrode surface with the reactant and simultaneously flushed any photo-induced reaction products which may tend to be adsorbed on the electrode. This technique has proven successful in detecting short lived excited state

species and estimating their lifetimes from kinetics of competing reactions. The capacity to estimate short lifetimes can be appraised by refering to earlier works (61) in which an excited state lifetime in the nanosecond domain was determined for the non-luminescent $Fe(bpy)_3^{2+}$.

Heterogeneous photoelectrochemical measurements were performed at SnO_2 modified electrodes in contact with deoxygenated 0.1 M KCl aqueous electrolyte. All measurements were made in the teflon cell described before. The arrangement was the same as that for the homogeneous study. The electrodes were irradiated with a collimated beam from a tungsten halogen lamp. Photocurrents were read directly from Kiethly model 177 multimeter. The electrode response under illumination was recorded on a strip chart. During irradiation the electrolyte was not circulated through the teflon cell. After each photocurrent reading, the illumination was manually interrupted and the electrode response in the dark (normal laboratory light) was allowed to attain electrochemical equilibrium then the electrolyte was circulated through the cell. There was no observable difference in the photocurrent when the electrolyte was stationary or in continuous circulation. Readings with a stationary electrolyte were preferred because the background current was smaller allowing the voltammeter to be kept at a more sensitive range.

2.6 Electronic Absorption Spectra

Solution electronic absorption spectra were taken with spectrograde acetonitrile in quartz cells of 1 cm and 0.1 cm lpathlength. Solid state spectra were recorded on SnO_2 modified electrode mounted in the position of the cell holder of the spectrophotometer. All measurements were made on Perkin Elmer 552, Cary 14 or 2290 spectrophotometer.

2.7 Flash Photolysis

2.7.1 Transient Absorption Measurements

Nanosecond flash photolysis experiments were performed on Model DL 2100 C dye laser by Phase-R Corporation using a Model DL-15 coaxial flash lamp. The Single Short Circuit operation was used in discharging the high voltage capacitor through the flash lamp to form a coaxial sheet discharge over the entire lamp thereby exciting the circulating dye solution in the inner tubing of the lamp. The flash lamp as well as the dye solution was cooled by tap water. The dye solution comprised of 2x10-4 M Laser Dye LD 490 (Exciton). The absorption maximum of this dye is at 396 nm and lasing wavelength range 480 nm. The probe consisted of a 250 Watt Xenon lamp operated from a stabilized power supply. It covered a spectral range from 240 nm to 900 nm. The flash beam and monitoring beam were made to pass through a quartz photolysis absorption cell at right angle to avoid

monitoring scattered light. The photodetection system consisted of a grating monochromator and a high gain photomultiplier. The photomultiplier output was displayed on a Tektronix 7633 storage oscilloscope and photographed.

2.7.2 Picosecond Flash Photolysis

Picosecond transient absorption spectra and fluorescence decay curves were measured by using a microcomputer controlled picosecond laser photolysis system of the Canadian Centre for Picosecond Laser Flash Photolysis located at this University. The excitation source consisting of a Quantel YG 402G Neodymium-doped YAG (Yttrium-Aluminum-Garnet) Oscillator, Brewster/Brewster Rod dimension 90 mm long x 7 mm diameter, was passively mode locked with Kodak 9740 dye solution.. It yielded a 30 ps pulse train at a maximum rate of 10 pps. The fundamental output is at 1064 nm with energy of a few micro joules pulse. Single pulse extraction was achieved by a PF 302 pulse slicer from Quantel. The pulse train entered the selector that consists of antireflection coated Glan-Taylor cross polarized prism. Between the prisms was positioned a KD*P double crystal pockels cell of half wave voltage 3.6 KV at 1064nm, Index of refraction 1.47, and an electro-optic coefficient of 25 pmV-1. The pockels cell and polarizer are used to achieve the pulse transmission mode (PTM). A Kryton based electronics triggered by the first (few) rejected mode locked pulse

supplied a short high voltage to the pockels cell to make them birefringent. The duration of the voltage pulse is such that only one pulse is rotated 90° angle and can pass through the analyser. The selected pulse from the pulse train is then successively amplified by a Quantel SF 410-07, 7 nm x 115 mm Nd:YAG rod. The amplified pulse of wave length 1064 nm, energy 60 to 80 mJ and width of 4 to 8 ps was then converted to 532 nm with approximately 20 percent effeciency by passing through a KDP type I crystal. The power output of the second harmonic is proportional to the square of the fundamental energy. Subsequent passage of the 532 and 1064 nm pulse through a KDP type II crystal produced the third harmonic at 355 nm by frequency mixing. This 355 nm pulse, energy of approximately 2.5 mJ was used for excitation. The frequency mixing technique does not convert all the 1060 nm light into the third harmonic. The unconverted fundamental is then focused into a Raman active fluid comprising of a 50% D_2O in H_2O by volume and resulted in the generation of a transient birefringent to produce a Stokes and anti-Stokes Raman effect. This produced a continuum of white light with a wavelength 400 to 600 nm with the same pulse width as the laser pulse. The 355nm pulse is directed to the sample throughthe cell holder. The transients transmission changes ofthe excited sampleare monitored with the picosecond continuum. The continuum passed through a beam splitter and divided in

two beams . One of the beams was directed to the sample to be used as the spectroscopic probe. The light transmitted by the excited sample is detected by a multichannel photodiodes array. The second continuum beam is directed to another polychromator-multichannel photodiodes arrangement and is used for spectral analysis of the light. Measurements were taken at different delay times between 20 ps to 10 ns. The delay time reflected the moment at which the probe pulse was detected by OMA after excitation of the sample. For each experimentally delayed period three sets of data were recorded. Each set consisted of four excitation shots, three recorded for the sample and one for the blank. An average value for the blank was based on the pooling of the data of the blank runs for all the different experimental periods. The average absorbance upon excitation of the sample for each delay period was based on the values of the nine shots used for exciting the sample. The transient spectra are presented as the average absorbance change between the blank and excited sample. The absorbance A (λ) of the transient species at wavelength λ can be given by the following equation:

$$A(\lambda) = \text{Log} \frac{I_1^E(\lambda)}{I_2^E(\lambda)} - \text{Log} \frac{I_1(\lambda)}{I_2(\lambda)} \qquad (12)$$

where I_F and I_1 are the intensities of the continum beams detected with and without excitation respectively, I_2 is the intensity of the transmitted light or radiant power and I_1 is the incident radiant power. The transient absorbance is calculated by a microprocessor connected to the multichannel photodiodes. Samples for transient absorbance spectroscopy were freshly prepared in spectrograde acetonitrile with an absorbance of 0.65 at 355 nm in a 2 mm cell. With the aid of microsyringes the samples were thoroughly deoxygenated by bubbling argon gas in the 2 mm cell tightly filled with rubber septum caps.

2.7.2 Pulse Fluorescence Measurements

Time resolved fluorescence was measured by the Electron Optical Chromoscopy Method using the experimental set up for the picosecond transient absorption spectroscopy with the appropriate modification. It employed a high speed time resolved photometer with a high gain microchannel plate incorporating a streak tube (Model HTV N895) and a video electronic readout system. This temporal photometer system consisted of the following: a Temporal-disperser (type No. C 979) which is a picosecond streak camera capable of resolving time better than 10 ps and producing profile of light events up to 10 ns. A Temporal Analyser (type C 1098) which is a rapid electronic readout system for processing video images. It integrates and outputs the video signal intensity along

the prescribed portion of a horizontal video time for every line. It analyses the video image for the streak camera and video camera, a video camera (SIT Camera type C100-18) which uses a highly sensitive pick up tube, a monitor, chart recorder and computer. The 355 nm light pulse from the third harmonic from the mode locked Nd:YAG laser was split by a dichronic beam splitter into a reference beam and sample beam. The sample beam was optically delayed by a roof-top prism and subsequently excited the sample in the cell. The sample fluorescence was collected from the sample cell front face and detected by the streak camera. The reference beam also entered the streak camera but because of the shorter light path arrived before the fluorescence. This reference pulse can be used to monitor the shape and duration of the exciting pulse. Colored glass filters (385 nm together with 485 nm Corning) as well as interference filters were placed before the streak camera entrance slit to select the fluorescence band and reject the intense laser pulse.

Samples for the pulse fluorescence spectroscopy were freshly prepared in spectrograde acetonitrile and in a 40% water/60% acetonitrile (by volume) solvent mixture. Sample solutions with absorbance of 0.61 at 355 nm in 2 nm cell were deoxygenated as before described and used for the fluorescence measurements.

Chapter 3

Results

General Remark

The results in this theses, are presented in a graphical, tabular, as well as the written form and are given in chapters 3 to 7. In some cases, the graphical and tabular results are cited in chapters other than that in which they are presented. In chapter 8 all the results are discussed. Therefore, for the purpose of convenience all graphical and tabular data are located at the end of each chapter in which they are described.

Results I

3.1 Electronic Absorption Spectra in Solution

The solution electronic absorption spectra of most of the $M(mnt)_2^{n-}$ complexes have been previously assigned. The two approaches described in the introduction are reported in Table 3-1. The importance of the absorption spectra in this study is to relate the assignments to photochemical results. The spectroscopic fine points were therefore ignored and the Gray assignment was followed without detailed comment. This choice is made because these assignments are based on one of the anionic complexes to be investigated in this work. There are also photochemical precedent favoring these assignments. The

assignments in Table 3-2 which are new are based on Gray's work. A representative molecular orbital diagram is shown in Figure 3-1.

3.2 Electrochemistry of $M(mnt)_2^{n-}$; M = Ni, Cu, Pd and Pt in CH_3CN

3.2.1 Characterization of Redox Reactions at SnO_2 electrode.

Since the solution photoelectrochemical measurements were at SnO_2 electrode the electrochemical behaviour of the above complexes were studied at this electrode by cyclic voltammetry and chronoamperometry. The solution electrochemistry of the metal dithiolates has been extensively studied by a number of groups and their redox behaviour is well characterized. These studies were however done in different electrolytes with different electrode systems. For the purpose of characterizing the reactions at SnO_2 and comparing reaction kinetics at Pt and SnO_2 electrodes the electrochemistry of Ni, Cu, Pd and Pt complexes were repeated under conditions identical to that at the SnO_2 electrode. The reference electrode was Ag/Ag^+ (0.1 M $AgNO_3$ in CH_3CN) and the electrolyte, 0.1M $NaClO_4$ in spectrograde acetonitrile in both cases.

Figures 3-2 and 3-3 show representative voltammetric response at 100 mV/sec at Pt and SnO_2 electrodes respectively. The voltammetric parameters from such waves are tabulated and compared in Table 3-3 and 3-4. The

redox reactions at the SnO_2 electrode, obtained by comparison with the known reactions at Pt electrode, are set out.

The shape of the waves for the current potential curves for the redox process $M(mnt)_2^{2-}/M(mnt)_2^{1-}$ where M = Ni, Cu and Pt at the SnO_2 electrode are symmetrical, well developed but unlike those of the Pt electrode in that they are broader. The ΔE_p (the anodic and cathodic peak separation) at the SnO_2 electrode is larger than that obtained for the same scan speed at the Pt electrode. The larger ΔE_p usually indicates slower heterogeneous electron transfer. The waves corresponding to the oxidation of $Ni(mnt)_2^{1-}$ and $Cu(mnt)_2^{1-}$ at SnO_2 electrode are not resolved, instead they appear to be very much diffused and merged with the background current of the electrolyte. The reduction of $Cu(mnt)_2^{2-}$ to the trianion and the oxidation of the monoanion to the neutral species have not been reported before. The wave at +0.96 in Figure 3-2 assigned to the oxidation reaction of the monoanion. It falls in the potential range for the oxidation of $Ni(mnt)_2^{1-}$. This is because the oxidation process of the monoanion results in the removal of an electron from a primarily ligand based orbital rendering the oxidation practically independent of the identity of the metal. The reversible wave at -1.07 V (Figure 3-2) is assigned to the $Cu(mnt)_2^{2-}/Cu(mnt)_2^{3-}$ redox reaction. A d^9 formulation can be considered for the metal ion in the $Cu(mnt)_2^{2-}$ which

makes it isoelectronic with the trianion of Nickel. The degree of metal contribution to the HOMO, $3b_{1g}$ is expected to be similar for $Ni(mnt)_2^{3-}$ and the dianion of Copper. Thus the reaction is a more metal centered reduction. This reduction potential is however approximately 1.0 V more anodic for the analogous process of the Nickel complex despite the addition of the extra electron to the $3b_{1g}$ orbital constitutes paring. The difference in the reduction potential of $Ni(mnt)_2^{2-}$ and $Cu(mnt)_2^{2-}$ lies in the nature of the metal ion and the metal character of the $3b_{1g}$ orbital. Since this orbital is predominantly metal based, the reduction of $Ni(mnt)_2^{2-}$ and $Cu(mnt)_2^{2-}$ can be approximated as placing the additional electron in the valence orbital of the metal ions. In such a situation the configurations $3d^8\ 4s^1$ and $3d^{10}$ are reached for Ni(I) and Cu(I) respectively. The 3d level of free Cu(I) ion is lower than the 4s level. In Ni(I) the ordering is reversed. The valence state ionization energy of Cu(I) is higher than NI(I) by about 2.05 eV. This means that the electron affinity for Cu(II) is higher than Ni(II). The electron affinity for the free ions do not quantitatively apply to the metal complexes since there is some contribution of ligand character to the $3b_{1g}$ orbital. It however seems to be a rational argument to suggest that this metal based orbital in the Copper complex is lower than in the Nickel thereby making it easier to be filled.

Similarily to the Ni, the redox process of $Pt(mnt)_2^{1-}$ /$Pt(mnt)_2^{0}$ was found to be irreversible at Pt and SnO_2 electrodes in acetonitrile. The reversibility of this reaction is dependent on the solvent since it was found to be reversible in dichloromethane. The wave associated with this anodic reaction at an SnO_2 electrode in acetonitrile is broad and diffuse. The $Pd(mnt)_2^{2-}$ complex show quasireversible reaction for the processes $Pd(mnt)_2^{0}/Pd(mnt)_2^{1-}$ and $Pd(mnt)_2^{1-}/Pd(mnt)_2^{2-}$ at the Sno_2 electrode. The wave for these reactions are broad and well separated with diffusional tails.

3.2.2 Kinetics of SnO_2 reaction in CH_3CN

The voltammetric peak separation at SnO_2 electrode from (Table 3-5) are larger than those at the Pt electrode for the corresponding reaction. In order to obtain a better understanding of the kinetics of the electrode reactions linear sweep voltammetric responses for Pt and SnO_2 electrodes at various scan rates in known concentrations of $Ni(mnt)_2^{2-}$ and $Pt(mnt)_2^{2-}$ were recorded. It should be mentioned that the electrodes used in this section for determining the kinetics of the electrode reactions were pretreated with dimethyldichlorosilane in the manner described in chapter 2 section 2.4.1. Figures 3-4(a) and 3-5(a) show the Pt and SnO_2 response respectively for the reaction $Ni(mnt)_2^{2-}/Ni(mnt)_2^{1-}$. While the analogous reaction at these electrodes for the

Platinum complex is shown in Figures 3-6(a) and 3-7(a).

For both Nickel and Platinum complexes at Pt electrode, the peak potentials show only a slight shift with increasing scan rate. The ratio of the anodic to the cathodic peak currents regardless of scan rate is unity indicating that no kinetic or other complication in the electrode process is occuring. The reaction products are stable and reversibly reactive. The peak currents increased with scan rate and a plot of peak current as a function of square root of the scan rate is shown in Figure 3-4(b) and 3-6(b) for the Nickel and Platinum complexes respectively. There is no deviation from linearity verifying that the reaction is reversible and in accordance with equation 9 for a semi-infinite diffusion process. The diffusion constants obtained from the slopes are 1.49×10^{-5} cm^2 sec^{-1} for the Nickel complex and 1.40×10^{-5} cm^2 sec^{-1} for the Platinum complex. These values are in agreement with the conventional diffusion constant of approximately 10^{-5} cm^2 sec^{-1} for diffusion limited current. Table 3-5 summarizes the voltammetric and kinetic parameters.

The peak separation ΔE_p which is a diagnostic test of a Nernstian behaviour is 70 mV for $Ni(mnt)_2^{2-}$ and 76 mV for $Pt(mnt)_2^{2-}$ at 30 mV/sec. These values are greater than the steady state value of 59 mV in aqueous solution at 25°C. The increase of 10 to 16 mV is not regarded as significant and could be due to the nature of the

electrolytic solution or a very small and insignificant uncompensated resistance in the cell. It is usually difficult to fully compensate cell resistances of non aqueous solutions even with positive feed back circuitry. In view of this, the small shift in peak potentials with scan rate cannot be considered as conclusive indication of irreversibility. The other factors such as equality in peak currents and linearity in Figures 3-4(b) and 3-6(b) should therefore be emphasized as indication of reversibility. Matsuda and Ayabe (62,63) showed that the shape of the voltammetric peak is a function of a dimensionless parameter Λ which is defined as

$$\Lambda = k_o/D^{1/2}(nF/RT)^{1/2}v^{1/2} \qquad (13)$$

where k_o is the standard heterogeneous rate constant for the electron transfer. For a reversible process they suggested a value greater than 10 for Λ and chose to use 15. From the diffusion coefficients of 1.49×10^{-5} and 1.40×10^{-5} cm^2 sec^{-1} for $Ni(mnt)_2^{2-}$ and $Pt(mnt)_2^{2-}$ respectively and the value of 15 for Λ, k_o for the Nickel complex was 6.26×10^{-2} cm/sec and k_o for the Platinum complex was 6.07×10^{-2} cm/sec at 30 mV/sec scan rate.

The behaviour of the Nickel and Platinum complexes at the SnO_2 electrode are different from that seen at the Pt electrode. Figures 3-5(a) and 3-7(a) show the peak

potential, E_p depends on scan rate but the ratio of the anodic and cathodic peak irrespective of scan rate is unity. Figures 3-5(b) and 3-7(b) show that the linearity predicted from the equation 9 is only obeyed at low scan rates. Deviation from linearity is seen at about 50 to 60 mV/sec. From the linear part of the curves at low speeds a "diffusion" constant of 2.06×10^{-6} cm^2sec^{-1} was obtained for $Ni(mnt)_2^{2-}$ and 5.22×10^{-6} cm^2sec^{-1} for $Pt(mnt)_2^{2-}$. These values are smaller than those obtained at Pt electrode (Table 3-5). The equality between the anodic and cathodic peaks for the particular scan rate inferred that the product of the electrode reaction was quantitatively converted to the initial reactant in the back sweep. The electrode process then cannot be complicated since both redox species are stable and appears to be readily available for reacting at the electrode.

The potential distribution at the semiconductor/electrolyte interface is different from that of a metal electrode. A potential drop does not only occur across the double layer but across the space charge layer below the surface. The measured potential versus a reference is then the sum of the potentials across the space charge and the double layers. Varying the potentials as in linear sweep voltammetry by applying an external voltage leads to variation of the band bending as in Figure 3-8 and variation in potential across the space charge layer.

This causes changes in the concentrations of holes and electrons which does not reside on the surface of the semiconductor, as it would in a metal, but in the space charge layer below the surface. The potential across the double layer remains essentially unchanged, it being insensitive to changes in the external potential. The variation in the potential distribution in the space charge layer region and the differential capacitance follow those for the double layer formed in a solution/metal electrode interface. The behaviour of the SnO_2 electrode in the linear sweep experiment is therefore similar to that of a Pt electrode where a significant charging current is flowing. The high resistance of 50 ohms of the SnO_2 electrodes along with the potential distribution at the interface under continuous variation in applied potential can account for the deviation from linearity in Figures 3-6(b) and 3-7(b), and the shift in the peak potentials with scan rate.

The resistance of the electrolyte solution cannot have significant effect on the scan rate behaviour since the solution is identical to that used with the Pt electrode. The cell resistance was calculated from the equation 14 below.

$$\psi = [(nF/RT)nFA(\sqrt{nFD/RT})^{1/2}CR_u)]^{-1} \qquad (14)$$

where R_u is the uncompensated cell resistance, ψ is a

dimensionless rate parameter obtained from peak separation values (63). Table 3-6 shows the variation of cell resistance with ψ and diffusion coefficient. The peak separations in Table 3-6 were chosen since they are the values obtained in the voltammograms; 72 mV at Pt electrode while the others were obtained at an SnO_2 electrode for the $Ni(mnt)_2^{2-}/Ni(mnt)_2^{1-}$ reaction. The diffusion coefficients of 1.49×10^{-5} and 2.06×10^{-6} cm^2 sec^{-1} were also those obtained at Pt and SnO_2 electrodes respectively for the same complexes. In table 3-6 the peak separations of 155 and 202 mV were used with the diffusion coefficient, 1.49×10^{-5} cm^2sec^{-1} obtained at Pt electrode to demonstrate the increase in cell resistance due to the SnO_2 electrode. Under identical conditions a diffusing species can only have a single diffusion constant. Pt electrodes are well characterized, frequently used stable electrodes for electrochemical kinetic studies. The diffusion coefficient for the Pt electrode used in this work is in agreement with conventional diffusion coefficient values and can be regarded as the true value for the diffusion for the $M(mnt)_2^{n-}$ species. Since the diffusion coefficient values at Pt eletrode are larger than those at SnO_2 electrode, it can be concluded that diffusion is not the limiting factor in the SnO_2 electrode process but the electron transfer steps. The number extracted from the i_p vs $v^{1/2}$ plot in Figures 3-5(b) and 3-7(b) as diffusion coefficients at the

SnO_2 electrode can then be regarded as a parameter associated with the heterogeneous electron transfer.

The variation of the peak potentials with scan rate, the equality of the anodic and cathodic wave regardless of scan rate and the large values of peak separations in indicative of a quasi-reversible reaction with electron transfer kinetic limitation. Using the Matsuda and Ayabe zone proposition (62,63), the rate constant for the quasi reversible process was calculated from the equation

$$k_o = Dv^{1/2} \qquad (15)$$

The value of D, the diffusion coefficient was taken as 1.49 x 10^{-5} cm^2/sec^{-1} and at scan speed of 10 mV/sec, k_o was calculated as 1.49 x 10^{-6} cm/sec. At 60 Mv/sec k_o is 3.65 x 10^{-6} cm/sec. A maximum scan rate of 60 mV/sec was used with equation 15 because deviation from linearity in the i_p vs $v^{1/2}$ plot was observed at this scan rate. These values are of the same magnitude as the "diffusion coefficient" obtained at SnO_2 electrode in the $i—v^{1/2}$ slopes.

Potential step chronoamperometric experiments were carried out to more closely examine the diffusional behaviour. The $i—t^{-1/2}$ plots for the $Ni(mnt)_2^{2-}$ complex in Figure 3-9 at Pt electrode and Figure 3-10 at SnO_2 electrode are also representative of $Pt(mnt)_2^{2-}$ complex. These plots indicate whether the electrode reaction is

governed by a semi-infinite diffusion process. The diffusion coefficient obtained from these plots for the complexes at the two electrodes are collected in Table 3-5.

The values of diffusion constants at both Pt and SnO_2 electrodes are very close and they are comparable to those obtained from the i_p vs $v^{1/2}$ slopes at Pt electrode. The Cotrell diffusion coefficient at SnO_2 electrode however do not agree with those obtained at the same electrode from the i_p vs $v^{1/2}$ plot. In the chronoamperometric technique the reaction appears to be diffusion limited irrespective to the nature of the electrode. This is in contrast to the observation under linear sweep experiments where the reaction at SnO_2 electrode is electron transfer limited.

The difference in the interfacial kinetics between the two techniques is probably a result of the potential distribution and relative energy levels at the SnO_2/ solution interface. As mentioned earlier, in linear sweep experiments, continuous variation in applied potential leads to a steady variation of band bending and in the potential across the space charge layer. This process has a relaxation time. Therefore, if there is an initial electrostatic equilibrium at the semiconductor/solution interface this equilibrium would have to undergo a constant change dictated by the changing potential. For potential sweep sufficiently fast the equilibrium may not be established. The lack of equillibrium is probably due

to the transport resistance in the space charge region under a fast potential sweep. Under a fast sweep concentration of charge in the space charge layer is continuously changing. This lack of equilibrium is probably the cause of slow heterogeneous electron transfer under the potential sweep experiment. In a chronoamperometric experiment the applied potential is constant, band bending is held constant and does not undergo a continuous steady change, the charging current will decay with a time constant R_uC_s (R_u is uncompensated cell resistance, C_s is space charge capacitance) and a static equilibrium is established. This equilibrium as well as the relative energy levels at the SnO_2/solution interface does not change since potential is constant. The concentration of charge in the space charge layer is also constant after equilibrium and always available at the semiconductor surface to react. Since the charge is readily available at the surface the current will be dependent on mass transport which in this situation is diffusion controlled.

$3a_u$, $4b_{3g}$	L(π^*)	L(π^*)	-8.70eV
$3b_{1g}$	(xy)	σ^*	-9.10eV
$4a_g$	(x^2-y^2)	π^*	-11.55eV
$4b_{2g}$	(xz)	π^*	-11.76eV
$3b_{1u}$, $2b_{2u}$, $2b_{3u}$, $2b_{1g}$	L(π)	L(π)	-12.40eV
$3b_{3g}$	(xy)	d	-12.60eV
$3a_g$	z^2	d	-13.00eV
$3b_{2g}$	xz	d	-13.26eV
$2a_g$	x^2-y^2	d	-13.60eV
$1b_{2u}$, $1b_{3u}$	L(σ)	L(σ)	-13.60eV

Figure 3-1 Simple MO Scheme of $Ni(mnt)_2^{-2}$ as prepared by Gray et al. (8).

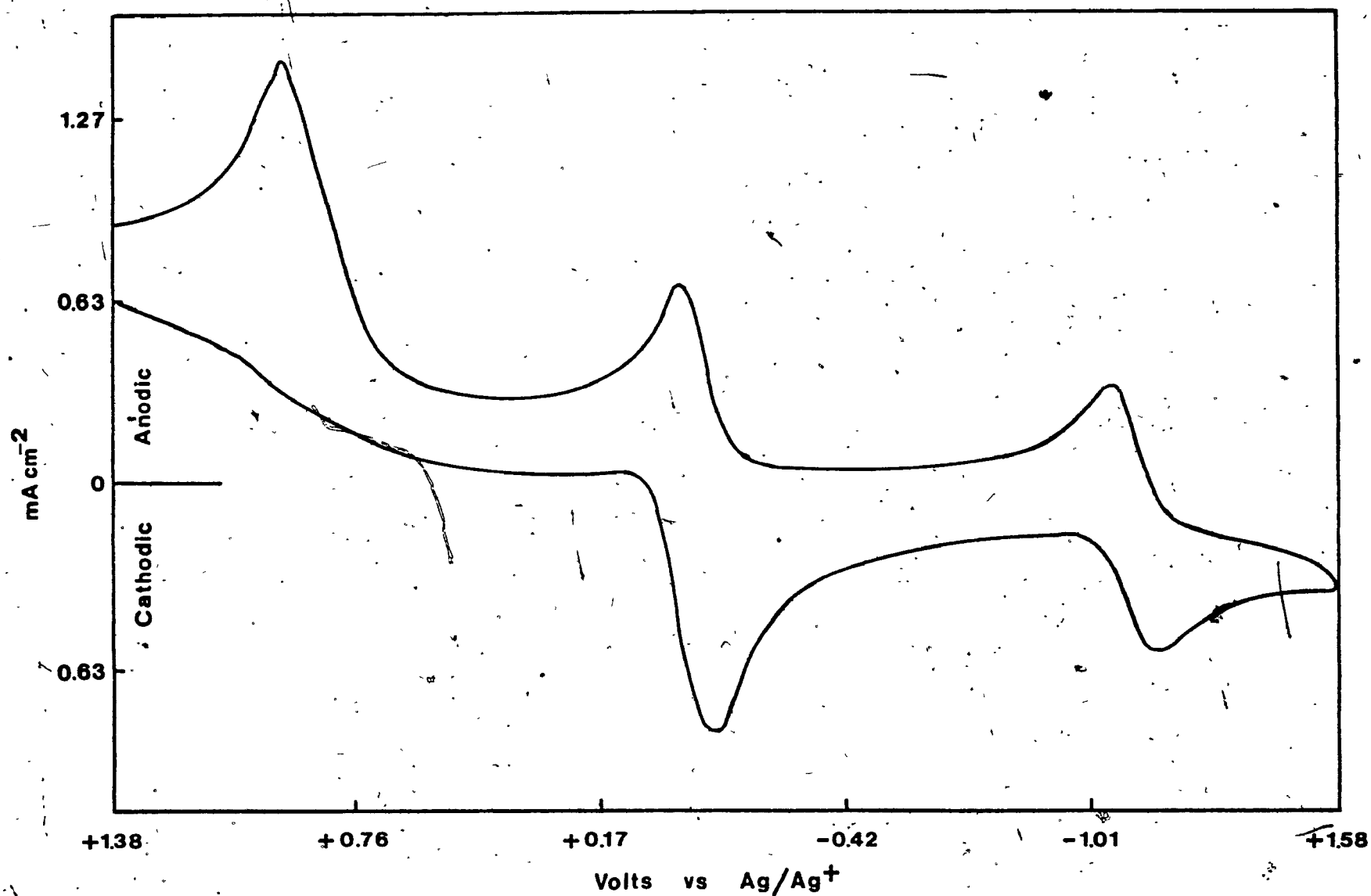

Figure 3-2. Cyclic voltammogram of $Cu(mnt)_2^{2-}$ at Pt electrode in 0.1 M $NaClO_4/CH_3CN$ solution. Scan rate 100 mV/sec.

Figure 3-3. Cyclic voltammogram of $Cu(mnt)_2^{2-}$ at SnO_2 electrode in 0.1 M $NaClO_4/CH_3CN$ solution. Scan rate 100 mV/sec.


0.13
0.06
0
0.06
0.13
mA cm⁻²
Anodic
Cathodic
1.35
+0.76
+0.17
-0.43
-1.02
-1.61
Volts vs Ag/Ag⁺

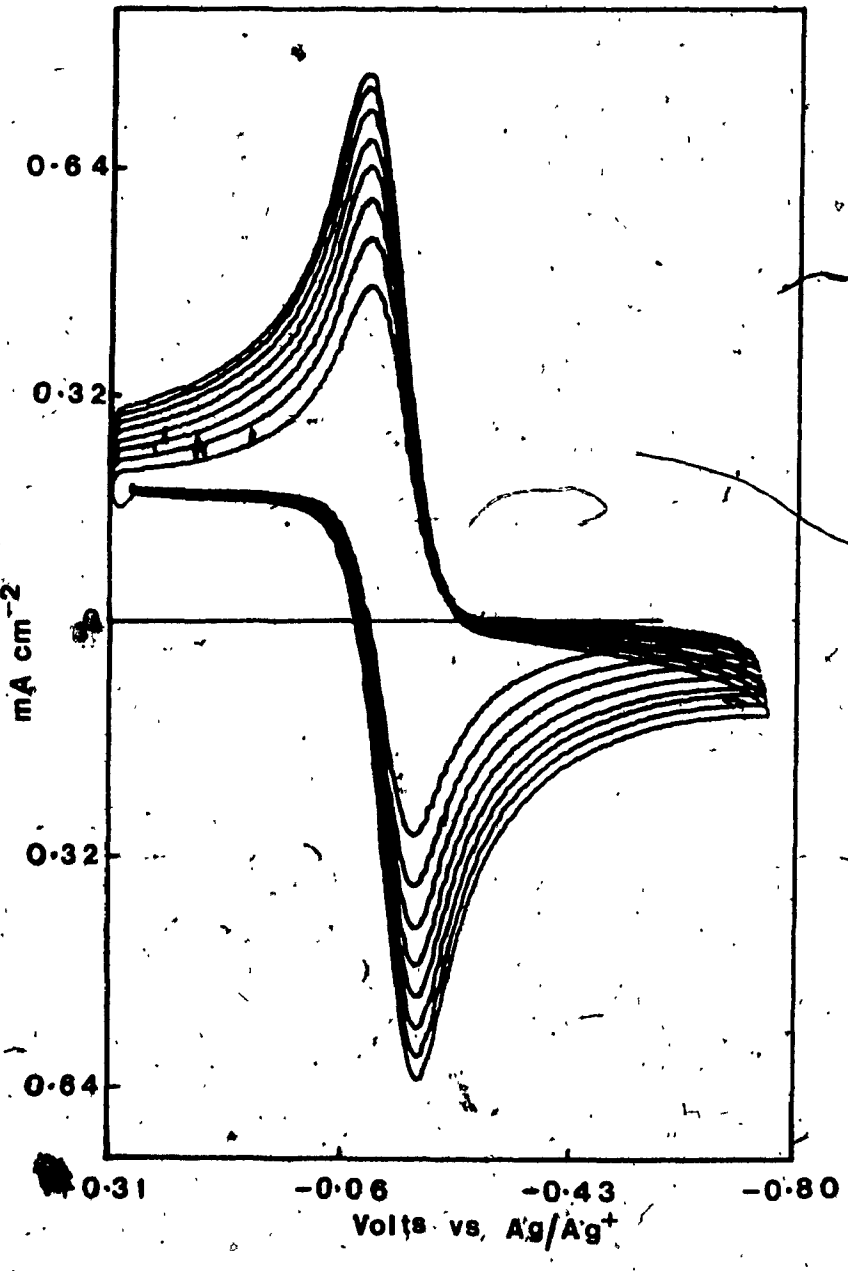

Figure 3-4 (a). Cyclic voltammograms at various scan rates; 30 to 100 mV sec at Pt electrode for 2.0×10^{-3} M $Ni(mnt)_2^{2-}$ in 0.1 M $NaClO_4/CH_3CN$ electrolyte.

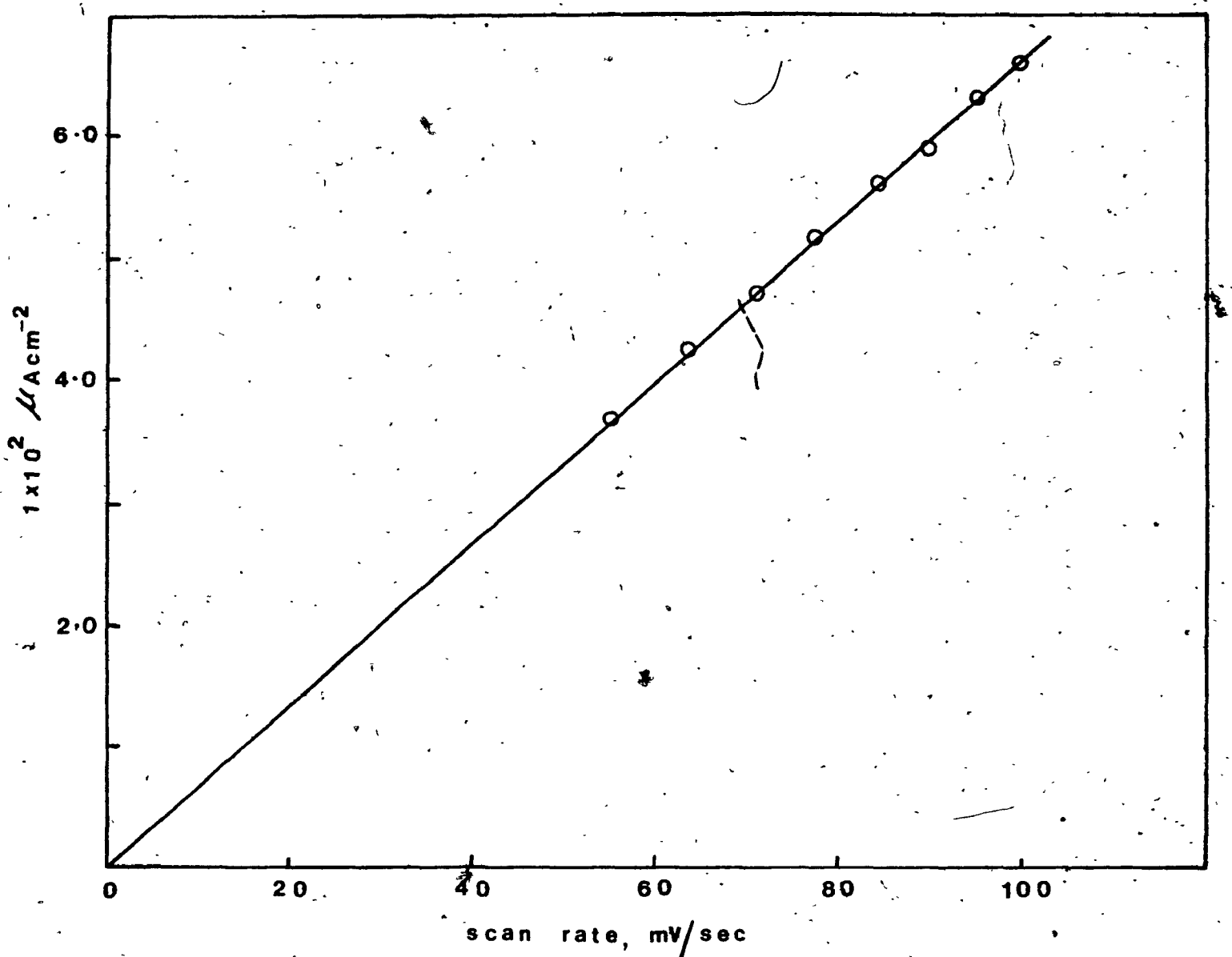

Figure 3–4 (b). Plot of cathodic peak current vs $v^{\frac{1}{2}}$ (v = scan rate) at Pt electrode for 2.0×10^{-3} M $Ni(mnt)^{2-}$ in 0.1 M $NaClO_4/CH_3CN$ electrolyte.

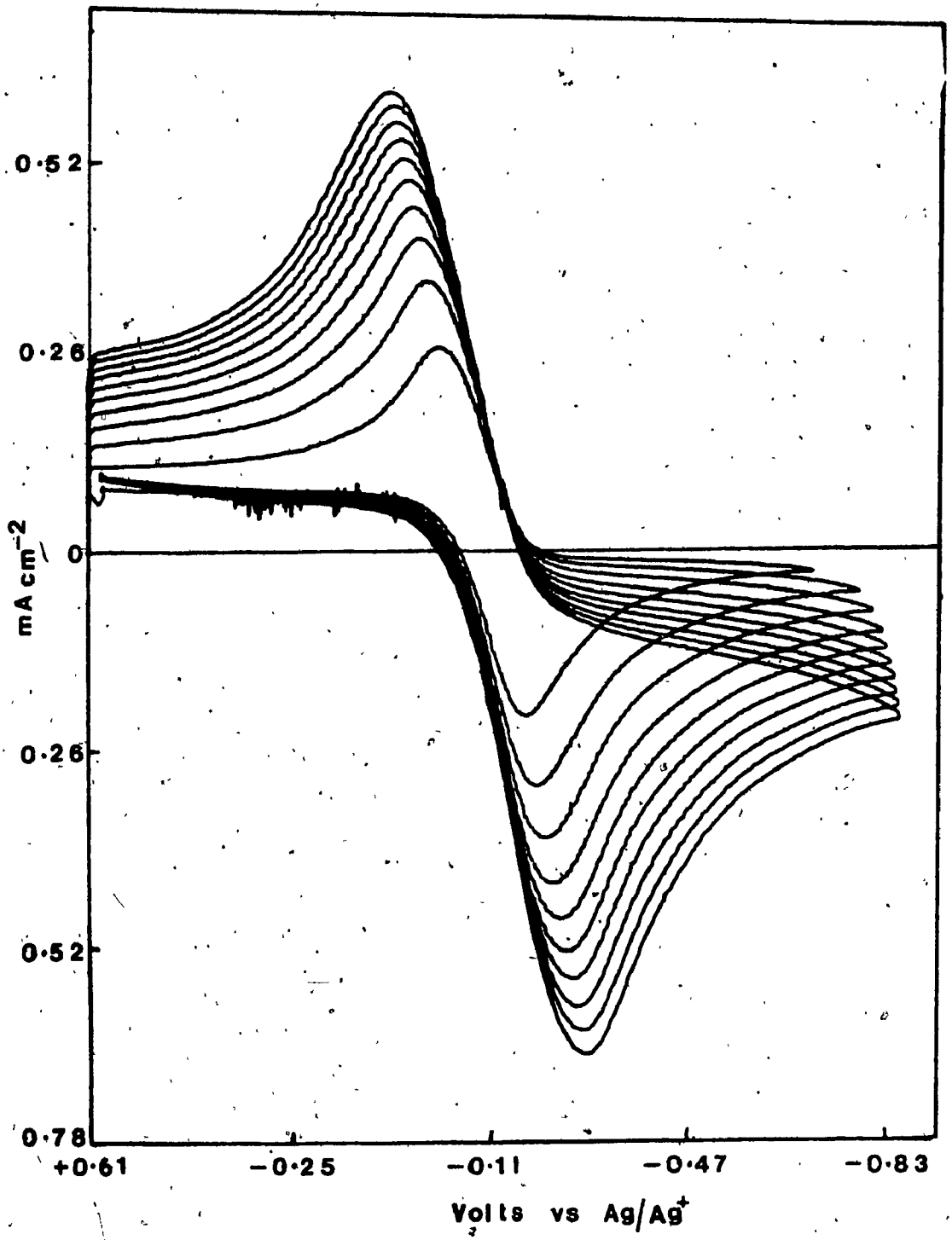

Figure 3-5 (a). Cyclic voltammgrams at various scan rates; 10 to 100 mV/sec at SnO_2 electrode for 2.0×10^{-3} M $Ni(mnt)_2^{2-}$ in 0.1 M $NaClO_4/CH_3CN$ electrolyte.

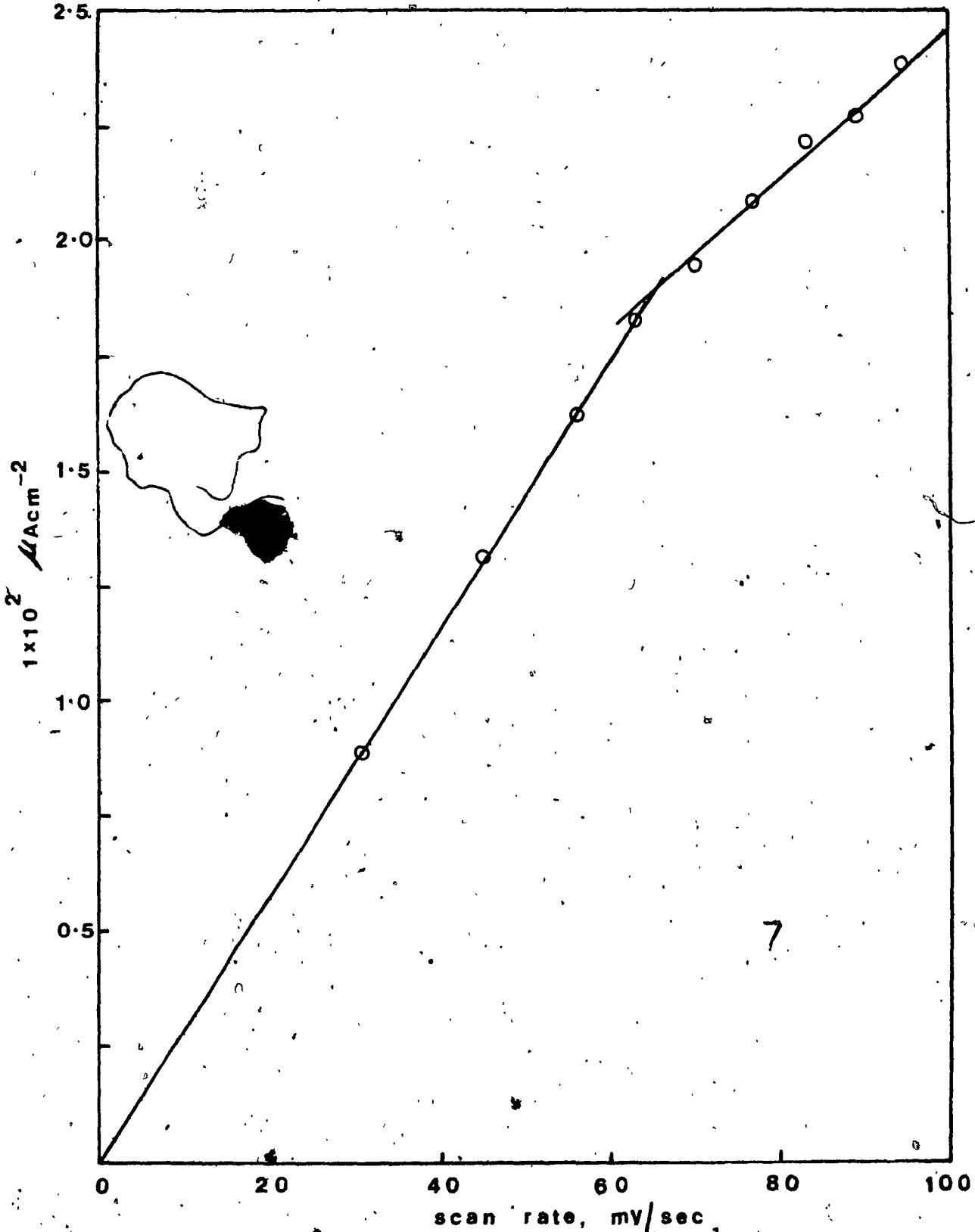

Figure 3-5 (b). Plot of cathodic peak current vs $v^{\frac{1}{2}}$ (v = scan rate) at SnO_2 electrode for 2.0×10^{-3} M $Ni(mnt)_2^{2-}$ in 0.1 M $NaClO_4/CH_3CN$ electrolyte.

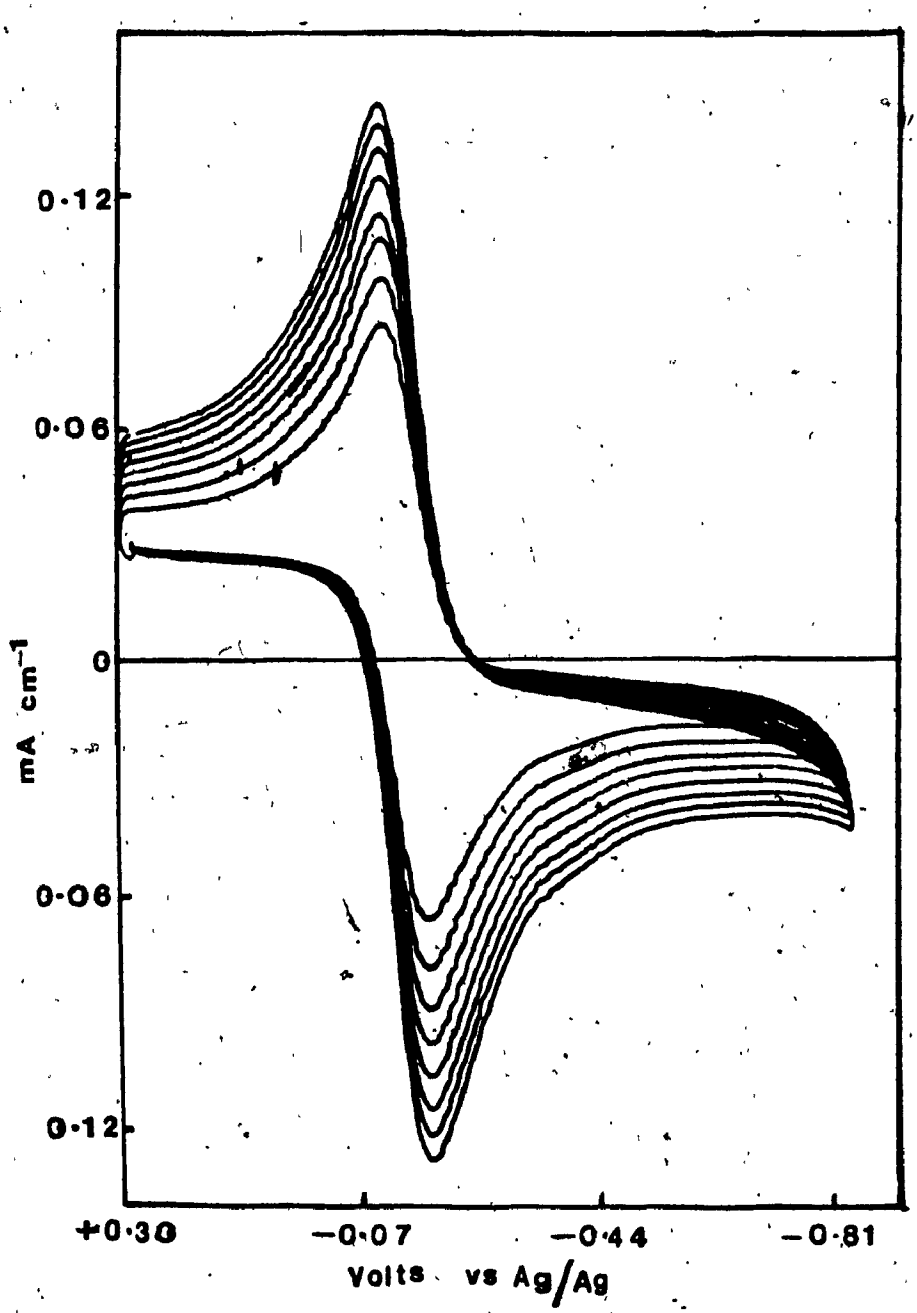

Figure 3-6 (a). Cyclic voltammograms at various scan rates; 30 to 100 mV/sec at Pt electrode for 8.58×10^{-4} M $Pt(mnt)_2^{2-}$ in 0.1 M $NaClO_4$/ CH_3CN electrolyte.

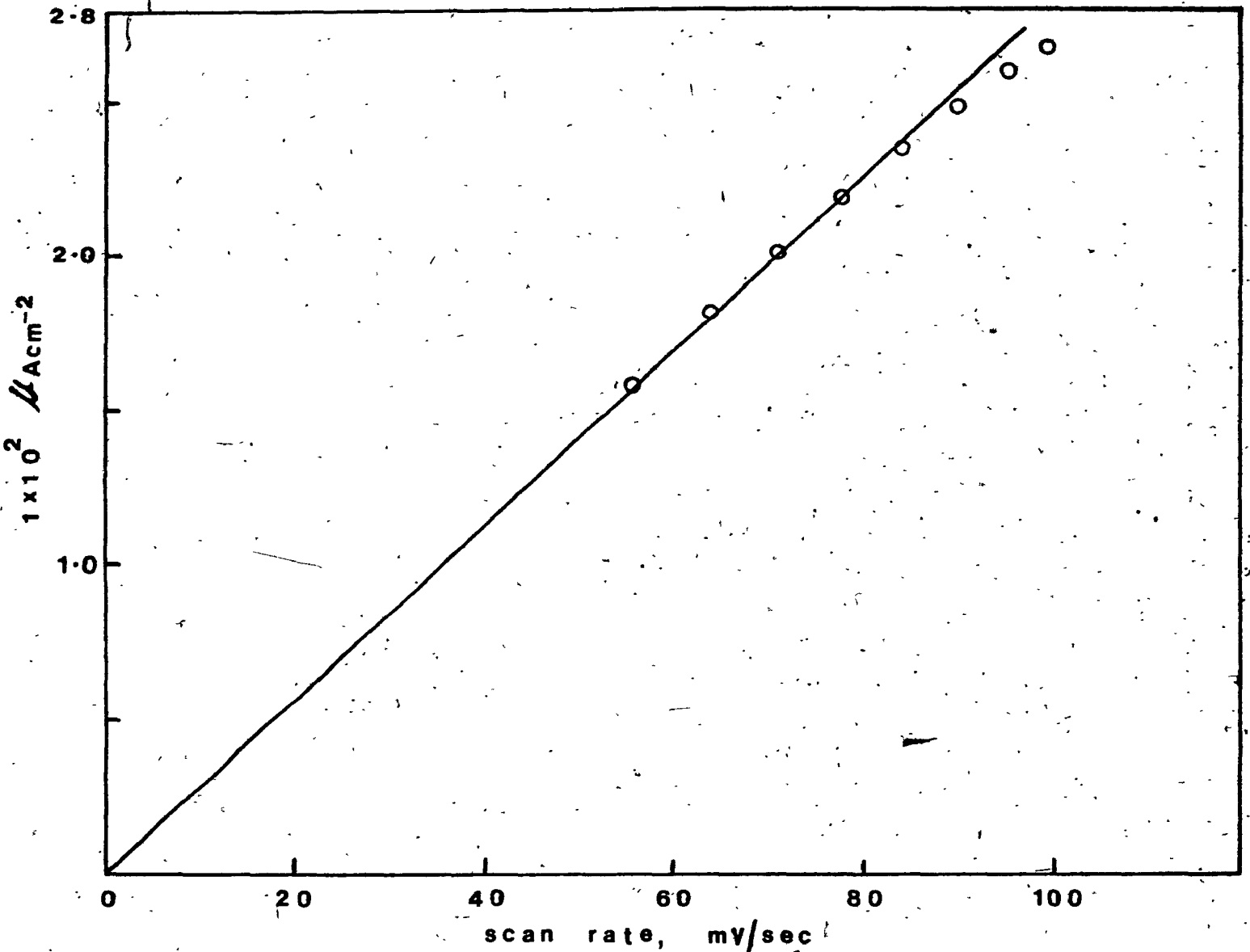

Figure 3-6 (b). Plot of cathodic peak current vs $v^{\frac{1}{2}}$ (v = scan rate) at Pt electrode for 8.58×10^{-4} M $Pt(mnt)_2^{2-}$ in 0.1 M $NaClO_4/CH_3CN$ electrolyte.

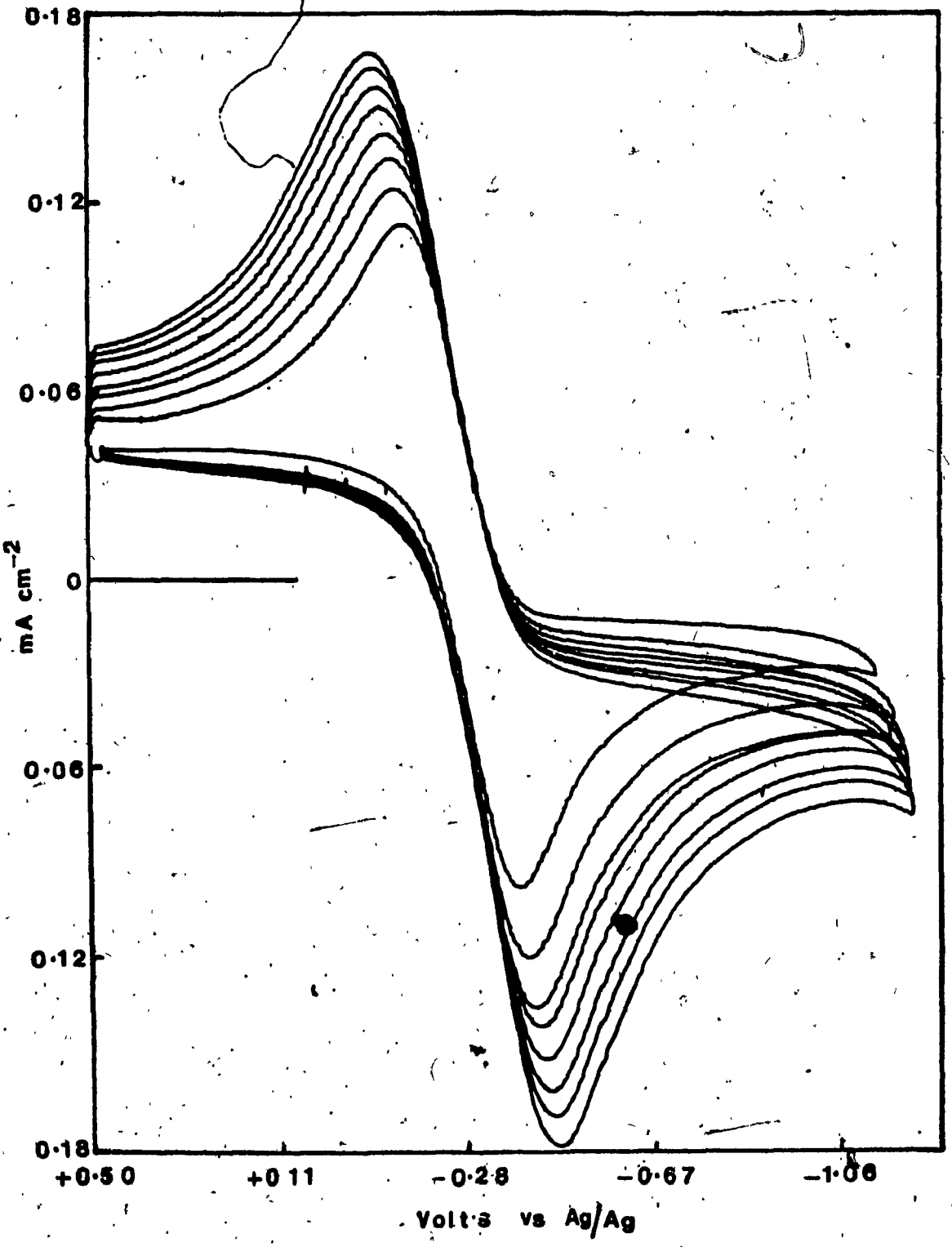

Figure 3-7 (a). Cyclic voltammograms at various scan rates; 30 to 100 mV/sec at SnO_2 electrode for 1 x 10^{-3} M $Pt(mnt)_2^{2-}$ in 0.1 M $NaClO_4/CH_3CN$ electrolyte.

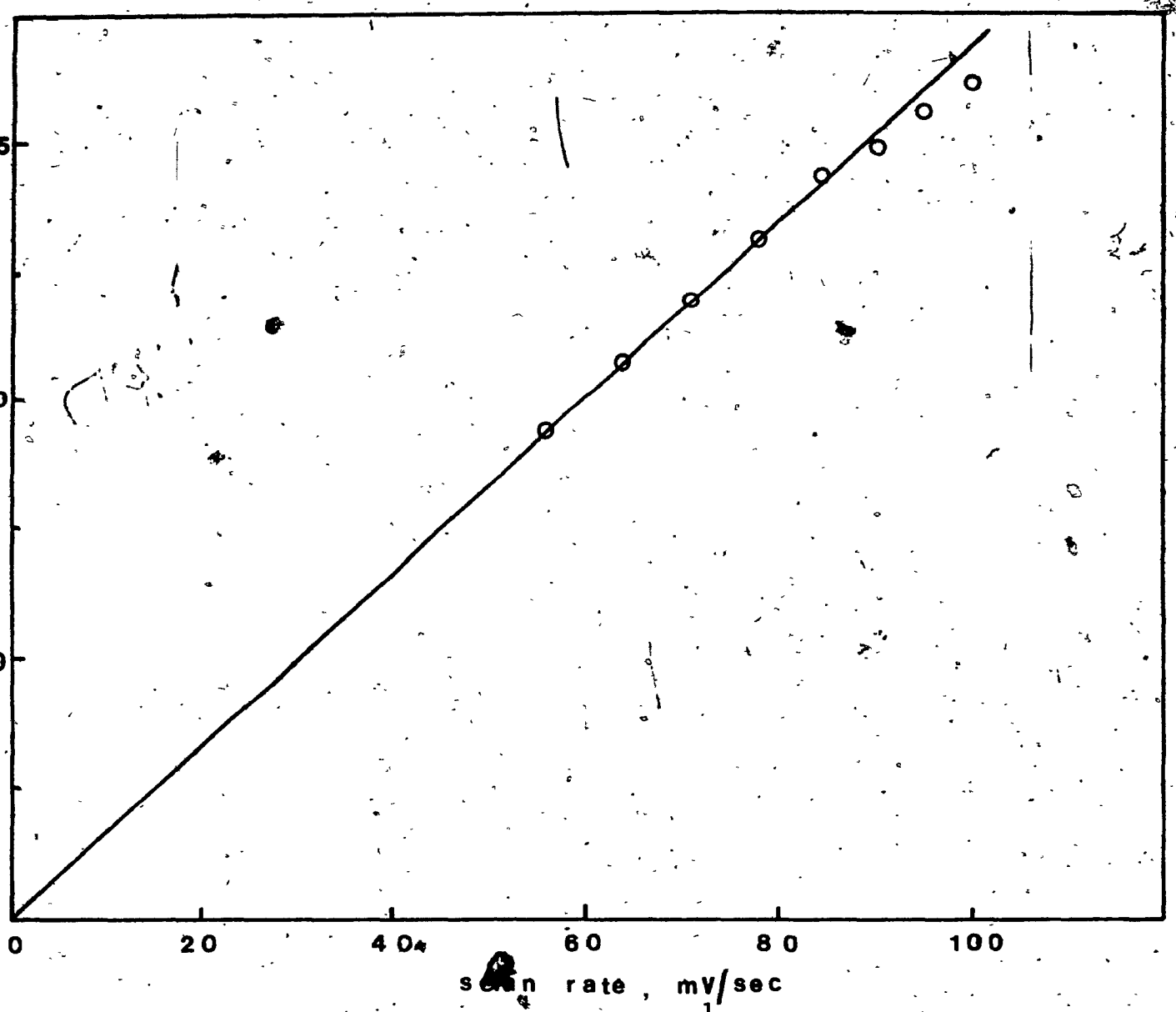

Figure 3-7 (b). Plot of cathodic peak current vs $v^{\frac{1}{2}}$ (v = scan rate) at SnO_2 electrode for 1×10^{-3} M $Pt(mnt)_2^{2-}$ in 0.1 M $NaClO_4/CH_3CN$ electrolyte.

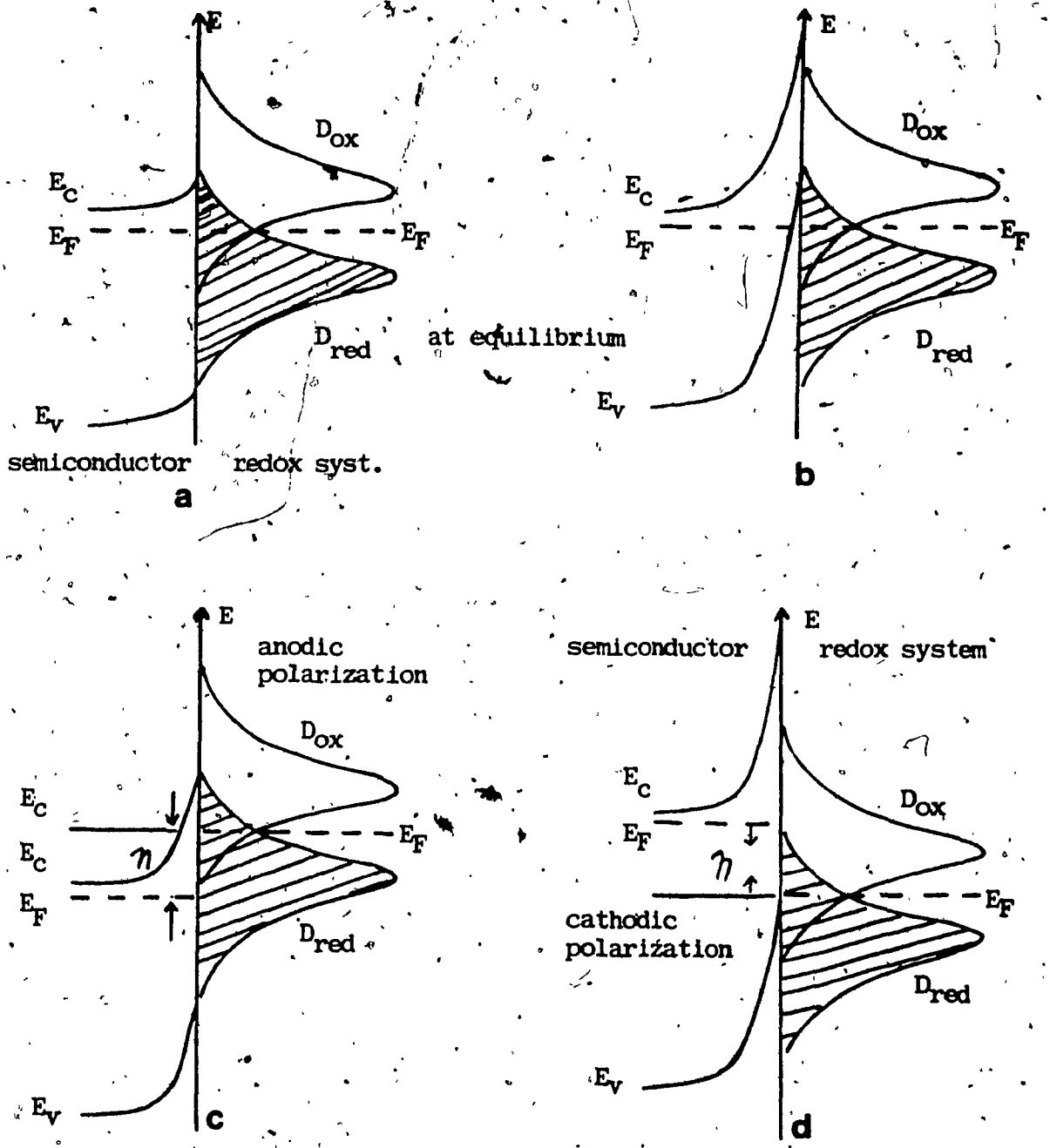

Figure 3-8. Relative position of energy levels at both sides of the semiconductor/electrolyte interface.
(a) and (b) at equilibrium; (c) at anodic polarization; (d) at cathodic polarization.
D_{red}, density of occupied states; D_{ox}, density of empty states; E_C, conduction band; E_V, valence band; E_F, Fermi level; η, external applied potential.

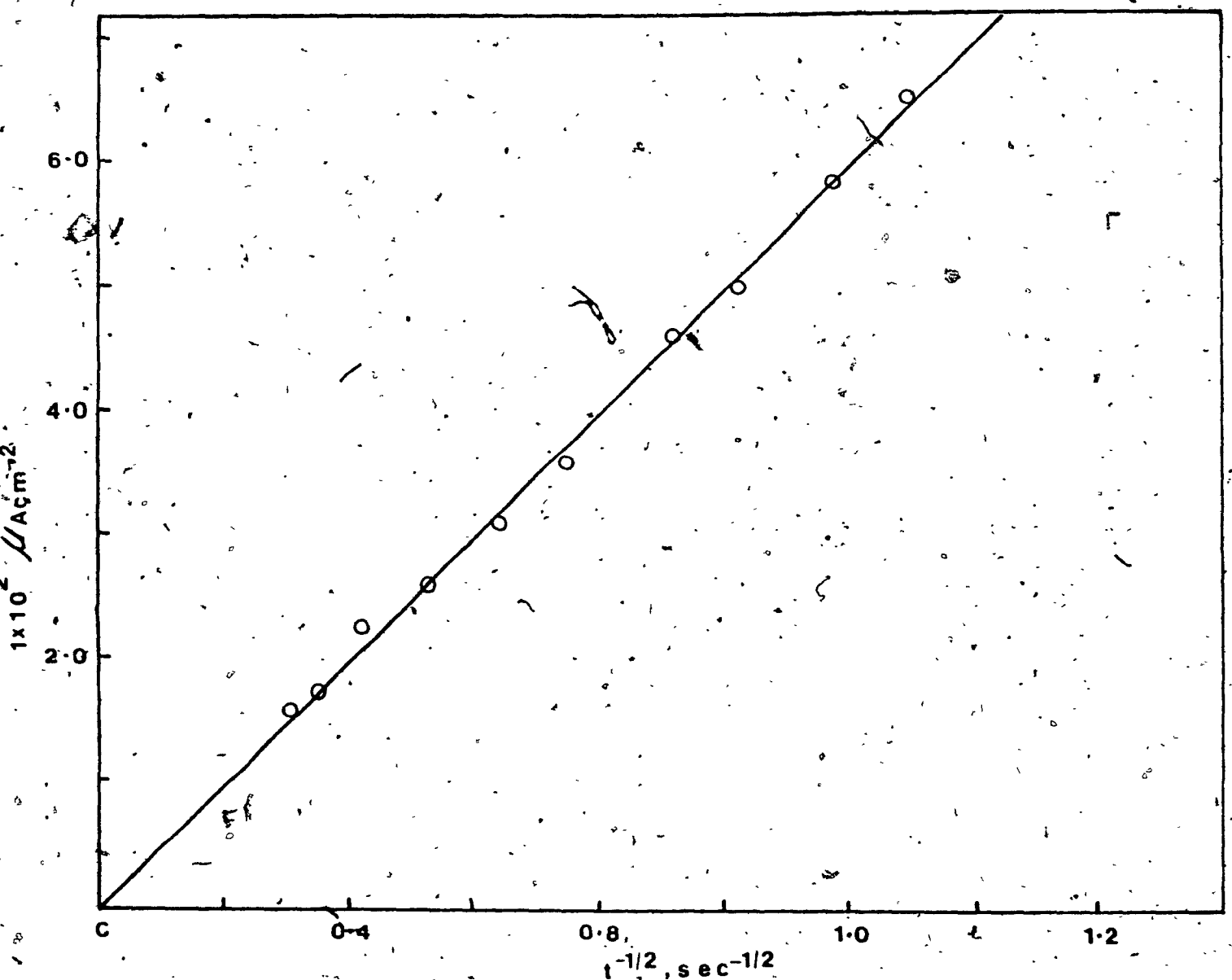

Figure 3-9. Plot of anodic current vs $t^{-\frac{1}{2}}$ (t = time) at Pt electrode for 2.0×10^{-3} M $Ni(mnt)_2^{2-}$ in 0.1 M $NaClO_4/CH_3CN$ electrolyte. Potential was stepped from -0.20 to +0.20 V vs Ag/Ag^+.

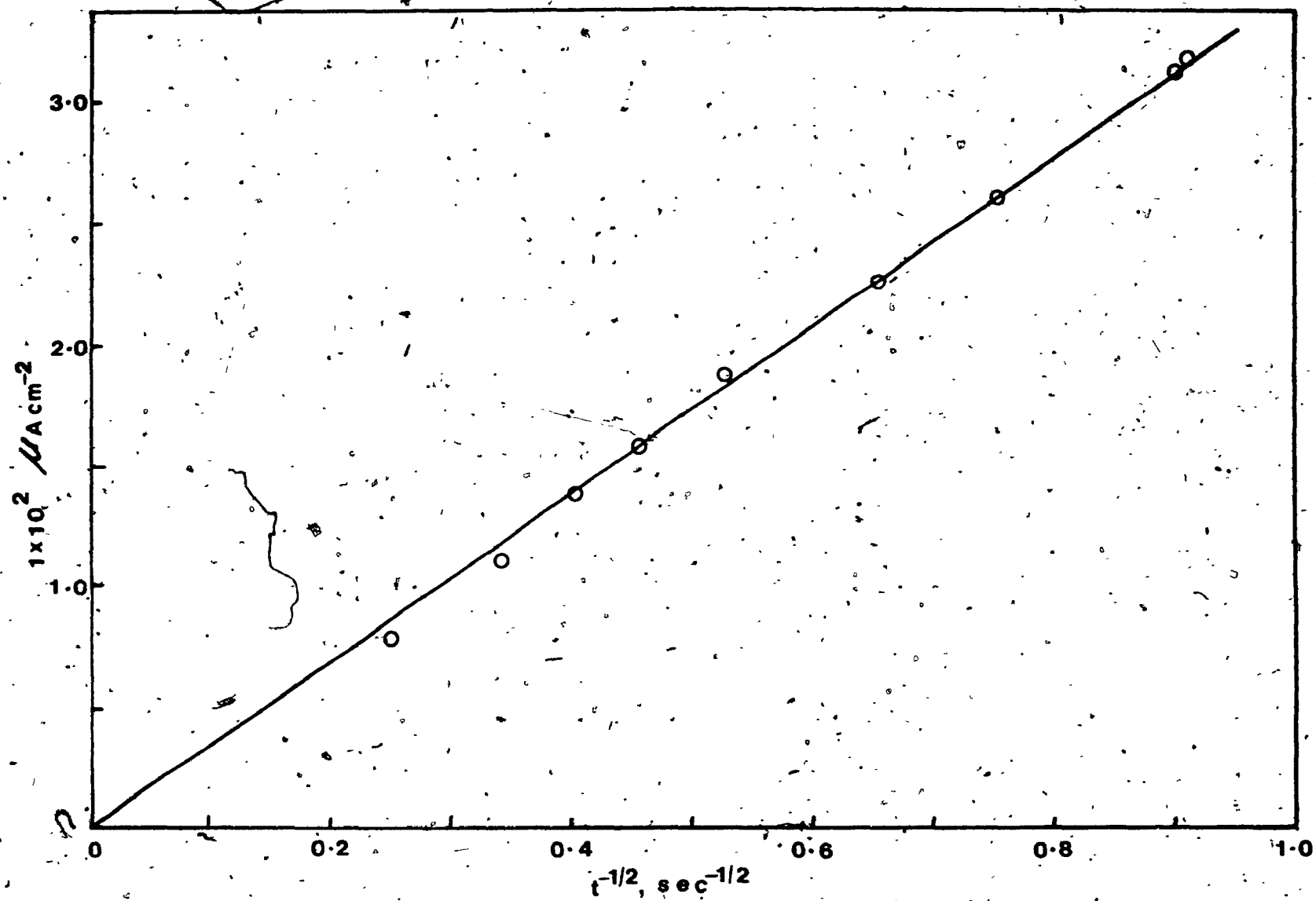

Figure 3-10, Plot of anodic current vs $t^{-\frac{1}{2}}$ (t = time) at SnO_2 electrode for 2.0×10^{-3} M $Ni(mnt)_2^{2-}$ in 0.1 M $NaClO_4/CH_3CN$ electrolyte. Potential was stepped from -0.40 to +0.20 V vs Ag/Ag^+.

TABLE 3-1

Electronic Absorption Spectra of $M(mnt)_2^{n-}$ complexes in Acetonitrile Solutions

Complex	$\bar{\nu}$ cm^{-1}	Wavelength nm	ε $dm^3 M^{-1} cm^{-1}$	Assignments a	Assignments b
$Ni(mnt)_2^{-2}$	11,690	855	30	$^1A_g \rightarrow {}^1B_{1g}(x^2-y^2 \rightarrow xy)$	c
	17,500	571	570	$^1A_g \rightarrow {}^1B_{3g}(xz \rightarrow xy)$	$^1A_g \rightarrow {}^1B_{2u}$, $^1B_{3u}(n=s \rightarrow M)$
	19,250	519	1,250	$^1A_g \rightarrow {}^1A_u(x^2-y^2 \rightarrow L\pi^*)$	$^1Ag \rightarrow {}^1B_{1g}(n=S \rightarrow M)$
	21,000	476	3,800	$^1A_g \rightarrow {}^1B_{2u}(xz \rightarrow L\pi^*)$	c
	26,400	378	6,600	$^1A_g \rightarrow {}^1B_{2u}, {}^1B_{3u}(L\pi \rightarrow xy)$	c
	31,300	319	30,000	$^1A_g \rightarrow {}^1B_{2u}(L\pi \rightarrow L\pi^*)$	c
	37,000	270	50,000	$^1A_g \rightarrow {}^1B_{2u}, {}^1B_{3u}(L\sigma \rightarrow xy)$	
$Pd(mnt)_2^{-2}$	15,700	637	64	$^1A_g \rightarrow {}^1B_{1g}(x^2-y^2 \rightarrow xy)$	$^1A_g \rightarrow {}^1B_{1g}(x^2-y^2 \rightarrow xy)$
	22,700	440	5,700	$^1A_g \rightarrow {}^1B_{2u}, {}^1B_{3u}(L\pi - xy)$	$^1A_g \rightarrow {}^1B_{1g}(n = s \rightarrow M)$
	25,800	387	2,840	$^1A_g \rightarrow {}^1A_u(x^2-y^2 \rightarrow L\pi^*)$	c
	30,800	325	20,200	$^1A_g \rightarrow {}^1B_{2u}(L\pi \rightarrow L\pi^*)$	c
	33,900	295	47,000	$^1A_g \rightarrow {}^1B_{2u}, {}^1B_{3u}(L\sigma \rightarrow xy)$	c
	37,800	266	45,000	c	c
	42,800	234	42,800	c	c
$Pt(mnt)_2^{-2}$	14,410	694	49	$^1A_g \rightarrow {}^3B_{1g}(x^2-y^2 \rightarrow xy)$	c
	15,650	639	56	$^1A_g \rightarrow {}^3B_{3g}(xz \rightarrow xy)$	c
	18,500	540	1,220	$^1A_g \rightarrow {}^1B_{1g}(x^2-y^2 \rightarrow xy)$	
				$^1A_g \rightarrow {}^1A_u(x^2-y^2 \rightarrow L\pi^*)$	c

Table 3-1 continued

Complex	$\bar{\nu}$ cm^{-1}	Wavelength nm[d]	ε $dm^3\ M^{-1}\ cm^{-1}$	Assignments a	Assignments b
$Pt(mnt)_2^{-2}$	21,100	473	3,470	$^1A_g \rightarrow {}^1B_{2u}(xz \rightarrow L\pi^*)$	c
	29,700	336	15,600	$^1A_g \rightarrow {}^1B_{2u}(L\pi \rightarrow L\pi^*)$	c
	32,300	309	13,400	$^1A_g \rightarrow {}^1B_{2u}, {}^1B_{3u}(L\pi \rightarrow L\pi^*)$	c
	38,500	260	17,000	c	c
	43,800	228	43,500	$^1A_g \rightarrow {}^1B_{2u}; {}^1B_{3u}(L\sigma \rightarrow xy)$	c
$Ni(mnt)_2^{-1}$	8,330	1,200[d]	329[d]	$4b_{2g} \rightarrow 4a_g(xz \rightarrow x^2-y^2)$	$4a_g \rightarrow 3b_{2g}(M \rightarrow \pi)$
	11,790	848[d]	8,000[d]	$3b_{1u}, 2b_{2u}, 2b_{3u} \rightarrow 4a_g(L\pi \rightarrow x^2-y^2)$	$2b_{3g} \rightarrow 3b_{2g}(M \rightarrow \pi)$
	16,666	600	668[f]	$3b_{3g} \rightarrow 4a_g$	$2b_{1u} \rightarrow 3b_{1g}(\pi \rightarrow M)$
	18,349	545[e]	798[f]	$3a_g \rightarrow 4a_g$	$n{=}S: \rightarrow 3b_{2g}(N{=}S: \rightarrow \pi)$
					$n{=}S: \rightarrow 3b_{1g}(n{=}S: \rightarrow \pi)$
	20,964	477	2,490[f]	$1b_{2u}, 1b_{3u} \rightarrow 4a_g(L\sigma \rightarrow x^2-y^2)$	$3b_{2g} \rightarrow 2a_u(\pi \rightarrow \pi)$
					$2a_g \rightarrow 3b_{1g}(n{=}S: \rightarrow M)$
	27,027	370[e]	7,114[f]	$2b_{3u}, 2b_{2u} \rightarrow 3b_{1g}(L\pi \rightarrow xy)$	$2b_{3g} \rightarrow 2a_u(M \rightarrow \pi)$
	32,154	311	33,873[f]	$3b_{1u} \rightarrow 4b_{3g}(L\pi \rightarrow L\pi^*)$	$1a_u \rightarrow 3b_{2g}(\pi \rightarrow \pi)$
	37,037	270	34,017[f]	$1b_{3u}, 1b_{2u} \rightarrow 3b_{1g}(L\sigma \rightarrow xy)$	c
	43,478	230	19,093[f]	c	c

[a] Given in Ref. 8

[b] Given in Ref. 15

c Not assigned

[d] Calculated from frequency (cm^{-1}) values of Refs. 8,9

[e] Shoulder

[f] Peak maximum and ε values are from this study.

TABLE 3-2

Electronic Absorption Spectra of $M(mnt)_2^{-n}$ Complexes in Acetonitrile Solutions

Complex	$\bar{\nu}$ / cm^{-1}	Wavelength / nm	ε / $dm^3\ M^{-1}\ cm^{-1}$	Assignments
$Cu(mnt)_2^{-2}$	8,299	1205[a]	94	$4a_g \rightarrow 3b_{1g}(x^2-y^2 \rightarrow xy)$
	21,097	474	4,537	$4b_{2g} \rightarrow 3a_u(xz \rightarrow L\pi^*)$
	23,256	430[b]	4,764	$2b_{3u}, 2b_{2u} \rightarrow 3b_{1g}(L\pi \rightarrow xy)$
	27,174	368	10,549	$3b_{3g}, 3a_g \rightarrow 3b_{1g}$
	28,736	348	10,501	$3b_{2g}, 2a_g \rightarrow 3b_{1g}$
	31,546	317	15,670	$3b_{1u} \rightarrow 4b_{3g}(L\pi \rightarrow L\pi^*)$
	35,842	279	23,156	$1b_{3u}, 1b_{2u} \rightarrow 3b_{1g}(L\sigma \rightarrow xy)$
	44,053	227	20,000	...
$Cu(mnt)_2^{-1}$	6,400	1563[a]	337	$4a_g \rightarrow 3b_{1g}(x^2-y^2 \rightarrow xy)$
	13,000	769[a]	110	$4b_{2g} \rightarrow 3b_{1g}(xz \rightarrow xy)$
	19,531	512[b]	1,159	$4a_g \rightarrow 3a_u(x^2-y^2 \rightarrow L\pi^*)$
	25,773	388[c]	16,477	$2b_{3u}, 2b_{2u} \rightarrow 3b_{1g}(L\pi \rightarrow xy)$
	31,250	320	9,364	$3b_{1u} \rightarrow 4b_{3g}(L\pi \rightarrow L\pi^*)$
	35,211	284	20,566	$3b_{3g} \rightarrow 4b_{3g}, 3a_u$
	37,037	270	21,911	$1b_{2u}, 1b_{3u} \rightarrow 3b_{1g}(L\sigma \rightarrow xy)$

Table 3-2 continued

Complex	$\bar{\nu}$ / cm^{-1}	Wavelength / nm	ε / $dm^3\ M^{-1}\ cm^{-1}$	Assignments
$Pd(mnt)_2^{-1}$	15,314	653	472	$4a_g \rightarrow 3b_{1g}(x^2-y^2 \rightarrow xy)$
	16,950	590[b]	580	$3b_{3g} \rightarrow 4a_g$
	18,382	544[b]	951	$3a_g \rightarrow 4a_g$
	20,704	483[c]	2,672	$4b_{2g} \rightarrow 3a_u, 4b_{3g}(xz \rightarrow L\pi^*)$
	28,818	347[b]	5,491	$3b_{1u} \rightarrow 4b_{3g}(L\pi \rightarrow L\pi^*)$
	36,496	274	45,000	$1b_{3u}, 1b_{2u} \rightarrow 3b_{1g}(L\sigma \rightarrow xy)$
	43,478	230	22,000	...
	9,000	1111[a]	13,800	$3b_{1u}, 2b_{2u}, 2b_{3u} \rightarrow 4a_g(L\pi \rightarrow x^2-y^2)$

[a] Calculated from frequency (cm^{-1}) values of Ref. 1,9,55.

[b] Shoulder

[c] Broad band probably contains two electronic transitions.

TABLE 3-3

Cyclic Voltammetry Parameters for Reversible or Quasi Reversible Redox Reactions of Metal Complexes of MNT at Pt Electrode in MeCN

	$E_{\frac{1}{2}}$[a]				ΔE_p		
Complex	+1 ⇌ 0	0 ⇌ -1	-1 ⇌ -2	-2 ⇌ -3	0/-1	-1/-2	-2/-3
$Ni(mnt)_2^n$	-	+0.82[b]	-0.14	-1.94[c]	-	0.13	-
$Cu(mnt)_2^n$	-	+0.96	-0.03	-1.07	-	0.06	0.10
$Pd(mnt)_2^n$	-	+0.48	+0.04	-2.17[c]	0.38	0.16	-
$Pt(mnt)_2^n$	-	+0.72	-0.16	-2.68[d]	0.07	0.07	-
	-	-	-	-2.97[d]	-	-	-

[a] Potential measured halfway between peak anodic and cathodic potentials at a scan rate of 100mV/sec.

[b] Irreversible in CH_3CN at Pt, the potential mentioned is the peak anodic potential.

[c] Value taken from Ref. 4,10 corrected to Ag/Ag^+ redox couple.

[d] See Ref. 4,10 for explanation.

TABLE 3-4

Cyclic Voltammetry Parameters for Reversible or Quasi Reversible Redox Reactions of Metal Complexes of MNT at SnO_2 Electrode in MeCN

Complex	$E_{\frac{1}{2}}$[a] 0 ⇌ -1	$E_{\frac{1}{2}}$[a] -1 ⇌ -2	$E_{\frac{1}{2}}$[a] -2 ⇌ -3	ΔE_p 0/-1	ΔE_p -1/-2	ΔE_p -2/-3
$Ni(mnt)_2^n$	a	-0.11	b	-	0.45	b
$Cu(mnt)_2^n$	b	+0.015	-1.17V	-	0.40	0.49
$Pd(mnt)_2^n$	+1.11[c]	-0.02	b	0.90	1.03	b
$Pt(mnt)_2^n$	+1.13	-0.13	b	-	0.39	b

[a] See corresponding footnotes to Table 3-3.

[b] See text for explanation

[c] Irreversible in CH_2CN at SnO_2 electrode, the potential mentioned is Epa, anodic the peak potential

Table 3-5

Apparent Diffusion Coefficient and Heterogeneous Rate Constant for $M(mnt)_2^{2-}$; M = Ni and Pt

Electrode	Complex	Scan Rate	Ag/AgCl[a] $E_p^b{}_{cat}$	Ag/AgCl[a] $E_p^c{}_{anod}$	ΔE_p^d	D_{app}^e	D_{app}^f	k_o^g
		mV/sec	Volts	Volts	mV	$cm^2\ sec^{-1}$	$cm^2\ sec^{-1}$	$cm\ sec^{-1}$
Pt	$Ni(mnt)_2^{2-}$	30	+0.08	+0.150	70	1.49×10^{-5}	2.11×10^{-5}	6.26×10^{-2}
		100	+0.07	+0.160	92			
Pt	$Pt(mnt)_2^{2-}$	30	+0.145	+0.145	76	1.40×10^{-5}	2.19×10^{-5}	6.07×10^{-2}[h]
		100	+0.053	+0.159	107			
SnO_2	$Ni(mnt)_2^{2-}$	30	+0.246	+0.159	162	2.06×10^{-6}	2.03×10^{-5}	1.49×10^{-6}[h]
		100	+0.234	+0.293	379			
SnO_2	$Pt(mnt)_2^{2-}$	30	-0.020	+0.219	239	5.22×10^{-6}	1.0×10^{-5}	1.49×10^{-6}
		100	-0.09	+0.291	381			

[a] Data obtained by adding +0.27 V to the E_p value measured in CH_3CN vs Ag/Ag^+

[b] Cathodic peak potential

[c] Anodic peak potential

[d] Anodic and cathodic peak separation

[e] Apparent diffusion coefficient obtained obtained from i_p vs $v^{\frac{1}{2}}$ plot.

[f] Apparent diffusion coefficient obtained from i vs $t^{-\frac{1}{2}}$ plot.

[g] Heterogeneous rate constant.

[h] Obtained from equation 15 with 10 mV/sec.

Table 3-6

Variation of Cell Resistance with Ψ and Diffusion Coefficients.

ΔE mV	Ψ	$D \times 10^5$ $cm^2\ sec^{-1}$	R_u Ohms	Scan Rate mV/sec
72	2	1.49	38	30
155	0.23	1.49	54	10
202	0.10	1.49	88	20
155	0.23	0.21	146	10
202	0.10	0.21	238	20

Chapter 4

Results II

4.1 Homogeneous Photoelectrochemistry in CH_3CN at SnO_2 electrodes

4.1.1 Photoelectrochemistry of $Ni(mnt)_2^{2-}$

The photoelectrochemical behaviour of $Ni(mnt)_2^{2-}$ in deaerated spectrograde acetonitrile was followed by measuring the photocurrent generated at the working SnO_2 electrode under irradiation with an argon ion laser. Figure 4-1 shows the dependence of photocurrents as a function of potential and complex concentration at constant laser intensity of 200 mW. The photowave between -0.5 V and -1.0 V is in the region where background currents are small enough to allow accurate measurements. The height of the wave is approximately linearly related to concentration (Figure 4-2). It is also proportional to approximately the first power of the Laser intensity as per Figure 4-3.

4.1.2 Photoelectrochemistry of $Ni(mnt)_2^{1-}$

The Photoelectrochemistry behaviour of this complex was investigated at potential +0.10 V to +0.70 V where the complex is stable. Potentials more cathodic than +0.1 V results in reduction while potentials anodic +0.7 V results in oxidation of the complex. Within this small potential window an anodic photocurrent was detectable

upon irradiation with the argon ion laser. The dependence of Photocurrent on concentration and potential is given in Figure 4-4. The wave is not define because the limiting current is probably reached at above +0.7 V where background currents become large. At about +0.5 V adsorption of the complex on the electrode surface was noticeable at high concentrations.

4.1.3 Photoelectrochemistry of $Pd(mnt)_2^{n-}$

The homologs with Pd were investigated under the same conditions as the $Ni(mnt)_2^{2-}$ and $Ni(mnt)_2^{1-}$ respectively but no photocurrents were detected. The complex was found to be stable under irradiation as indicated by the absorption spectrum before and after irradiation.

4.1.4 Photoelectrochemistry of $Pt(mnt)_2^{2-}$

Unlike the $Pd(mnt)_2^{2-}$ the $Pt(mnt)_2^{2-}$ complex exhibited similar behaviour to that of the $Ni(mnt)_2^{2-}$. It was examined within the potential range of -0.3 to +1.0 V under 100 mW visible irradiation from a Xenon lamp. A water filter and a U.V. cut off filter were used to remove the unwanted irradiation. Photocurrent saturation appeared at about -0.7. There are also indications of a photocurrent concentration dependence. The dependence of photocurrent on potential at two levels of concentration is shown in Figure 4-5.

4.1.5 Photoelectrochemistry of $Cu(mnt)_2^{2-}$

Figure 4-6 shows the behaviour of $Cu(mnt)_2^{2-}$ upon irradiation with an argon ion laser at the SnO_2 electrode. No important photocurrents were found in the potential region where the 2- oxidation state of the complex exists but at potentials sufficiently cathodic for $Cu(mnt)_2^{3-}$ to be the important species at the electrode, anodic photocurrents arise. The photocurrents were found to be dependent linearly on the first power of the laser intensity and on concentration (Figure 4-7).

4.2 Quenching of Photocurrents.

The cathodic photocurrents of $Pt(mnt)_2^{2-}$ and $Ni(mnt)_2^{2-}$ as well as the anodic photocurrents of $Cu(mnt)_2^{3-}$ are at least partially quenched by oxygen. Figure 4-8 show the photoelectrochemical behaviour of the electrolyte solution saturated with oxygen as well as the electrolyte with different concentrations of $Ni(mnt)_2^{2-}$ and oxygen. Typically oxygen saturated currents are about 60 percent of those in deaerated, oxygen free, solutions.

The oxygen effect on the photocurrents of $Cu(mnt)_2^{3-}$ is given in Figure 4-6(b). This photocurrent was completely quenched. This may not be of direct significance for the $Cu(mnt)_2^{3-}$ excited state since oxygen may reoxidize the trianion itself but it seems significant in the other cases.

Pyridine was also found to quench the

photoelectrochemistry of $Ni(mnt)_2^{2-}$. Increasing the pyridine concentrations by the addition of various amounts of the quencher to a solution of $Ni(mnt)_2^{2-}$ resulted in a decrease of the photocurrent. Figure 4-9 shows the photoelectrochemistry of 4.0×10^{-3} M of $Ni(mnt)_2^{2-}$ in the presence of the various quantities of the quencher. The photocurrents observed were analyzed in using the Stern-Volmer equation:

$$i_o/i_q = k_q/k_{-1}\,[Py] \qquad (16)$$

where i_o and i_q are the photocurrents in the absence and in the presence of the quencher. A plot of i_o/i_q observed at -0.7 V as a function of the concentration of the quencher [Py] is shown in Figure 4-10. It is evident from both Figures 4-9 and 4-10 that there is appreciable quenching by the pyridine but at the high concentrations the quenching process does not give an accurate Stern-Volmer behaviour. Deviation from the Stern-Volmer relationship is especially pronounced at -0.6 V and at more anodic potentials where the limiting photocurrent of $Ni(mnt)_2^{2-}$ is not observed.

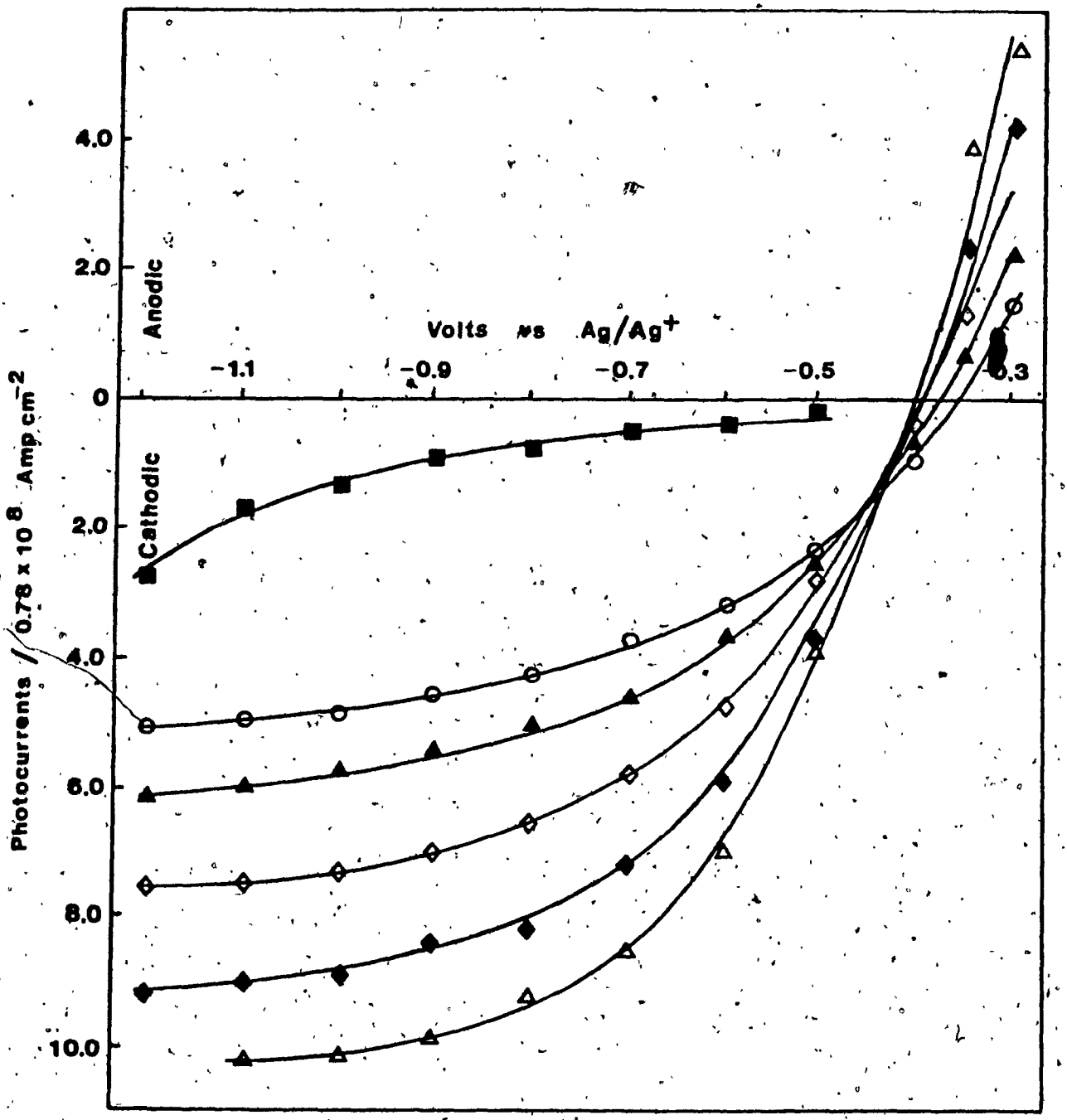

Figure 4-1. The dependence of photocurrents of $Ni(mnt)_2^{2-}$ on potential in 0.1 M $NaClO_4/CH_3CN$ electrolyte. Concentration of $Ni(mnt)_2^{2-}$: 0 M (■); 2×10^{-3} M (○); 4×10^{-3} M (▲); 6×10^{-3} M (◇); 8×10^{-3} M (◆) and 1×10^{-2} M (△). Irradiation Source: Argon ion Laser in multimode; 200 mW.

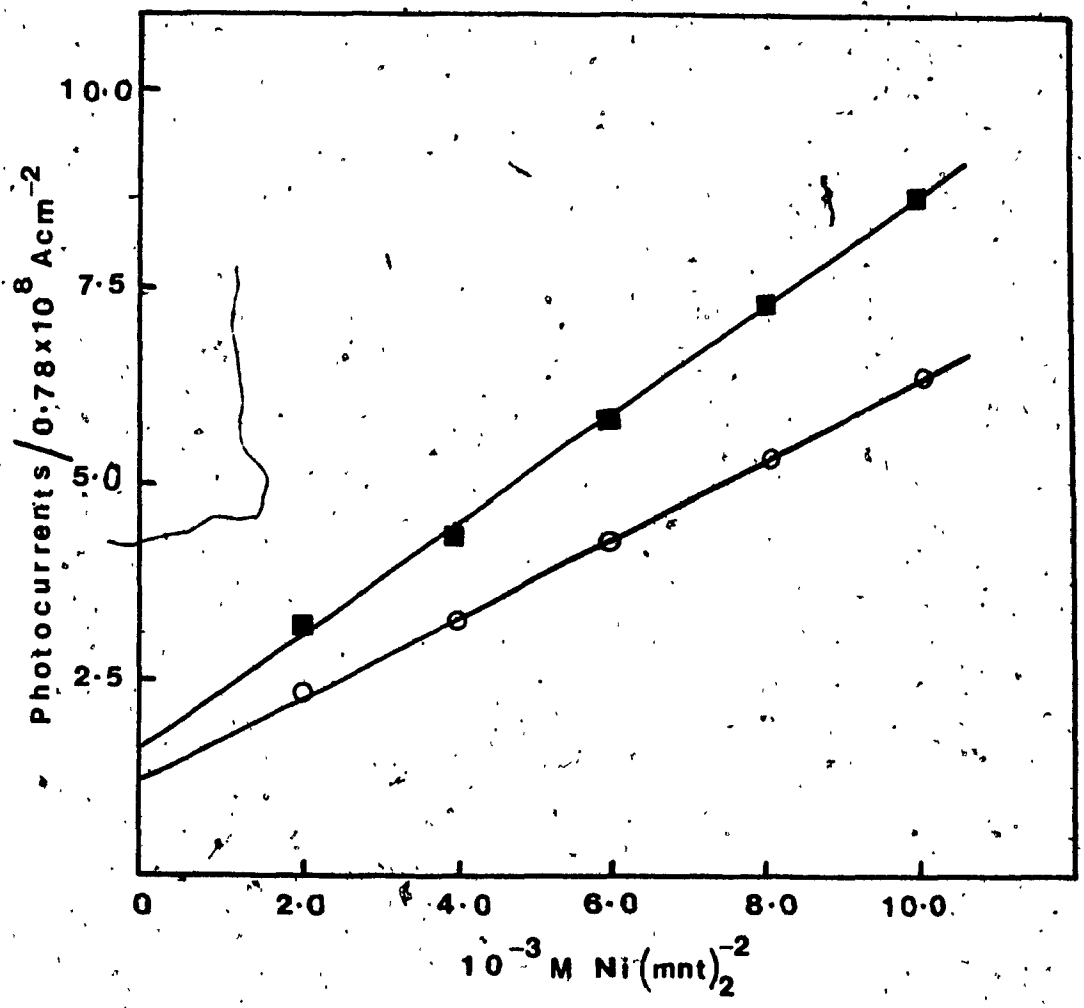

Figure 4-2. The dependence of cathodic photocurrents on concentration of $Ni(mnt)_2^{2-}$. Irradiation Source: Argon ion Laser in multimode; 200 mW; (■) -0.8 V; (○) -0.6 V.

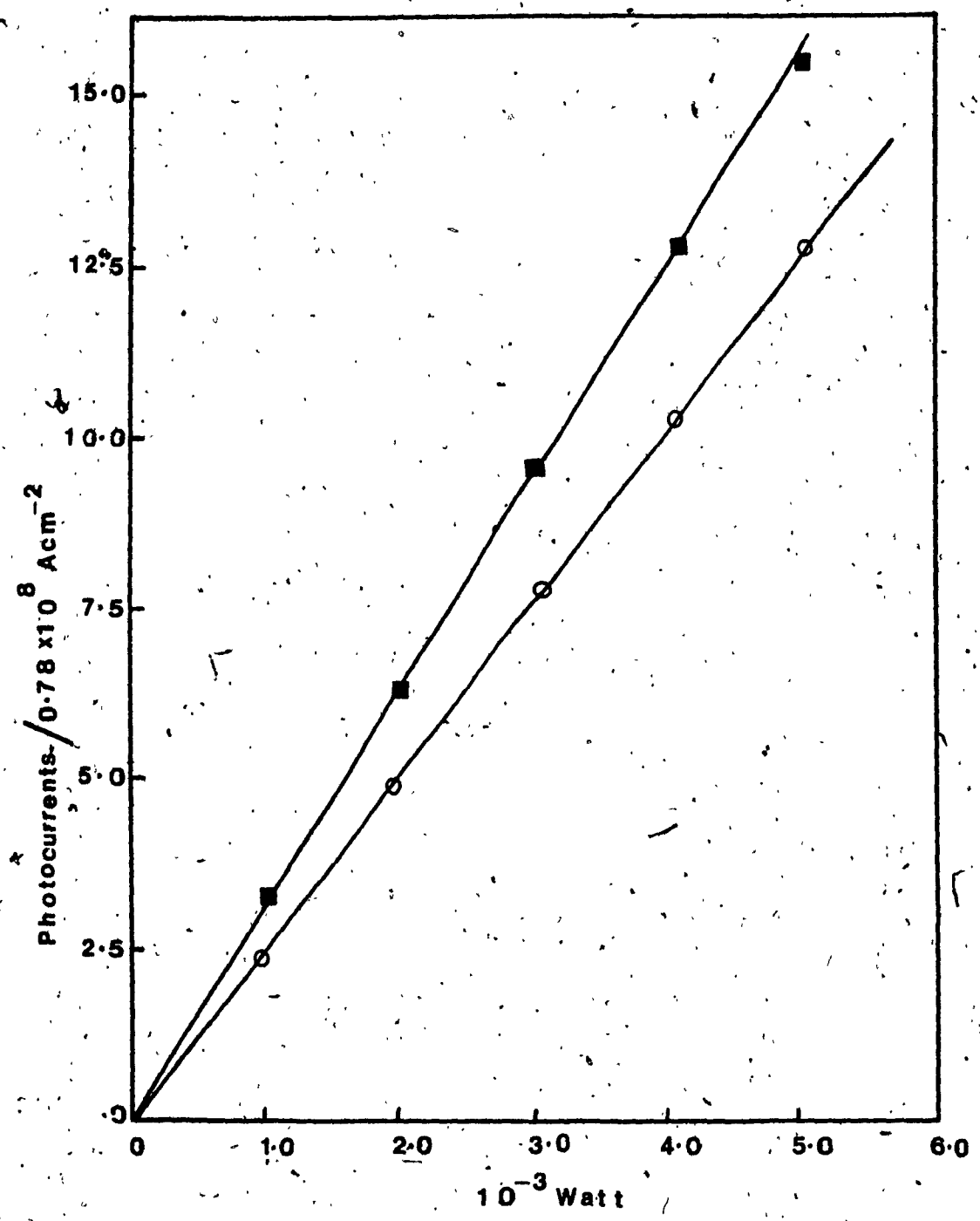

Figure 4-3. The dependence of cathodic photocurrents on the first power of laser intensity: (■) -0.8 V; (O) -0.6 V; concentration of $Ni(mnt)_2^{2-}$ 6 x 10^{-3} M.

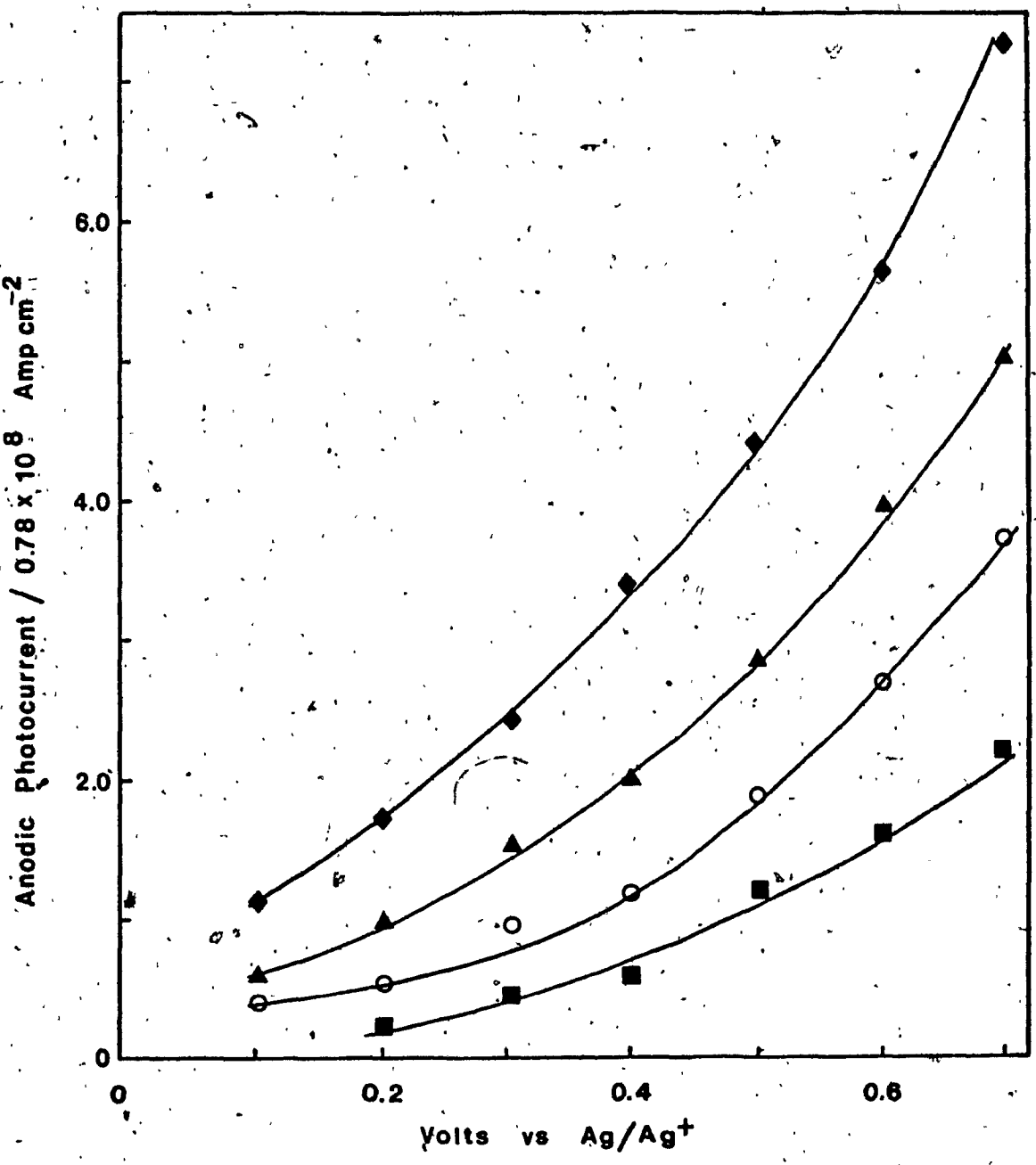

Figure 4–4. The dependence of photocurrents on potential and concentration of $Ni(mnt)_2^{1-}$ in 0.1 M $NaClO_4/CH_3CN$ electrolyte. $Ni(mnt)_2^{1-}$ concentration: 0 M (■); 2×10^{-3} M (○); 4×10^{-3} M (▲); and 8×10^{-3} M (◆). Irradiation Source: Argon ion Laser in multimode; 200 mW.

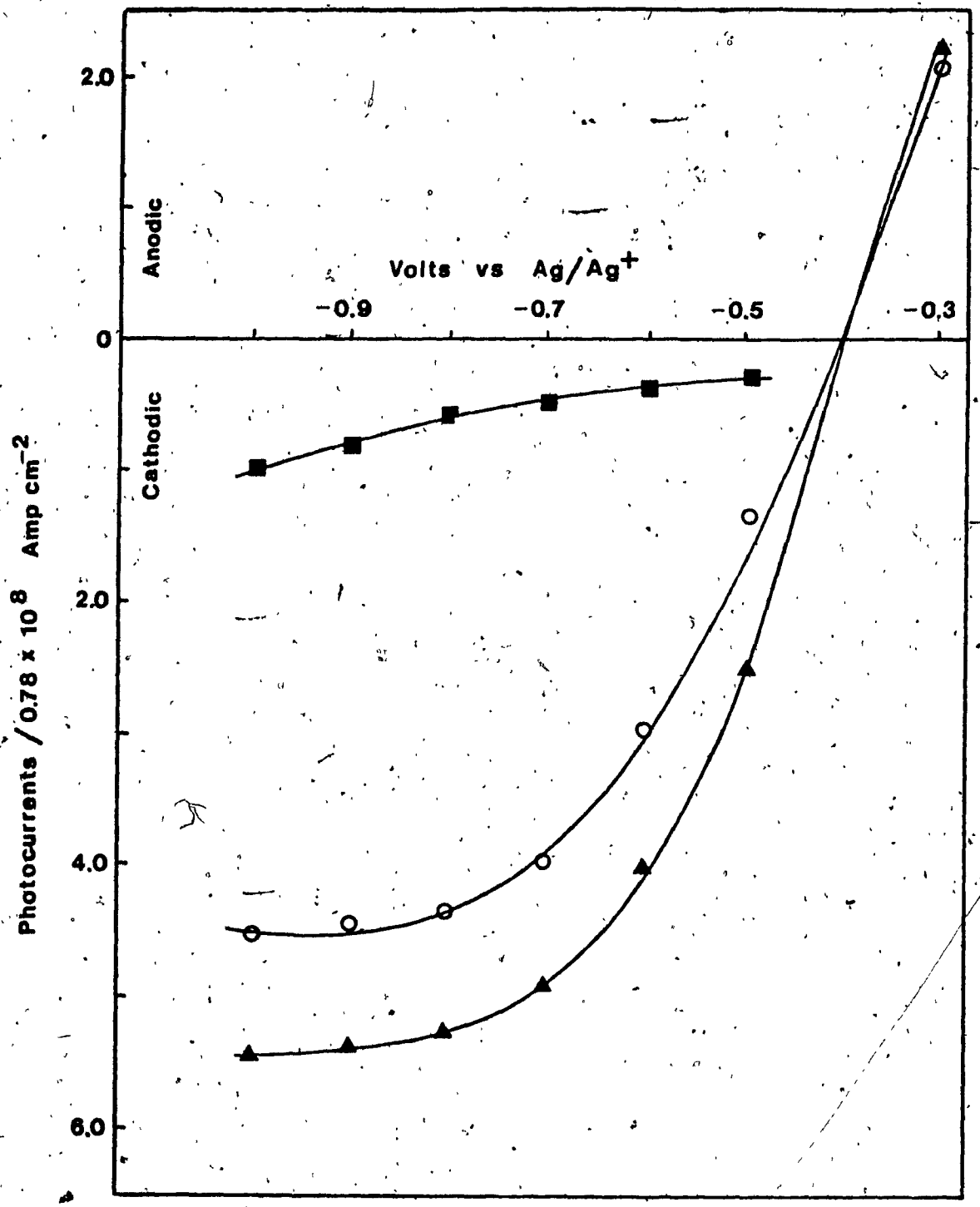

Figure 4-5. The dependence of Photocurrents on potential and concentration of $Pt(mnt)_2^{2-}$ in 0.1 M $NaClO_4/CH_3CN$ electrolyte. $Pt(mnt)_2^{2-}$ concentration: 0 M (■); 2×10^{-3} M (○); 4×10^{-3} M (▲). Irradiation Source: Xenon lamp with I.R. and U.V. cutoff filters; 100 mW.

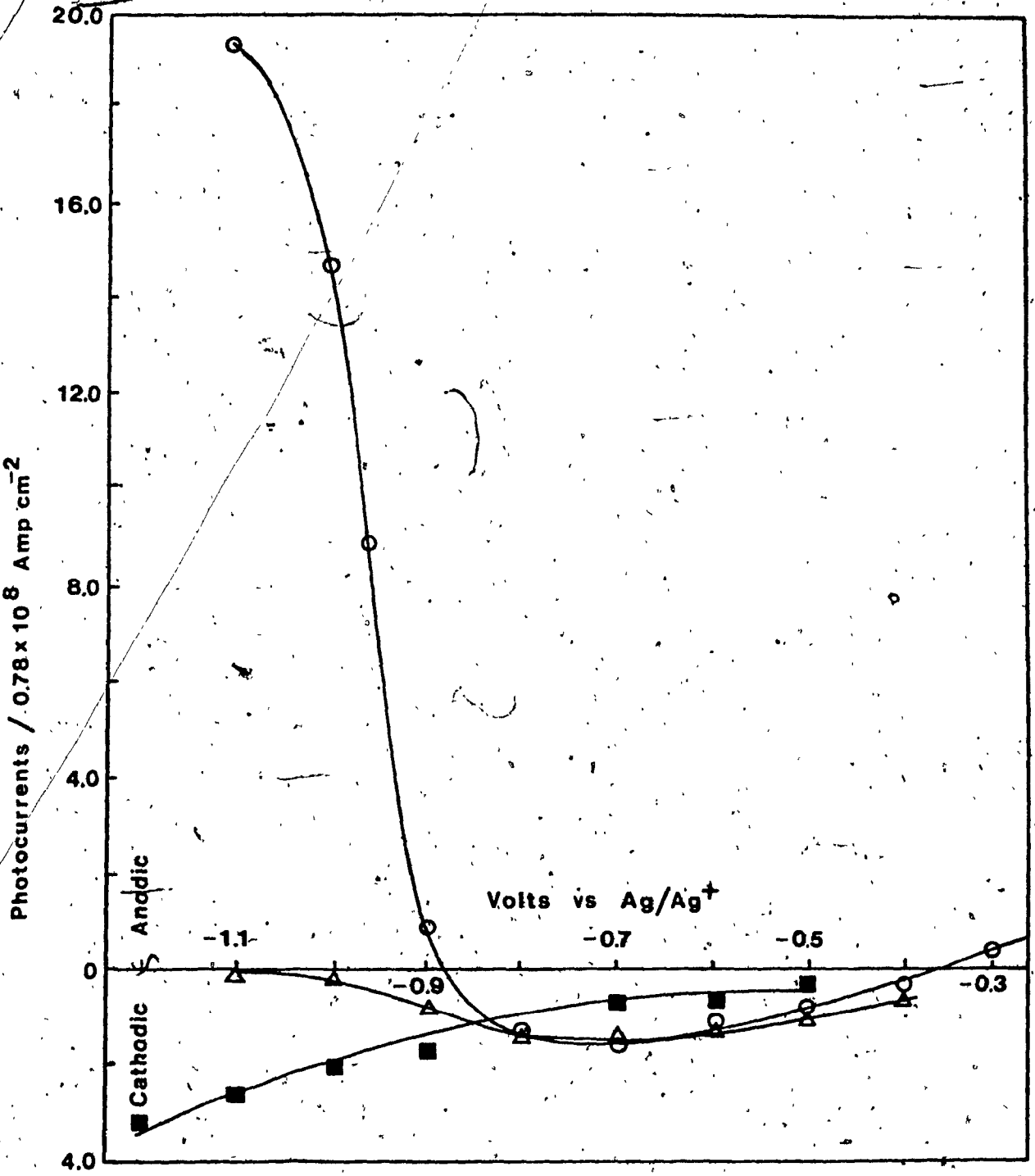

Figure 4-6. The effect of potential and oxygen on photocurrents of $Cu(mnt)_2^{2-}$ in 0.1 M $NaClO_4/CH_3CN$ electrolyte. Electrolyte saturated with O_2 gas (■); 2×10^{-3} M $Cu(mnt)_2^{2-}$ in electrolyte saturated with O_2 gas (△); 2×10^{-3} M $Cu(mnt)_2^{2-}$ in electrolyte (O). Irradiation Source: Argon ion Laser in multimode; 200 mW.

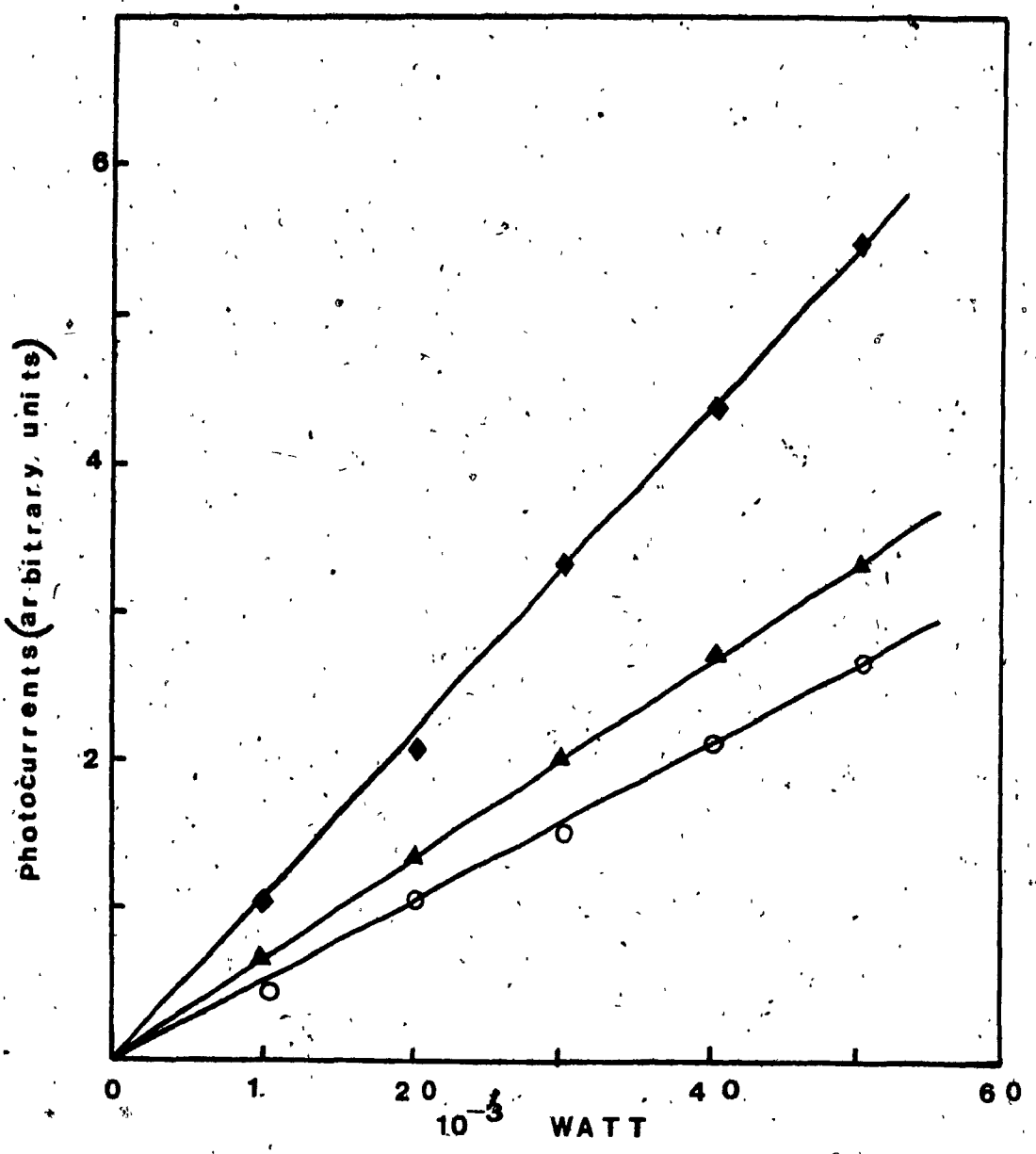

Figure 4-7. The dependence of anodic photocurrents on the first power of laser intensity: concentration of $Cu(mnt)_2^{2-}$: 2×10^{-3} M (O); 4×10^{-3} M (▲); 8×10^{-3} M (◆); Potential: -1.0 V vs Ag/Ag^{+}. Irradiation Source: Argon ion Laser in multimode.

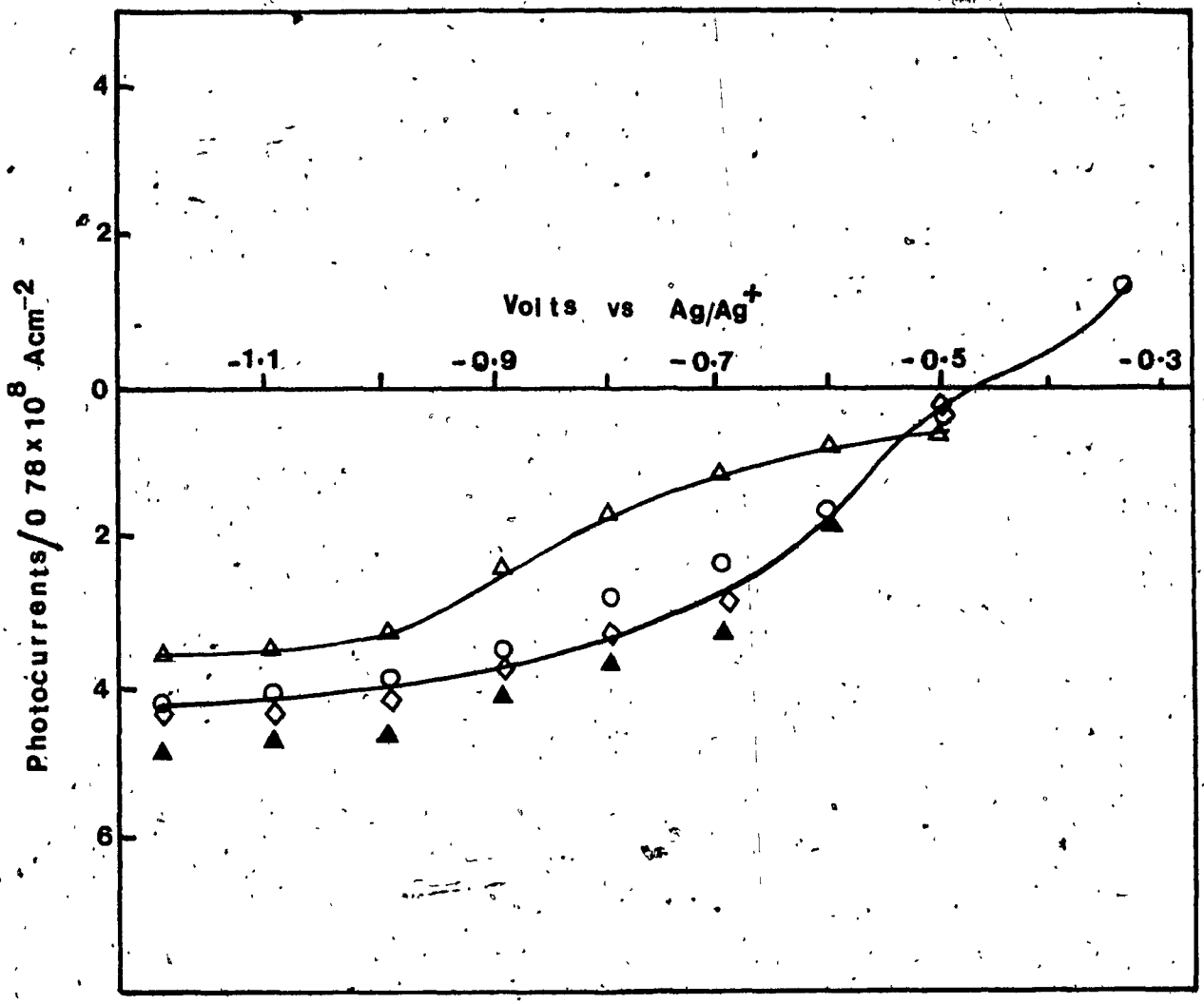

Figure 4–8. Effect of oxygen on the photocurrents of $Ni(mnt)_2^{2-}$ (△) electrolyte saturated with O_2. Concentrations of $Ni(mnt)_2^{2-}$ are: (○) 2.4×10^{-3} M; (▲) 4.7×10^{-3} M; (◇) 1.24×10^{-3} M.

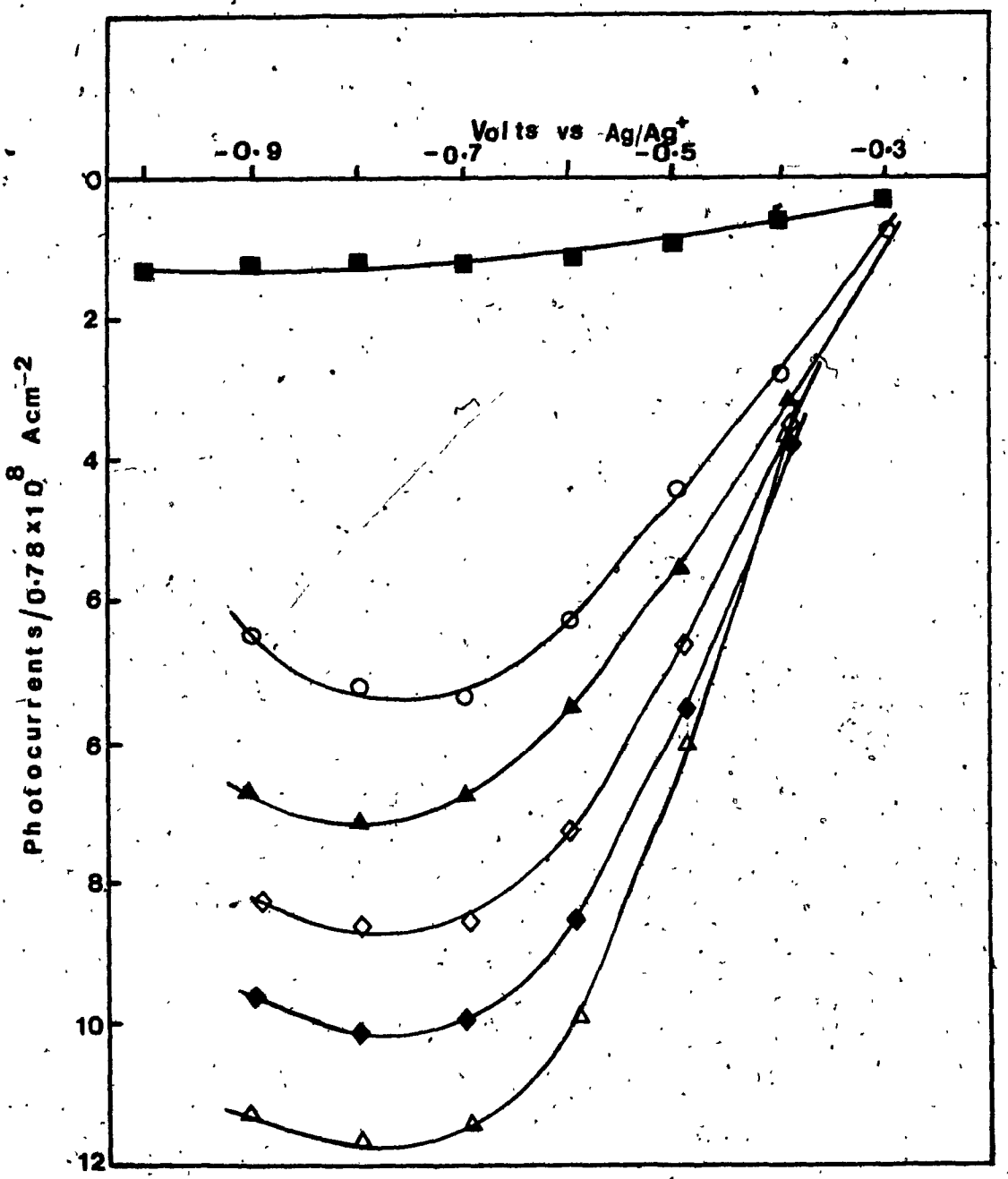

Figure 4–9. Decrease in Cathodic photocurrents of 4×10^{-3} M $Ni(mnt)_2^{2-}$ with pyridine. Concentrations of pyridine are: (△) nil; (◆) 1.24×10^{-3} M; (◇) 2.47×10^{-3} M; (▲) 4.95×10^{-3} M; (O) 9.89×10^{-3} M; (■) electrolyte containing only 1×10^{-2} M pyridine. Irradiation Source: Xenon lamp with I.R. and U.V. cutoff filters; 100 mW.

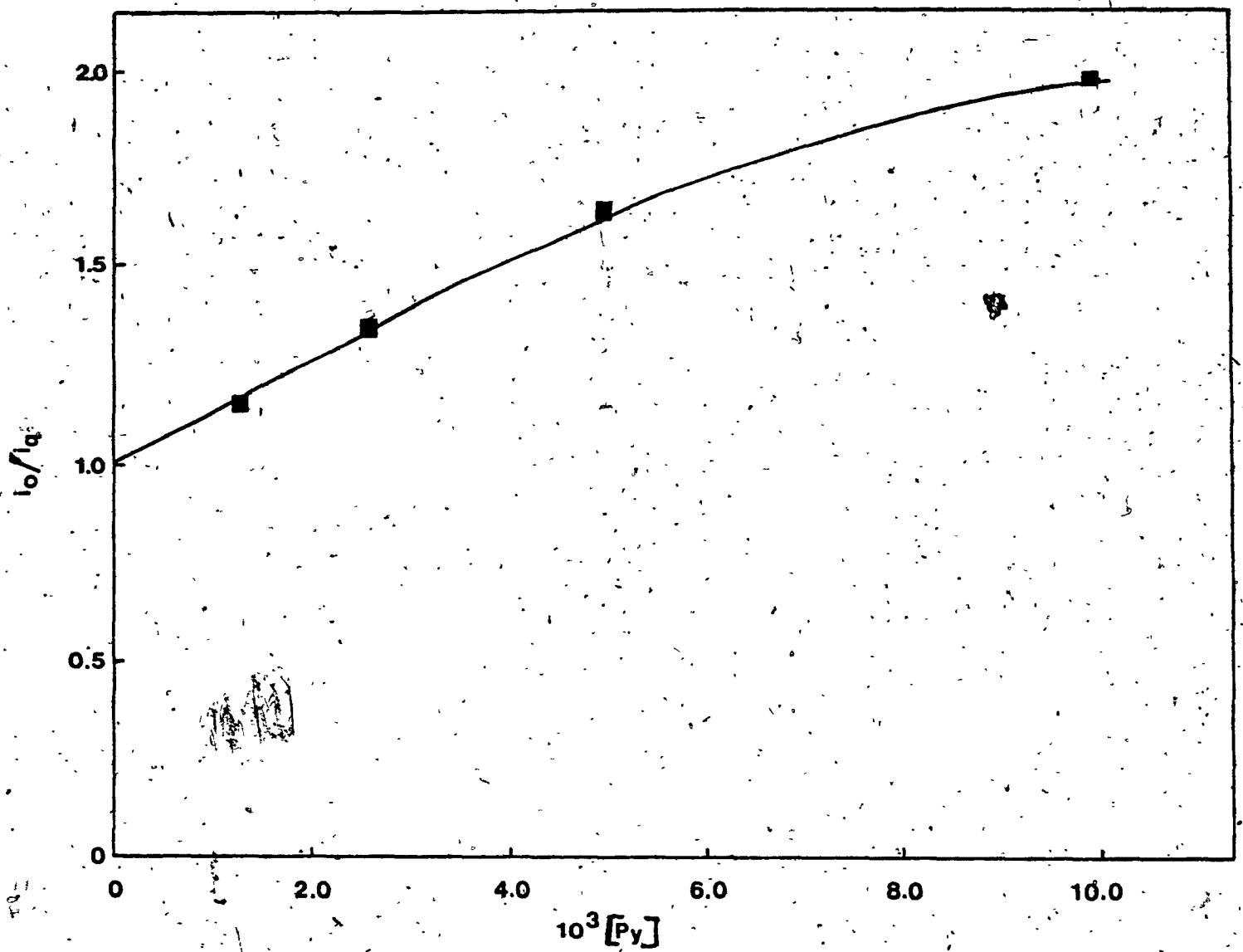

Figure 4-10. Stern Volmer plot for quenching of $Ni(mnt)_2^{2-}$ photocurrents by pyridine. Irradiation Source: Xenon lamp with I.R. and U.V. cutoff filters; 100 mW.

Chapter 5

Results III

5.1 Electronic Absorption Spectra of SnO_2-QPVP-$M(mnt)_2^{2-}$ Modified Electrodes

The homogeneous photoelectrochemistry of the dithiolate complexes studied demonstrated that the $Ni(mnt)_2^{2-}$ and $Pt(mnt)_2^{2-}$ are the most interesting for their photo-induced electron transfer reactions at the SnO_2 electrode. In an attempt to enhance the photoreaction, these complexes were immobilized on SnO_2 electrodes to produce chemically modified electrodes where their photoelectrochemistry would be studied. Immobilization of these complexes does not cause any chemical change of the complexes since the technique involved is the process where a tetraethylammonium cation is exchanged for a quaternized pyridinium ion. This was established by comparison of the absorption spectra of the electrodes to solution spectra. Figure 5-1 shows the near U.V. and visible spectrum of $Ni(mnt)_2^{2-}$ in solution and the spectrum of $Ni(mnt)_2^{2-}$ incorporated into the polymer which formed a modified electrode, SnO_2-QPVP-$Ni(mnt)_2^{2-}$. The spectrum of the SnO_2-QPVP-$Ni(mnt)_2^{2-}$ was the first recorded then all the complex was removed from the electrode by ion exchange with ClO_4^- ions in 10 ml of 1.0 M $NaClO_4$ in acetonitrile. The spectrum of this solution was then recorded and compared to the spectrum of the SnO_2QPVP-$Ni(mnt)_2^{2-}$. The

film spectrum as well as that of the solution spectrum for the complex removed from the polymer are in qualitative agreement with the spectrum of a freshly prepared solution of the complex. This indicates that the complex did not undergo any chemical change in the loading process. The peaks in the near U.V. region for the solution and the modified electrode fall at approximately the same wavelength. In the visible region, the 472 nm band that appears in the solution spectrum is shifted to the red in the polymer film on the electrode by approximately 8nm. It is also broader due to the environmental effects which freeze out molecular motions.

From the known solution extinction coefficient of 3800 l $M^{-1}cm^{-1}$ and an absorbance value of 0.413 obtained for this solution at 472 nm. It was determined that this solution contained about 1.09 x 10^{-6} moles of $Ni(mnt)_2^{2-}$ complex. The area of the SnO_2 electrode was determined as 4.34 cm^2 and the average thickness of the polymeric coating containing the complex was measured as 0.94 μm. From the area and thickness of the film the modified electrode was estimated to contain approximately 2.64 x 10^{-7} moles of $Ni(mnt)_2^{2-}$ per cm^2. The optical density of the visible band (472 nm) of the SnO_2-QPVP-$Ni(mnt)_2^{2-}$ was found to be 1.087. This would mean that the extinction coefficient for the complex in the polymer matrix is 42,000. This value is considerably larger than that found

for the solution spectrum and indicates severe problems with light scattering. This is confirmed by the irreproducibility of absorbance.

Since the electronic absorption of SnO_2-QPVP-$M(mnt)_2^{2-}$ cannot give a quantitative spectrum, it was not used to determine the amount of complex incorporated in the film. The solution spectrum was used for this purpose for all the electrodes. On this electrode, and all other modified electrodes used in this study, the ion exchange was found to be less than 100%. This means that in all the electrodes there was large amount of Cl^- ion remaining in the film. Based on the vinyl pyridium unit, the molar ratio of QPVP to $M(mnt)_2^{2-}$ was found to be between 12.5 and 6.4 for all the modified electrodes of this study. In terms of the ratio of cationic charge of the QPVP to the anionic charge of the $M(mnt)_2^{2-}$ values between 6.25 and 3.2 were obtained. From these values it was estimated that between 16 and 31% of the cationic sites on the polymer was neutralized by $M(mnt)_2^{2-}$ with the remaining sites retaining Cl^- ions.

5.2 Heterogeneous Electrochemistry at Pt and SnO_2 Modified Electrodes.

5.2 Solvent/Electrolyte System and workable Potential Window of Pt and SnO_2 Modified Electrodes.

Although the objective of the modified electrodes is the study of their photoelectrochemical behaviour, their thermal electrochemistry is important and cannot be

neglected. It is a situation analogous to any photochemical studies where the behaviour of the ground state of the molecule must be known as a prerequisite.

The $M(mnt)_2^{2-}$ complexes are known to be insoluble in water. It is therefore not surprising that aqueous solution of KCl, NaCl, LiCl or the Bromide and Fluoride salts of these metals proved to be satisfactory electrolytes. The ion exchange partition coefficient for $M(mnt)_2^{2-}$ into the polymer film is favourable versus the halide anions because it is a hydrophobic anion. It is not leached out from the polymer coating even after prolonged soaking in the salt solution in the dark or under irradiation or under cathodic or anodic polarization. The ground state of the molecules $Ni(mnt)_2^{2-}$ and $Pt(mnt)_2^{2-}$ are also stable in the presence of water. They were prepared from aqueous solution or washed with water in the preparative procedure and no reactivity with water was observed.

Since some chemically modified electrodes are known to exhibit electrocatalytic as well as other types of catalytic behaviour described before, it is necessary to establish the workable potential window of the modified electrode and the electrolyte/solvent system. In this study the potential window of the Pt-QPVP and SnO_2-QPVP without any $M(mnt)_2^{2-}$ incorporated into the polymer film was first established in 0.1 M KCl aqueous electrolyte.

The initial polymer in this study containing chloride counter ions is soluble in water and insoluble in acetonitrile but on exchanging the chloride ions for perchlorate it becomes insoluble in water. Polymer coatings on Pt and SnO_2 electrodes were subjected to such an exchange reaction by immersion in acetonitrile solution containing 1.0 M $NaClO_4$. The coatings were rendered water insoluble and stable for use in contact with 0.1 M KCl electrolyte.

Figures 5-2(a) and 5-3(a) show the respective cyclic voltammeteric behaviour for Pt-QPVP and SnO_2-QPVP modified electrodes in contact with 0.1 M KCl aqueous electrolyte. Both modified electrodes were scanned at 100 mV/sec and both exhibit a reduction with a corresponding oxidation wave. For the Pt modified electrode the reduction peak occurs at -0.77 V and the oxidation at -0.61 V making the peak separation, ΔE_p approximately 160 mV. For the SnO_2 modified electrode the peak separation is greater. The anodic peak remains at -0.60 V but the cathodic peak shifted by 240 mV to a potential of -1.01 V.

Cyclic linear sweep of the electrodes to a potential slightly anodic of the cathodic polymer peak shows no electrochemical activity. Figures 5-2(b) and 5-3(b) show this behaviour. No Faradaic response was observed even after several repeated cycles. In this potential region the polymer is inactive and stable. However when the $M(mnt)_2^{2-}$ complex was incorporated into the polymer film

two additional peaks; a cathodic and the anodic counterpart was observed in the potential region where the polymer is not electroactive. Figure 5-4 show the cyclic voltammetric behaviour at the various scan rates on a Pt modified electrode with $Ni(mnt)_2^{2-}$ incorporated into the polymer film (Pt-QPVP-$Ni(mnt)_2^{2-}$). In this electrode the pair of peaks at +0.35 V and +0.11 V can be attributed to the redox reaction of the complex while those at -0.55 V and -0.70 V are similar to the redox process for the Pt-QPVP electrode in Figure 5-2(a) since they fall in the same potential region.

The cathodic peak for both Pt-QPVP and SnO_2-QPVP electrodes Figures 5-2(a) and 5-3(a) can be assigned to a reduction of the pyridinium cation to a pyridinyl radical. This radical cation does not appear to undergo complete electrochemical oxidation to the original reactant. On both electrodes it appeared the cathodic wave is twice as large as the anodic counterpart. N-Alkyl pyridinium ions were shown to undergo dimerization (64) to form a tetrahydrobipyridine species upon electrochemical reduction between -1.32 and -1.28 V vs SCE. In the reaction below two moles of N-methyl pyridinium cation were consumed after reduction to produce the dimer. On the back sweep (anodic direction of a cyclic linear potential scan) the dimer was proven to oxidize to a viologen type cation radical at about -.46 V vs SCE.

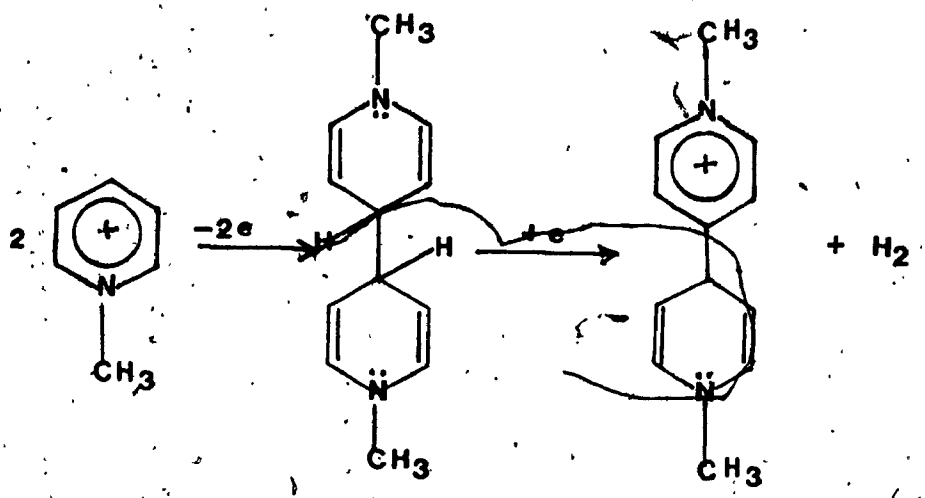

In the QPVP polymer the only electroactive group is the N-benzyl pyridinium unit and it is similar to the N-methyl-pyridinium monomer. It is conceivable then that a similar reaction is occuring in the film upon reduction on the modified electrode. The benzylic group is a better stabilizing group for radicals than the methyl, and can be responsible for the shift in the redox potential. An ECE mechanism similar to that outlined for the monomeric species can explain the surface voltammogram. In the reduction process two monomer units in the polymer are reduced. They then react to produce one mole of the dimer which then undergoes a one electron oxidation. The ratio of electrochemical charge transfer in the cathodic to the anodic process is 2:1 and this is reflected in the area of

the cathodic and anodic peak of the voltammetric surface wave as a ratio of 2:1.

For the modified electrode of Pt-QPVP-Ni(mnt)$_2^{2-}$ the reduction of the N-benzyl pyridinium cation to the pyridinyl radical was observed at -0.70 V. The radical cation of this electrode, unlike the electrodes with no Ni(mnt)$_2^{2-}$ incorporated into the polymer film undergo quantitative re-oxidation. The area of the anodic peak at -0.55 on the back sweep of the voltammetric wave (Figure 5-4) equals the area of the cathodic peak at scan rates up to 100 mV/sec. It would appear then that when the complex is incorporated into the polymer film, the pyridinyl cation radicals are difficult to undergo chemical reaction to form a dimer. The pyridium cations are probably separated from each other by the complex so that after reduction, there is no adjacent radical cation available to react. In this way the complex is useful in preventing the degradation of the polymer.

5.2.2 Electrochemistry of M(mnt)$_2^{2-}$, M = Pt, Ni on Modified Electrodes: Characterization of the ChargeTransport Process; Effect of Film Thickness and Loading.

In the potential region where the polymer is not electroactive the modified electrodes with Ni(mnt)$_2^{2-}$ and with Pt(mnt)$_2^{2-}$ incorporated in the polymer coating were examined for the electrochemical behaviour. A number of Pt and SnO_2 modified electrodes were initially prepared

under parallel conditions in which the thickness of the film and the amount of $M(mnt)_2^{2-}$ incorporated in the polymer film were varied to determine the effect of thickness and loading on the electrochemical behaviour. These electrodes are listed in Table 5-1 along with their respective thickness loadings, quantities of polymer and other parameters which may influence the electrode behaviour. Cyclic voltammetric waves were recorded at different scan rates for both Pt and SnO_2 modified electrodes in contact with 0.1 M KCl aqueous electrolyte. These are shown in Figure 5-5(a) to 5-11(a). The corresponding peak currents i_p vs the square root of scan rate, $v^{1/2}$ are shown in Figures 5-5(b) to 5-11(b).

There is wide variation in values of ΔE_p For the Pt modified electrodes, ΔE_p ranged from 120 to 180 mV at scan rate 30 mV/sec and 150 to 208 mV at 100 Mv/sec. For the SnO_2 modified electrodes ΔE_p values are from 170 to 298 mV at 30 mV/sec and 230 to 373 mV at 100 mV/sec. Values of ΔE_p for each of these electrodes along with the anodic and cathodic peak currents are given in Table 5-2. The voltammetric wave shapes are quite distorted and asymmetric for some of the electrodes. Electrodes 1, 4 and 6 of Table 5-1 are the typical examples. These electrodes exhibited sluggish oxidation while the reduction process by comparison, was faster. The anodic wave (Figures 5-5(a), 5-8(a) and 5-10(a)) is smaller than

its cathodic counterpart. The cathodic peaks are narrower or sharper than the anodic peaks. In electrodes 3, 5 and 7 (Table 5-2) the anodic peak current equals that of the cathodic at all scan rates (Figure 5-7(a), 5-9(a) and 5-11(a)), and the wave shapes are more symmetrical. Among the electrodes with asymmetric peaks the ratio of cathodic to anodic peak currents varied from 1.3 to 1.9 This indicate discrepencies of about 30 to 90% in the charge transferred between the anodic and the corresponding cathodic peaks.

The charge or area under the waves varies substantially with scan rate even if the baseline is included in the charge. The variation in peak shape and charge is associated with the appearance of tailing in the surface wave. Tailing is more pronounced for those voltammetric waves recorded at higher scan rates especially for the SnO_2 modified electrodes.

The peak currents, i_p vs $v^{1/2}$ are linear for the Pt modified electrodes (Figures 5-5(b) to 5-11(b). This linear relationship was only observed at slow scan rates below 50 or 60 mV/sec at the SnO_2 modified electrodes. Linearity indicates that the Randles-Sevick equation is obeyed for the Pt modified electrode up to scan rate of 100 mV/sec but only to 50 or 60 mV/sec for the SnO_2 modified electrode. From the slopes of this linear relationship apparent diffusion coefficients were calculated. These are given in Table 5-2 and range from 1

x 10^{-11} to 5 x 10^{-14} cm^2sec^{-1}. In the Randles -Sevick equation the concentration of the electroactive specie in terms of moles per cm^2 must be known. This was determined from the relationship

$$C = N/Al \qquad (17)$$

where N is the amount of $M(mnt)_2^{2-}$ in the polymer film, A is the area of the electrode and l is thickness of the film. In this calculation it is assumed that the complex is distributed uniformly in the polymer matrix.

Chronoamperometric experiments were also performed on these electrodes. The Pt and SnO_2 modified electrodes were respectively polarized at +0.4 and +0.5 V respectively. These potentials are beyond the oxidation potential of the $M(mnt)_2^{1-}$ in the film and the change in current was recorded as a function of time. Plots of the current, i vs $t^{-1/2}$ are shown in Figures 5-5(c) to 5-11(c). The linear portion of the i vs $t^{-1/2}$ plots obey the Cotrell equation (equation 11). The apparent diffusion coefficient, D_{app} obtained from the slopes of the i vs $t^{-1/2}$ plots for the different electrodes are given in Table 5-2. Values obtained for D_{app} by this technique range from 1.2 x 10^{-11} to 1.0 x 10^{-13} cm^2sec^{-1}.

Analysis of the wave shapes and other voltammetric parameters are made in comparion to that expected for a monolayer adsorbed species on an electrode surface and to

those obtained from voltammetric studies of $M(mnt)_2^{2-}$ in CH_3CN.

The general shape of the voltammetric surface waves of the Pt and SnO_2 modified electrodes are different from that expected from a monolayer and submonolayer species. They are broader and more diffuse with non zero peak separation. The full width half maximum E_{FWHM} is greater than 90.6 mV.

A comparison of the voltammetric parameters of Table 3-5 for the homogenous solution species with those of Table 5-2, for the modified electrodes show some interesting behaviour. It is important to note that there is not a large difference between the cathodic peak potentials on the modified electrodes and those of the monomeric species in dilute solution. The difference in the values also do not follow any consistent pattern. There is however an increase of 150 to 200 mV in the anodic peak potentials of the modified electrodes compared to that observed at the bare electrodes in solution. The potentials of the modified electrodes were measured with respect to Ag/AgCl (Sat. KCl) reference. The potentials of the solution species were measured with respect to Ag/Ag^+ (0.1 M $AgNO_3/CH_3CN$) reference and were adjusted to the aqueous reference by adding +0.27 V. These adjusted potentials are also shown in Table 3-5. The increase in the anodic peak potentials for the modified electrodes reflects a more difficult oxidation process in the film.

The ΔE_p for the Pt modified electrodes were found to be between 150 to 200 mV at scan rate 100 mV/sec and between 120 to 180 mV at 30 mV/sec. This is larger than the ΔE_p values for the homogeneous solution reactions which were between 107 and 92 mV at 100 mV/sec and 76 and 72 mV at 30 mV/sec (Table 3-5). The ΔE_p for SnO_2 modified electrodes do not show the same pattern of behaviour as the Pt modified electrodes. The SnO_2 modified electrodes exhibited ΔE_p values which are comparable to those observed for the solution reactions at the bare SnO_2 electrode.

Unlike the solution reactions where all the voltammetric peaks are symmetrical and the electrode response close to a Nernstian behaviour (for the reactions at Pt electrode) not all the surface waves for the modified electrodes are symmetric and exhibit a peak ratio of unity (Figure 5-5(a), 5-8(a) and 5-10(a)). The variation of film thickness does not explain this behaviour. For example electrode 7 which is 2 μm thick and electrode 5 which is 4 μm thick (Table 5-1) show equal anodic and cathodic peaks. Electrode 3 and 6 which are both 2 μm thick show different behaviour. In electrode 6 the anodic and cathodic peaks are unequal while in 3 they are equal and symmetric.

The major factor which appears to influence the wave shape and distortion can be found by examining the amount

of the complex in the polymer film. Each mole of the dianion complex should ideally coexist with two moles of the N-alkylated vinylpyridine units since each pyridinium unit has one positive charge. For all the electrodes of Table 5-1 the quantity of complex anion incorporated in the film is less than that required to completely neutralize the film. This means that along with the complex diahion there is also Cl^- ion in the film so that when the concentration of the complex dianion is increased, the chloride content in the film is decreased. Tables 5-1 and 5-2 show an interesting correlation between the fraction of the complex in the polymer film, the chloride content in the film, and the behaviour of the electrodes. The correlation is more meaningful when the contents of the film is expressed in terms of charge neutralization. The positive charge on the polymer was obtained from the number of moles of vinylpyridinium units per square centimeter. The charge on the dianion complexes were obtained in a similar manner. The percentage of cationic sites neutralized by the complex was obtained from the charge ratio, and the difference from 100 reflected percentage neutralization by Cl^- ions. Electrodes 3, 5 and 7 showed a polymer to complex molar ratio greater than 10. In these electrodes only 15 to 16% of the charge on the polymer coatings were neutralized by the electroactive dianion complex. These are the electrodes that exhibited equal anodic and cathodic waves.

In electrode 1 where the polymer/complex ratio is only 6.4 and 31% of the cationic charge in the polymer was neutralized by the complex the wave shape is not symmetrical, the anodic wave is smaller than the cathodic. In electrodes 2, 4, 6 the percentage positive charge on the polymer neutralized by the $M(mnt)_2^{2-}$ complex is between 15 to 31%. These results are graphically represented in Figure 5-12 where a plot of percentage cationic charge neutralized by the complex vs the ratio of cathodic to anodic peak currents (i_{pc}/i_{pa}) is shown. At lower value of i_{pc}/i_{pa} a linear relationship exist but at values greater than 1.8 the curve tends to level. This result demonstrated that the amount of complex loaded into the film is the significant factor that affects the wave shape. When the fraction of the cationic sites neutralized by the complex is low the waves are more symmetrical and reversible while at high fraction of 30% alteration in the symmetry of the waves is observed and the electrode behaves less reversibly.

The behaviour of the redox reactions of the modified electrodes with respect to the character of the charge transfer process is similar to that observed at the bare Pt electrode. The direct proportionality of i_p vs $v^{1/2}$ in the Randles-Sevick equation and the i vs $t^{-1/2}$ in the Cotrell equation for the modified electrodes are typical of the homogeneous solution. These equations are based on

a semi-infinite volume of diffusing reactant in contact with the electrode such that the depletion layer of the diffusion profile never reaches the cell wall. In the modified electrodes the electroactive species is confined to the polymer film on the electrode. The thickness of the film can then be regarded as the cell dimension and this is very small. It therefore means that a linear relationship between i_p and $v^{1/2}$ and i and $t^{-1/2}$ can only be obtained when the rate of diffusion in the film is very slow in comparison to diffusion rates in the homogeneous solution. The apparent diffusion coefficients for the modified electrodes are indeed very much smaller than the diffusion coefficient for the homogeneous solutions. Diffusion coefficients in solution are approximlately 1 to 2×10^{-5} cm^2 sec^{-1}. Apparent diffusion coefficient for the modified electrodes are between 1×10^{-11} 5×10^{-14} cm^2 sec^{-1}. These values for the D_{app} are in agreement with literature values for other types of modified electrodes.

In the chronoamperometric experiments the plots are linear for times up to 4 sec and the current does not fall off. Sustenance of the current for such long time showed that the electroactive species in the film has not been depleted and also indicate a slow diffusional process. For the linear cyclic scans tailing is evident in the surface waves. The tailing is more pronounced at fast scan rates particularily for the SnO_2 modified electrodes.

Tailing indicates that a large portion of the electroactive species remains unoxidized or unreduced as the potential is swept past the redox peak. The diffusion like tailing is also suggestive of a rate of charge transfer in the film which is comparable to the voltammetric time scale, i.e. that D_{app} is small enough that the oxidized form of the complex in the film does not remain in equilibrium with the applied potential.

The linear i_p vs $v^{1/2}$ relationship for the modified electrode (low scan speed for SnO_2) suggests that the electrode reaction is reversible. The peak separations are however larger than the 59 mV require for a reversible behaviour by solution reactant and far from the ideal behaviour for a surface adsorbed specie on a bare electrode. The area of the anodic and cathodic peak is an obvious indication that the electrode does not behave reversibly. Tailing also supports this conclusion. In view of the i_p--$v^{1/2}$ behaviour which indicate reversibility and the other voltammetric observations which indicate irreversibility, the modified electrodes can be regarded as behaving only partially reversible.

It is not very clear whether the thickness of the film has any real significance with repect to the reversibility of these modified electrodes. Electrodes 2 and 5 (Table 5-2) were compared. On electrode 2 the thickness was measured as 3 m, with 0.96×10^{-3} mol/cm^3

of $Pt(mnt)_2^{2-}$ in the film. The peak separation is 150 mV (at 30 mV/sec) and D_{app} was estimated to be approximately 2×10^{-12} cm^2sec^{-1}. In electrode 5 which is similar, the thickness was measured as 3.5 to 4 μm with 0.62×10^{-3} mol/cm^3 of $Pt(mnt)_2^{2-}$ incorporated in the film. The peak separation was 120 mV and D_{app} approximately equal to 1×10^{-13} cm^2sec^{-1}. In these two electrodes the peak separations are not in agreement with the apparent diffusion coefficient. The larger ΔE_p usually indicate slower electron transfer and in this situation the D_{app} is expected to be smaller when the reaction is diffusion controlled. Should the difference in the peak separations of electrodes 2 and 5 be considered insignificant or the peak separations be ignored in this analysis one can conclude that the apparent diffusion coefficient decreases with increasing film thickness. Electrodes 3 and 7 were also compared to 4 and 6. These electrodes are the same type. Their thickness is approximately 2 μm but the waves shapes of electrodes 3 and 7 would indicate a behaviour closer to reversibility than electrode 4 and 6. Electrodes 3 and 7 have anodic and cathodic peak ratio of unity while in 4 and 6 the peaks are unequal at this sweep rate.

The fraction of the complex in the polymer film does not appear to influence the apparent diffusion coefficient. Electrodes 6 and 7 (Table 5-2) were compared. These electrodes are of the same type, with

thickness of about 2 μm. The fraction of $Ni(mnt)_2^{2-}$ in the polymer film is different; 0.28 or 28% of the cationic sites on the polymer was neutralized by the complex for electrode 6 and 0.17 or 17% for electrode 7. The apparent diffusion coefficients for the cathodic reactions are however very close 4.97×10^{-12} cm^2 sec^{-1} (electrode 6) and 7.23×10^{-12} cm^2 sec^{-1} (electrode 7). Other examples are electrodes 1 and 7 in which the fraction is varied but the apparent diffusion coefficient is approximately equal. Since the D_{app} is independent of the fraction of complex in the film or the loading it can be concluded that electron exchange by hopping between localized 2- and 1- redox sites does not contribute significantly to the charge transport.

However, a comparison of the apparent diffusion coefficients obtained from the i_p vs $v^{1/2}$ slopes for the anodic and the cathodic peaks for a particular electrode shows that they are influenced by by the amount of complex in the film. When the fraction is large the cathodic peak is greater than the anodic peak or the reaction $M(mnt)_2^{1-}$ ---> $M(mnt)_2^{2-}$ is more favorable than the reaction $M(mnt)_2^{2-}$ ---> $M(mnt)_2^{1-}$. Typical examples of such behaviour were seen in electrode 1, 4 and 6. In electrode 1 the D_{app} for the cathodic reaction is 2.55×10^{-11} cm^2 sec^{-1} while for the anodic reaction it is $7:14 \times 10^{-12}$ cm^2 sec^{-1}. This usual behaviour cannot be directly attributed to the

higher fraction of the complex alone, but a high fraction in conjunction with other factors associated with the polymer film may be responsible. A large quantity of the complex is solution does not show such a behaviour.

In the chronoamperometric experiments where the modified electrodes were polarized at +0.4 (Pt) and +0.5 V (SnO_2) the apparent diffusion coefficients determined from the $i—t^{-1/2}$ slopes for the oxidation reaction are greater than those obtained from the anodic peak currents of the i_p vs $v^{1/2}$ slopes for the same electrode. The D_{app} from the Cotrell plots are comparable to those obtained from the cathodic peak current in the i_p vs $v^{1/2}$ slopes. This indicates that there is no special barrier to electron transfer from the dianion in the linear sweep experiment. The surface waves also show that the peaks are repeatable and therefore the oxidation does proceed during the stop time at the anodic limit. It is likely that the smaller anodic peak in the surface waves and the corresponding smaller apparent diffusion coefficient are probably due to factors which influence D_{app} and are also affected by the continuous changing potential under the cyclic scan.

The larger and narrower cathodic and the board anodic wave pattern of Figures 5-5(a), 5-8(a) and 5-10(a) can be generally interpreted in terms of the interaction parameter g_o and g_R postulated by Brown and Anson (37). The shift in the anodic peak in the surface wave to more anodic potential would then suggest that in these

electrodes there is attractive force between molecules of $R_2(M(mnt)_2^{2-})$. The energy needed to overcome this attractive force is represented by the increase in the anodic peak potential. This explanation is not sufficient since it does not give molecular information but is still helpful as a guide to a more detailed explanation.

Molecular interpretation was obtained by analysing the electrode process as the potential is swept pass the peak potential. In such cyclic sweep the scan was initiated at a potential more anodic than the oxidation peak potential of the modified electrode. The electrode was first polarized at this potential and an equilibrium was established in an attempt to satisfy the Nernst equation. At this time the complex is oxidized. To compensate for the change in oxidation state Cl^- ions from the electrolyte diffuse into the polymer film. After the sweep was initiated and continued past the reduction peak potential; the complex is reduced and Cl^- ion is expelled. The processes occuring in this half of the scan are electron transfer and expulsion of Cl^- ions. On the anodic half of the scan electron transfer occurs but with uptake of Cl^- ions. Since the electron transfer is fast, the sluggish oxidation can then be attributed to a slow uptake of Cl^- ions. The slow intake of Cl^- ions is probably due to the occurance of a process or processes in the film after reduction. After reduction the complex

gain an electron and becomes multiply charged. Murray et al (65) have suggested electrostatic cross-linking by multiple charged species, and has associated cross-linking to broader peaks and peaks with diffusional tails. It is possible that the rate of uptake and exodus of chloride ions is associated with the extent of electrostatic cross-linking by the dianion of the $M(mnt)_2^{2-}$ between two segments of the polymer. Electrostatic cross-linking can produce a more compact and more organized film which will be difficult for the Cl^- ions to penetrate. Thus on polarizing the electrode before initiating the scan some of the electrostatic cross-linking is slowly destroyed because of the removal of negative charge from the complex. The oxidation occurs first followed by breaking up of cross-linkages then the influx of Cl^- ions into the film. After passing the reduction peak potential in the forward sweep, the dianion is regenerated, chloride ions are expelled and cross-linkage increased. On the anodic backsweep there is no significant variation in the ratio of the oxidized to the reduced complex until the oxidation peak potential is reached. At potentials cathodic to the oxidation peak potential the major component in the film is the dianion and cross-linking as well as organization of the film may be substantial. The diffusion of chloride ions and solvent into the film is thus retarded. Therefore as the potential is sweep past the anodic peak potential the quantity of $M(mnt)_2^{2-}$ oxidize is limited by

the rate at which Cl^- ions can diffuse into the film from the electrolyte. The electrostatic cross-linkage can be regarded as a stronger interaction of the dianion within the polymer matrix. Since only the dianion can be involved in the cross-linking the oxidation peak is only affected. It is broader and shift to a more anodic values by comparison with the cathodic peak potential of the modified electrodes and the bare electrodes.

The ion exchange partition coefficient may also affect the exchange of chloride ions. The exodus of chloride ions is probably easier in the presence of the dianion than the monoanion because the ion-exchange partition coefficient for $M(mnt)_2^{2-}$ is probably greater than $M(mnt)_2^{1-}$. It was found for example that only a very limited amount of $Ni(mnt)_2^{-1}$ exchanges into the polymer film on the electrode when the conditions parallel those used for $Ni(mnt)_2^{2-}$.

In the QPVP polymer the counter ions or co-ions are chloride ions. As the amount of $M(mnt)_2^{2-}$ in the polymer film of the modified electrodes is increased the amount of chloride ions in the film is decreased. $NI(mnt)_2^{2-}$ which was precipitated by QPVP is expected to replace all the chloride ions of the polymer. This precipitated QPVP-$Ni(mnt)_2^{2-}$ polymer is insoluble in most common solvents except dimethylsulfoxide (DMSO). This is probably because of extensive cross-linkage. The deposition of a DMSO

solution of the QPVP $Ni(mnt)_2^{2-}$ polymer on SnO_2 electrodes to form a thin film was found to be difficult. The solvent is not very volatile and took several days to evaporate. When it did evaporate the film became very brittle, peeled off from the electrode surface and cracked as soon as it was exposed to water. The cracked film appeared to be very crystalline in appearance. This would suggest that as the amount of the $M(mnt)_2^{2-}$ in the film is increased the polymer becomes more compact and organized and is more impermeable to solvent and Cl^- ions. Coatings with low concentrations of $M(mnt)_2^{2-}$ as in electrode 3 and 5 (Table 5-1 contain more chloride ions in the polymer film than electrode 1. There would be less electrostatic cross-linkage in these electrodes and the polymer film would be less compact and not well organized. Exchange of chloride ions between neighbouring cationic sites is less hindered. At the polymer/electrolyte interface this exchange may occur without major difficulty. Chloride ions from the electrolyte can then penetrate and migrate through the polymer film more easily than in an organized compact polymer film. An easy flow of chloride ions from the electrolyte into the polymer film would then favour the symmetry of the voltammetric wave as seen in electrode 3 and 5.

5.2.3 Effect of Supporting Electrolyte

As noted in the previous section the change in

oxidation state in the electrochemical reaction of the modified electrodes must be accompanied by migration of charge compensating counter ions. Ion mobility in ion exchange polymer is known to be a strong function of ion size, charge and concentration (66,67). If electrochemically induced change in the polymer ionic composition is large then the properties of the counter ion can be important in the kinetics of the electrode reaction. It is expected that smaller ions would encounter less difficulty in penetrating and migrating through the polymer film from the electrolyte. Aqueous electrolytes of 0.1 M NaBr, NaCl and NaF were used to determine the anion effect while 0.1 M LiCl, NaCl and KCl were used to establish the cation effect. Both SnO_2-QPVP-$Ni(mnt)_2^{2-}$ and SnO_2-QPVP-$Pt(mnt)_2^{2-}$ modified electrodes were examined for the ion effect. Figure 5-13 shows the voltammetric wave for SnO_2-QPVP-$Ni(mnt)_2^{2-}$ while Figure 5 14(a) shows the behaviour of SnO_2-QPVP-$Pt(mnt)_2^{2-}$ modified electrodein the 0.1M NaBr, NaCl and NaF electrolytes. The voltammetric parameters are summarized in Table 5-3 and 5-4. The peak separation is increased as the anion is varied from F > Cl > Br. The peak current follow the opposie pattern. Larger currents were observed for the electrodes when they were in contact with the Bromide electrolyte. These currents decreased in the order of Br > Cl > F.

The voltammetric response of the electrodes in the

presence of 0.1 M LiCl, NaCl, and KCl did not show any variation in the voltammetric parameters as the cations of the electrolyte were changed from Li, Na to K. This is because the cations in the electrolyte are not actively involved in the charge neutralization process of the polymer film upon the change in oxidation state.

The voltammetric response is therefore sensitive only to anions of the electrolyte and the migration of these anions through the polymer film for charge neutrality is probably contributing significantly to the kinetics of the oxidation reaction of the electrodes. The trend in the voltammetric response is however contrary to what was anticipated. This unexpected trend suggests that additional factors other than the size of the charge compensating counter ion have significant influence on the behaviour of the electrode, notably in hydration.

5.2.4 Effect of Soaking the Modified electrodes in Methanol and Water

In the kinetics of counter ion diffusion solvent transport can be important. Solvent can be carried along by the counter ion into the polymer and expand the polymer thereby changing the pressure in the film. This effect in combination with the high concentration of redox sites can induce thermodynamic activity which will be reflected in the voltammetric wave. The phenomenon of polymer swelling promoted by solvents of polarity similar to the polymer

can have a similar effect. Even non solvents are known to penetrate amorphous polymers in the absence of defect by a process which involves local segmental motion of the polymer (47). Therefore despite the insolubility of QPVP-$M(mnt)_2^{2-}$ in water, penetration of this solvent into the QPVP-$M(mnt)_2^{2-}$ electrode cannot be excluded without verification. The procedure adopted in preparing the QPVP-$M(mnt)_2^{2-}$ modified electrodes include no experimental proof that the coating is solvent free. The QPVP coating on Pt and SnO_2 electrodes was deposited from methanol solution. Since the QPVP with Cl^- as counter ion is soluble in methanol these $M(mnt)_2^{2-}$ free cationic sites can trap methanol and influence the charge transport process.

The electrode used to record the waves of Figure 5-13 was examined for the effect of methanol and water. After the voltammograms of Figure 5-13 were recorded the SnO_2-QPVP-$Ni(mnt)_2^{2-}$ was left in a vacuum oven at 35°C for 12 hrs. Subsequent to cooling to room temperature the voltammetric waves of Figure 5-15 were recorded in 0.1 M NaF and NaCl electrolytes. The vacuum heating was expected to remove any or all of the methanol trapped in the film during the preparation.

The electrode was then soaked in water for 35 mins. This is meant to determine whether there is uptake of this solvent by the polymer coating and its effect on the performance of the electrode. The voltammetric response shown in Figure 5-16 was obtained in 0.1 M NaF and NaCl

after the electrode was removed from the water. There was no visible indication of swelling or entrapment of water in the polymer coating.

The electrode was again used to determine the effect of methanol. It was immersed in methanol for 5 mins. rinsed copiously with water and the voltammetric waves of Figure 5-17 recorded.

The SnO_2-QPVP-$Pt(mnt)_2^{2-}$ electrode used in Figure 5-14 was treated in the same manner to demonstrate the effect of water and methanol. After vacuum heating, cooling to room temperature and soaking in water for 35 mins the SnO_2-QPVP-$Pt(mnt)_2^{2-}$ was used to record the voltammogram of Figure 5-18(a) in 0.1 M NaCl electrolyte. Figure 5-18(b) was then subsequently recorded in the same electrolyte after the electrode was exposed to methanol vapor for 8 hrs.

The responses of both $Pt(mnt)_2^{2-}$ and $Ni(mnt)_2^{2-}$ modified electrodes to exposure to water and methanol are similar. The voltammetric waves of Figure 5-16, 5-17 and 5-18(b) clearly demonstrated this similarity and provide further insight and understanding of the factors governing the charge transport process. A comparison of Figure 5-13 and 5-14 which were recorded after the electrodes were freshly prepared and Figures 5-15 and 5-18(a) after vacuum heating show a drastic change in the response. The waves recorded with a freshly prepared electrode showed better

behaviour than those recorded after heating. The peak currents after heating decreased, there is more tailing particularly in the anodic peaks. The peak separation also increased. These are the tendencies that are indicative of a irreversible behaviour. This response seemed to verify that the freshly prepared electrode contained methanol inside the polymer matrix and the solvent aids in the charge transport process. On heating, the trapped methanol was removed and charge transport was retarded. The exposure of the electrodes after heating to methanol either by direct immersion in the solvent or to the vapor also supported the retention of methanol in the polymer matrix in the preparative procedure since from Figure 5-17 and 5-18(b) the electrodes showed improved performance as compared to Figure 5-16 and 5-18(a).

Exposure or soaking the electrodes in water does not improve their behaviour this is evident by comparing Figures 5-16and 5-17. This is surprising. As mentioned earlier there was a maximum average of 30% cationic sites on the modified electrodes that is associated with $M(mnt)_2^{2-}$ dianions and the remaining 70% with Cl^- ions. Since the QPVP with associated Cl^- ion is soluble in water these sites on the surface of the polymer coating in contact with aqueous electrolyte should be solvated by water and provide channels or pores for water to diffuse into the polymer coating. Water can also modifiy the conductivity by increasing the dielectric constant of the

system and enhancing the dissociation of the ionically bound Cl^- ions in the polymer. The electrochemical results suggest that this is not occuring in the polymer film. A plausible explanation for this unexpected behaviour is the distribution of the $M(mnt)_2^{2-}$ species in the polymer film. The technique of loading the complex unto the polymer coated electrode is an ion exchange one where the outer surface contacting the $M(mnt)_2^{2-}$ solution would first incorporate the complex which would then diffuse into the interior of the polymer film. It is possible that the cationic sites on the outer surface of the coating is fully neutralized by $M(mnt)_2^{2-}$ while the interior of the film consists of both $M(mnt)_2^{2-}$ and Cl^- ions. This would mean that from the polymer/electrolyte interface to the polymer/electrode interface the concentration of $M(mnt)_2^{2-}$ decreases providing a concentration gradient in the film. In such a situation there would probably exist at the polymer/electrolyte interface insignificant or no cation sites with associated chloride counter ions. The cations associated with $M(mnt)_2^{2-}$ are insoluble in water and cannot be solvated to provide pores for water to diffuse. The complex $[(C_2H_5)_4N]_2\ M(mnt)_2$ is slightly soluble in methanol and solubility of QPVP is greater in methanol than water. The solvation of cationic sites with $M(mnt)_2^{2-}$ as counter ions by methanol can provide for methanol to diffuse into the

polymer.

The different responses of the electrodes after exposure to water and methanol is important in understanding the behaviour when they were in contact with different electrolytes and also helpful in determining the limiting process in the diffusion kinetics.

The electrochemical response for both $Ni(mnt)_2^{2-}$ and $Pt(mnt)_2^{2-}$ modified electrodes are in agreement with the hydration sequence of the halide ions. Fluoride, the smallest ion is heavily hydrated and the least mobile. Bromide on the other hand is least hydrated and most mobile. Since it was shown that water does not penetrate the polymer coating, it is resonable to suggest that the most heavily hydrated ion would have the most difficulty in diffusing into the polymer from the electrolyte. These observations implied that diffusion of counter ion from the electrolyte solution into the polymer film at the polymer electrolyte interface is the determing process in the counter ion diffusion kinetics.

Since water or the hydrated counter ions is difficult to penetrate the polymer film well when the modified electrode is immersed in water or aqueous electrolyte, mobility by self diffusion appears to be unlikely. The modified electrodes in contact with aqueous electrolyte incorporate counter ion from the electrolyte due to a potential gradient which occurs when the complex in the polymer at the electrode/polymer interface starts

oxidizing. Upon oxidizing a net transfer of electric charge from the polymer to the electrode occurs and results in a violation of electro-neutrality of the polymeric film. Conservation of neutrality at the electrode/polymer interface is established by migration of Cl^- ions from the bulk polymer matrix to the cationic sites near the electrode. The site to site migration of the counter ion is the only plausible mechanism for counter ion transport in the polymer since the average film thickness of the polymer is 2 to 3 μm and this a long distance for ion migration or jump in any one step. With methanol trapped in the film the transport process is enhanced probably due to segmental motion of the pendant pyridinium group which can move closer and aid in Cl^- ion transfer.

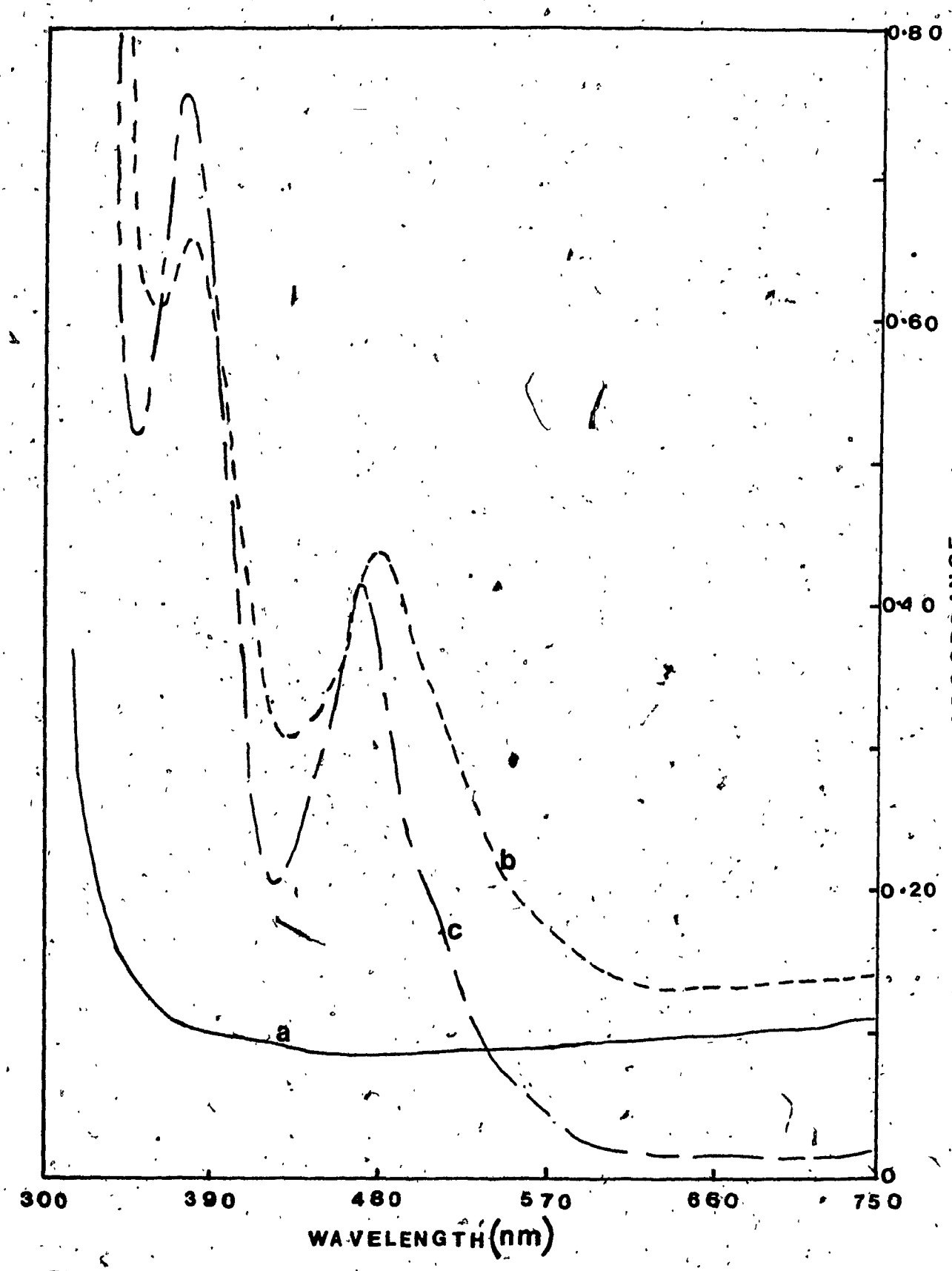

Figure 5-1. Absorption spectra of SnO_2-QPVP (a); SnO_2-QPVP-$Ni(mnt)_2^{2-}$ (b) and $Ni(mnt)_2^{2-}$ in acetonitrile (c).

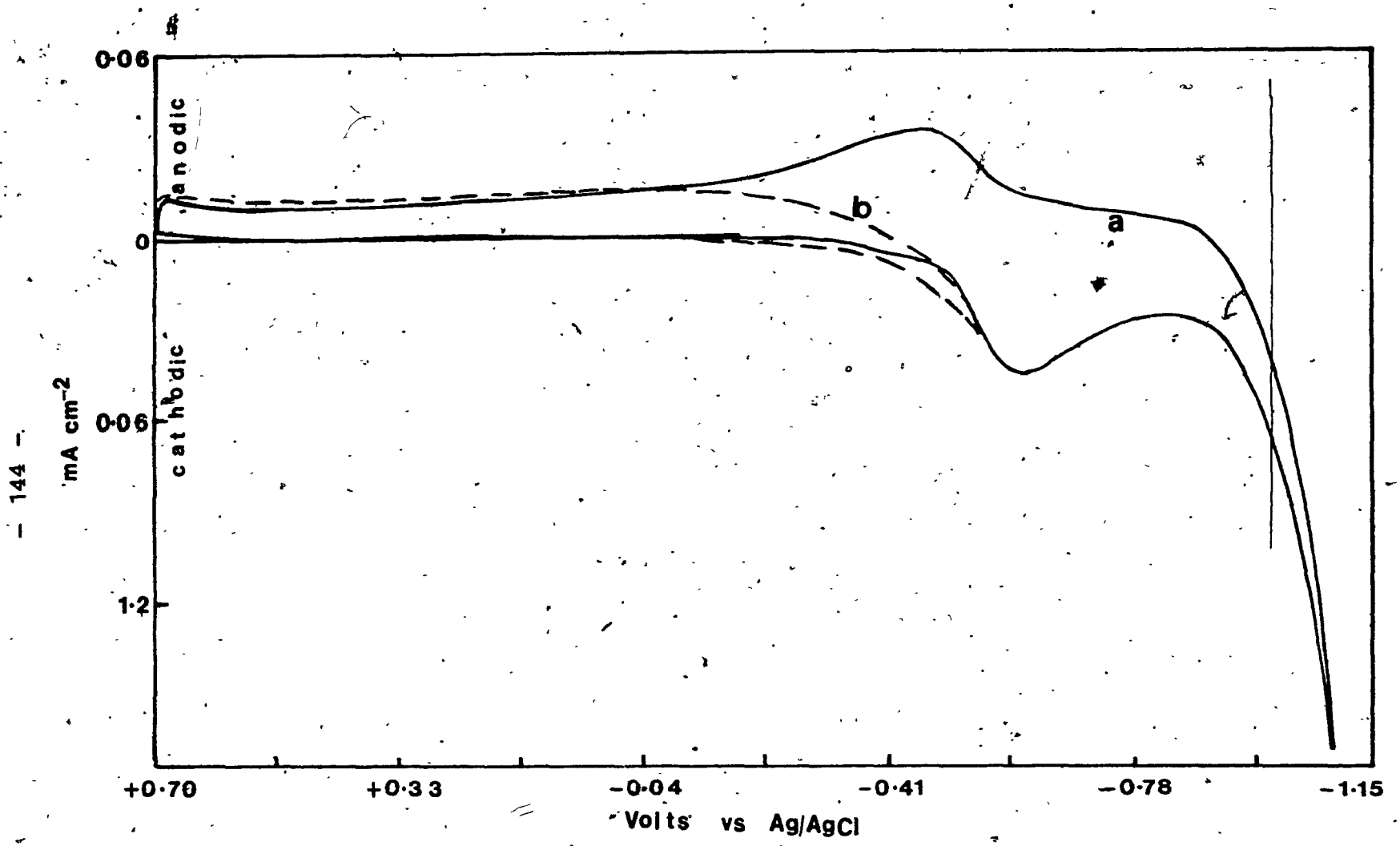

Figure 5–2. Cyclic voltammetric waves for Pt–QPVP within the potential window +0.70 to -1.15 V (a) and +0.70 to -0.60 V (b) in contact with 0.1 M KCl aqueous electrolyte.

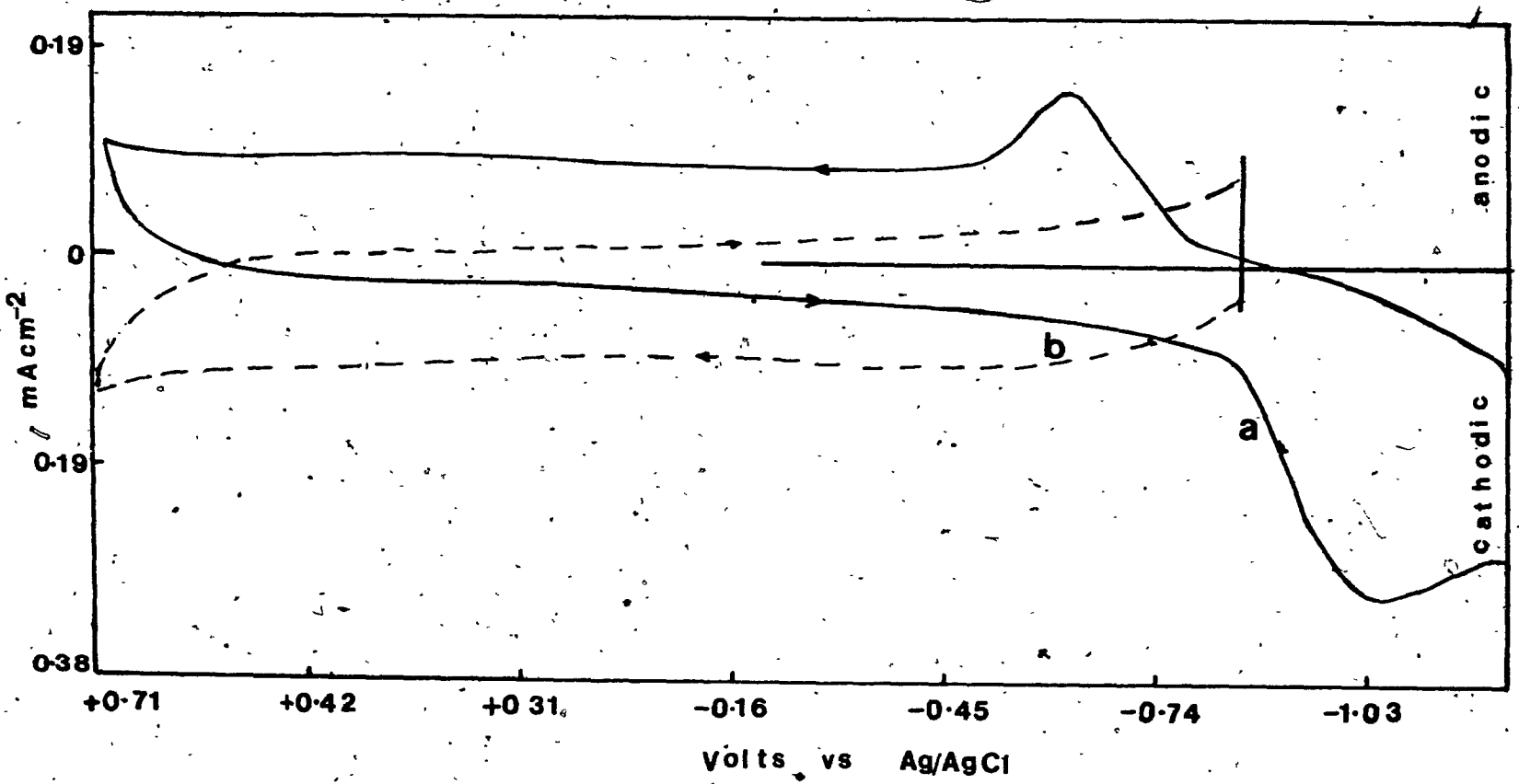

Figure 5-3. Cyclic voltammetric waves for SnO_2-QPVP within the potential window +0.71 to -1.22 V (a) and +0.71 to -0.86 V (b) in contact with 0.1 M KCl aqueous electrolyte.

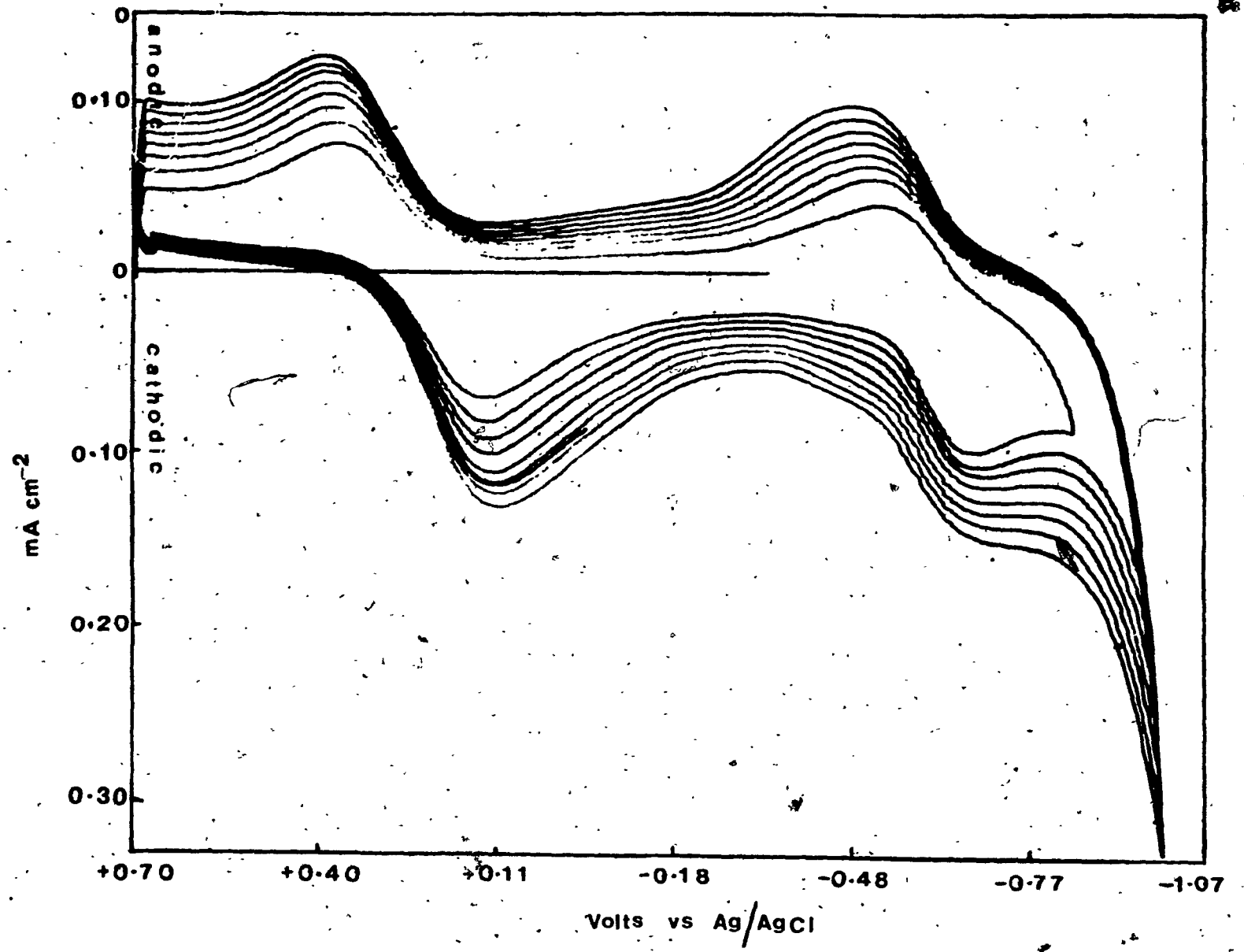

Figure 5-4. Cyclic voltammetric waves at various scan rates (30 to 100 mV/sec) for Pt-QPVP-Ni$(mnt)_2^{2-}$ in contact with 0.1 M KCl aqueous electrolyte.

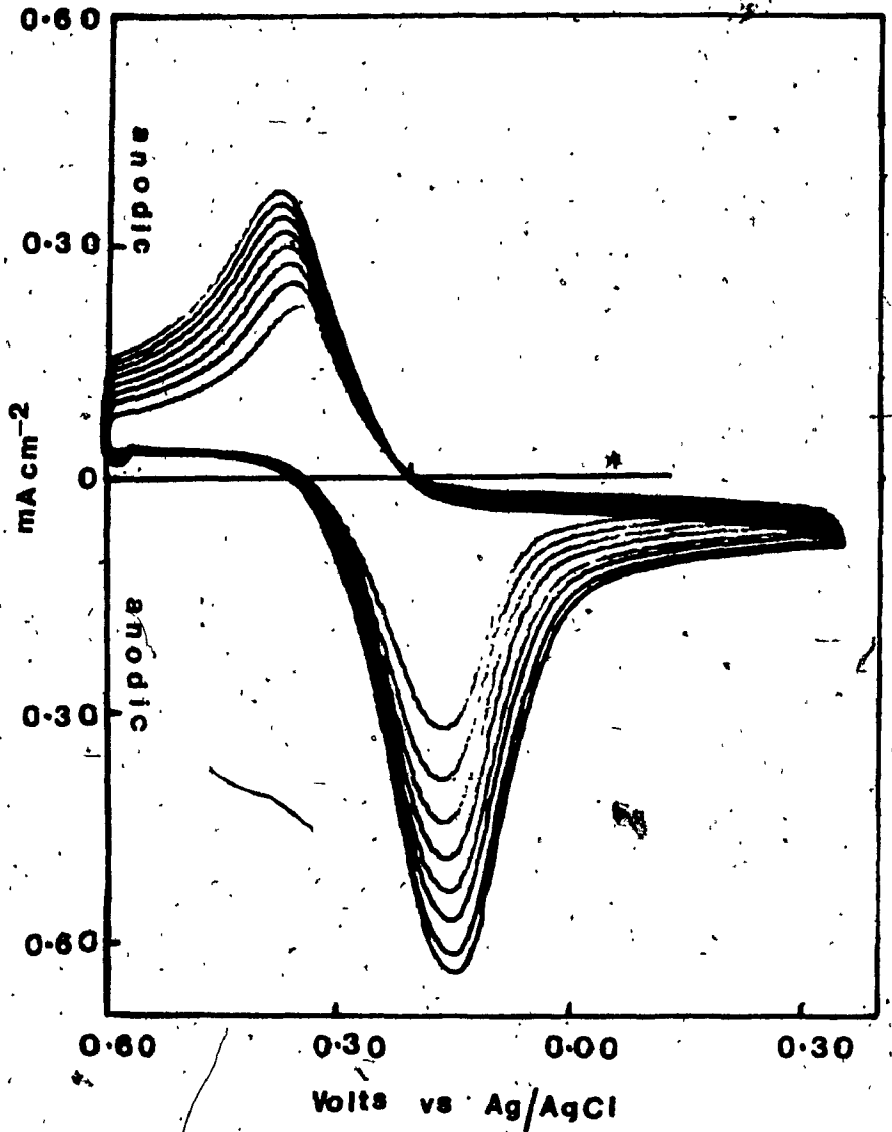

Figure 5-5 (a). Voltammetric surface waves at scan rates 30 to 100 mV/sec for Electrode 1; Pt-PVP-Pt(mnt)$_2^{2-}$ in contact with 0.1 M aqueous electrolyte.

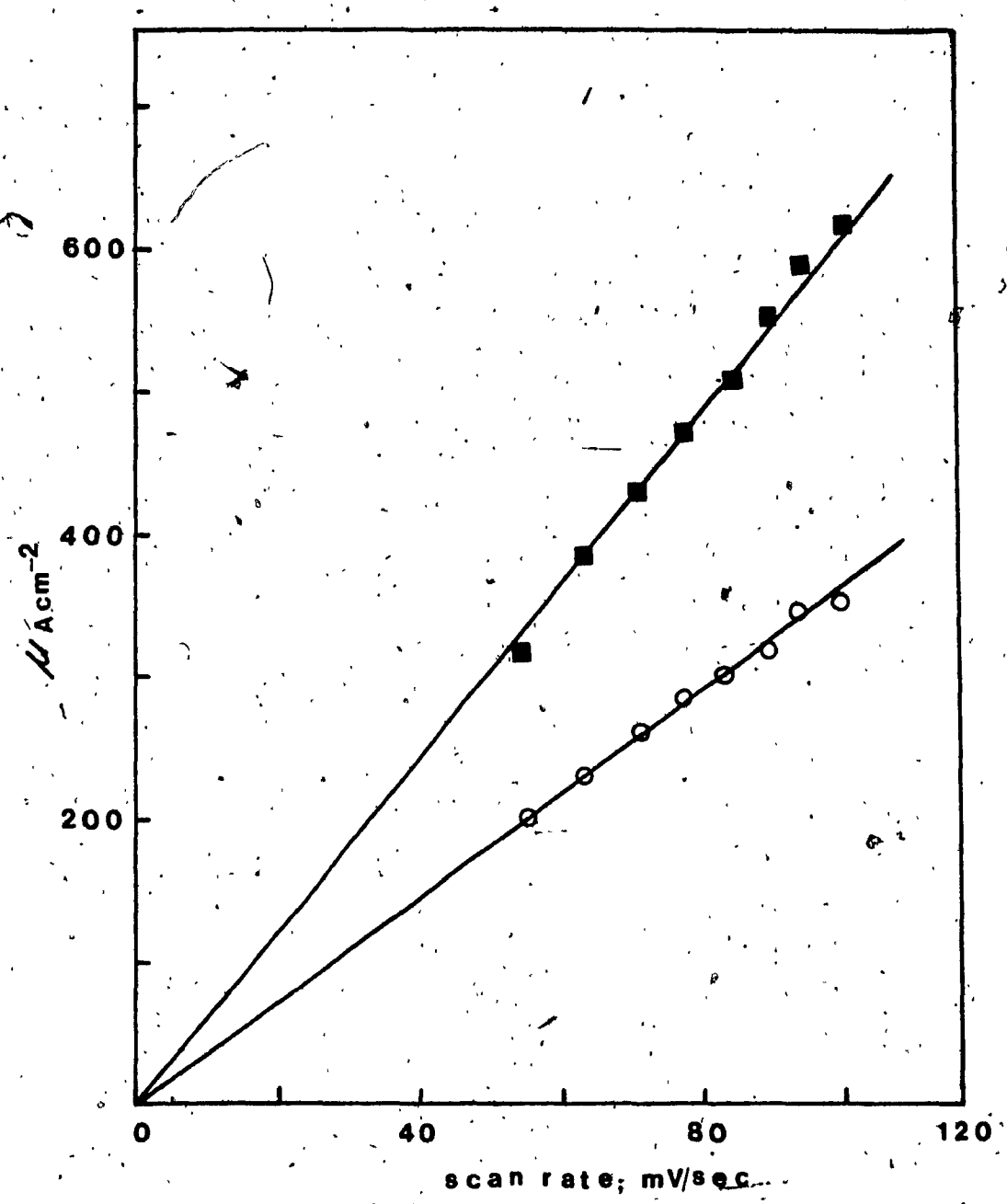

Figure 5-5 (b). Plots of cathodic (■) and anodic (O) peak currents vs $v^{\frac{1}{2}}$ (v = scan rate) for Electrode 1; Pt-QPVP-Ni(mnt)$_2^{2-}$.

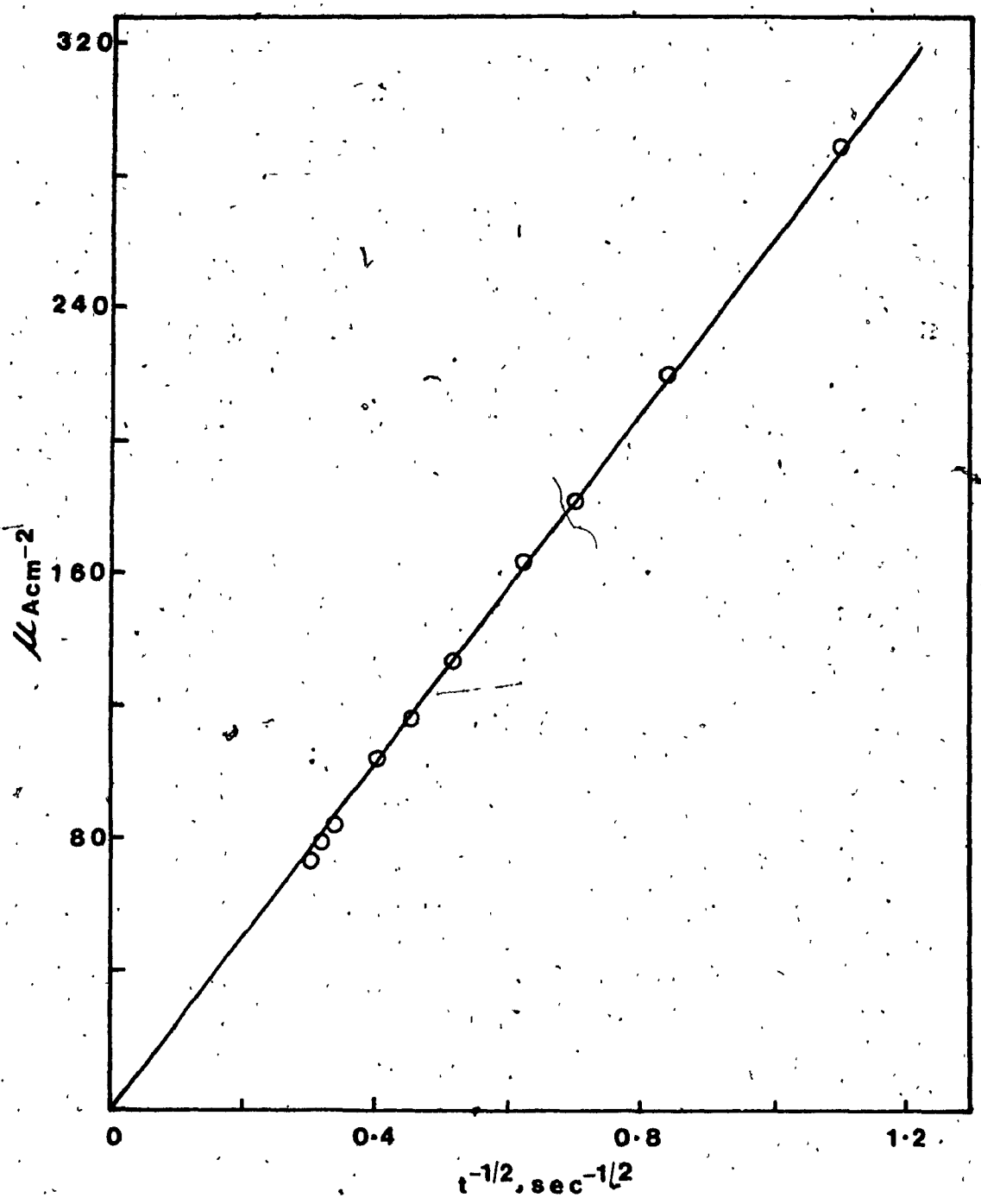

Figure 5-5 (c). Plot of anodic current vs $t^{-\frac{1}{2}}$ for Electrode 1; Pt-QPVP-Ni(mnt)$_2^{2-}$. Potential was stepped from -0.20 to +0.40 V.

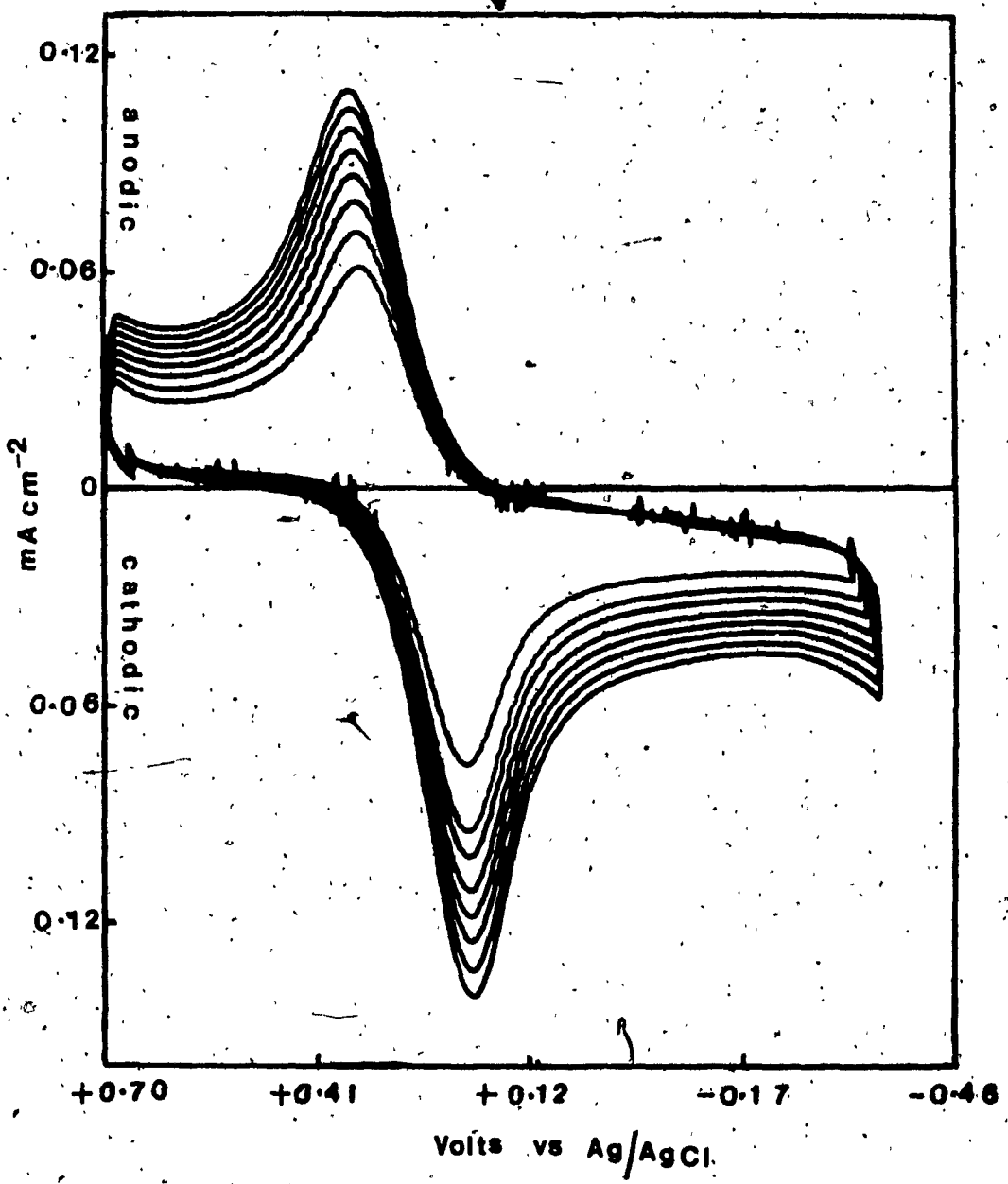

Figure 5-6 (a). Voltammetric surface waves at scan rates 30 to 100 mV/sec for electrode 2; Pt-QPVP-Ni(mnt)$_2^{2-}$ in contact with 0.1 M KCl aqueous electrolyte.

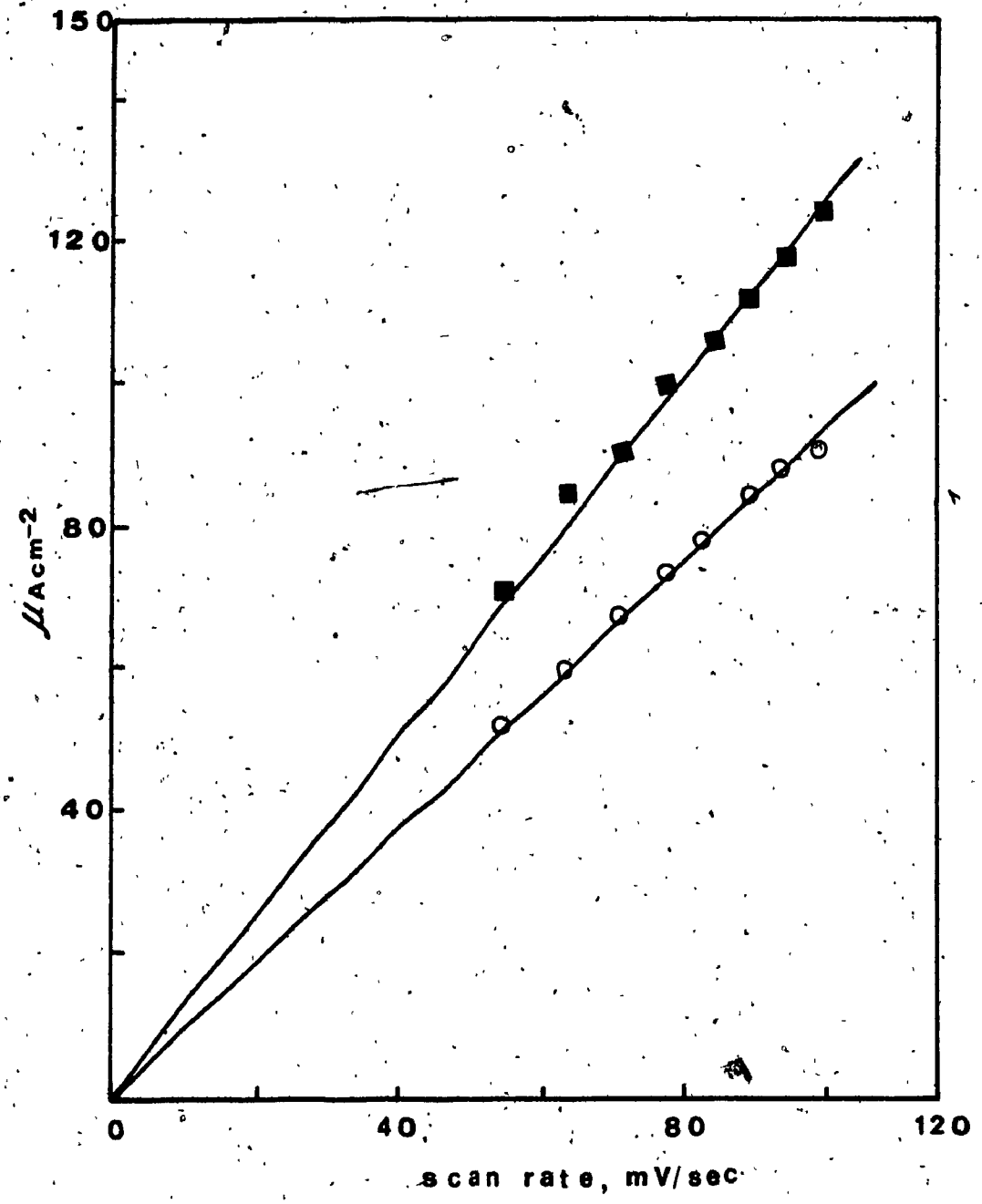

Figure 5-6 (b). Plots of cathodic (■) and anodic (O) peak currents vs $v^{\frac{1}{2}}$ (v = scan rate) for Electrode 2; Pt-QPVP-Pt$(mnt)_2^{2-}$.

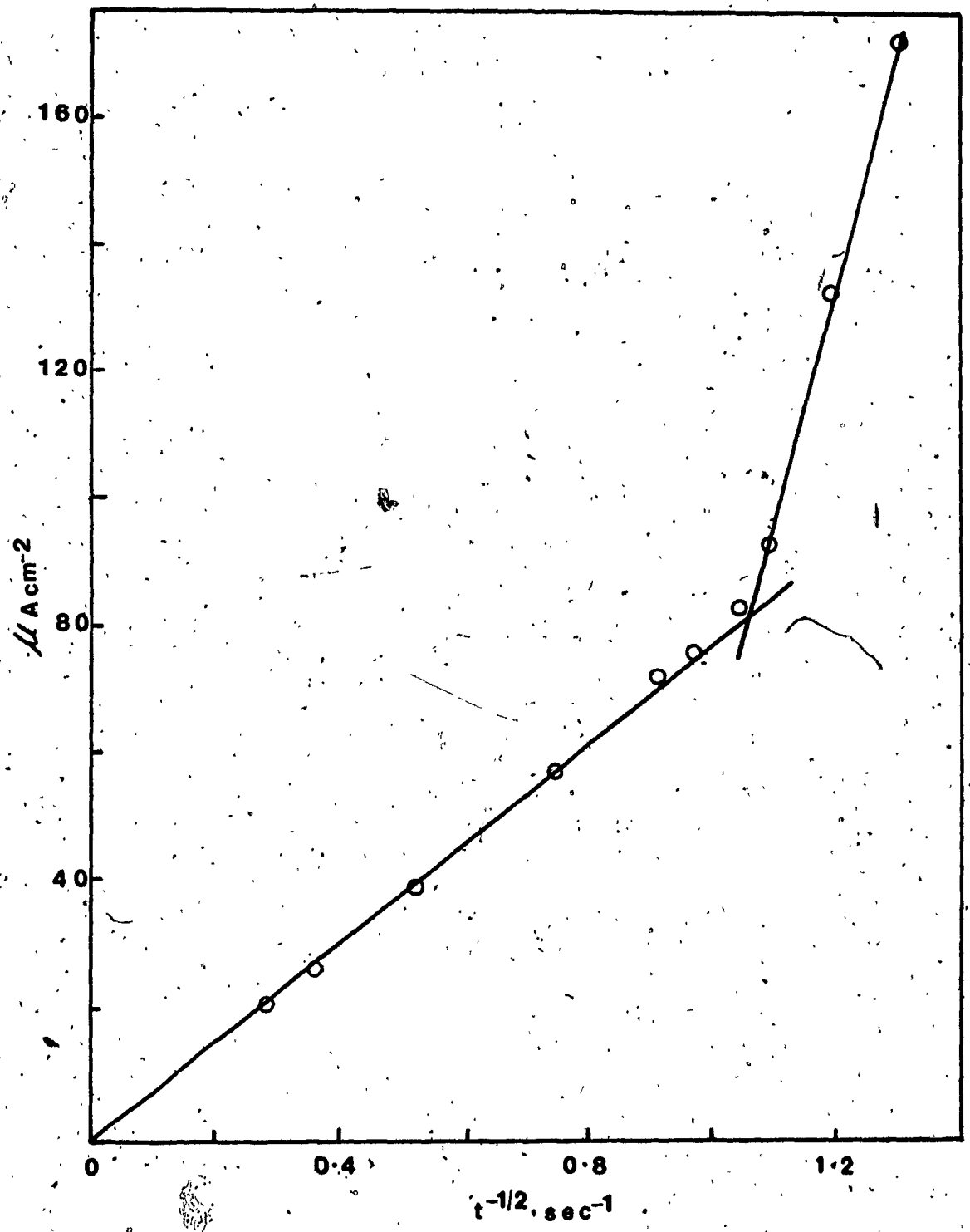

Figure 5-6 (c). Plot of anodic current vs $t^{-\frac{1}{2}}$ for Electrode 2, Pt-QPVP-Pt$(mnt)_2^{2-}$. Potential was stepped from -0.20 to +0.40 V.

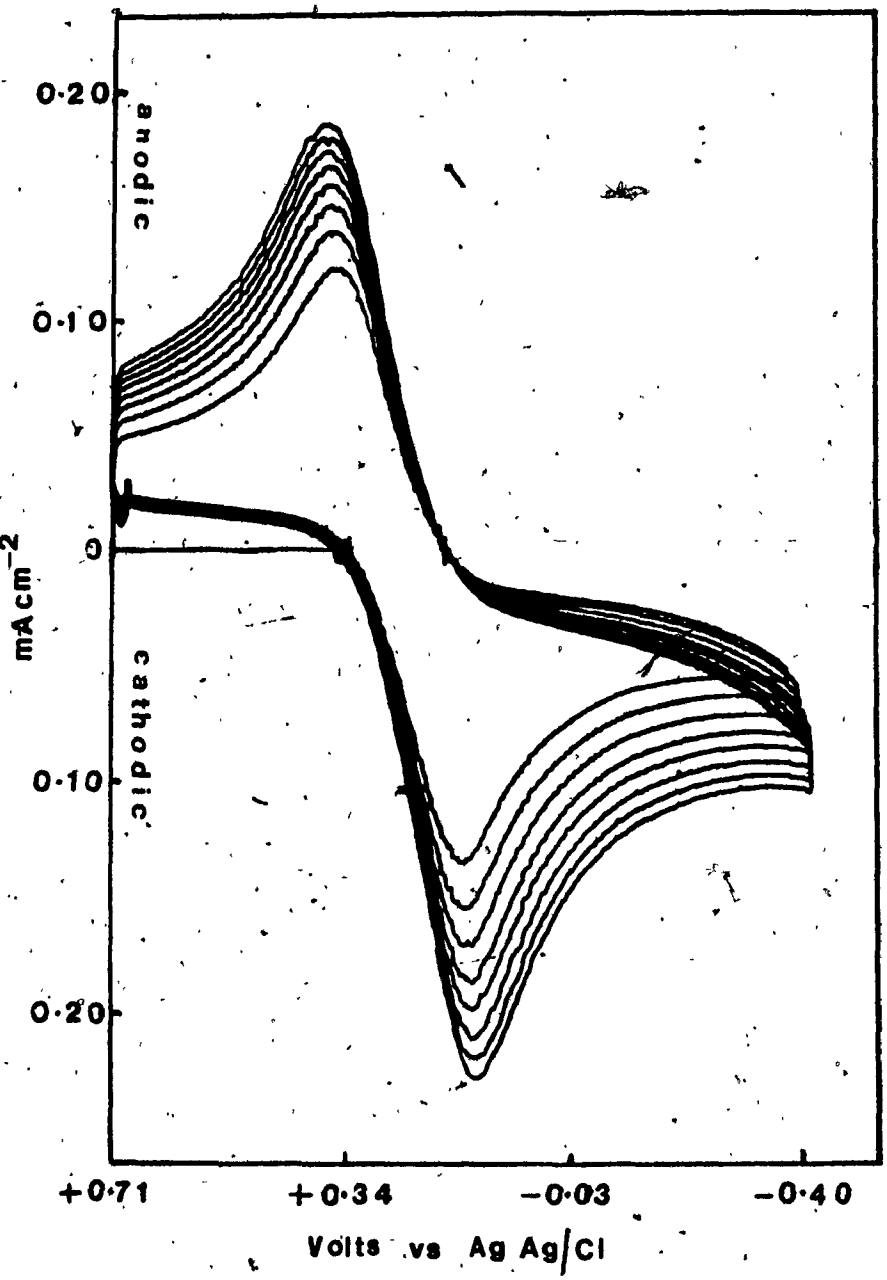

Figure 5-7 (a). Voltammetric surface waves at scan rates 30 to 100 mV/sec for Electrode 3; SnO_2-QPVP-Ni(mnt)$_2^{2-}$ in contact with 0.1 M KCl aqueous electrolyte.

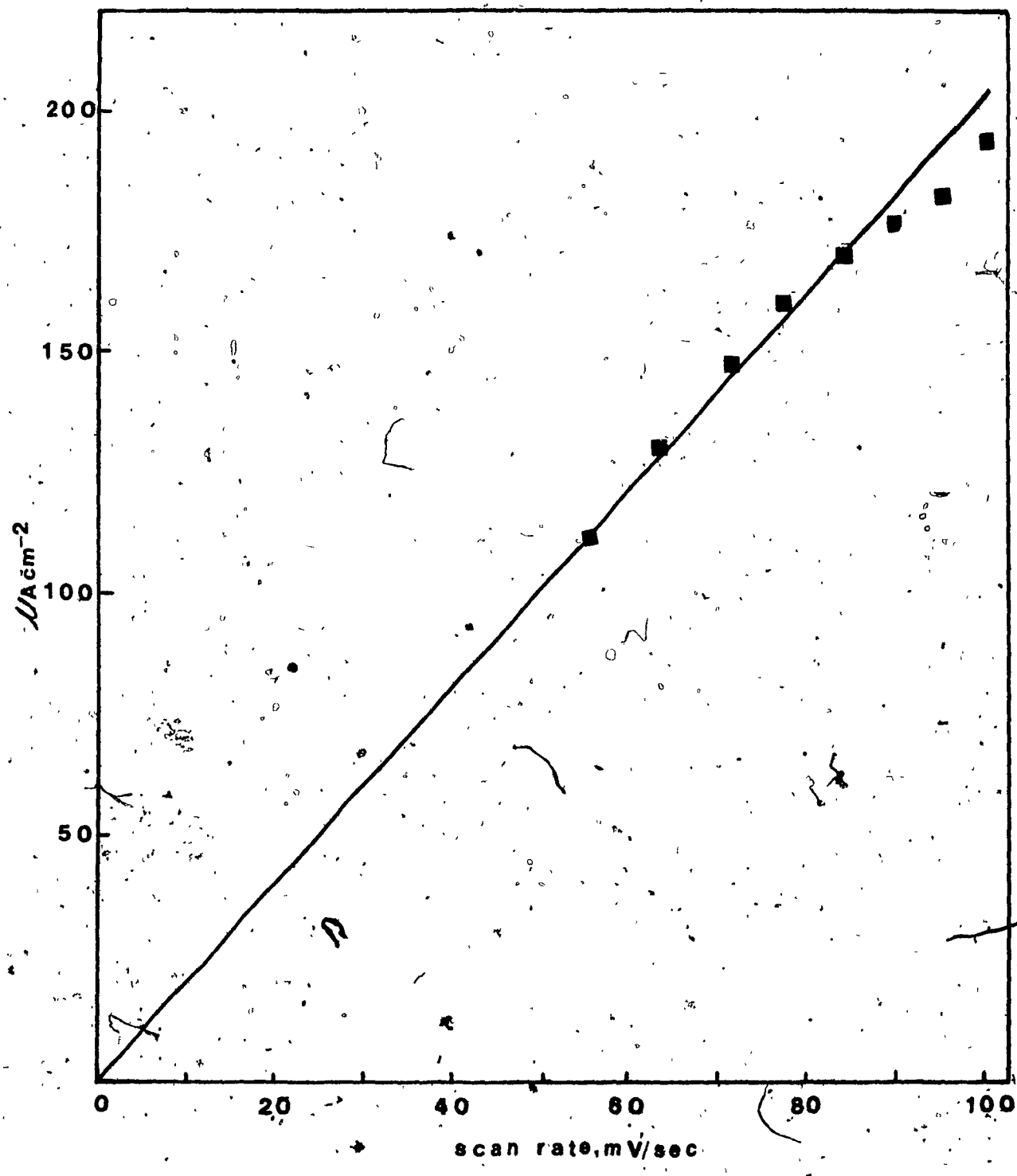

Figure 5-7 (b). Plot of cathodic peak current (■) vs $v^{\frac{1}{2}}$ (v = scan rate) for Electrode 3; SnO_2-QPVP-Ni(mnt)$_2^{2-}$.

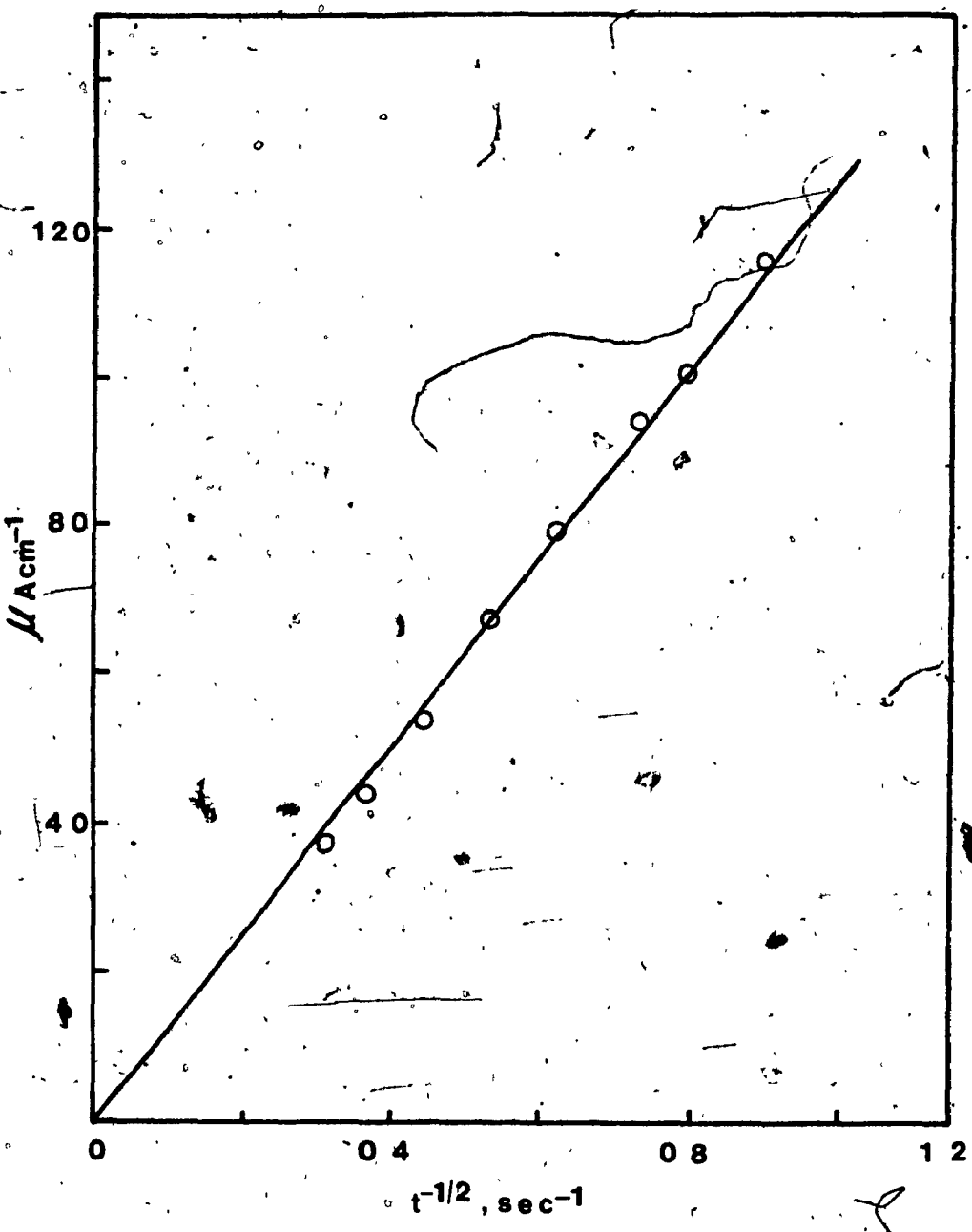

Figure 5-4 (c). Plot of anodic current vs $t^{-\frac{1}{2}}$ for Electrode 3; SnO_2-QPVP-Ni(mnt)$_2^{2-}$ for Electrode 3; SnO_2-QPVP-Ni(mnt)$_2^{2-}$. Potential was stepped from -0.20 to +0.50 V.

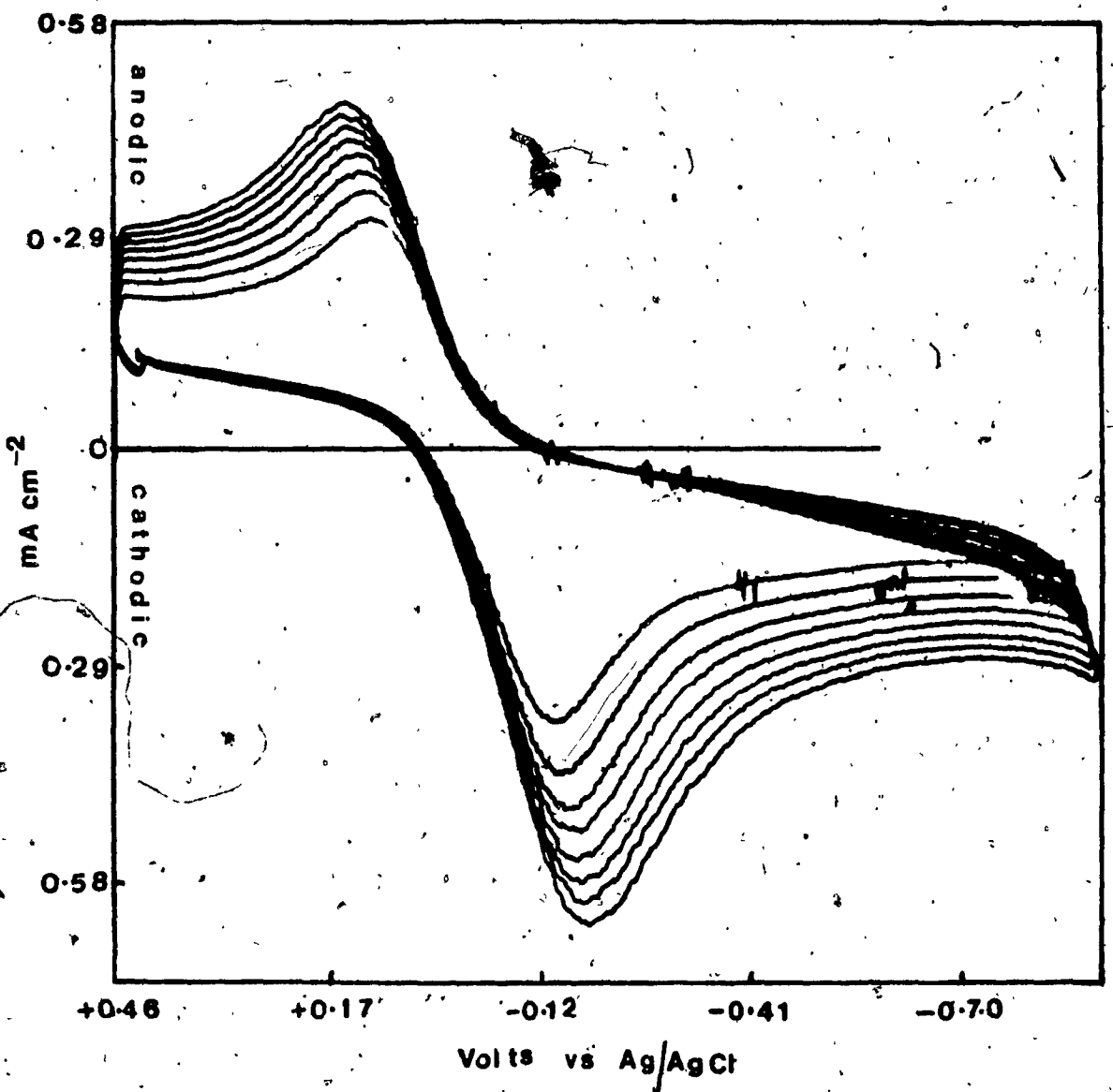

Figure 5-8 (a). Voltammetric surface waves at scan rates 30 to 100 mV/sec for Electrode 4; SnO_2-QPVP-$Pt(mnt)_2^{2-}$ in contact with 0.1 M KCl aqueous electrolyte.

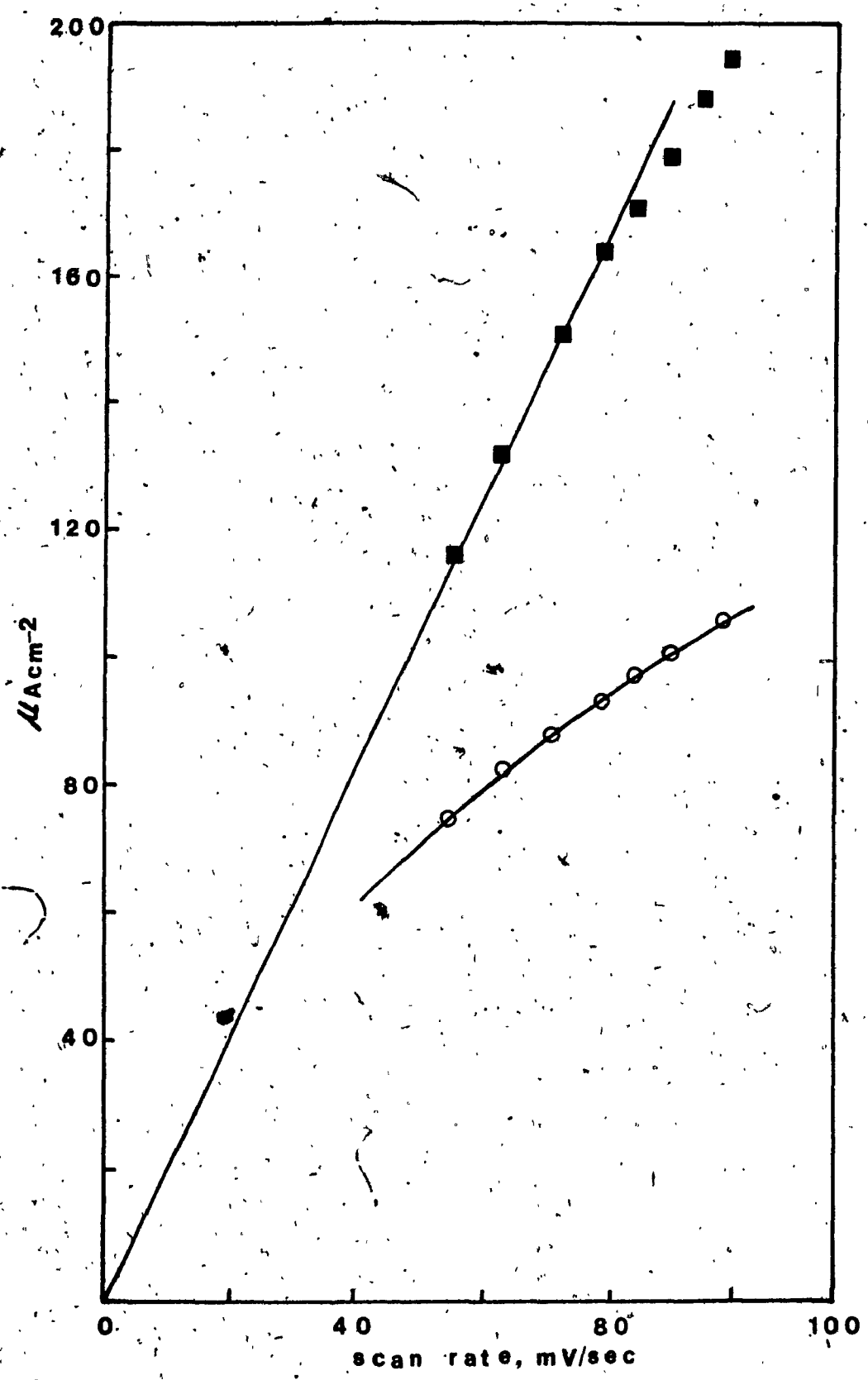

Figure 5-8 (b). Plots of cathodic (■) and anodic (○) peak currents vs $v^{\frac{1}{2}}$ (v = scan rate) for Electrode 4; SnO_2-QPVP-Pt$(mnt)_2^{2-}$.

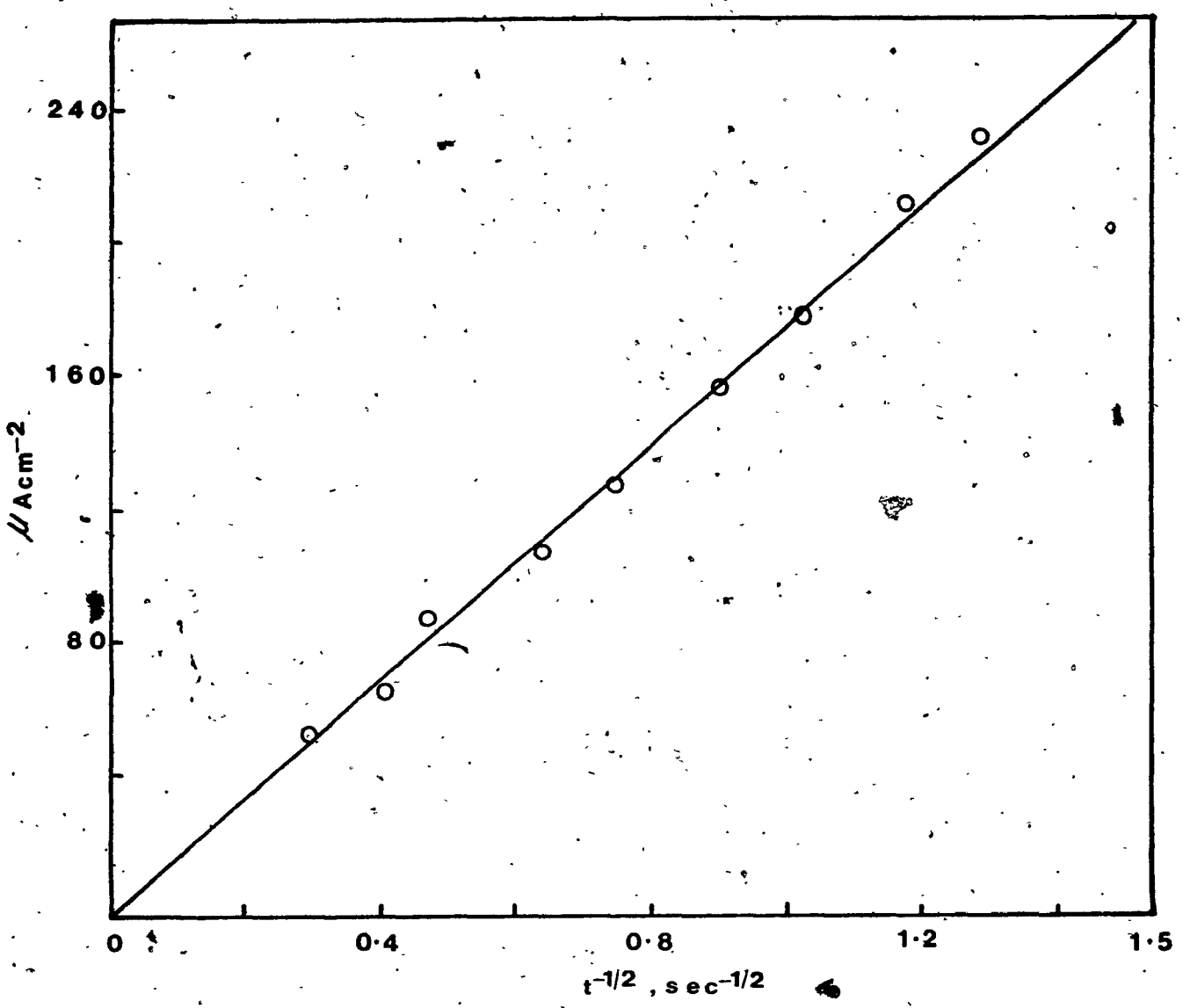

Figure 5-8 (c). Plot of anodic current vs $t^{-\frac{1}{2}}$ for Electrode 4; SnO_2-QPVP-Pt$(mnt)_2^{2-}$. Potential was stepped from -0.20 to +0.50 V.

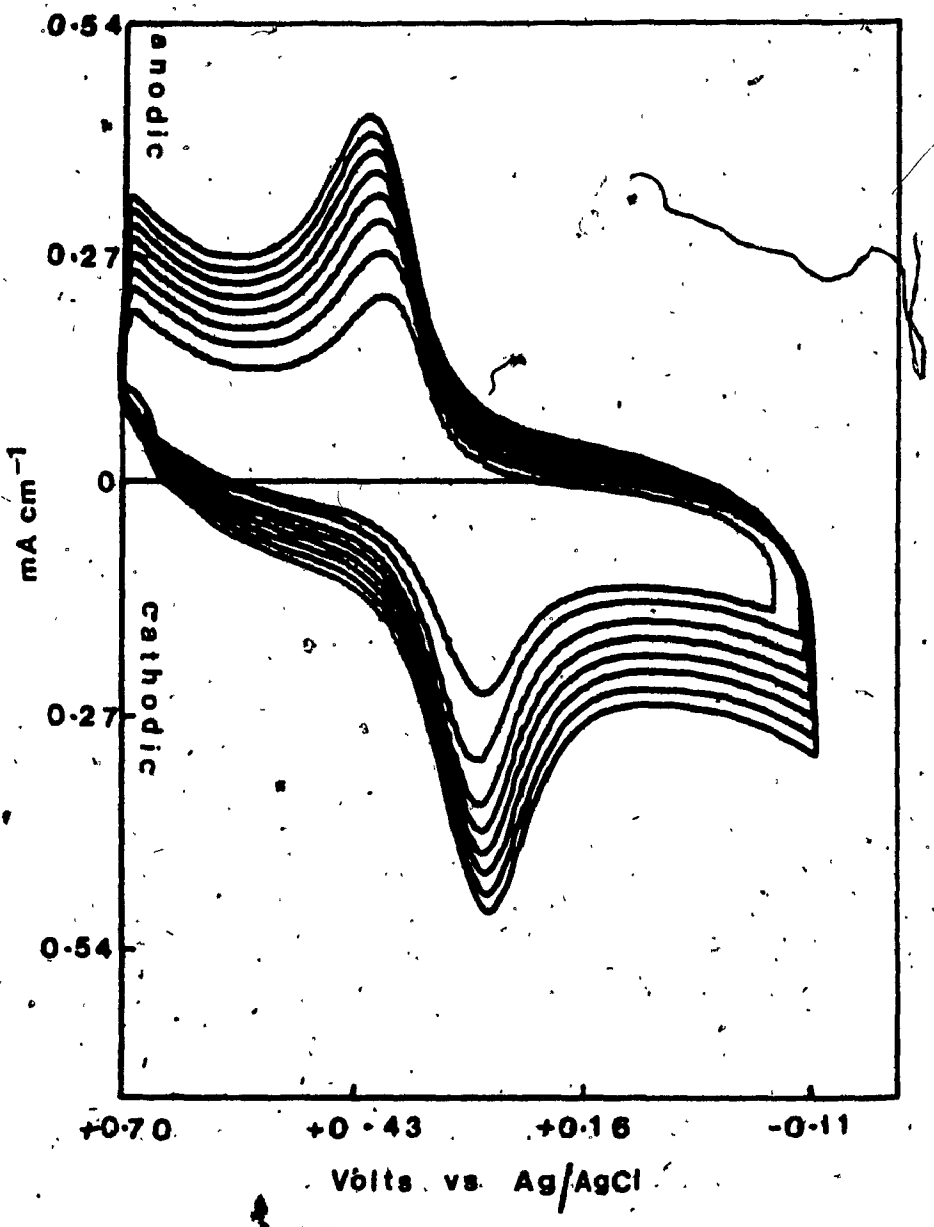

Figure 5-9 (a). Voltammetric surface waves at scan rates 30 to 100 mV/sec for Electrode 5; Pt-QPVP-Pt$(mnt)_2^{2-}$ in contact with 0.1 M KCl aqueous electrolyte.

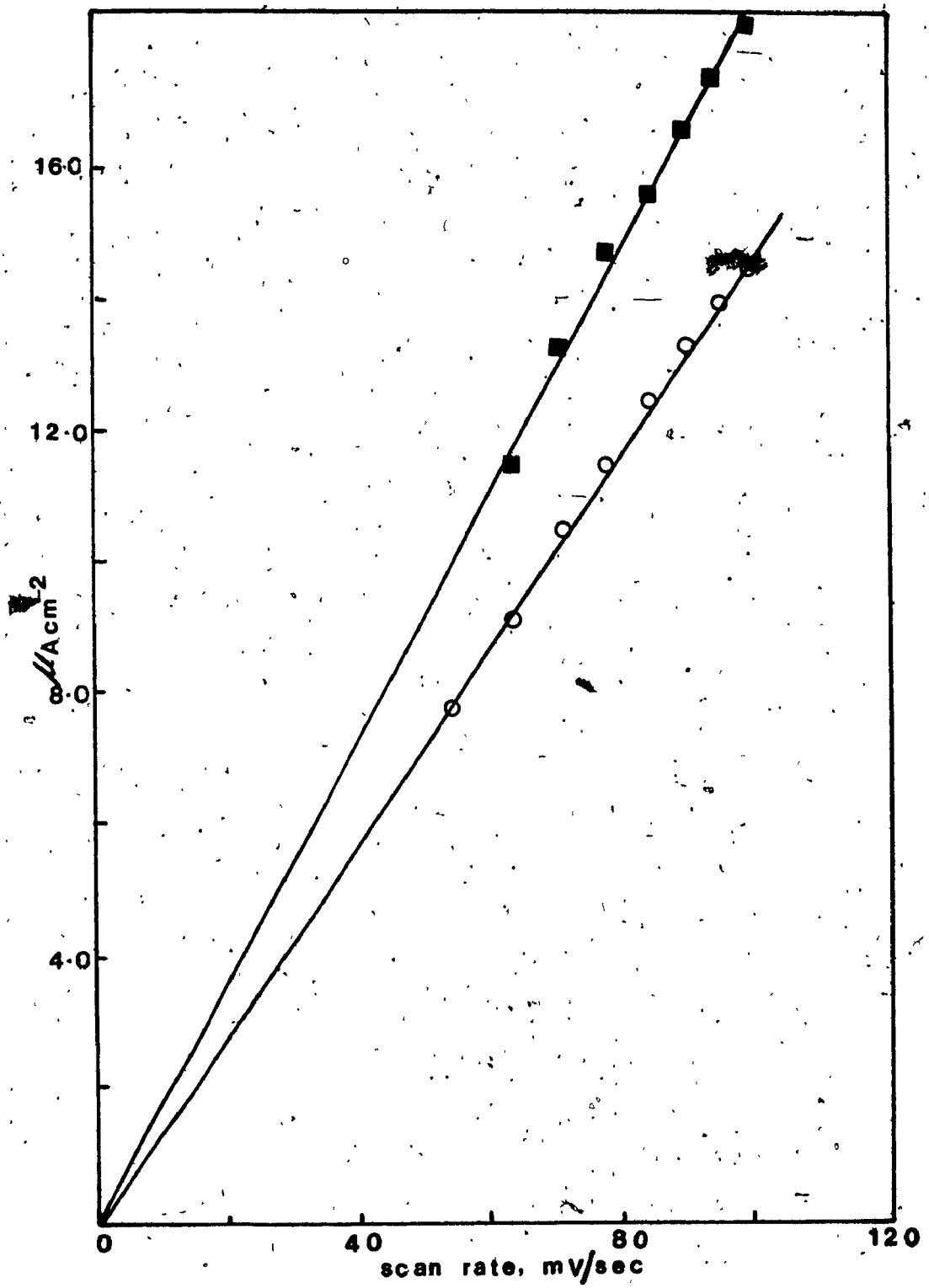

Figure 5-9 (b). Plots of cathodic (■) and anodic (O) peak currents vs $v^{\frac{1}{2}}$ (v = scan rates) for Electrode 5; Pt-QPVP-Pt$(mnt)_2^{2-}$.

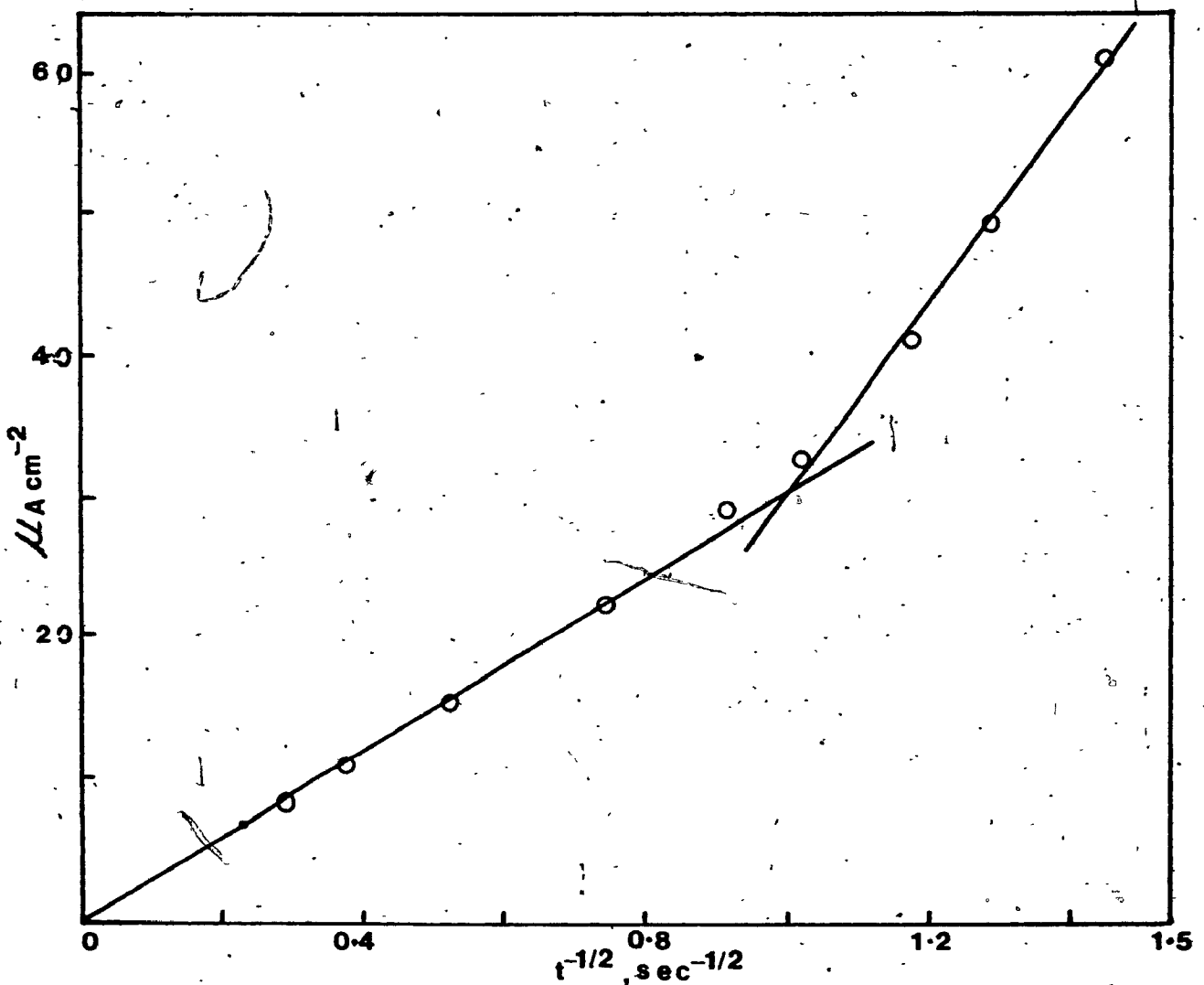

Figure 5-9 (c). Plot of anodic current vs $t^{-\frac{1}{2}}$ for Electrode 5; Pt-QPVP-Pt$(mnt)_2^{2-}$. Potential was stepped from -0.20 to +0.40 V.

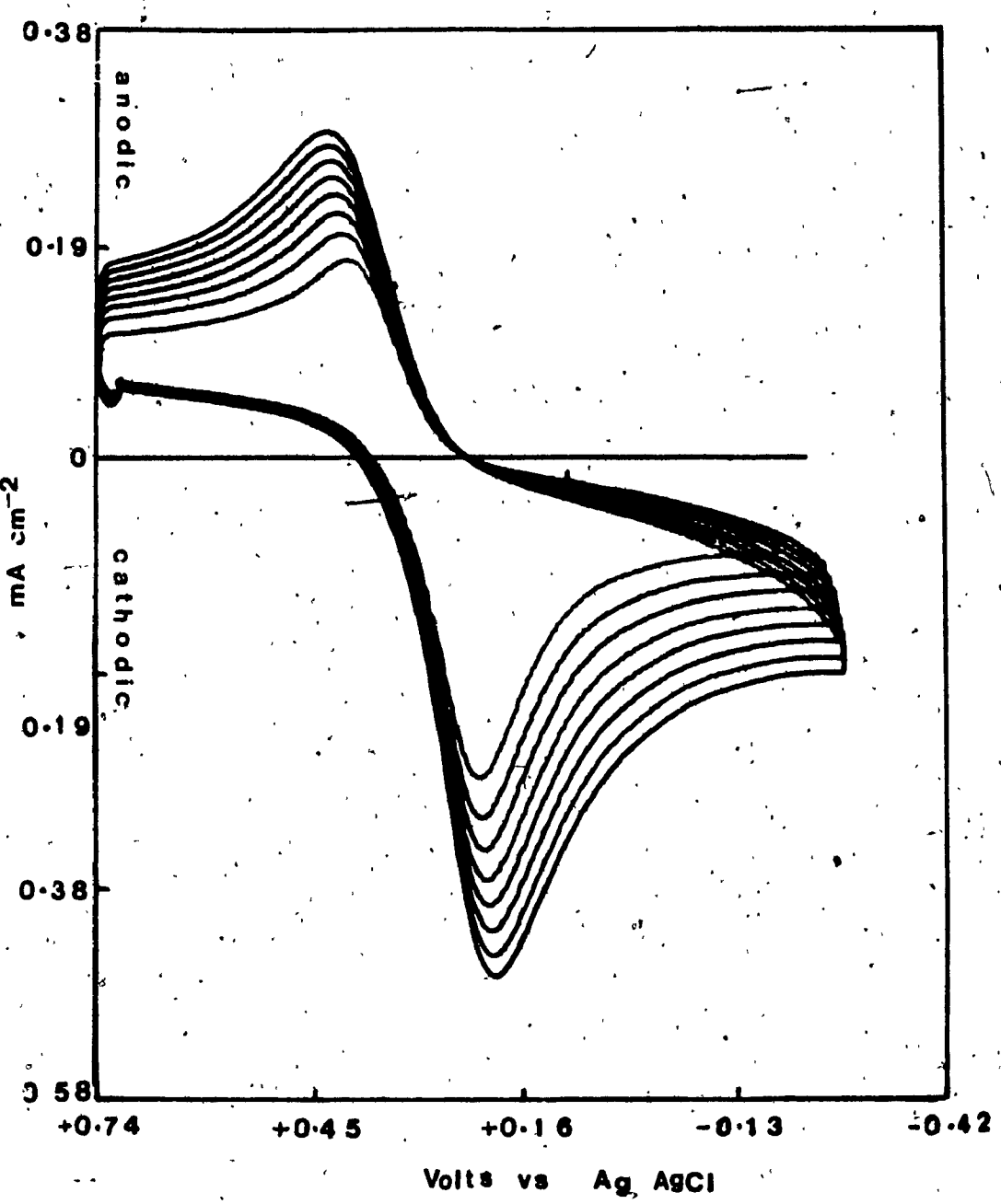

Figure 5-10 (a). Voltammetric surface waves at scan rates 30 to 100 mV/sec for Electrode 6; SnO_2-QPVP-Ni(mnt)$_2^{2-}$ in contact with 0.1 M KCl aqueous electrolyte.

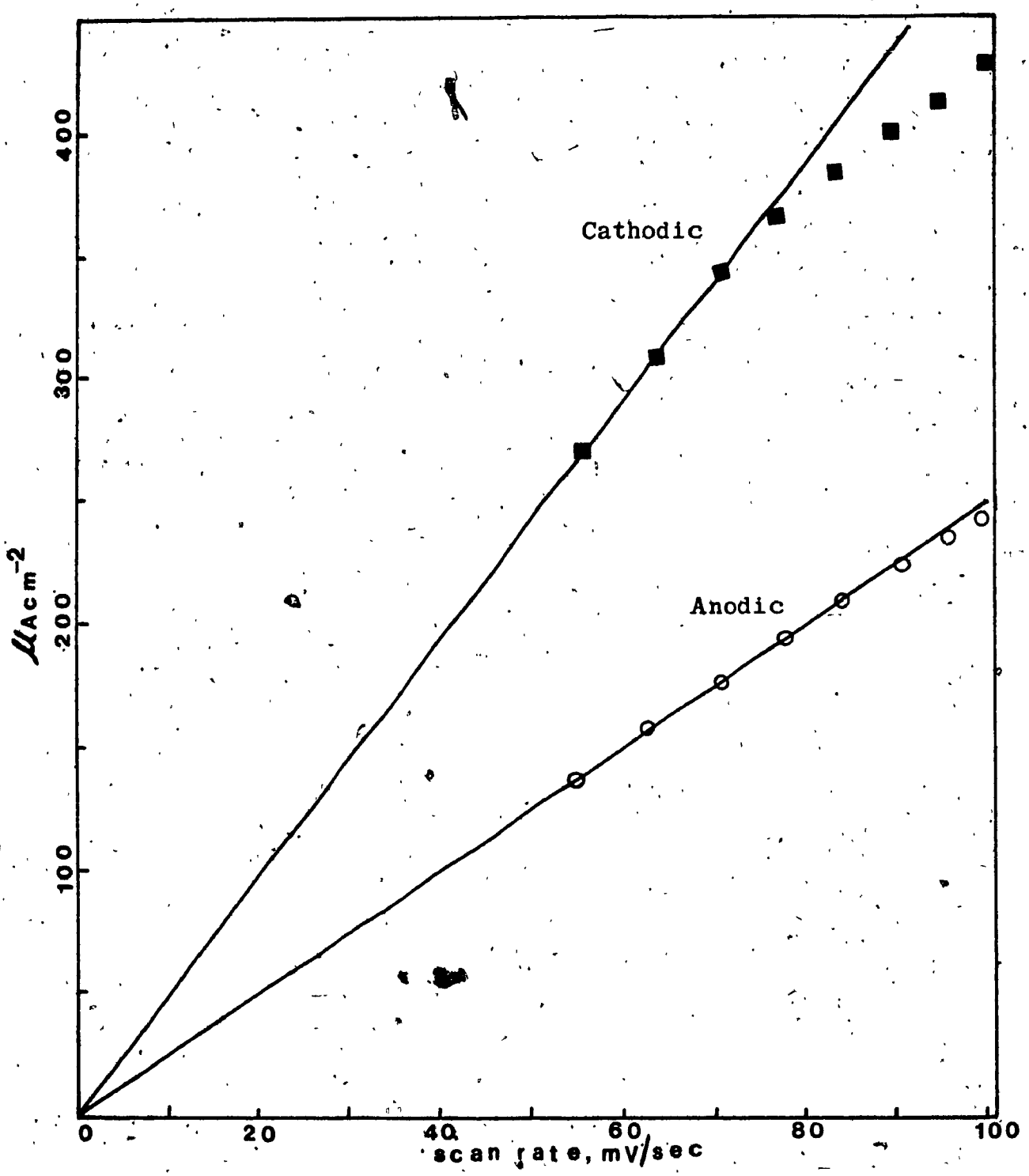

Figure 5-10 (b). Plots of cathodic (■) and anodic (O) peak currents vs $v^{\frac{1}{2}}$ (v = scan rate) for Electrode 6; SnO_2-QPVP-Ni(mnt)$_2^{2-}$.

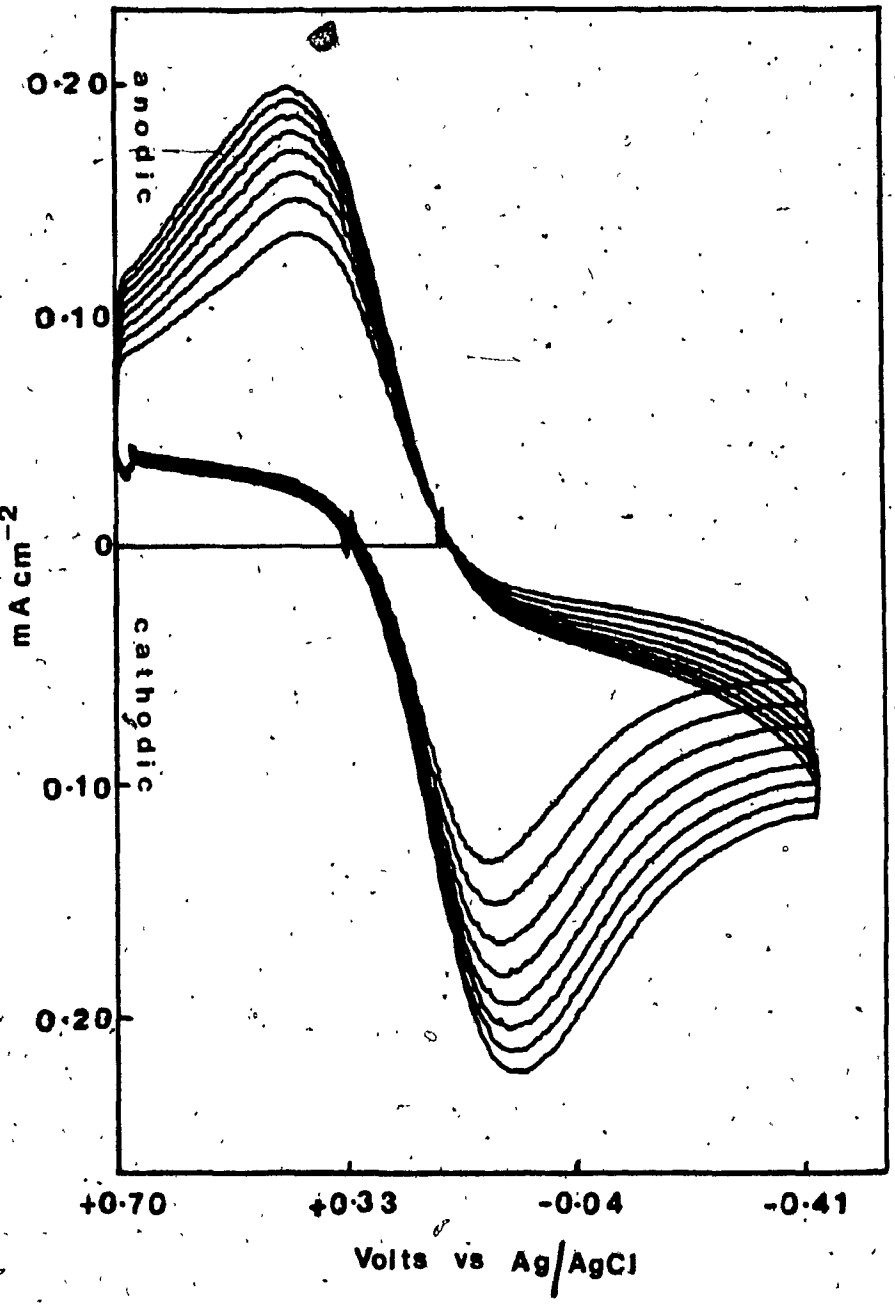

Figure 5-11 (a). Voltammetric surface waves at scan rates 30 to 100 mV/sec for Electrode 7; SnO_2-QPVP-$Ni(mnt)_2^{2-}$ in contact with 0.1 M KCl electrolyte.

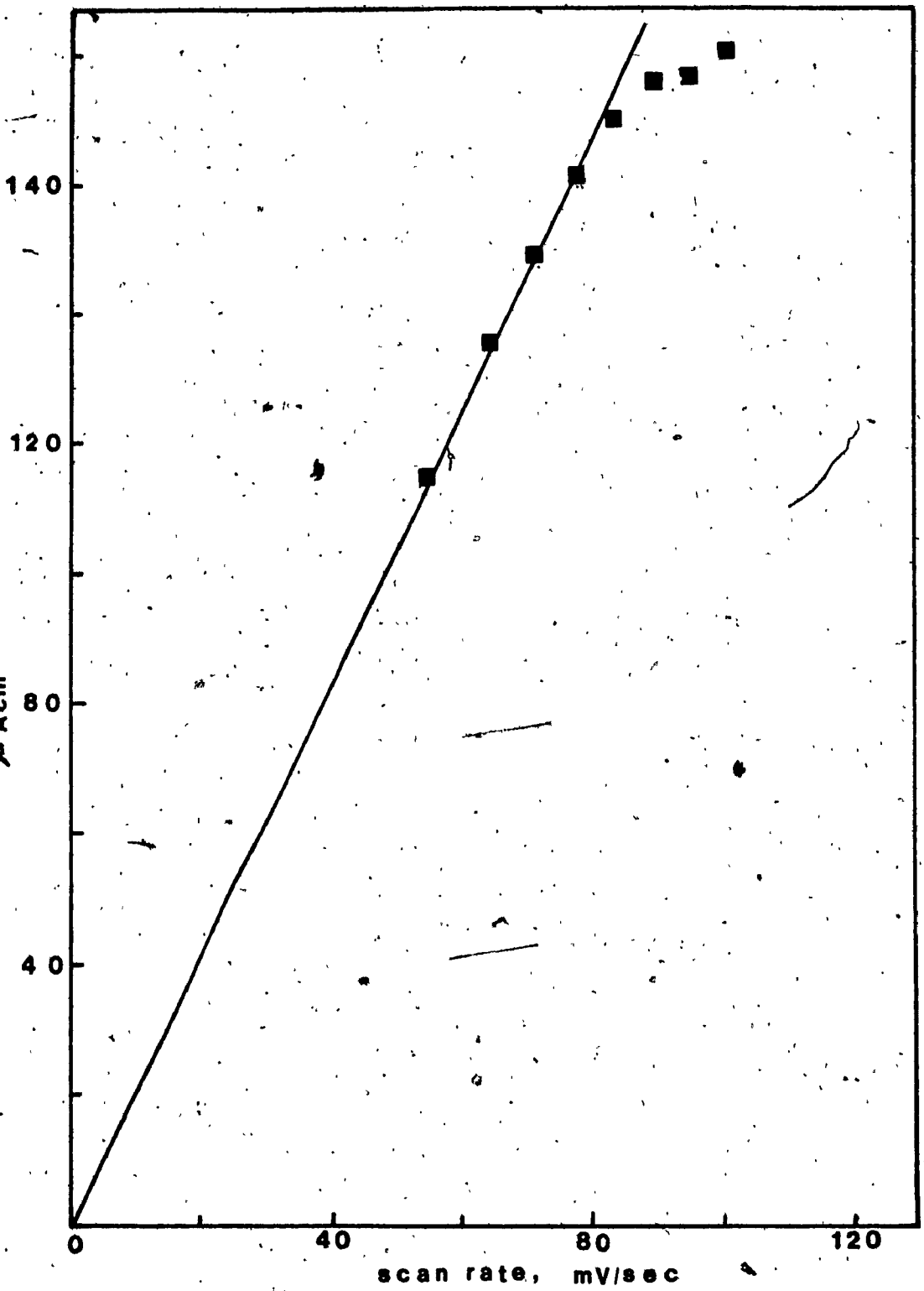

Figure 5-11 (b). Plots of cathodic (■) peak currents vs $v^{\frac{1}{2}}$ (v = scan rate) for Electrode 7; SnO_2-QPVP-Ni(mnt)$_2^{2-}$.

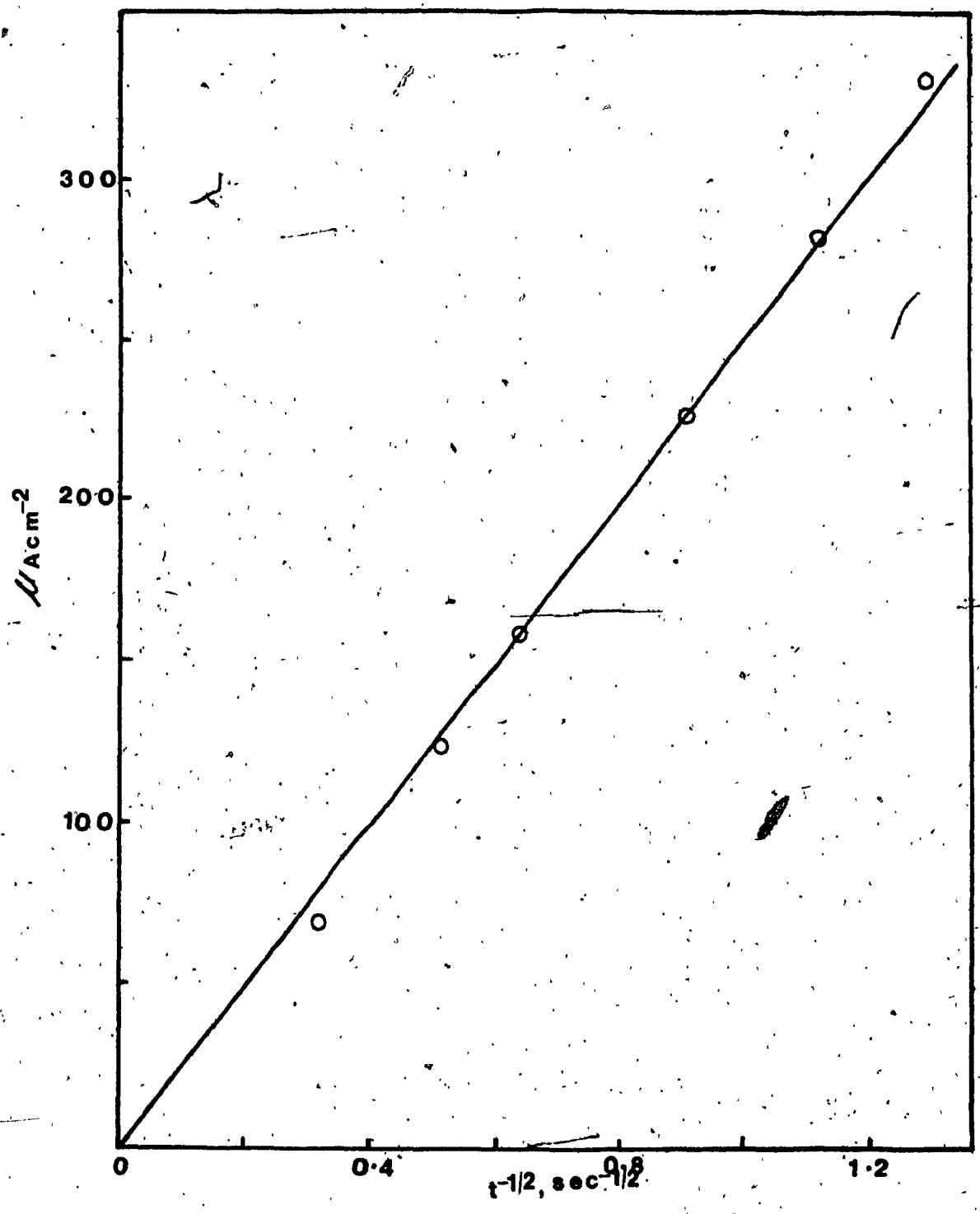

Figure 5-11 (c). Plot of anodic current vs $t^{-\frac{1}{2}}$ for Electrode 7; SnO_2-QPVP-Ni(mnt)$_2^{2-}$. Potential was stepped from -0.20 to +0.50 V.

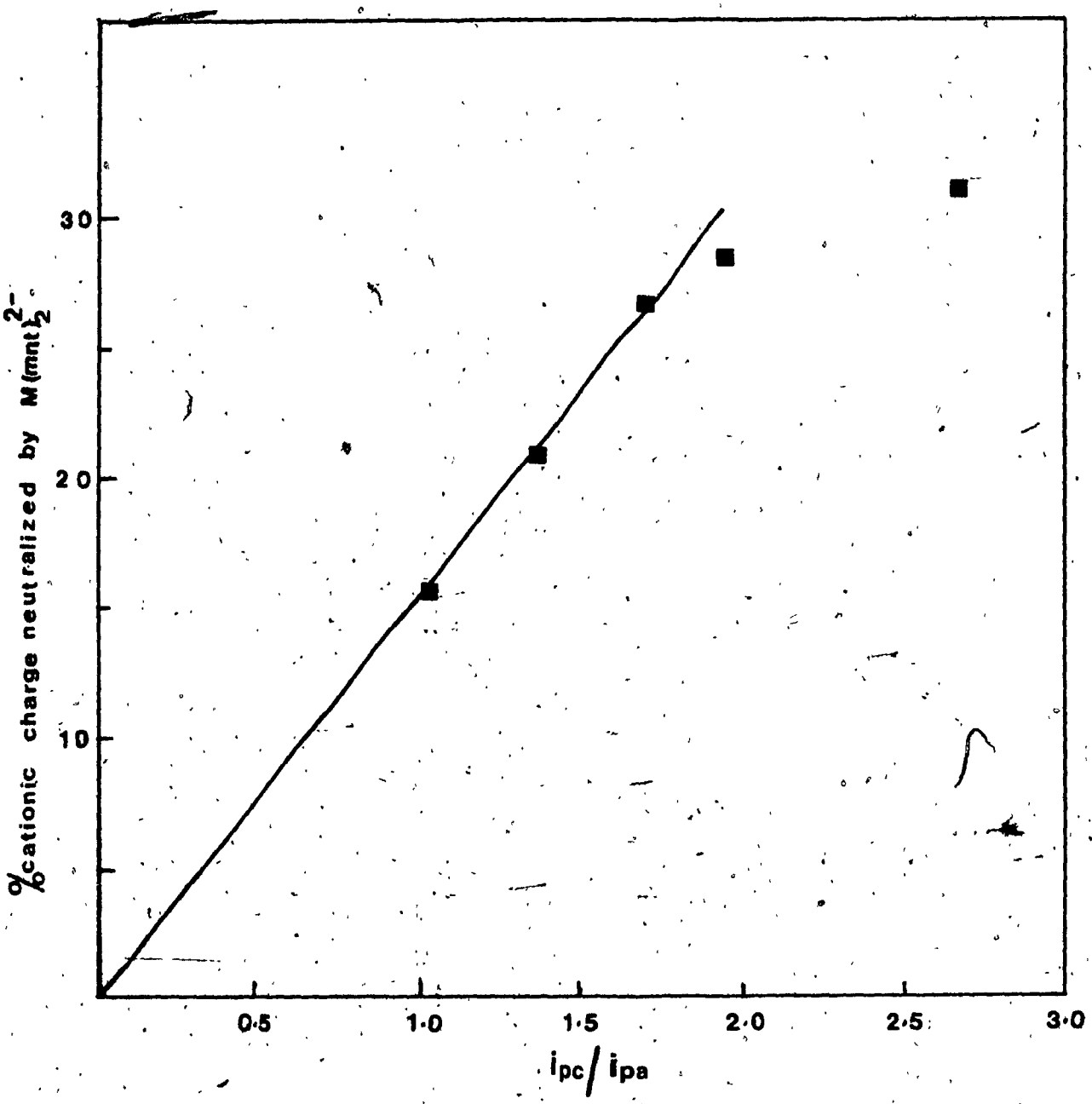

Figure 5-12. Plot of percentage cationic charge of QPVP polymer film neutralized by $M(mnt)_2^{2-}$; M = Pt and Ni vs ratio of cathodic to anodic peak current (i_{pc}/i_{pa}).

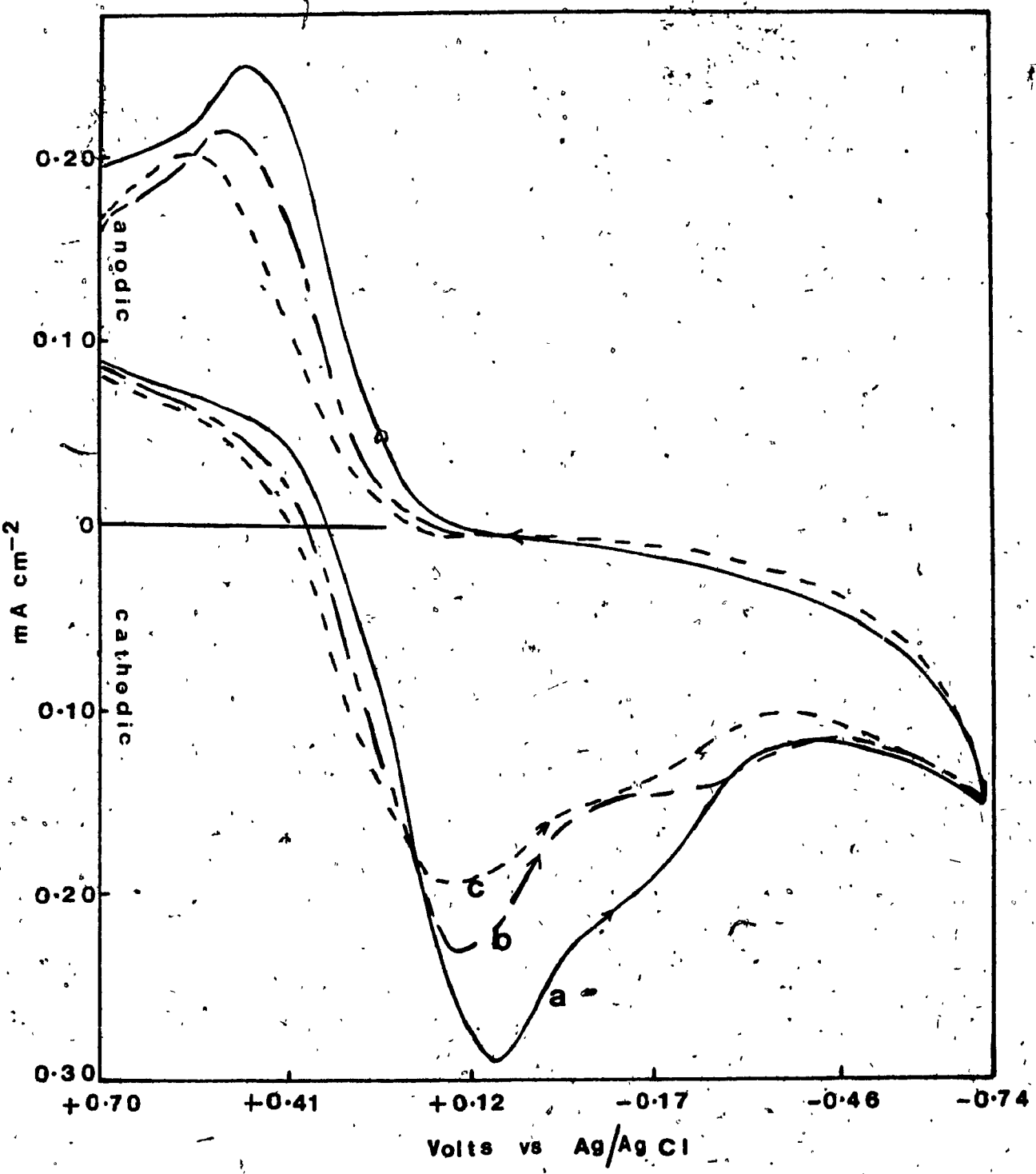

Figure 5-13. Cyclic voltammetric waves at 30 mV/sec for SnO_2-QPVP-Ni$(mnt)_2^{2-}$ in contact with 0.1 M NaBr (a), 0.1 M NaCl (b) and 0.1 M NaF (c) aqueous electrolytes.

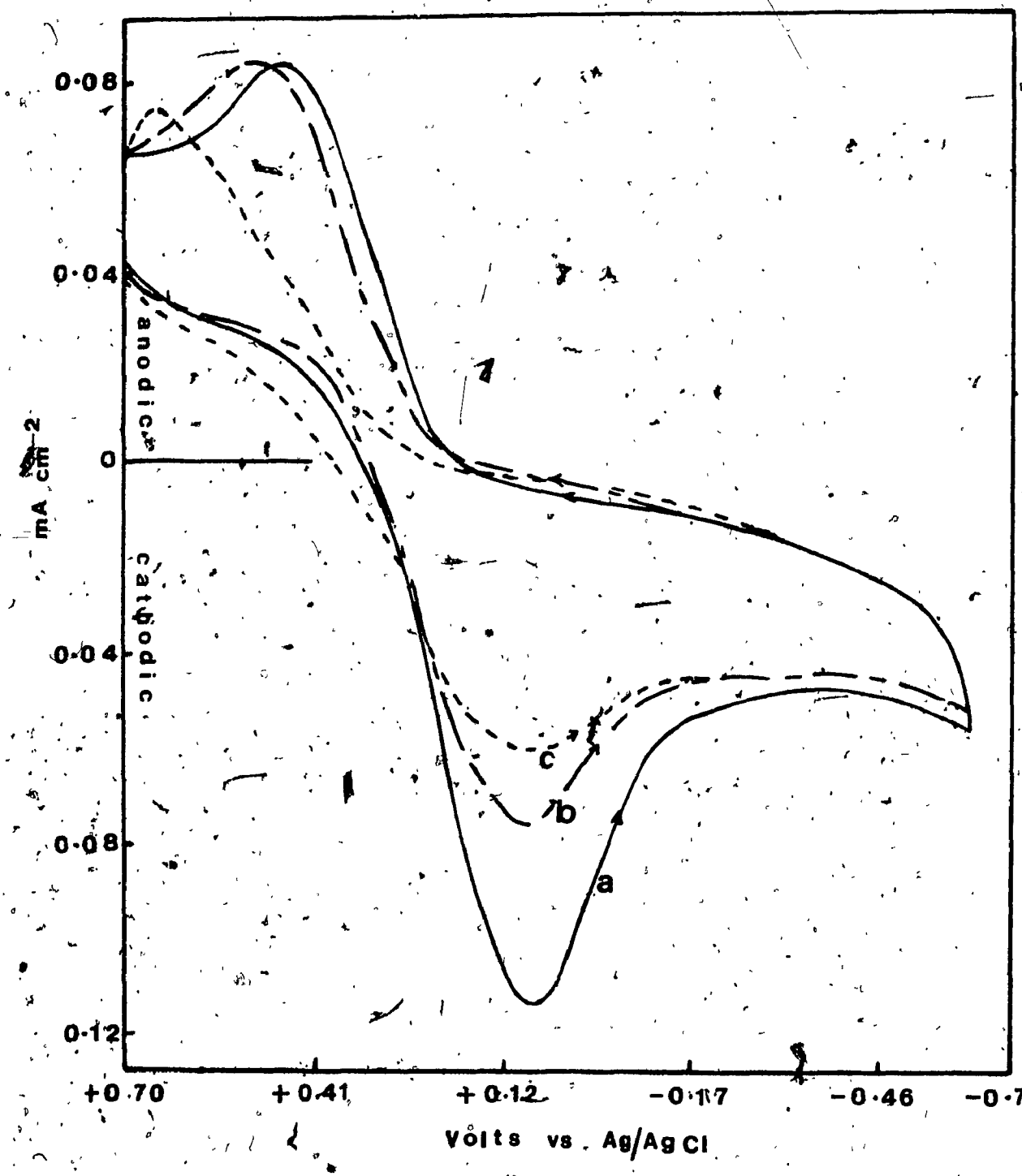

Figure 5-14. Cyclic voltammetric waves at 30 mV/sec for SnO_2-QPVP-Pt$(mnt)_2^{2-}$ in contact with 0.1 M NaBr (a); 0.1 M NaCl (b) and 0.1 M NaF (c) aqueous electrolyte.

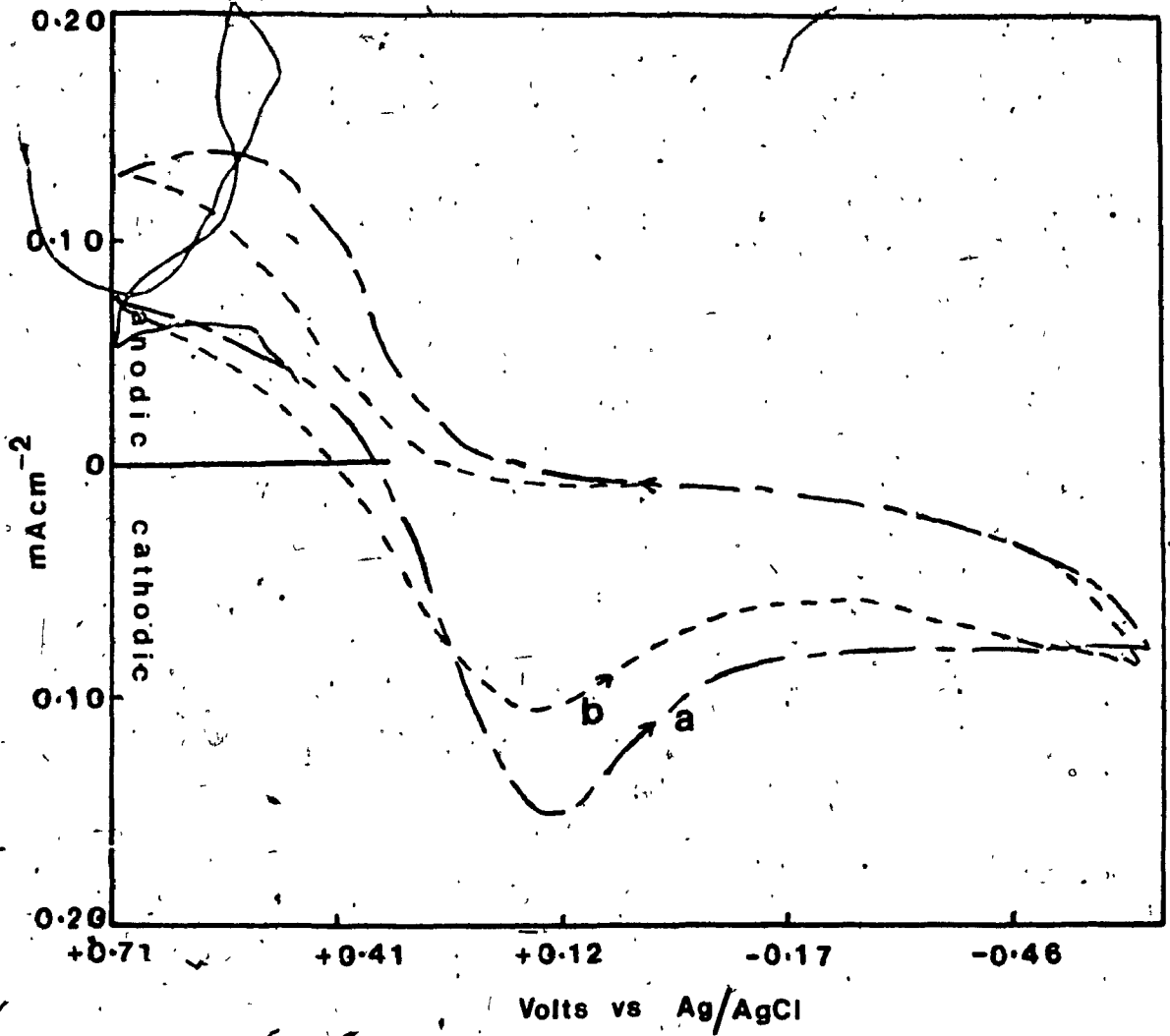

Figure 5-15. Cyclic voltammetric waves for SnO_2-QPVP-Ni(mnt)$_2^{2-}$ in contact with 0.1 M NaCl (a) and 0.1 M NaF (b) aqueous electrolytes after vacuum heating electrode at 35 ^{o}C for 12 hrs.

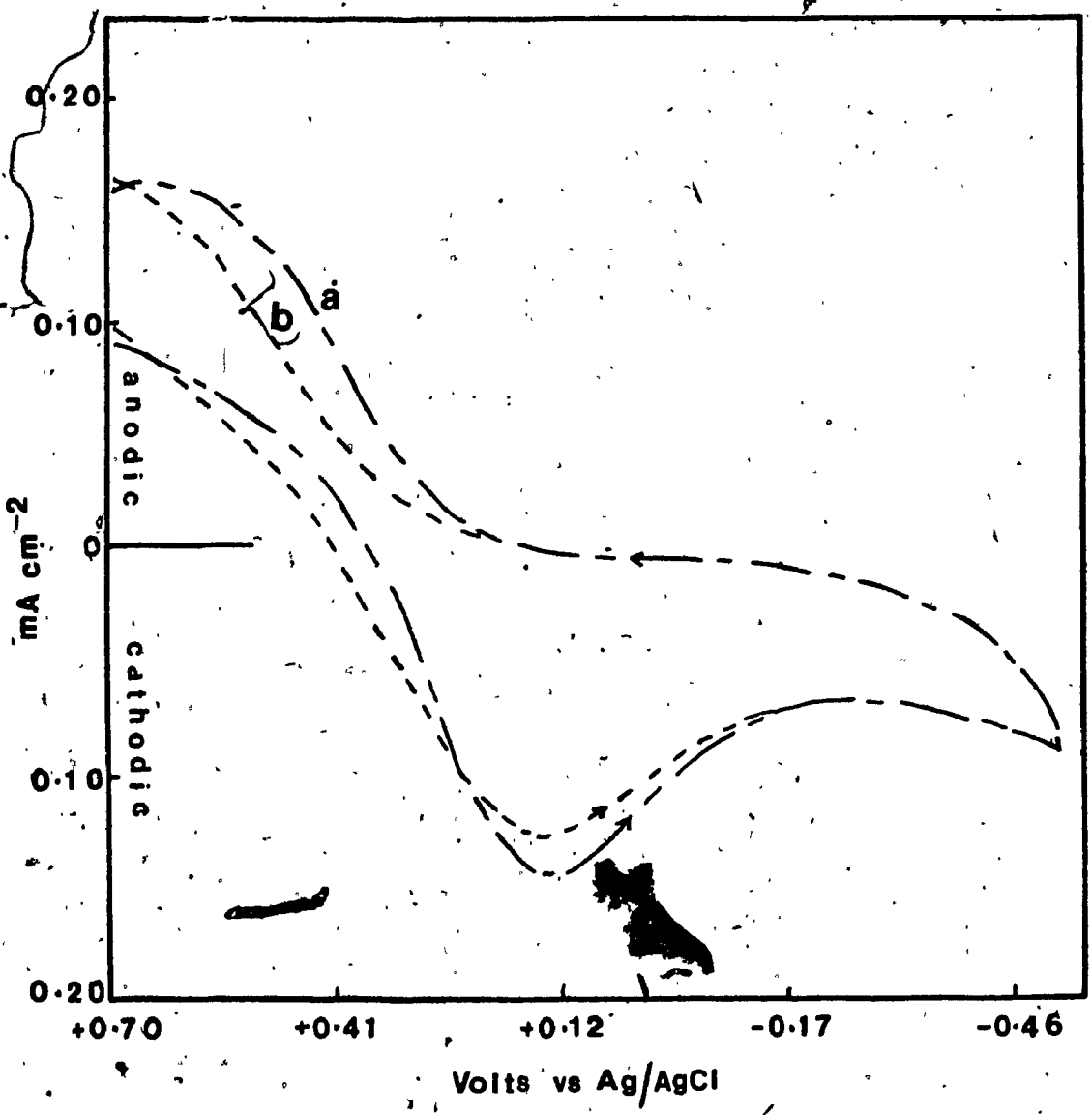

Figure 5-16. Cyclic voltammetric waves for SnO_2-QPVP-Ni(mnt)$_2^{2-}$ in contact with 0.1 M NaCl (a) and 0.1 M NaF (b) aqueous electrolytes after soaking electrode in water for 35 mins.

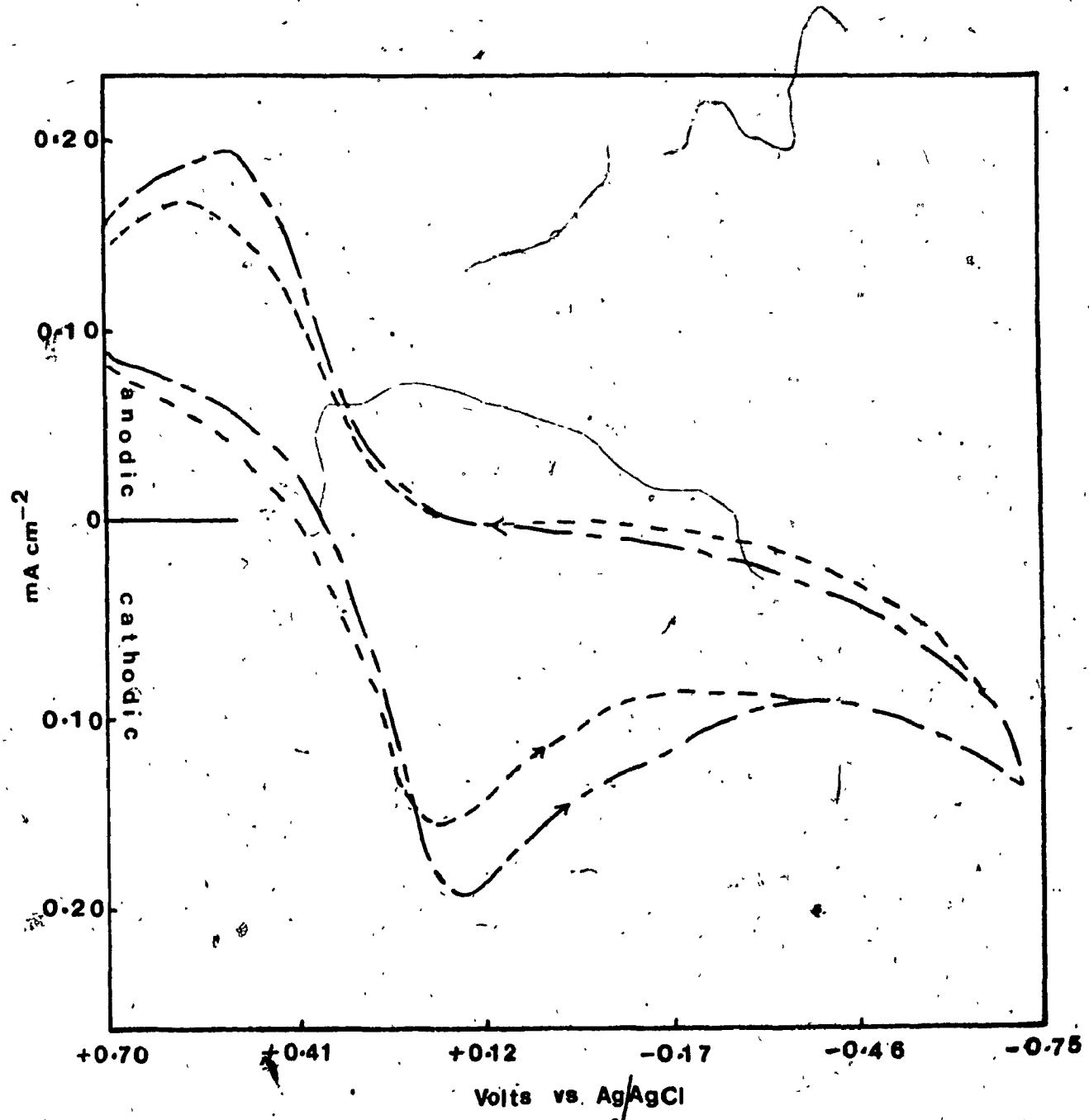

Figure 5-17. Cyclic voltammetric waves for SnO_2-QPVP-Ni(mnt)$_2^{2-}$ in contact with 0.1 M NaCl (a), and 0.1 M NaF (b) aqueous electrolytes after soaking electrode in methanol for 5 mins.

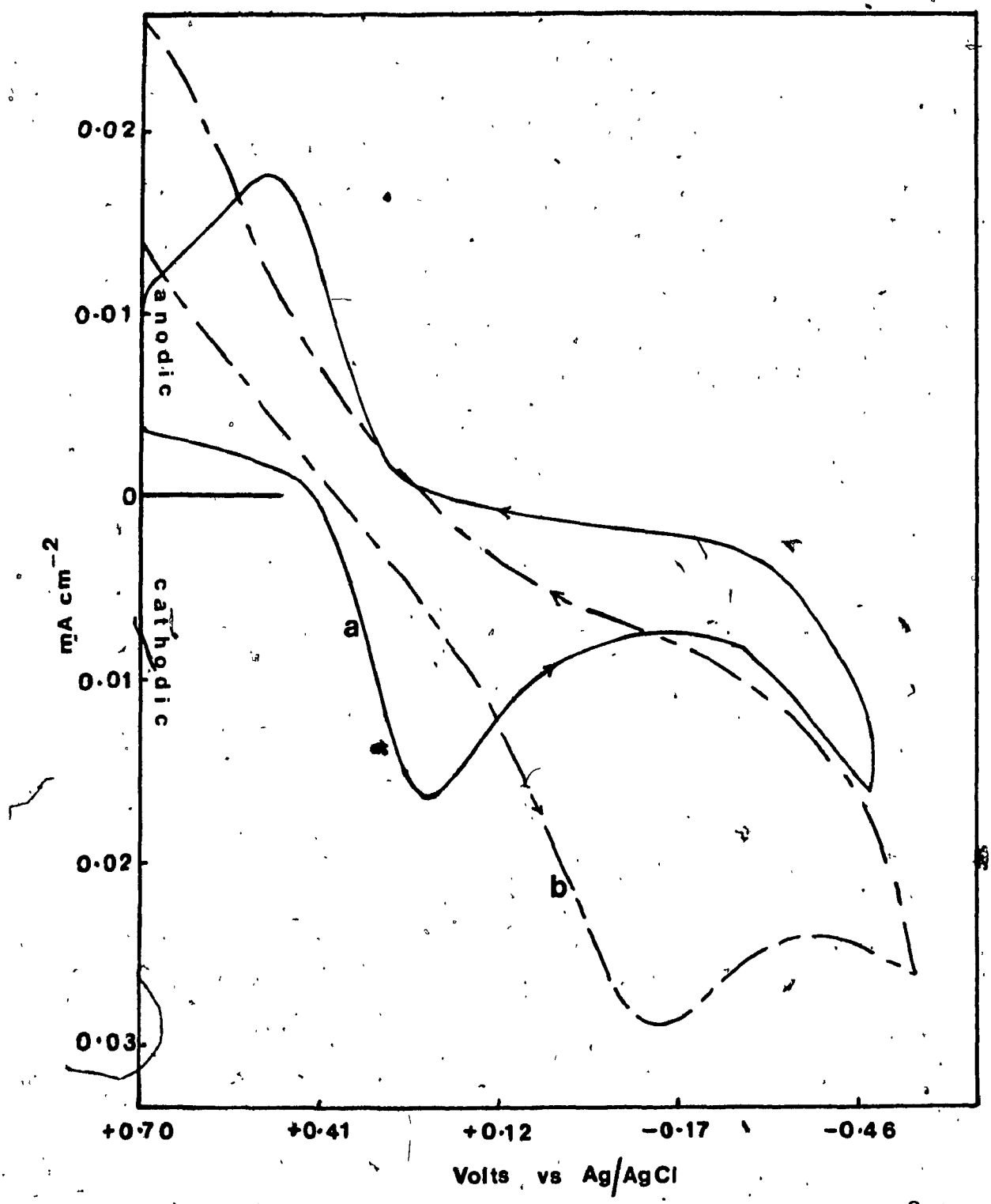

Figure 5-18. Cyclic voltammetric waves for SnO_2-QPVP-Pt(mnt)$_2^{2-}$ in contact with 0.1 M NaCl aqueous electrolyte; (a) after heating electrode for 35 mins, (b) after exposing electrode to methanol vapour for 8 hrs.

Table 5-1

Properties of Modified Electrodes Used in Electrochemistry

No	Modified Electrode	Conc. of complex $M\ cm^{-3}$	Conc. of complex $M\ cm^{-2}$	Conc. of polymer $M\ cm^{-2}$	Thickness (l) μm	Ratio of $\frac{[QPVP]}{[M(mnt)_2^{2-}]}$	% QPVP neutralized by $M(mnt)_2^{2-}$
1	Pt-QPVP-$Ni(mnt)_2^{2-}$	1.39×10^{-3}	4.18×10^{-7}	2.68×10^{-6}	3	6.4	31.14
2	Pt-QPVP-$Pt(mnt)_2^{2-}$	0.96×10^{-3}	2.88×10^{-7}	2.66×10^{-6}	3	9.2	21.62
3	SnO_2-QPVP-$Ni(mnt)_2^{2-}$	0.87×10^{-3}	1.92×10^{-7}	2.36×10^{-6}	2.2	12.3	16.24
4	SnO_2-QPVP-$Pt(mnt)_2^{2-}$	1.24×10^{-3}	2.24×10^{-7}	1.66×10^{-6}	1.8	7.4	26.88
5	Pt-QPVP-$Pt(mnt)_2^{2-}$	0.62×10^{-3}	2.48×10^{-7}	3.25×10^{-6}	[illegible]	12.5	15.27
6	SnO_2-QPVP-$Ni(mnt)_2^{2-}$	1.23×10^{-3}	2.46×10^{-7}	1.73×10^{-6}	2	7.03	28.43
7	SnO_2-QPVP-$Ni(mnt)_2^{2-}$	0.94×10^{-3}	1.88×10^{-7}	2.25×10^{-6}	2	12	16.67

Table 5-2

Apparent Diffusion Coefficients and Voltammetric Parameters for Modified Electrodes 1 to 7 of Table 5-1.

#	Scan Rate	E_{pc}	E_{pa}	E_p	i_{pc}	i_{pa}	$\frac{i_{pc}}{i_{pa}}$	D^a_{app}	D^b_{app}
	mV/sec	Volts	Volts	mV	A/cm^2	A/cm^2		cm^2 sec^{-1}	cm^2 sec^{-1}
1	30	+0.17	+0.35	180	320	120	>1	$D_c = 2.55 \times 10^{-11}$	1.20×10^{-11}
	100	+0.166	+0.37	208	615	264		$D_a = 9.14 \times 10^{-12}$	
2	30	+0.19	+0.35	150	71	52	≈1	$D_c = 2.29 \times 10^{-12}$	2.20×10^{-12}
	100	+0.20	+0.37	160	124	92		$D_a = 1.38 \times 10^{-12}$	
3	30	+0.14	+0.35	210	112	112	1	$D_c = D_a =$	8.08×10^{-12}
	100	+0.12	+0.37	249	195	195		7.17×10^{-12}	
4	[illegible]	+0.12	+0.40	280	121	78	>1	$D_c = 4.17 \times 10^{-12}$	6.41×10^{-12}
	[illegible]	+0.08	+0.43	350	195	134		$D_a = 1.78 \times 10^{-12}$	
5	30	+0.23	+0.36	120	7	[illegible]	1	$D_c = D_a =$	1.03×10^{-13}
	100	+0.20	+0.38	150	18	15		9.05×10^{-12}	
6	30	+0.21	+0.38	170	137	69	>1	$D_c = 4.98 \times 10^{-12}$	
	100	+0.18	+0.41	230	214	132		$D_a = 1.34 \times 10^{-12}$	
7	30	+0.089	+0.43	298	117	117	1	$D_c = D_a =$	2.41×10^{-11}
	100	+0.061	+0.39	373	181	181		7.22×10^{-12}	

[a] apparent diffusion coefficient obtained from i_p vs $v^{\frac{1}{2}}$ plot; D_c: obtained from cathodic waves. D_a: obtained from anodic waves.

[b] apparent diffusion coefficient obtained from i vs $t^{-\frac{1}{2}}$ plot upon polarization beyond the anodic wave potential.

Table 5-3

Effect of Electrolyte on Peak Potentials of SnO_2-QPVP-Ni(mnt)$_2^{2-}$

Electrolyte	E_{pc}^{a} Volts	E_{pa}^{b} Volts	E_{p}^{c} mV
0.1 M NaBr	+0.074	+0.453	379
0.1 M NaCl	+0.099	+0.483	384
0.1 M NaF	+0.130	+0.532	402

[a] E cathodic peak potential

[b] E anodic peak potential

[c] E peak separation in mV.

Table 5-4

Effect of Electrolyte on Peak Potentials of SnO_2-QPVP-Pt(mnt)$_2^{2-}$

Electrolyte	E_{pc}^{a} Volts	E_{pa}^{b} Volts	E_{p}^{c} mV
0.1 M NaBr	+0.054	+0.44	100
0.1 M NaCl	+0.073	+0.47	397
0.1 M NaF	+0.054	+0.64	586

a,b,c see corresponding footnotes to Table 5-3

Chapter 6

Results IV

Heterogeneous Photoelectrochemistry.

6.1 Photoeffects of SnO_2-QPVP electrode without $M(mnt)_2^{2-}$ in the polymer film.

The photoelectrochemical response of SnO_2-QPVP without $M(mnt)_2^{2-}$ incorporated in the polymer film was necessary in order to determine any background thermally induced "photocurrent" resulting from light perturbing the SnO_2-QPVP/electrolyte interface. The QPVP coating on the SnO_2 electrode was rendered insoluble in the aqueous electrolyte by previously exchanging the Cl^- ions in the film for ClO_4^- ions from a 0.1 M $NaClO_4/CH_3CN$ solution. The multimeter detection system did not show any photocurrents for the bare SnO_2-QPVP electrode in the potential range of +0.2 V to -0.6 V (potentials beyond this range were not examined.)

6.2 Photoelectrochemistry at SnO_2-QPVP-$Ni(mnt)_2^{2-}$ electrodes (electrodes 8 & 9).

For the purpose of convenience, the numbering sequence of Tables 5-1 and 5-2 is continued. The use of electrodes 8 and 9 for the heterogeneous photoelectrochemical measurements is now described. The physical properties are given in Table 6-1. Except for the loading all the other properties are the same or very close.

Figure 6-1 shows the photocurrent profile generated by electrode 8 on illumination from the SnO_2 coated glass side, the back-side of the electrode. The generation of the photocurrent was instantaneous and remained quite steady during the period of illumination. There is a slight increase in the photocurrent with time at -0.6 V but this is probably due to an increase in the background current as the redox potential of the polymer is approached. The light and the corresponding dark period following the illumination were approximately equal. Upon interrupting the light the photocurrents promptly decayed to the original dark current values. Photocurrents were recorded at potentials between +0.1 V and -0.6 V inclusively commencing at +0.1 V with readings at each 0.1 V interval scanning in the cathodic direction. Four sets of photocurrents measurements were taken, the initial and three repeats. The dependence of the photocurrents on potential is shown in Figure 6-2. Curve (a) is the first set or initial photocurrents measured at +0.1 V to -0.6 V. Curves (b), (c) and (d) in the same figure represent the second, third and fourth set respectively obtained by repeating the measurements in the same manner as the first. In all these curves the photocurrent increases with increasing cathodic potential and tend to level at about -0.4 V. It is also obvious from this figure that the photocurrent at each potential decreased as the

measurements were repeated. The voltammetric waves before and after the photoelectrochemical measurements were recorded at scan rate of 30 mV/sec and shown in Figure 6-3(a) and (b) respectively. The response of the electrode before and after the photoelectrochemical measurements were not the same. A more symmetric anodic and cathodic wave shape for the redox reaction of the complex was obtained before the measurements; the area under the peaks was approximately equal and the peak separation was found to be about 220 mV. After the measurements both, the anodic and cathodic peaks for the redox reaction of the complex decreased. The decrease is greater for the anodic peak. The peak separation was also increased by 100 mV to 300 mV. The visible spectrum of the electrode before and after the photoelectrochemistry was also recorded and shows only a slight increase in the peak at 472 nm.

Photoelectrochemical measurements were repeated in a similar manner on electrode 9. The response of this electrode under back-face illumination was similar to electrode 8. The photocurrents were instantaneous, and in the dark, there is an immediate decay. The photocurrents remained constant during each period of illumination but the dark, background current increased slightly with time giving a deceptive appearance that the photocurrent is time dependent. Figure 6-4 shows the current increases with potential and starts leveling at -0.4 V. Unlike

electrode 8, the photocurrents produced by this electrode showed a negligible decrease as the measurements were repeated. The values of a second and third measurements are very close to that of the first one shown in curve (a) of Figure 6-4. However, on polarizing the electrode under continuous illumination through a water filter for 1 hr, the photocurrent decreased, particularly at potentials more cathodic than -0.3 V (curve b, Figure 6-4). Further polarization under irradiation for an additional hour revealed a smaller decrease (curve (c).

The voltammetric responses before, during and after the photoelectrochemistry were recorded and given in Figure 6-5. Curve (a) was obtained before the photoelectrochemistry curve (b) after the third set of photocurrent measurements while curves (c) and (d) were those after polarization at -0.4 V under illumination for 1 and 2 hr, respectively. The waves corresponding to the reaction, $Ni(mnt)_2^{2-} \rightleftharpoons Ni(mnt)_2^{1-}$ in the film are not symmetrical, the anodic peak is smaller than its cathodic counter-part, in all the voltammetric curves. The peak currents for oxidation as well as the reduction before and after the third photoelectrochemical measurements are comparable and the voltammetric response closely parallel. After simultaneous polarization and irradiation of the electrode the peak currents for the redox reaction of the complex decreased (curves (c) and (d). The optical

absorption spectrum of the electrode, did not show significant differences before and after the PEC measurements, there was only a slight increase in absorbance after the photoelectrochemistry. This could be due to scattering or merely a slight change in the position of the electrode in the spectrophotometer.

6.3 Photoelectrochemistry of SnO_2-QPVP-Pt(mnt)$_2^{2-}$

6.3.1 Effect of Starting Potential on Photowave.

The photoelectrochemistry of SnO_2-QPVP-Pt(mnt)$_2^{2-}$ electrodes were studied in the potential range of 0.0 and -0.6 V and photocurrents were measured at every 0.1 V interval. Measurements can be started at either 0.0 V or at -0.6 V. The effect of starting the measurements at -0.6 or 0.0 V on the shape of the photowave was illustrated with electrodes 10 and 11. These electrodes were irradiated through the SnO_2-glass side, the back-side. Photocurrent measurements on electrode 10 were started from 0.0 V and scanned in a more cathodic direction to -0.6 V.

The current profile under illumination is presented in Figure 6-6. An instantaneous response was observed upon irradiation and did not level with time. The photocurrent increased slowly as the irradiation was continued. Upon interrupting the light and maintaining the electrode under normal laboratory illumination there was prompt drop in the photocurrent to steady value larger

than the initial dark current value. Subsequent to this fast drop there was a slow decay to a value equal to the initial dark current. Both the instantaneous response and the slow increase in photocurrent over a period of 2 mins were measured at different potential. These two values along with their sum, which refects the total photocurrent, varied with potential as shown in Figure 6-7. The "instantaneous photocurrent" (curve (a) slowly increases with potential to about -0.3 V then levels. The slow component curve (b) is fairly constant from 0.0 to -0.2 V. Between -0.2 and -0.3 V there is a decrease and at potentials -0.3 to -0.6 it remains constant again. The total photocurrents as shown in curve (c) are controlled by curve (a).

Electrode 10 was immediately exploited for a second measurement under the same conditions to determine whether it is reproducible. The photocurrent profile was similar to that observed in the first photoelectrochemical measurements. The response of the electrode under illumination consisted of the prompt and the slow photocurrents both of which vary with potential. The photocurrent values however are not quantitatively the same. Figure 6-8 curve (a) shows the prompt photocurrent has decreased. The decrease is pronounced in the potential region -0.3 to -0.6 V in that the shape of the curve in this region differs from that of Figure 6-7 (a).

Instead of leveling after -0.3 V it starts falling to produce a curve with a maximum at -0.2 V. The slow component, curve (b) of Figure 6-8 decreased in the potential region 0.0 to -0.3 V after which it increased steadily. The sum of the prompt and slow photocurrents, curve (c), is reduced compared to the previous measurement but the shape of the curve is similar.

The voltammetric as well as the spectral responses of the electrode before and after the photoelectrochemical measurements are given in Figures 6-9 and 6-10 respectively. The voltammetric response after the photoelectrochemical measurements decreased. Both anodic and cathodic peaks for the reaction of the complex became smaller.

The spectral response was also altered. The change in the spectrum was evident since the $Pt(mnt)_2^{2-}$ originally incorporated in the film was orange/red and after the photoelectrochemistry a green coloration appeared. The main band in the visible at 472 nm decreased with successive PEC measurements while a small peak at about 445 to 450 nm started to appear. In the near infra-red region the weak intensity absorption at 855 nm began to increase.

Measurements on electrode 11 were similar to those for electrode 10 except that scan was started at -0.6 V and continued in the anodic direction to 0.0 V. The response profile under illumination was similar to

electrode 10. It consisted of both an instantaneous and a slow photocurrent. The shape of the photocurrent curves as a function of potential is shown in Figure 6-11. The prompt photocurrents curve (a) increased slowly with potential between 0.0 V and -0.3 V after which there is a steep increase and at -0.5 V there is the tendency to flatten. The slow photocurrent, curve (b) increased linearly with potential up to -0.3 V after which the current remained constant. The sum of the two component is shown in curve (c). Photoelectrochemical measurements on electrode 11 were repeated under the same conditions as the first measurement. The photoresponse pattern again consisted of the prompt and slow photocurrents. These values are plotted as a function of potential in Figure 6-12.

Each component of this second measurement was found to be smaller than the counterpart in the first runs. Five other additional measurements were subsequently taken on this electrode in the same electrolyte under the same conditions as the first and second. In each case the response under illumination is similar to that seen before in the second run. The instantaneous as well as the slow photocurrent varied with potential. The instantaneous photocurrent were in close agreement with those obtained in the second photoelectrochemical measurements. The slow photocurrent decreased with each repeated measurement.

The voltammogram and the spectra were also recorded before, during and after the photoelectrochemical measurements these are shown in Figure 6-13 and 6-14 respectively.

6.3.2 Effect of Irradiation from Back and Front side of Electrode.

Electrode 12 and 13 were used to examine the effect of illumination of the electrode from the back-side through the SnO_2 coated glass disc and from the front side through the electrolyte. A schematic representation of the electrode under irradiation is shown in Figure 6-15. The amount of loading, film thickness and related properties of these electrodes are given in Table 6-1. The high concentration of the complex in the film was intentional so that a large quantity of the complex is at the SnO_2/polymer interface. It was achieved by soaking the QPVP coated SnO_2 disc in acetonitrile for 10 mins before the usual mild heating in the acetonitrile solution of the complex. Electrode 12 was irradiated from the back-side while electrode 13 was irradiated from the front side. Photocurrent measurements for both electrode were commenced at -0.6 V and continued to 0.0 V. The photoresponse was similar to the other modified electrodes with $Pt(mnt)_2^{2-}$ incorporated into the polymer film in that the total photocurrent consists of the prompt and the slow components. Figures 6-16 and 6-17 respectively for electrode 12 while Figures 6-18 and 6-19 are those

obtained for electrode 13. These electrodes were also characterized by their voltammetric and spectral responses before and after the photoelectrochemical measurements. Unlike the other modified electrodes which showed a clear orange-red color after the complex has been incorporated into the polymer, these two electrodes were only translucent and scattering is significant. For both electrodes the voltammetric response decreased after the photoelectrochemical measurements but there is not significant change in their spectrum.

6.3.3 Effect of Prolonged Irradiation under Potentiostatic Conditions on Voltammogram and Spectrum.

Electrode 14 was used to determine the effect of prolonged irradiation under constant potential on the voltammetric and spectral response. The electrode was polarized at -0.4 V and irradiated from the SnO_2 side through a water filter for approximately 10 hrs. The electrolyte solution was circulated through the cell at a rate of 20 ml per min. The voltammograms before and after irradiation is given in Figure 6-20. Response (a) shows the redox potential of the complex and the polymer before irradiation are in their expected potential region. After irradiation (response (b)) the waves corresponding to the oxidation and reduction of the incorporated $Pt(mnt)_2^{2-}$ were greatly reduced. The wave for the reduction of the polymer was not observed since at -0.5 V bubbles

vigorously evolved from the surface of the modified electrode. This voltammetric scan was repeated several times on the same day and on two following days and on each occasion an identical voltammetric response was observed with gas bubbles appearing at the electrodein the -0.5 V potential region. The electrode after irradiation did not show any sign of sogginess. The film was intact and robust as before irradiation, but the color of that portion of the electrode that was exposed to both electrolyte and irradiation had changed from orange-red to green. The spectrum before and after irradiation Figure 6-21 is similar to that of Figure 6-13 obtained on electrode 11.

6.3.4 Effect of acidic Electrolyte.

Electrode 15 was used to determine the effects of acidic electrolyte on the photocurrent as well as the voltammetric and spectral response. The photoelectrochemistry of this electrode was initially examined in 0.1 M KCl (pH 6.02) and then in 0.1 M HCl (pH 1.58) starting from 0.0 V to -0.6 V. The use of 0.1 M KCl electrolyte before 0.1 M HCl is merely to establish that there is not unusual behaviour of the electrode. A behaviour similar to electrode 10 was found. In 0.1 M HCl the response of the electrode was different. In the first attempt with the HCl electrolyte the prompt photo-response was not observed in the potential region of 0.0 V to - 0.4

V but the slow photocurrents persisted. In the second and other subsequent attempts the slow photocurrents were very small. In the region -0.4 to -0.6 V, a prompt response was observed in all the attempts. This response profile reached a limit very quickly and showed no sign of further increase or decrease within a 2.5 min period of illumination. Figure 6-22 (a) and (c) show the variation of the photocurrents as a function of potential for the first and second attempt in the HCl electrolyte. The voltammetric response was also greatly altered in the presence of HCl. Figure 6-23 (a) is the voltammogram recorded at 30 mV/sec after the photoelectrochemical measurements in the KCl electrolyte. It showed no unusal behaviour. Response (b) in the same figure was obtained in 0.1 M HCl before the photoelectrochemical measurements while (c) was recorded after the photoelectrochemical measurements. In (b) the waves corresponding to the redox reaction of the complex were significantly reduced particularly the reduction wave. At about -0.48 a pair of small anodic and cathodic waves began appearing. The reduction of the polymer appeared at -1.2 V and no oxidation on the back sweep was seen. In (c) the anodic wave at -0.4 shifted to about -0.34 V. The current is increased and there is no corresponding reduction wave but a prewave on the anodic back-sweep was observed at -0.15 V. In the forward cathodic sweep a small prewave was

found at about -0.6 V which was followed by rapid evolution of gas from the modified electrode surface due to solvent decomposition.

The polymer film on the electrode after removal from the cell was stable and was not soaked. The color however, was changed. The initial orange-red color has changed to green. The spectrum of the electrode before and after the PEC measurements in 0.1 M HCl is given in Figure 6-24. The 472 nm band in the visible decreased and the broad absorption in the IR region increased after the photoelectrochemistry in the acid electrolyte.

6.3.5 Effect of the Electrode behaviour on Acid Treatment.

Electrode 16, was subjected to chemical treatment by 6.0 M HCl acid solution and the reaction followed spectrophotometrically before the photoelectrochemistry was performed.

Before this experiment a preliminary observation of an SnO_2-QPVP-$Pt(mnt)_2^{2-}$ electrode immersed in 0.1 M KCl and another in 0.1 M KCl was made. No precaution was taken to eliminate laboratory illumination. The electrode in 0.1 M KCl showed no visible change for over a period of three months after which time the observation was abandoned. The electrode in 0.1 M HCl showed the appearance of a green coloration after 5 to 6 weeks. The spectrum of the electrode after the prolonged exposure to the acid solution showed a decreased in absorbance at 472 nm with

the appearance of the green color similar to that obtained after prolonged irradiation in contact with 0.1 M KCl. The rate of reaction with the acid was enhanced by a more concentrated acid solution was shown with electrode 16. This electrode was immersed in the acid solution for a short period of time, taken out and washed with distilled water then dried in vacuum at 50° C before the spectrum was recorded. This process was repeated several times. The total time the electrode was immersed in the acid solution was not more than 8 min. The spectrum obtained before after each acid treatment is shown in Figure 6-25. As the contact time with the acid increased, the 472 nm band of $Pt(mnt)_2^{2-}$ decreased and the low intensity band at 855 increased. The complex was finally removed from the polymer by a perchlorate ion exchange in acetonitrile. The spectrum of this solution was taken and found to be in qualitative agreement with that in Figure 6-32 namely, $Pt(mnt)_2^{1-}$.

The voltammetric response in 0.1 M KCl was also followed during the various stages of acid treatment. Figure 6-26 shows the changes. The redox waves for the reaction $Pt(mnt_2^{2-}/Pt(mnt)_2^{1-}$ gradually disappear during the acid treatment. The final voltammetric wave curve (c), was similar to that obtained after the photoelectrochemistry in 0.1 M KCl solution in the previous section.

The photoelectrochemical behaviour shown in Figure 6-27 similar to that of Figure 6-22 in 0.1 M HCl. Curve (b) is the second attempt in the measurement.

6.3.6 Scanning Electron Microscopy.

Scanning Electron Microscopy (SEM) although limited in resolution for monolayer films was employed to examine the surface features of the SnO_2-QPVP-$Pt(mnt)_2^{2-}$ electrodes before and after photoelectrochemical experiments. To reduce the build up of electrical charge, the modified electrodes were mounted on a stub and coated with a gold film of approximately 10 nm in a E-5100 gold sputtering system (Polaron Equipment Ltd.). They were examined and photographed with a Hitachi-520 Scanning Electron Microscope.

Figure 6-28 (a) and (b) compared the micrographs before and after the photoelectrochemistry. Both micrographs showed that the polymer films were cracked. This is believed to occur during the gold coating procedure and in the process of examining the electrodes under vacucum in the electron beam. The polymer film of these electrodes was thick (not a monolayer) and contained solvent i.e. methanol used in the drop evaporation technique. The high vacuum condition of the sputtering technique should result in removal of the trapped solvent, and cracking of the polymer film. Local heating by the electron beam irradiation also contributes to this effect.

The effect of dissipation of beam energy was noticable at the beginning of the irradiation of the electrodes. When the electrodes were examined under the electron beam irradiation, movements of the polymer coating on the SnO_2 surface were clearly detected and the cracks appeared on the screen. The QPVP polymer film itself has a smooth even surface with the complex dispersed in the QPVP film. The micrograph obtained for the electrode before the photoelectrochemistry (Figure 6-28(a) showed the complex may be present in small crystals clustered and embedded in the polymer. The dark feature of the complex would suggest that such crystals are inside the polymer film below the surface. After the photoelectrochemistry gross change occurs in the topology of the complex in the film. The micrograph (Figure 6-28(b) show the new larger crystals. The white feature of these crystals would suggest that they are on the surface of the polymer film or partially protruding out of the film.

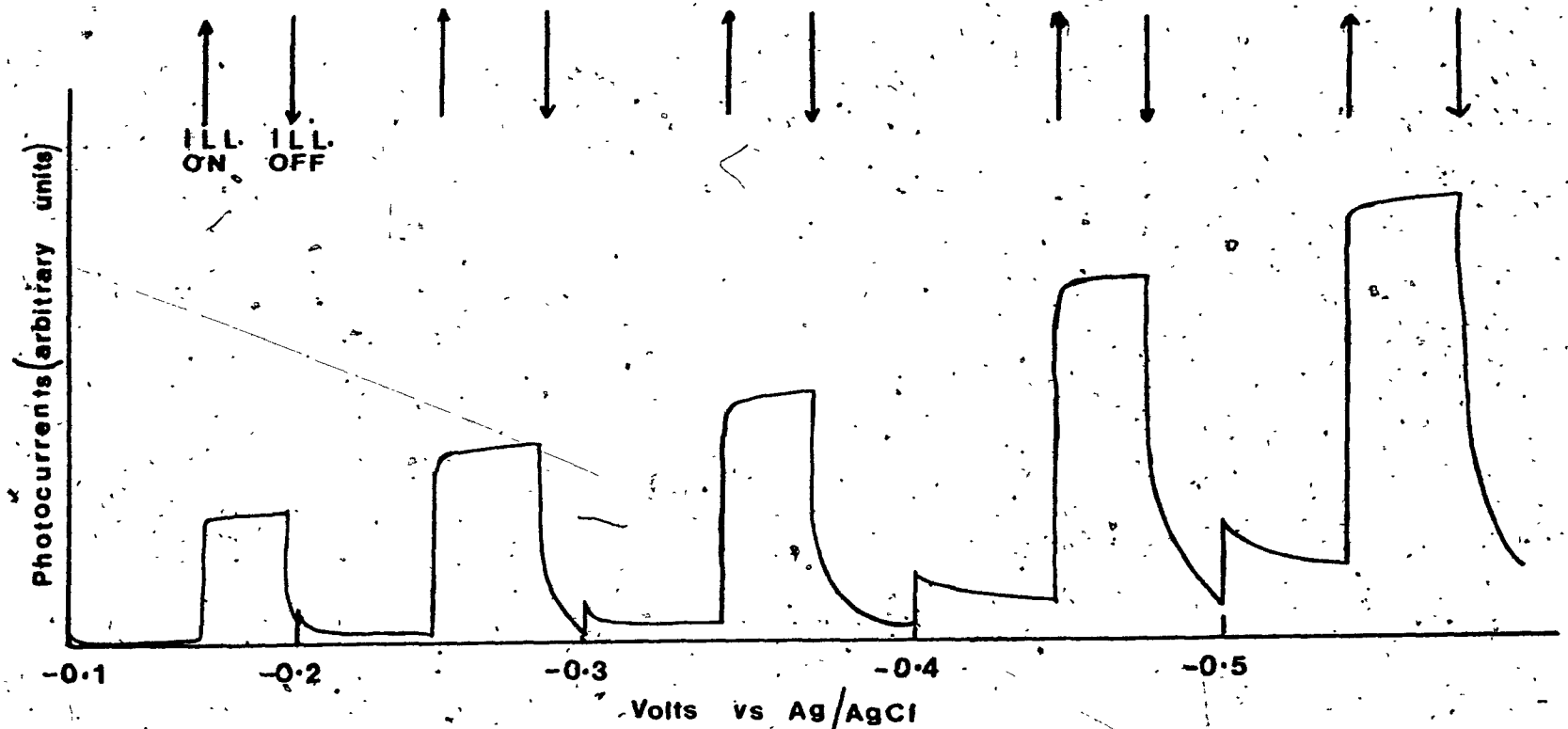

Figure 6-1. response of cathodic photocurrent at SnO_2-QPVP-Ni(mnt)$_2^{2-}$ electrode to illumination.

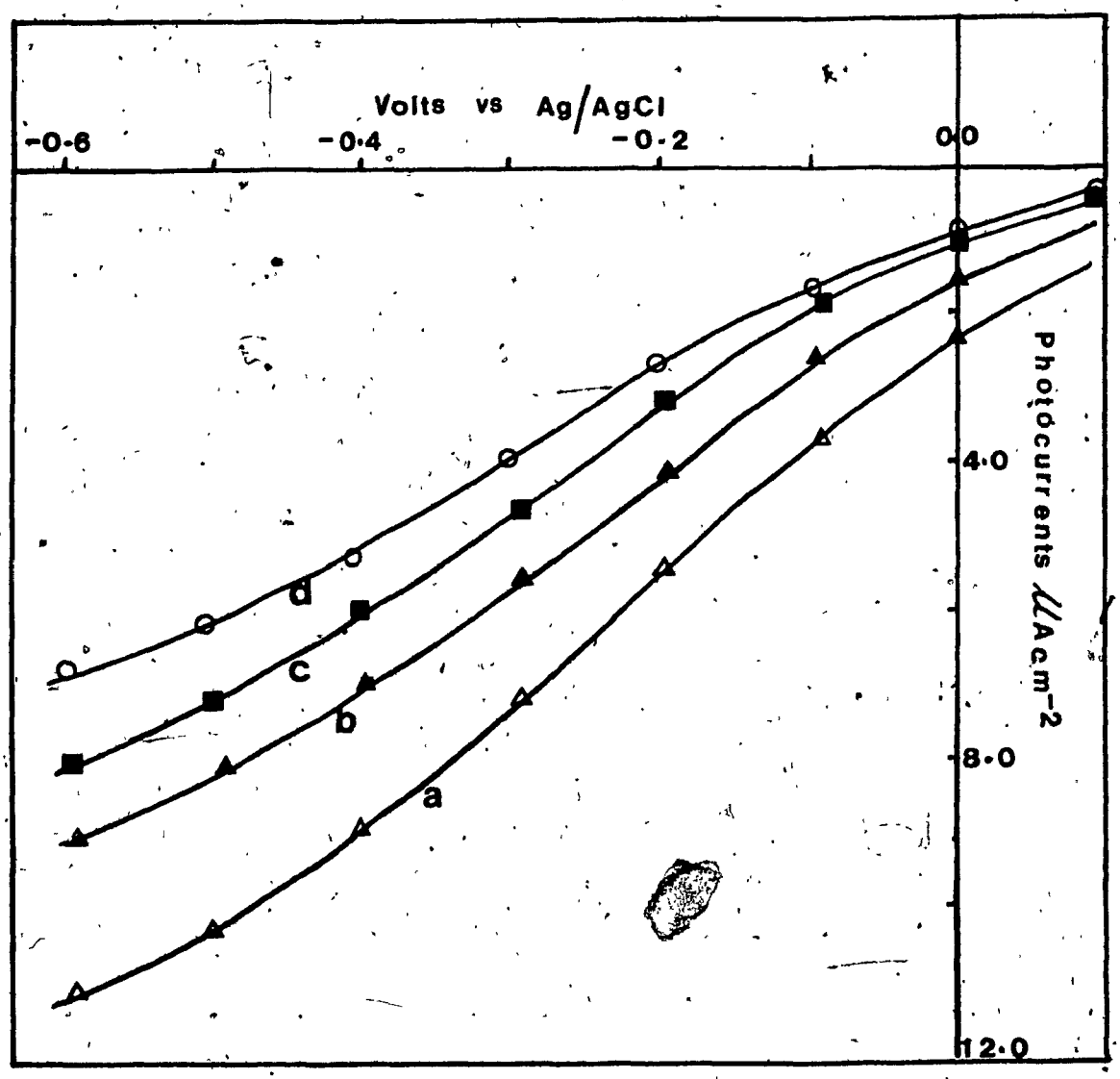

Figure 6-2. The dependence of cathodic photocurrent on potential for Electrode 8, SnO_2-QPVP-Ni(mnt)$_2^{2-}$ in contact with 0.1 M KCl aqueous electrolyte. Curves (a), (b), (c), (d) are the first, second, third and fourth measurements, respectively.

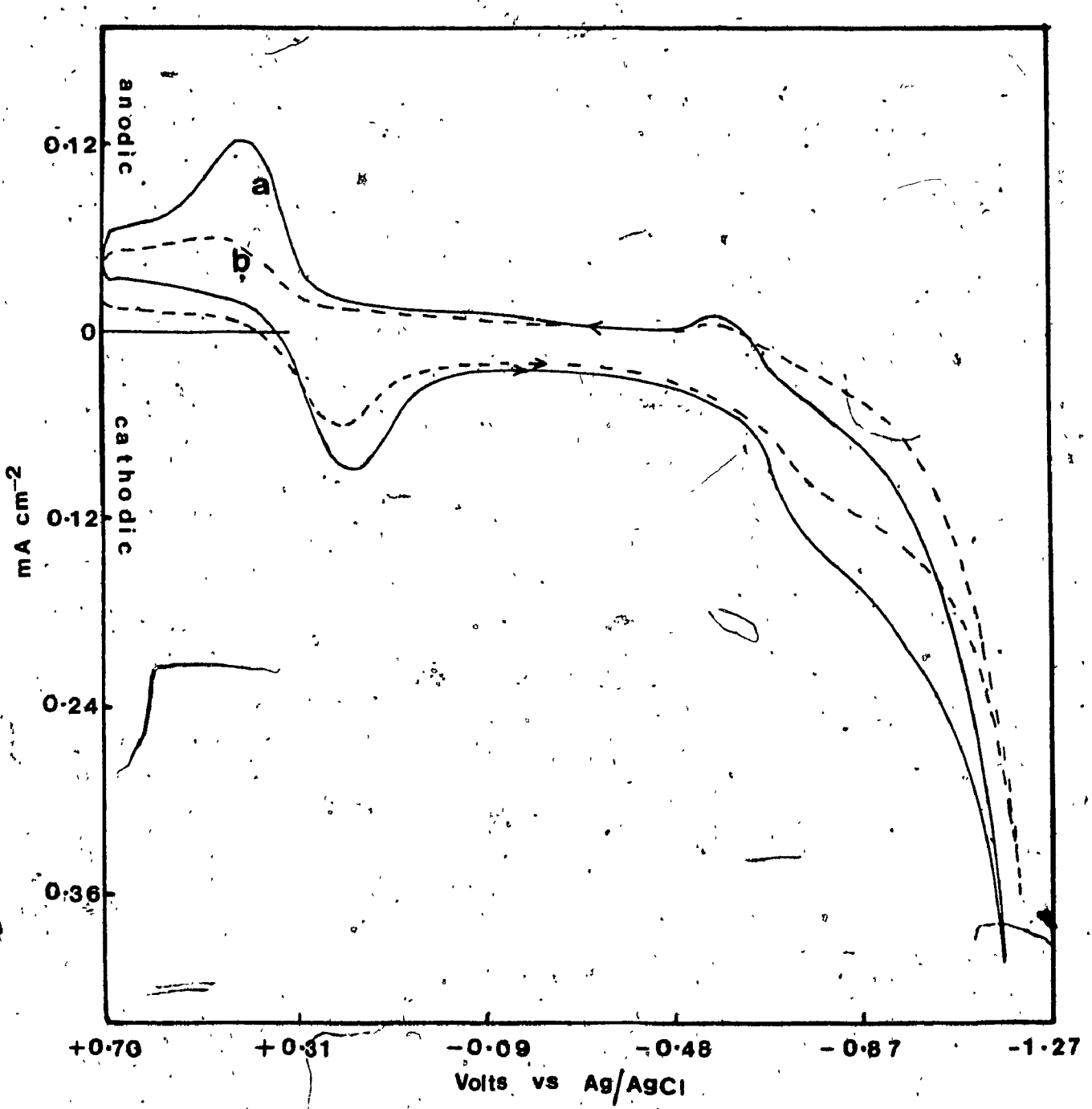

Figure 6-3. Cyclic voltammetric waves for Electrode 8; SnO_2-QPVP-Ni(mnt)$_2^{2-}$ in contact with 0.1 M KCl aqueous electrolyte. Response before photoelectrochemical measurements (a). Response after photoelectrochemical measurements (b).

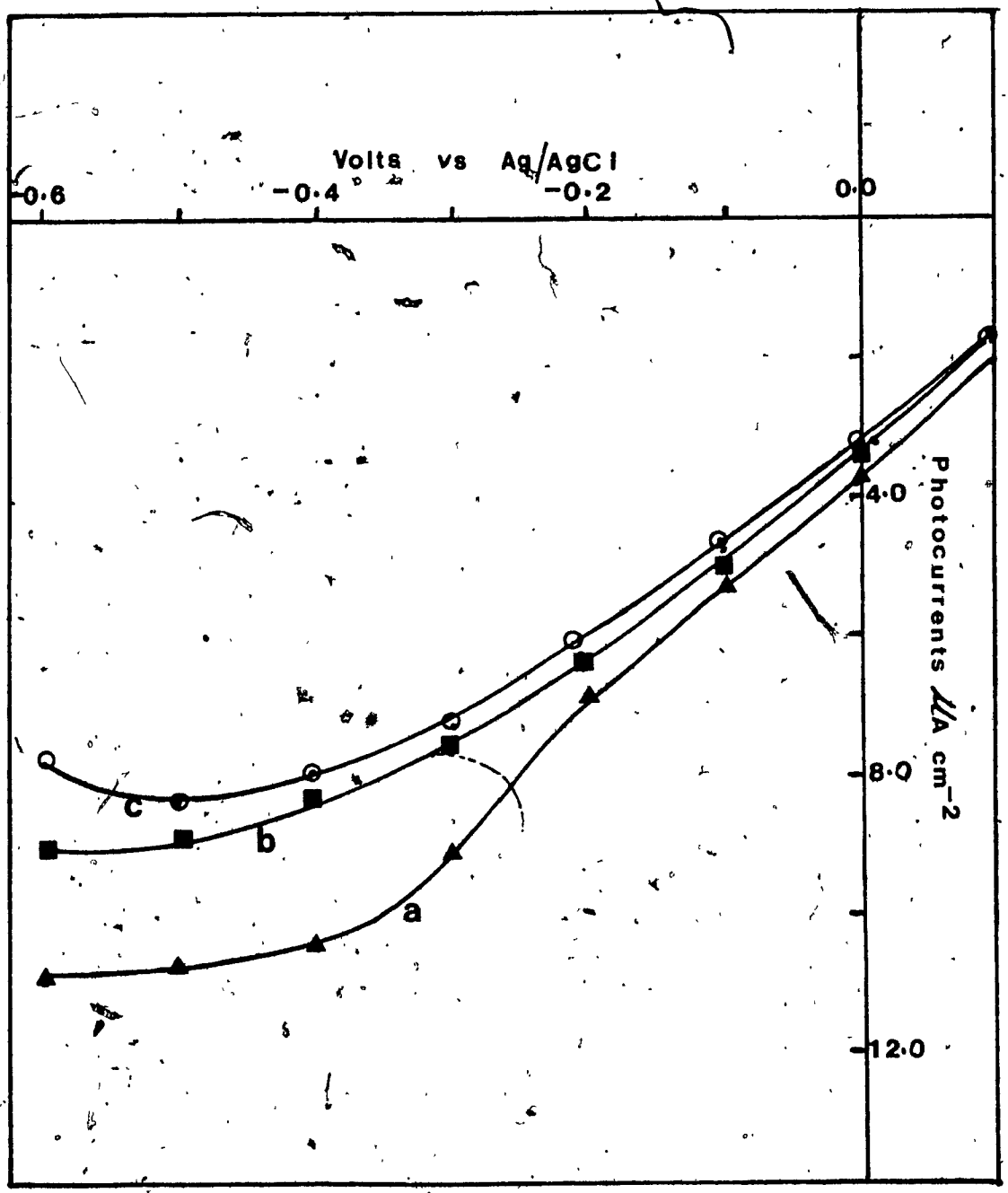

Figure 6-4, The dependence of cathodic photocurrent on potential for Electrode 9; SnO_2-QPVP-Ni$(mnt)_2^{2-}$ in contact with 0.1 M KCl aqueous electrolyte. Curve (a): Photocurrent for the first measurement. Curves (b) and (c): photocurrents after polarization at -0.4 V under irradiation for 1 and 2 hr, respectively.

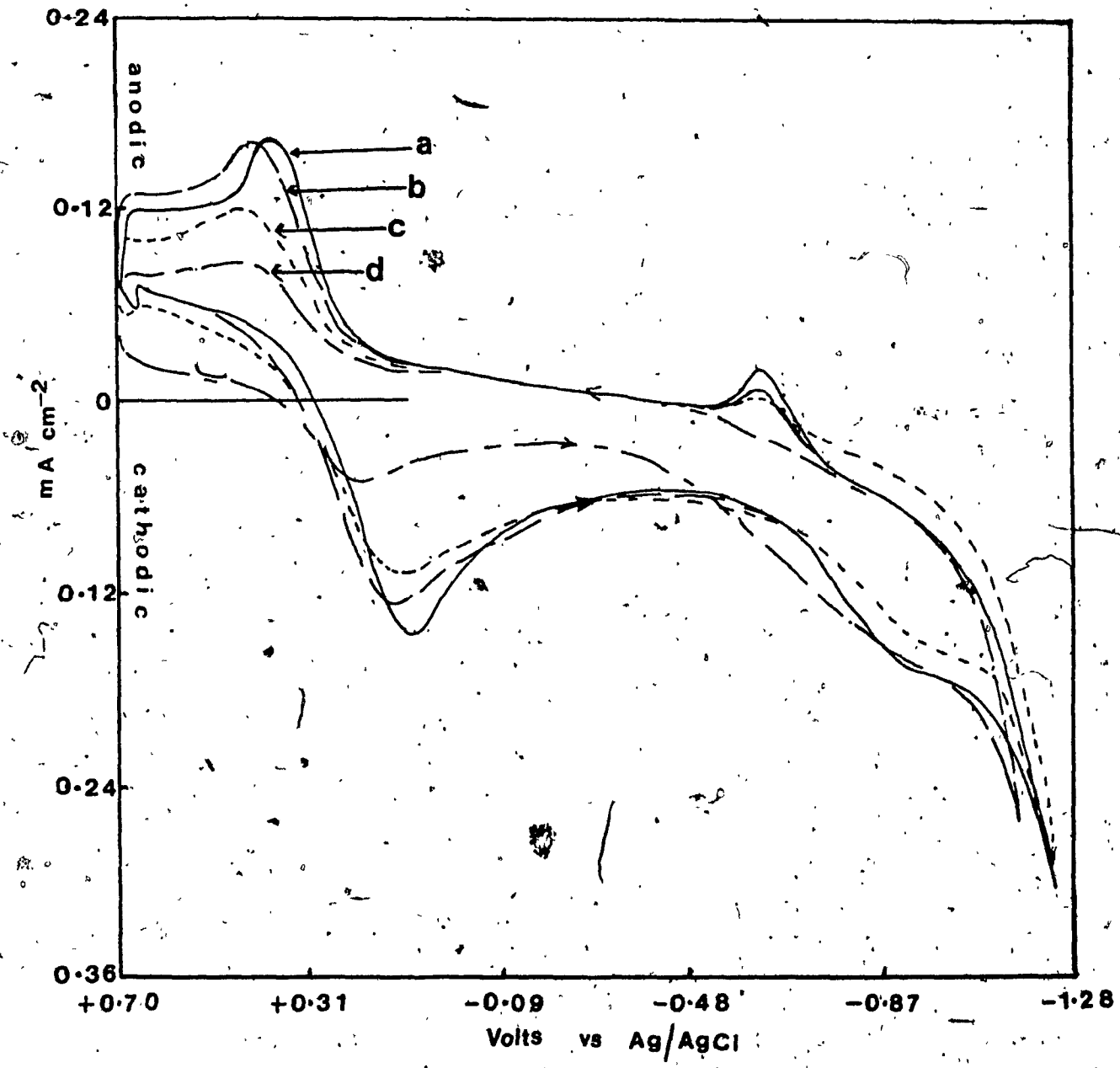

Figure 6-5. Cyclic voltammetric waves for Electrode 9, SnO_2-QPVP-$Ni(mnt)_2^{2-}$ in contact with 0.1 M KCl aqueous electrolyte: (a) before photoelectrochemical measurements; (b) after third set of photoelectrochemical measurements; (c) and (d) after polarization at -0.4 V under illumination for 1 and 2 hr, respectively.

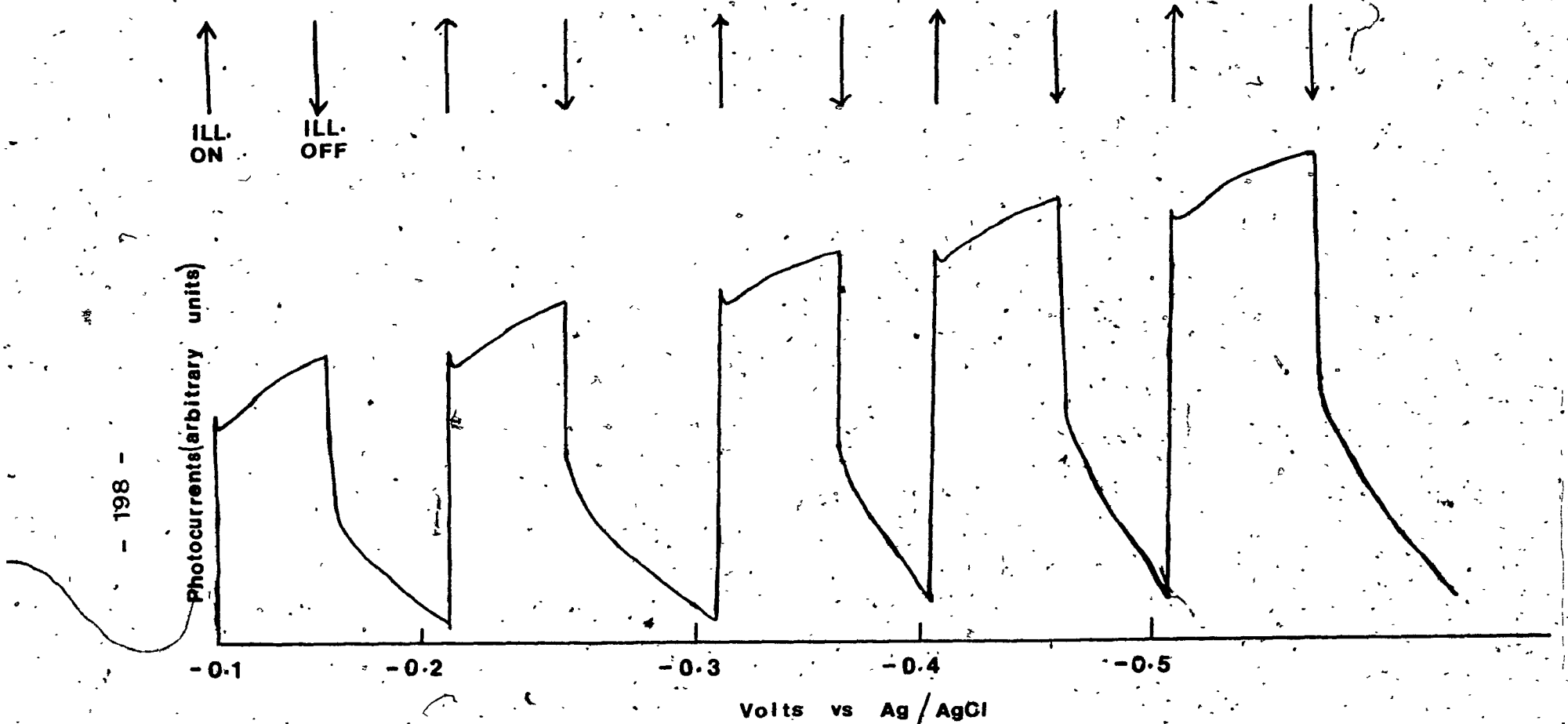

Figure 6-6. Response of cathodic photocurrents at SnO_2-QPVP-Pt(mnt)$_2^{2-}$ electrode to illumination.

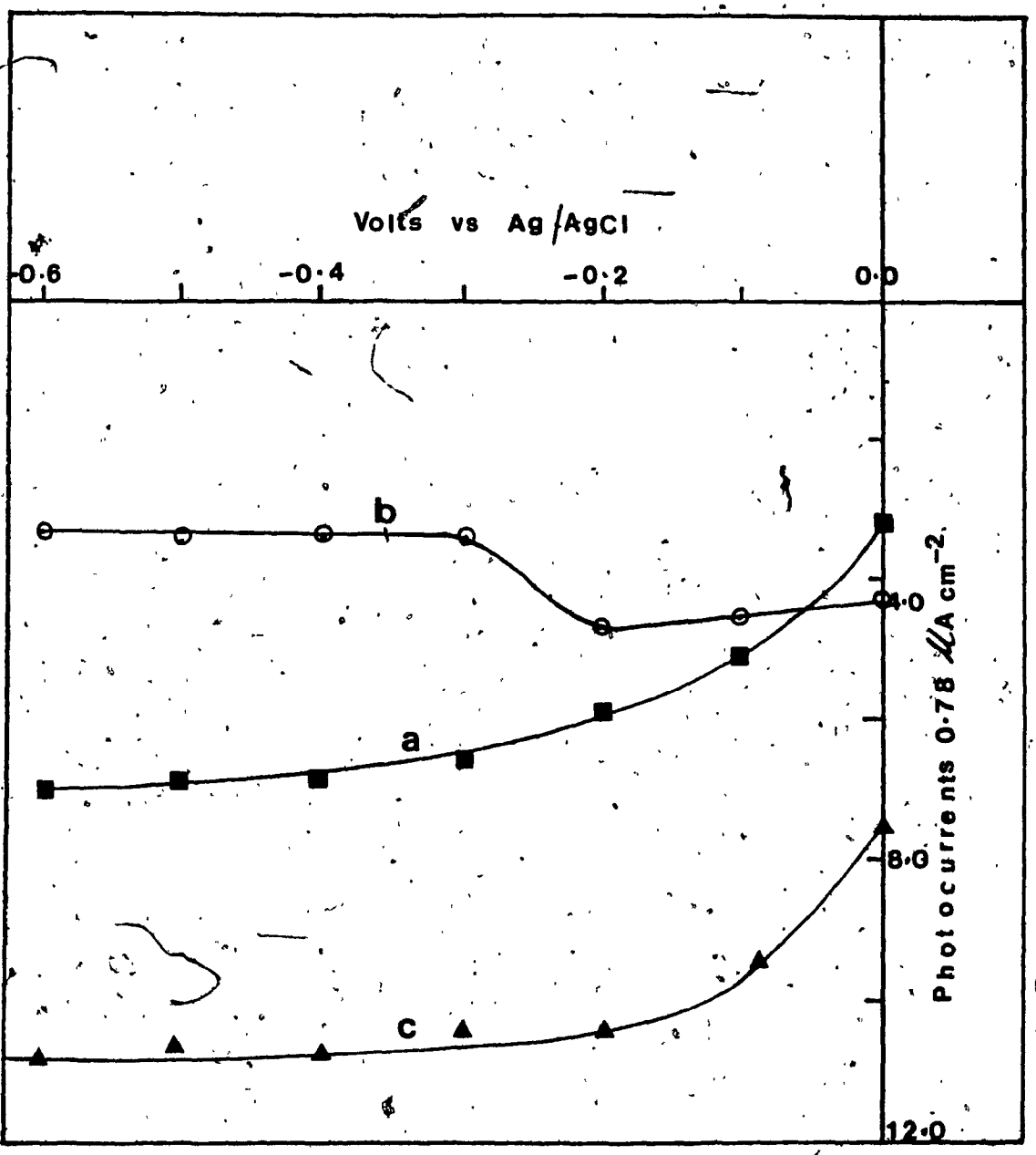

Figure 6-7. The dependence of cathodic photocurrents (first measurement) on potential for Electrode 10, SnO_2-QPVP-Pt(mnt)$_2^{2-}$ in contact with 0.1 M KCl aqueous electrolyte. (a) prompt photocurrent; (b) slow photocurrent; (c) total photocurrents. Measurements were started at 0.0 V.

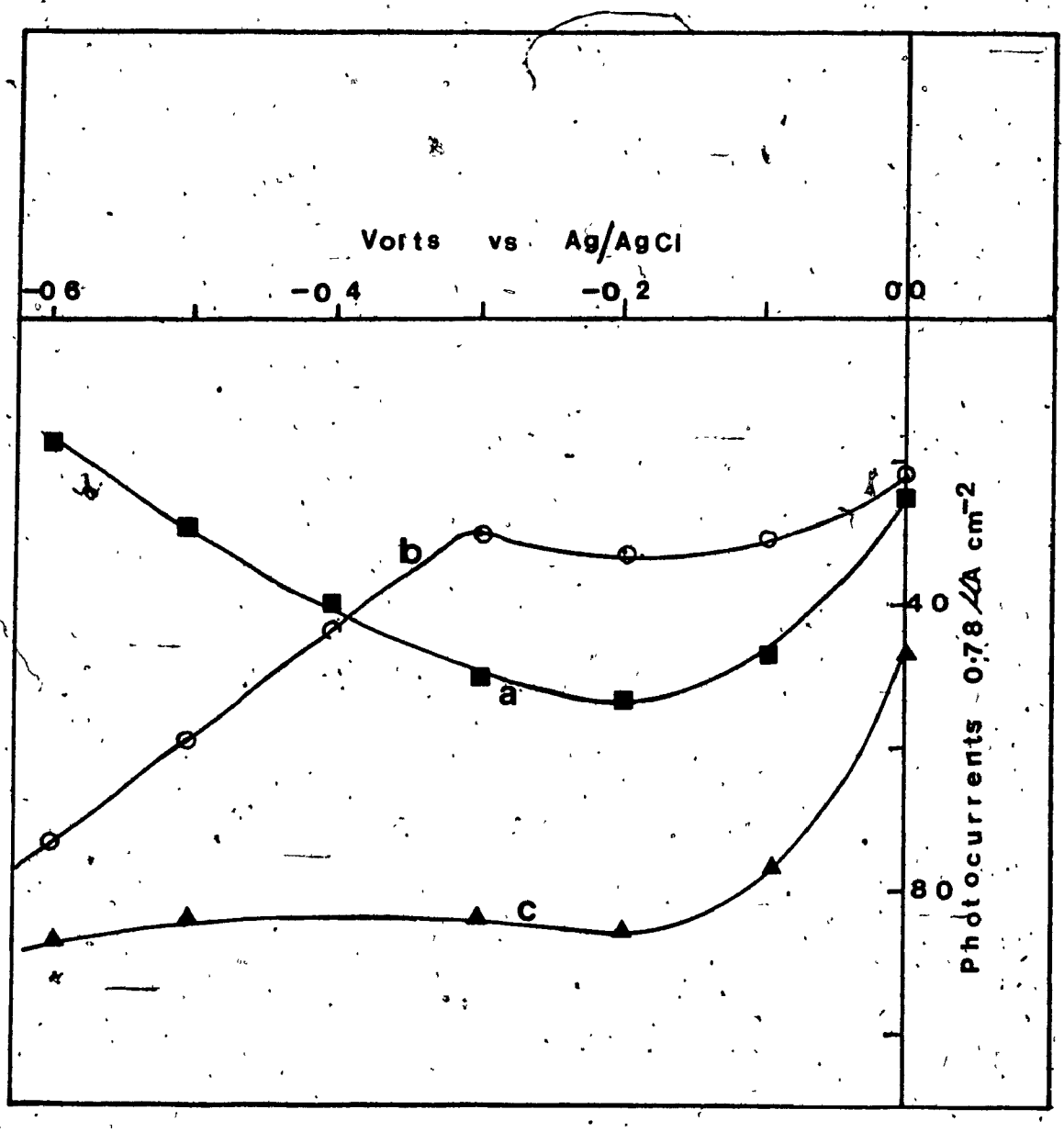

Figure 6-8. The dependence of cathodic photocurrents (second measurement) on potential for Electrode 10, SnO_2-QPVP-Pt(mnt)$_2^{2-}$ in contact with 0.1 M KCl aqueous electrolyte. (a) prompt photocurrent; (b) slow photocurrent;. (c) total photocurrents. Measurements were started at 0.0 V.

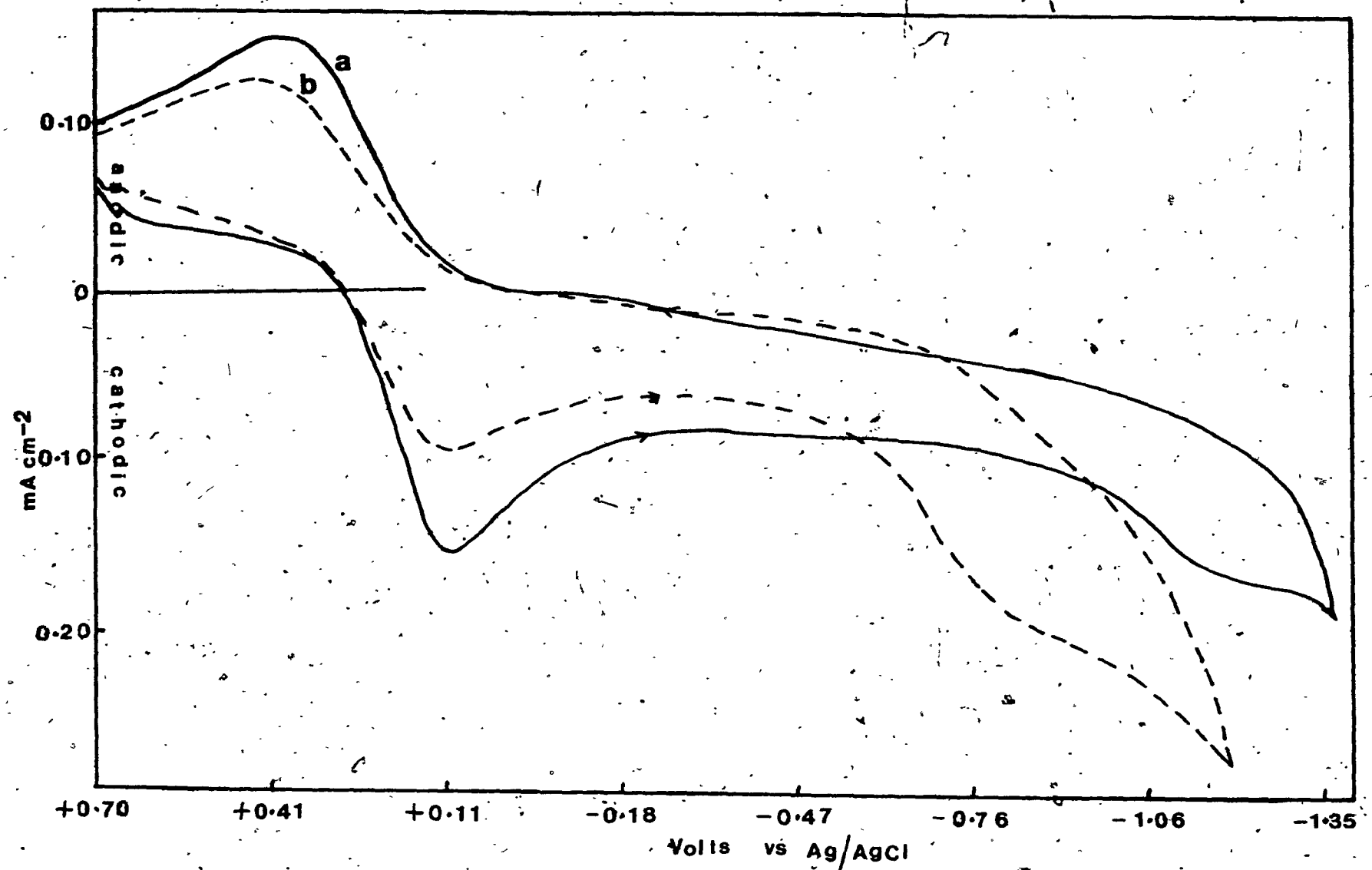

Figure 6-9. Cyclic voltammetric waves for Electrode 10, SnO_2-QPVP-Pt$(mnt)_2^{2-}$ in contact with 0.1 M KCl electrolyte. (a) before photoelectrochemical measurements; (b) after photoelectrochemical measurements.

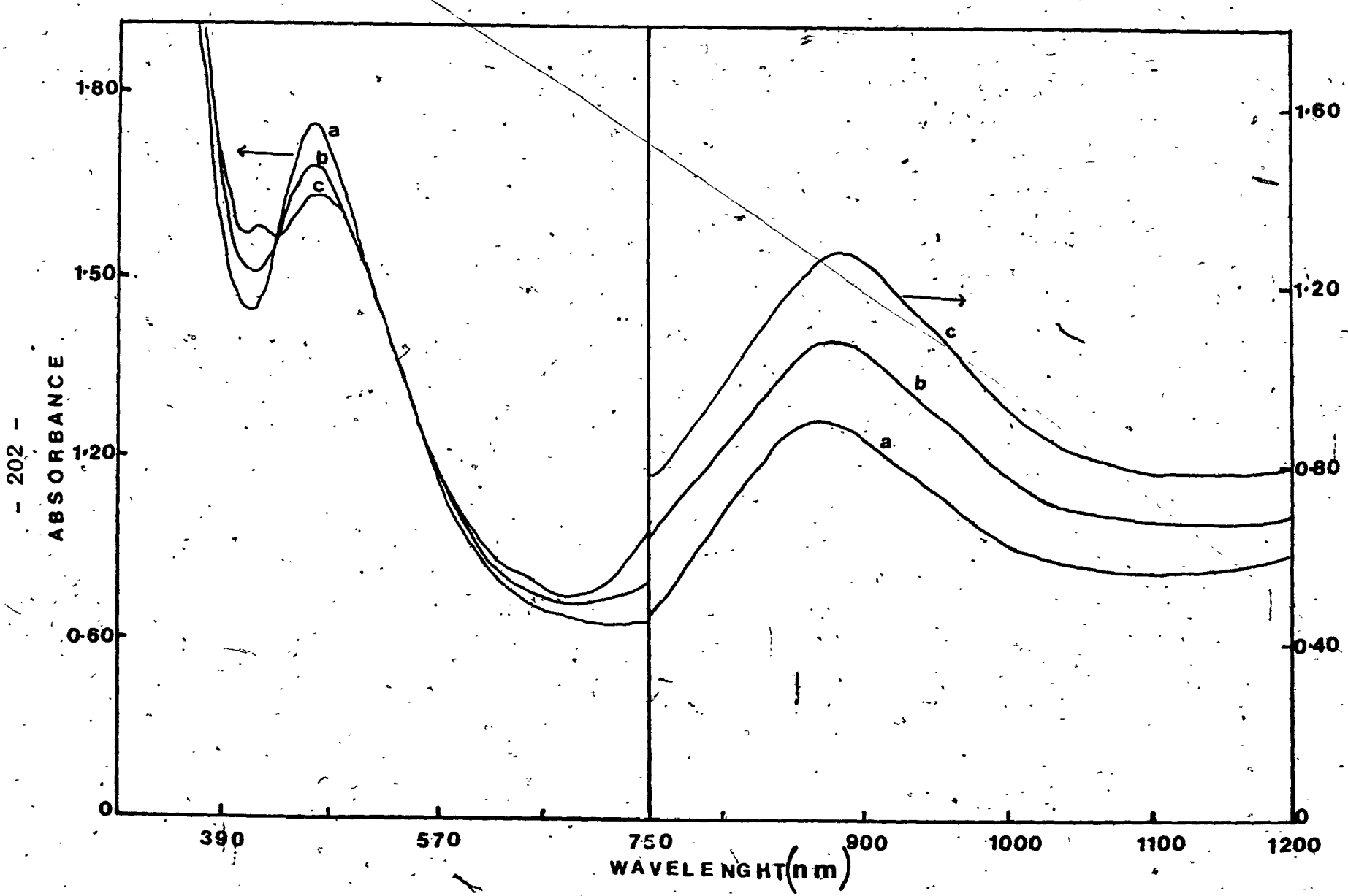

Figure 6-10. Absorption spectra for Electrode 10, SnO_2-QPVP-Pt(mnt)$_2^{2-}$; (a) before photoelectrochemistry; (b) and (c) after the first and second photoelectrochemical measurements.

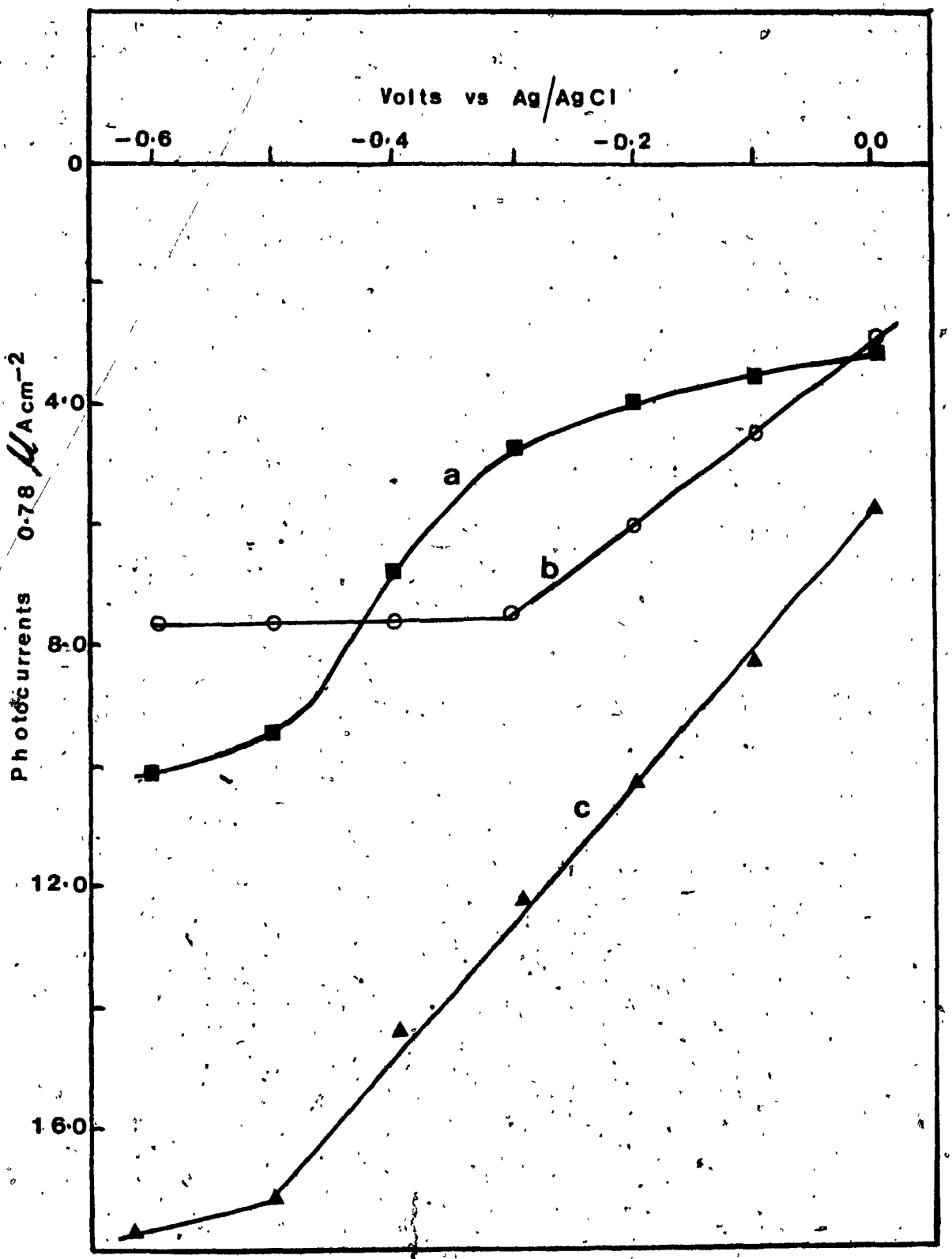

Figure 6-11. The dependence of cathodic photocurrents (first measurement) on potential for Electrode 11; SnO_2-QPVP-Pt(mnt)$_2^{2-}$ in contact with 0.1 M KCl electrolyte. (a) prompt photocurrent; (b) slow photocurrent; (c) total photocurrents. Measurements were started at -0.6 V.

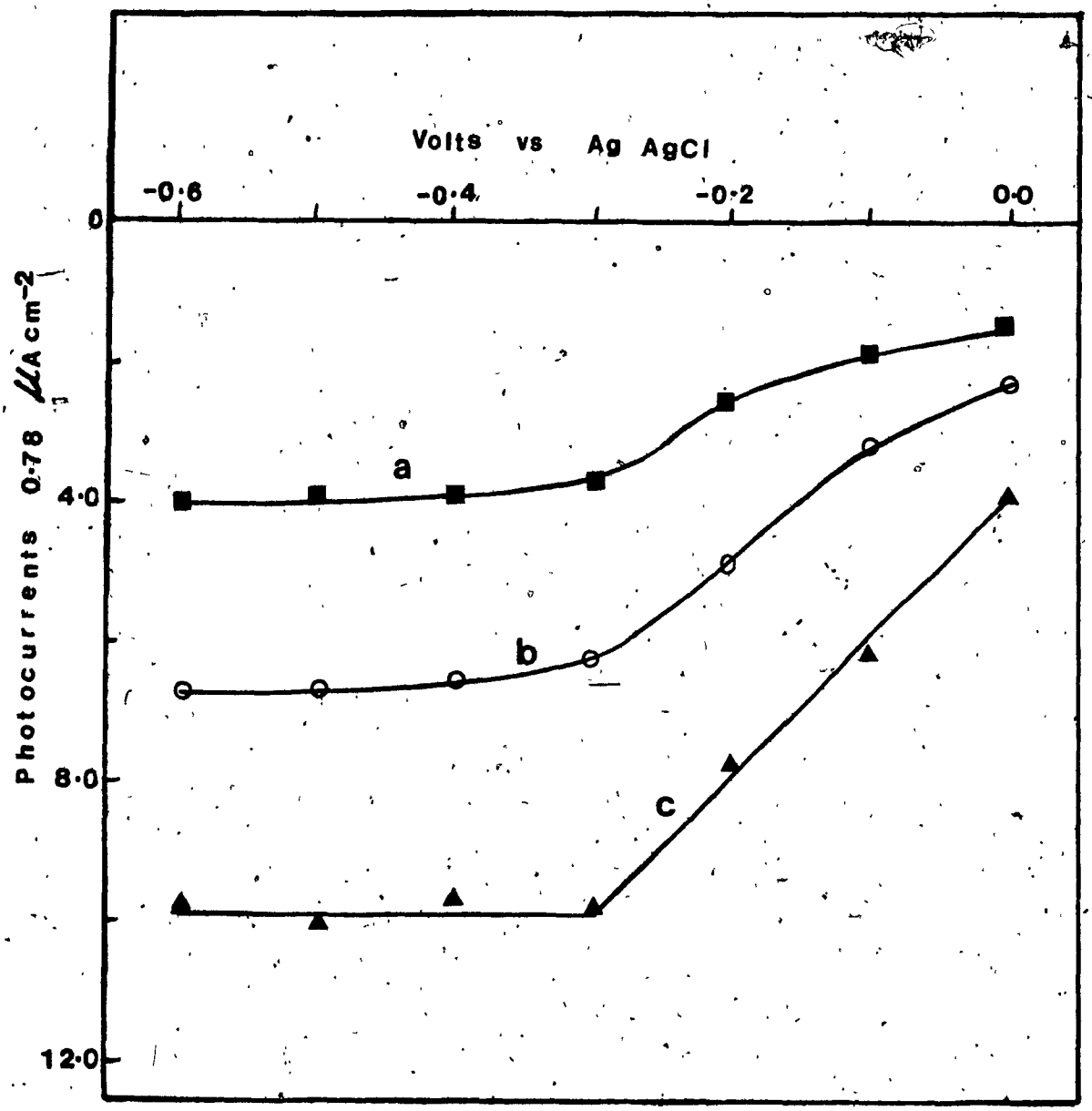

Figure 6-12. The dependence of cathodic photocurrents (second measurement) on potential for Electrode 11; SnO_2-QPVP-Pt(mnt)$_2^{2-}$ in contact with 0.1 M KCl aqueous electrolyte; (a) prompt photocurrent; (b) slow photocurrent; (c) total photocurrents. Measurements were started at -0.6 V.

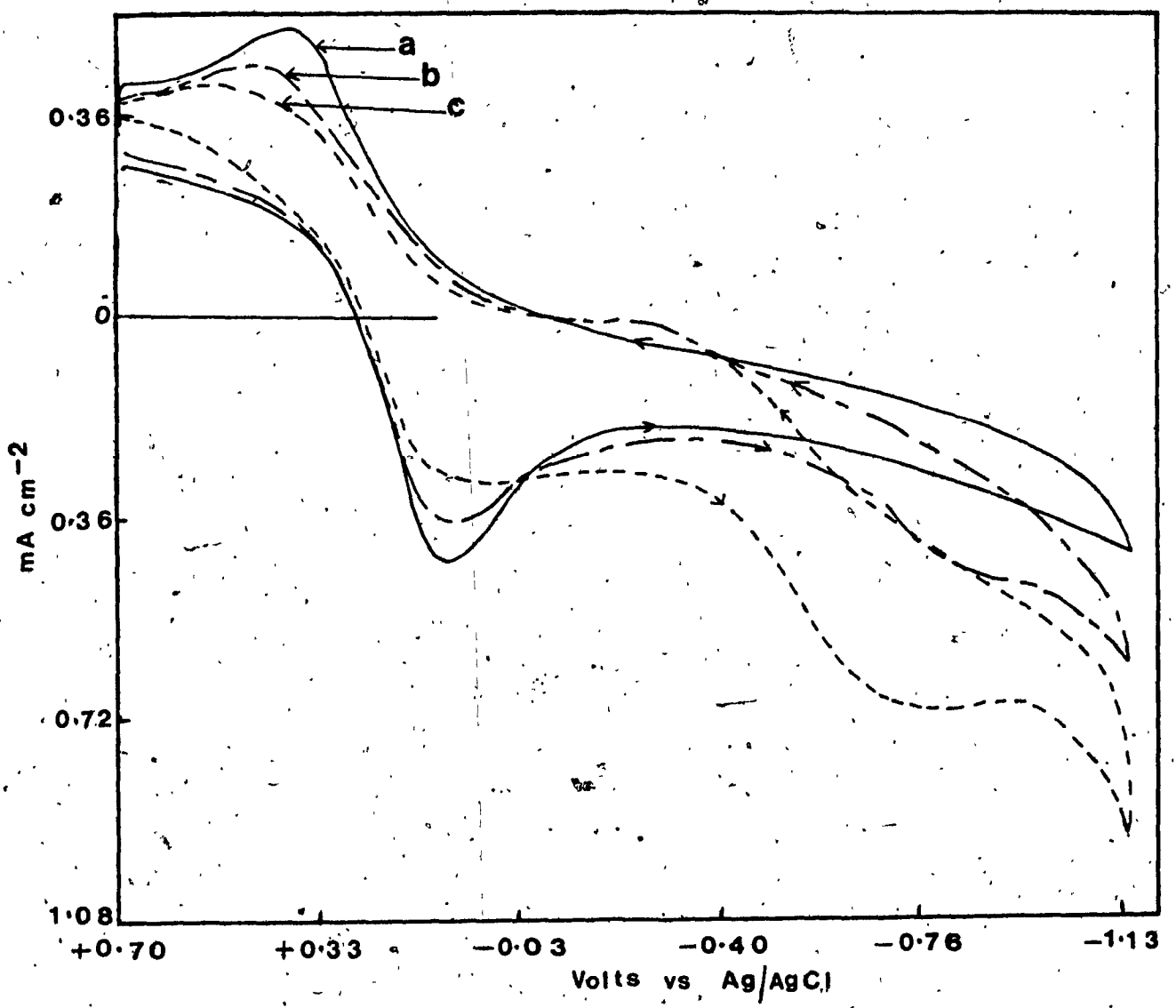

Figure 6-13. Cyclic voltammetric waves for Electrode 11; SnO_2-QPVP-Pt$(mnt)_2^{2-}$ in contact with 0.1 M KCl aqueous electrolyte electrolyte. (a) before photoelectrochemical measurements; (b) and (c) after first and second photoelectrochemical measurements, respectively.

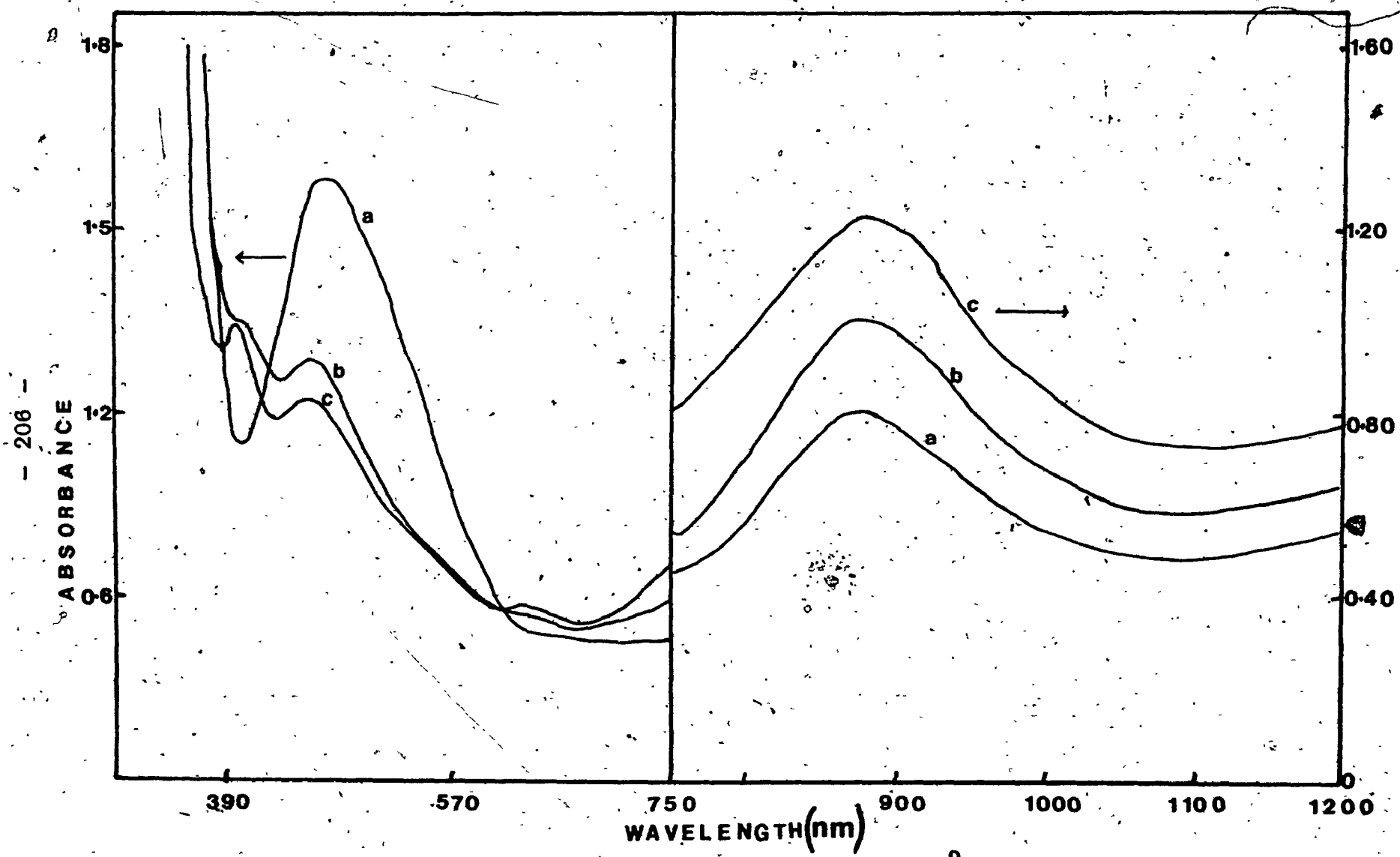

Figure 6-14. Absorption spectra for Electrode 11; SnO_2-QPVP-Pt(mnt)$^{2-}$. (a) before photoelectrochemistry; (b) and (c) after first and second photoelectrochemical measurements.

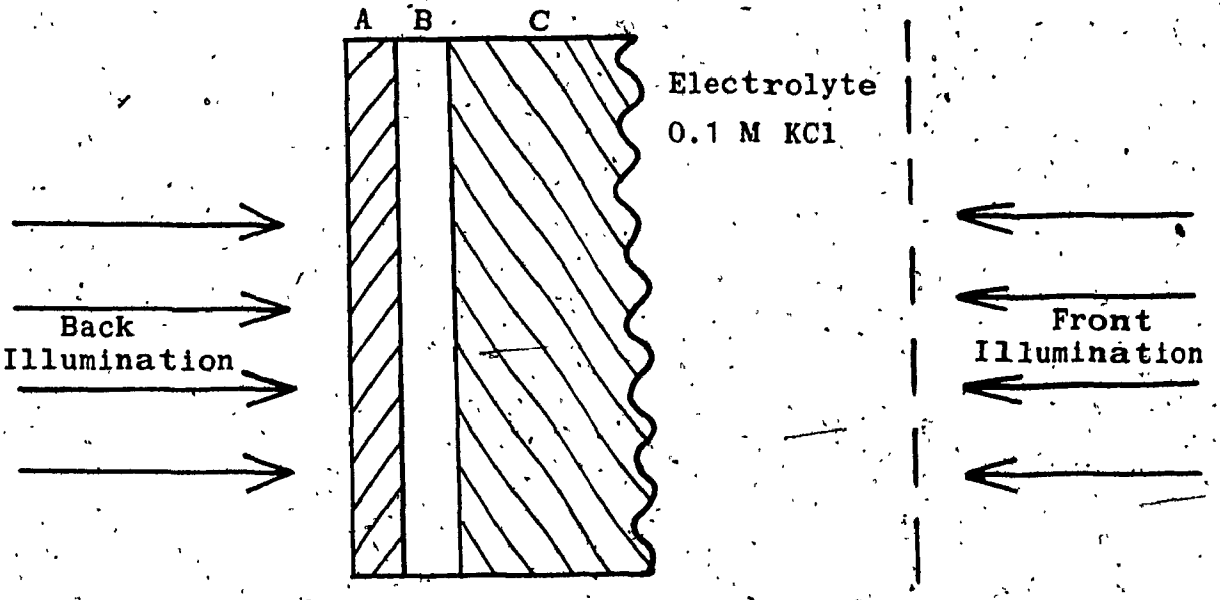

Figure 6-15. Schematic representation of Back and Front illumination:
(A) Glass
(B) SnO_2 layer
(C) QPVP polymer layer with $M(mnt)_2^{2-}$.

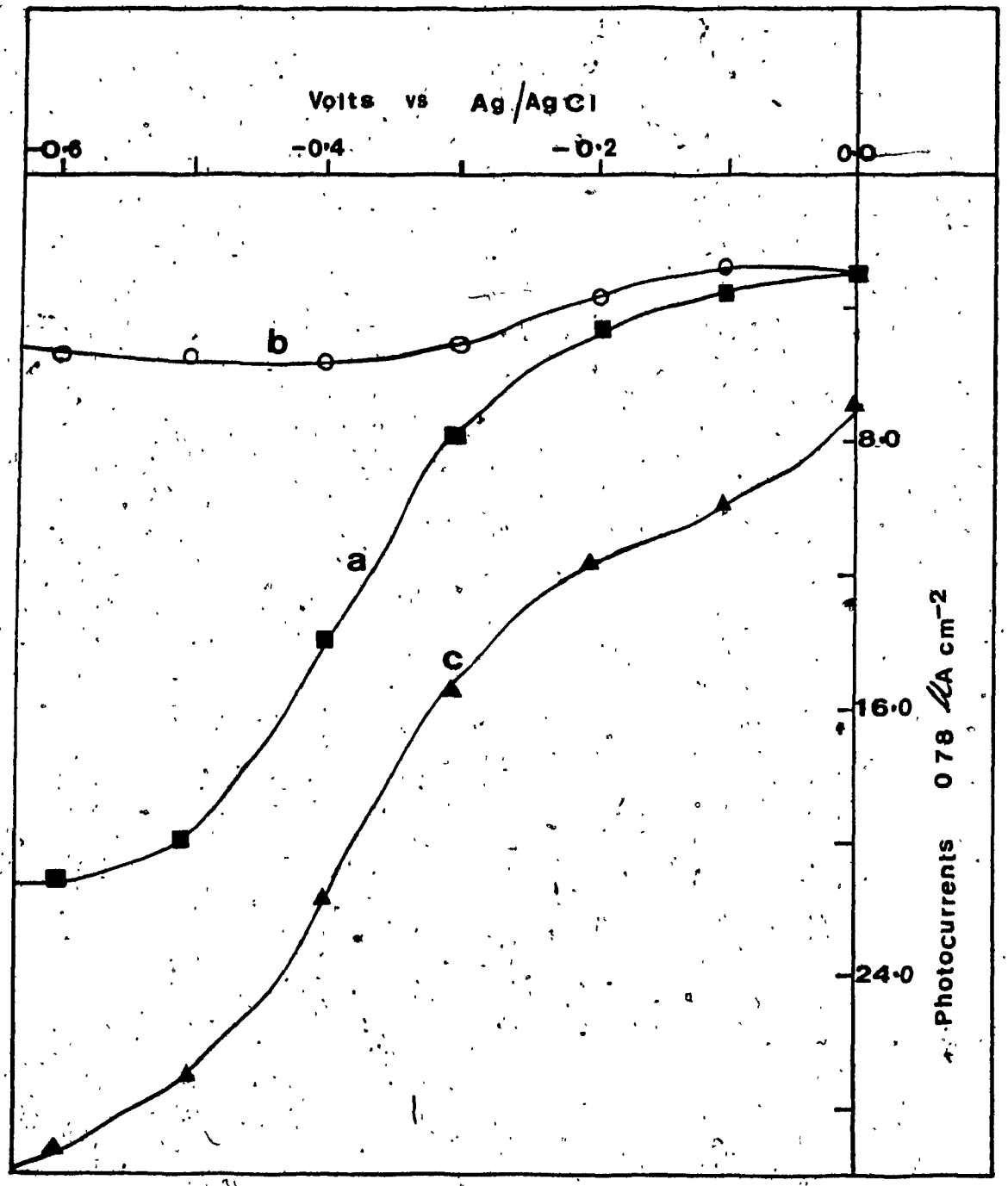

Figure 6-16. The dependence of cathodic photocurrents (first measurement) on potential for Electrode 12; SnO_2-QPVP-Pt(mnt)$_2^{2-}$ in contact with 0.1 M KCl aqueous electrolyte. Electrode was irradiated from SnO_2 side. (a) prompt photocurrent; (b) slow photocurrent; (c) total photocurrents.

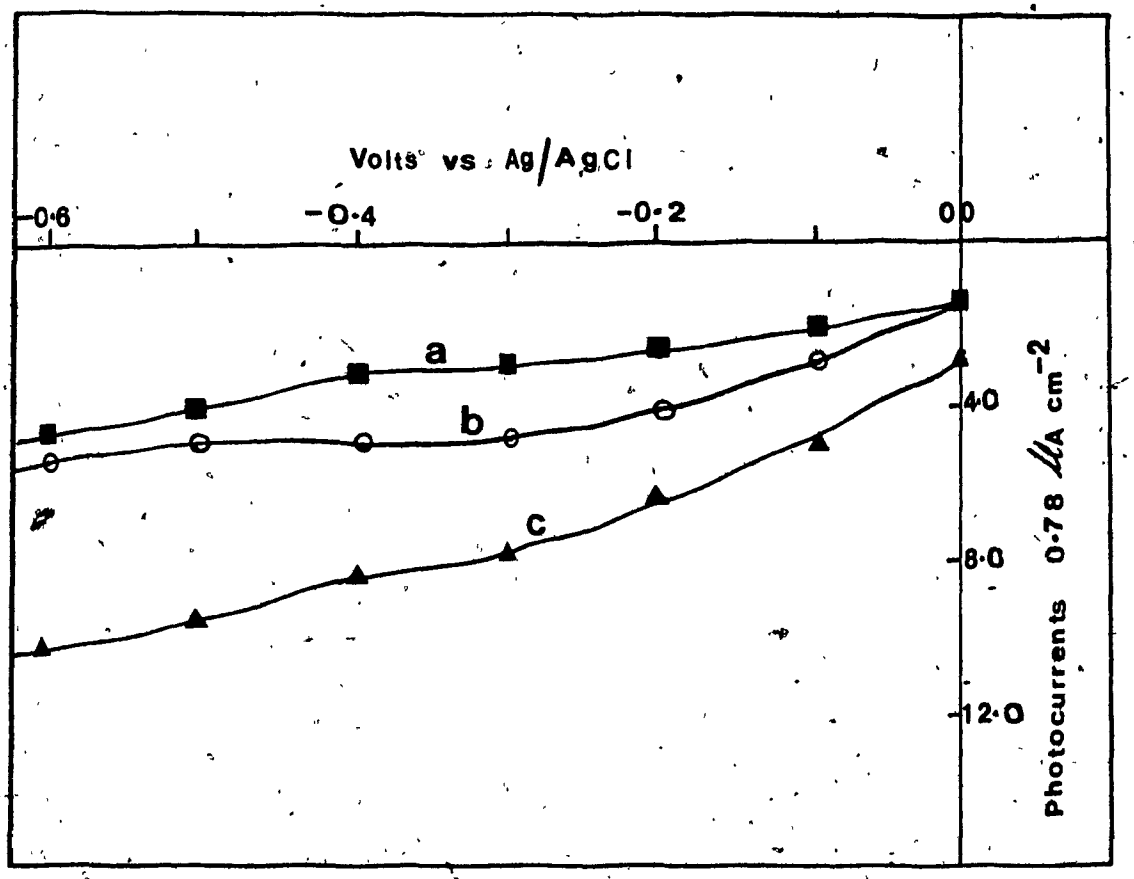

Figure 6-17. The dependence of cathodic photocurrents (second-measurement) on potential for Electrode 12; SnO_2-QPVP-Pt(mnt)$_2^{2-}$ in contact with 0.1 M KCl aqueous electrolyte. Electrode was irradiated from SnO_2 side. (a) prompt photocurrent; (b) slow photocurrent; (c) total photocurrents.

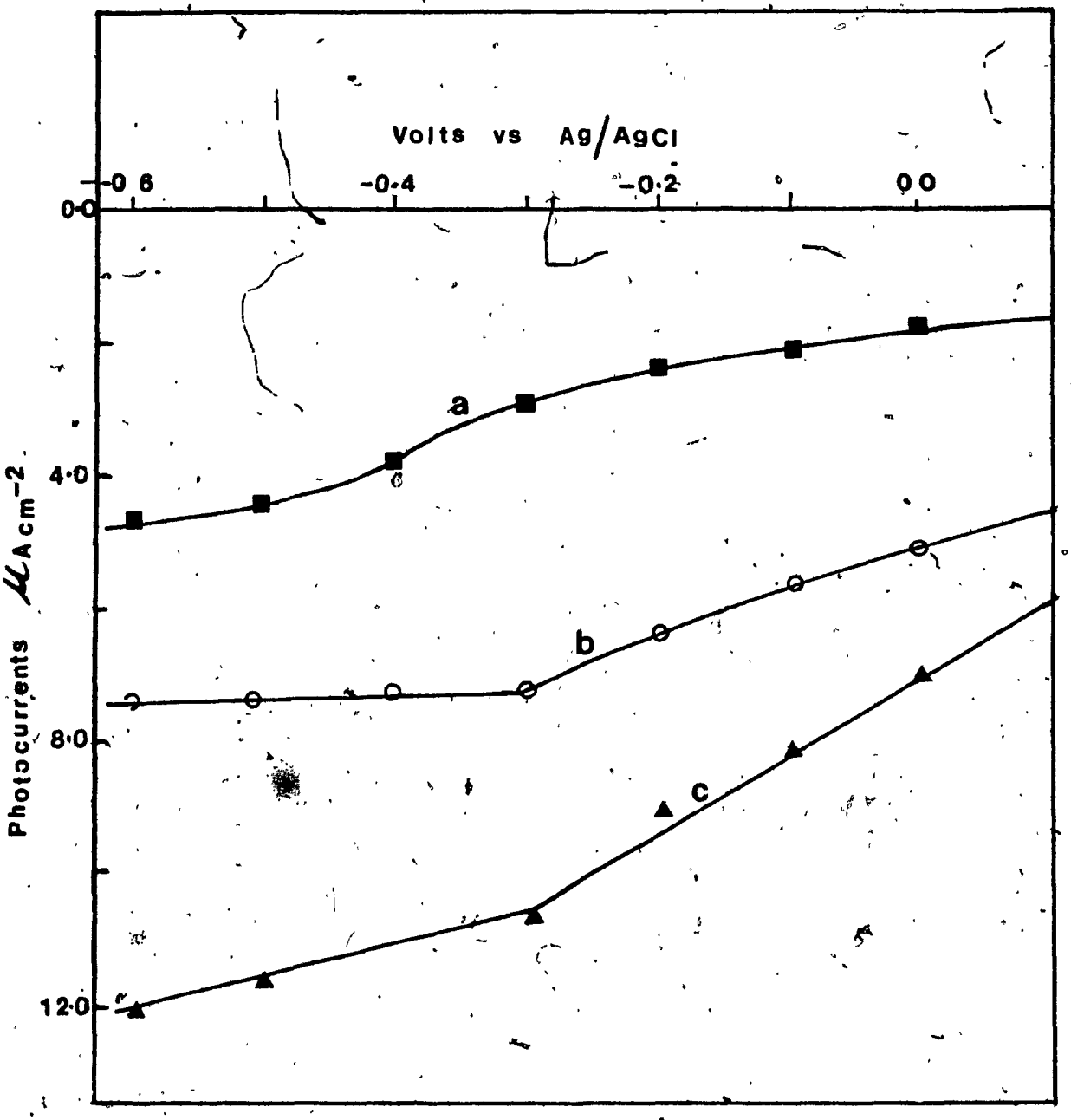

Figure 6-18. The dependence of cathodic photocurrents (first measurement) on potential for Electrode 13; SnO_2-QPVP-Pt(mnt)$_2^{2-}$ in contact with 0.1 M KCl aqueous electrolyte. Electrode was irradiated from electrolyte side. (a) prompt photocurrent; (b) slow photocurrent; (c) total photocurrent.

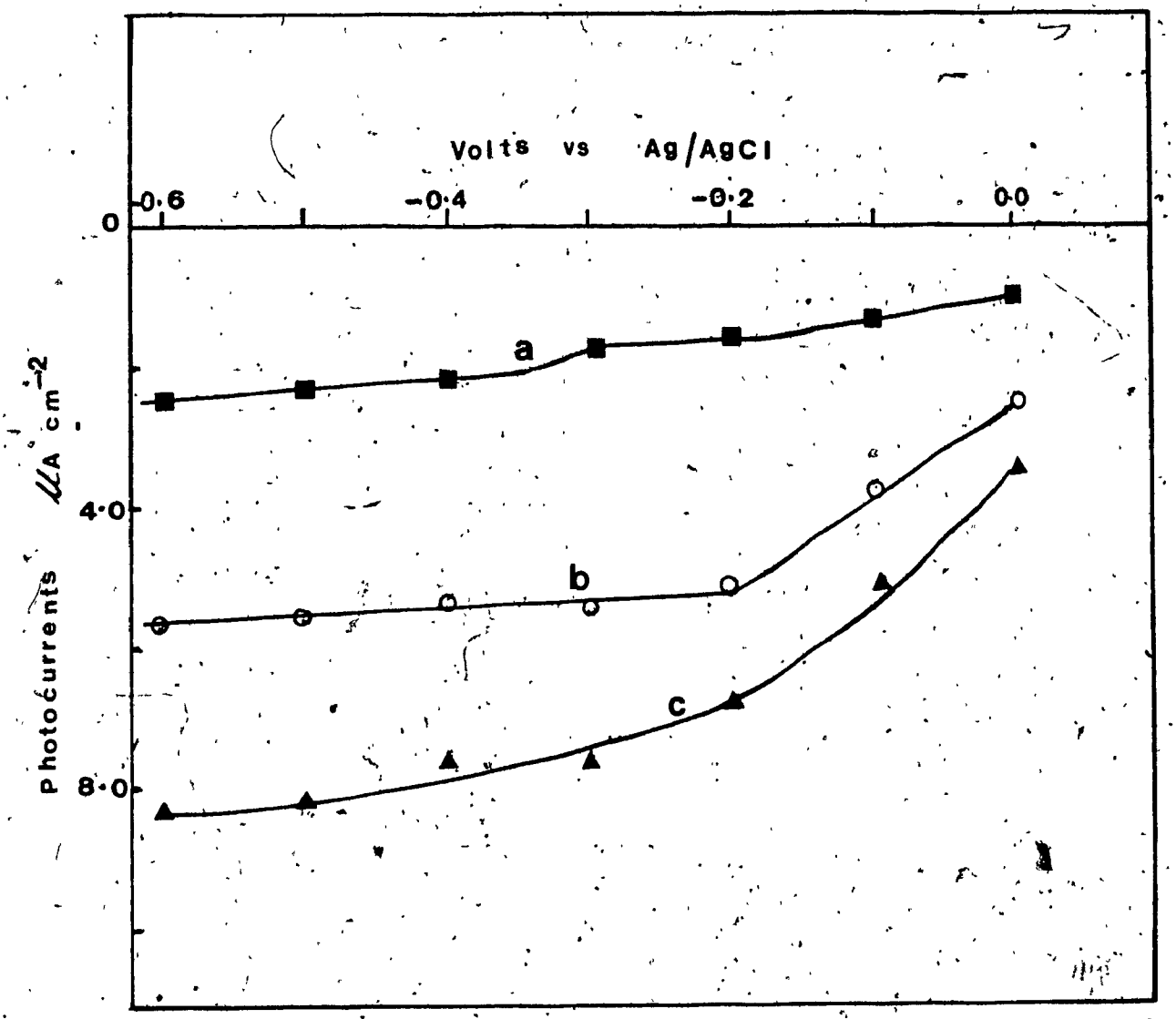

Figure 6-19. The dependence of cathodic photocurrents (second measurement) on potential for Electrode 13; SnO_2-QPVP-Pt(mnt)$_2^{2-}$ in contact with 0.1 M KCl aqueous electrolyte. Electrode was irradiated from electrolyte side. (a) prompt photocurrent; (b) slow photocurrent; (c) total photocurrent.

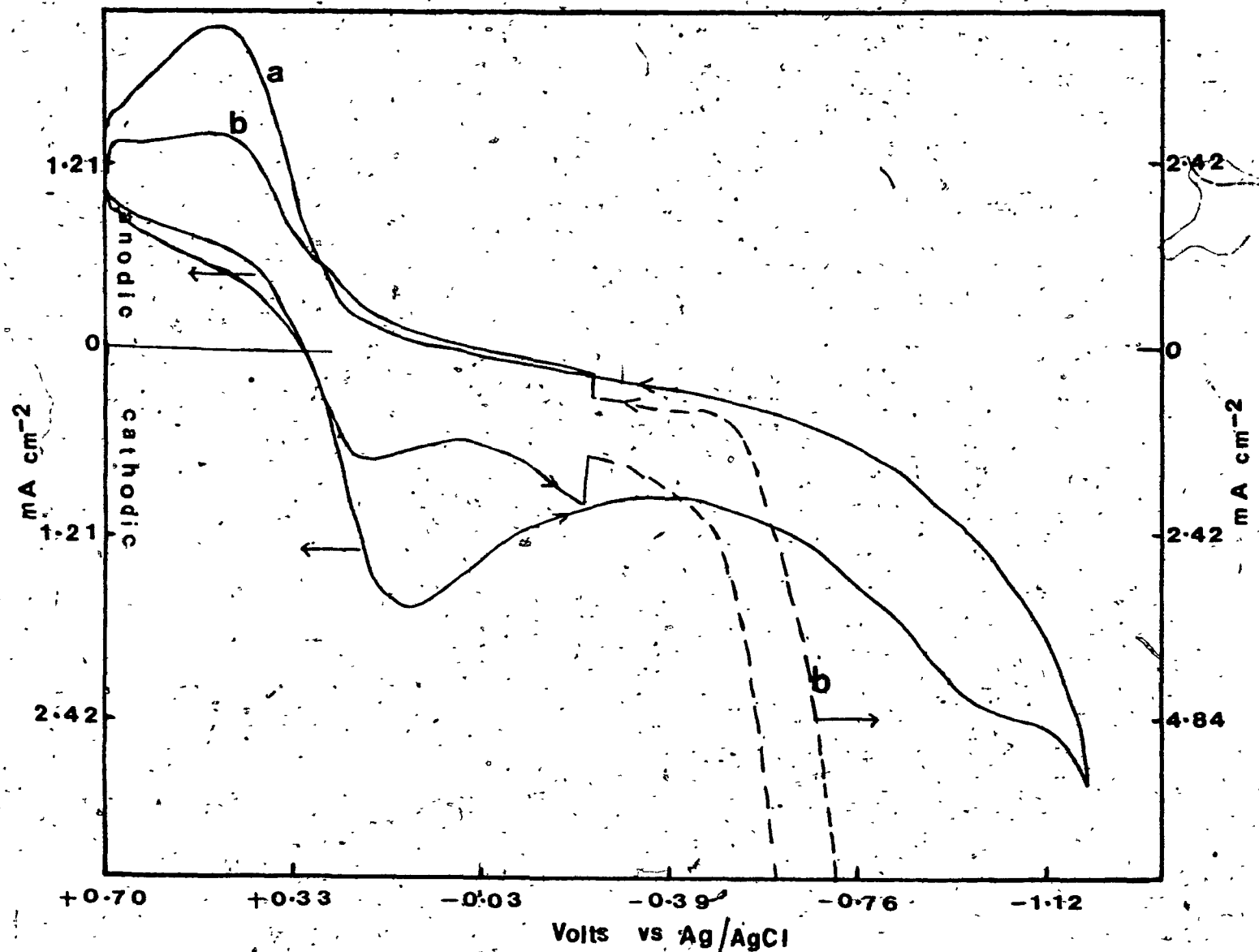

Figure 6-20. Cyclic voltammetric waves of Electrode 14; SnO_2-QPVP-Pt(mnt)$_2^{2-}$ in contact with 0.1 M KCl aqueous electrolyte. (a) before irradiated and polarized at -0.4 V; (b) after irradiated and polarized at -0.4 V for 10 hrs.

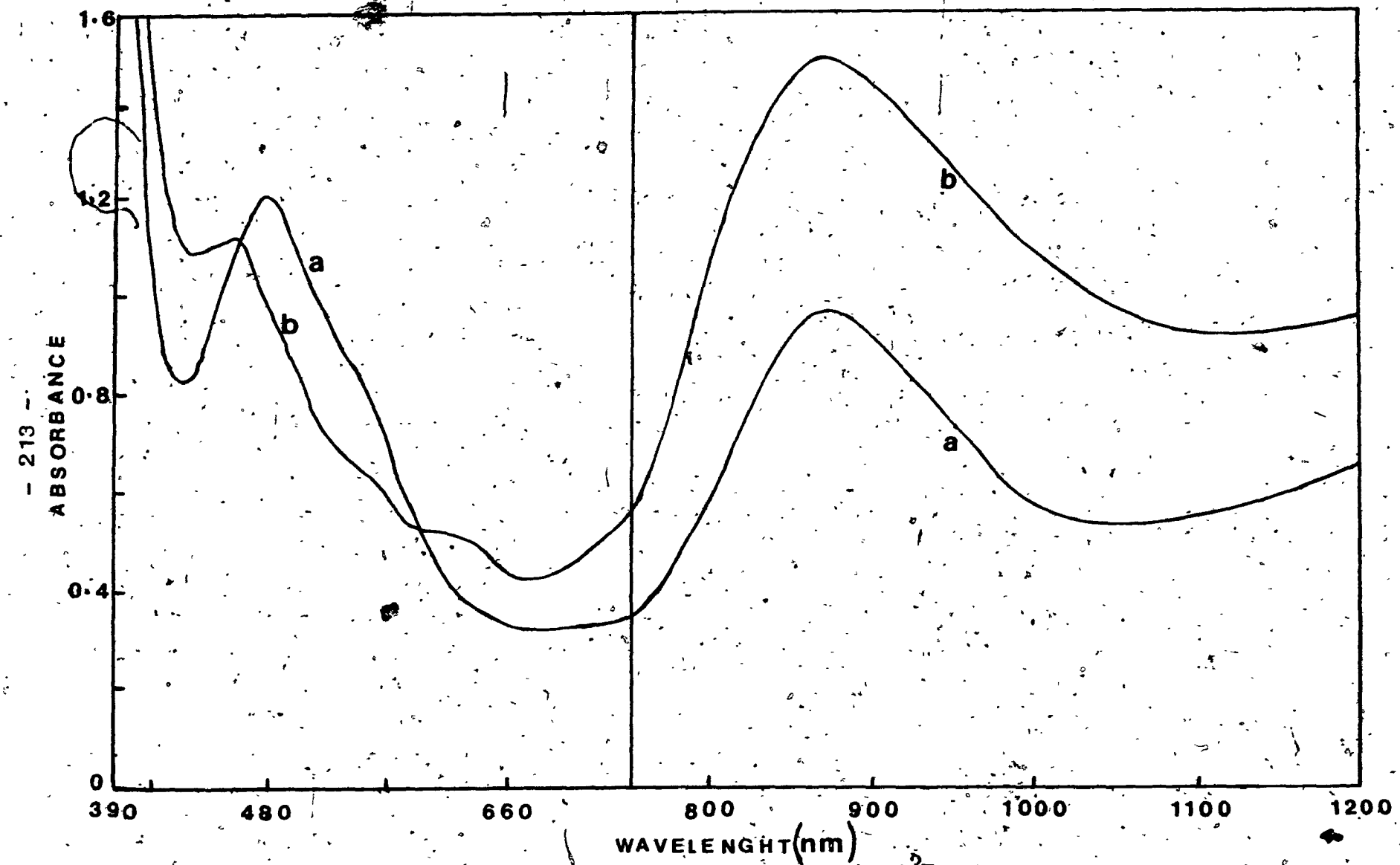

Figure 6-21. Absorption spectra of Electrode 14; SnO_2-QPVP-$Pt(mnt)_2^{2-}$; (a) before irradiation and polarization; (b) after irradiation and polarization for 10 hrs.

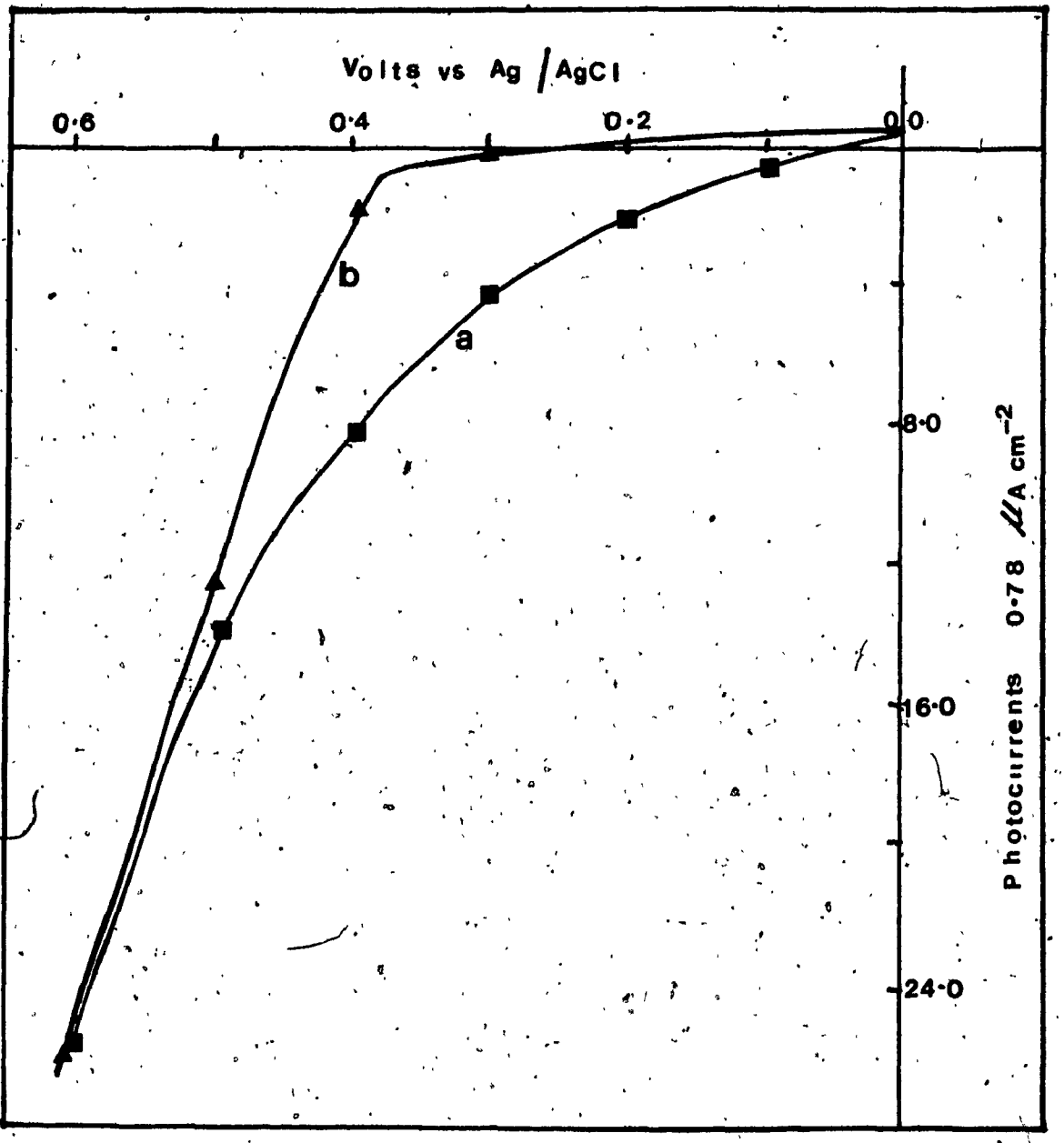

Figure 6-22. Photoelectrochemical behaviour of Electrode 15; SnO_2-QPVP-Pt$(mnt)_2^{2-}$ in contact with 0.1 M HCl electrolyte. (a) cathodic photocurrents from first measurement; (b) cathodic photocurrents from second measurement.

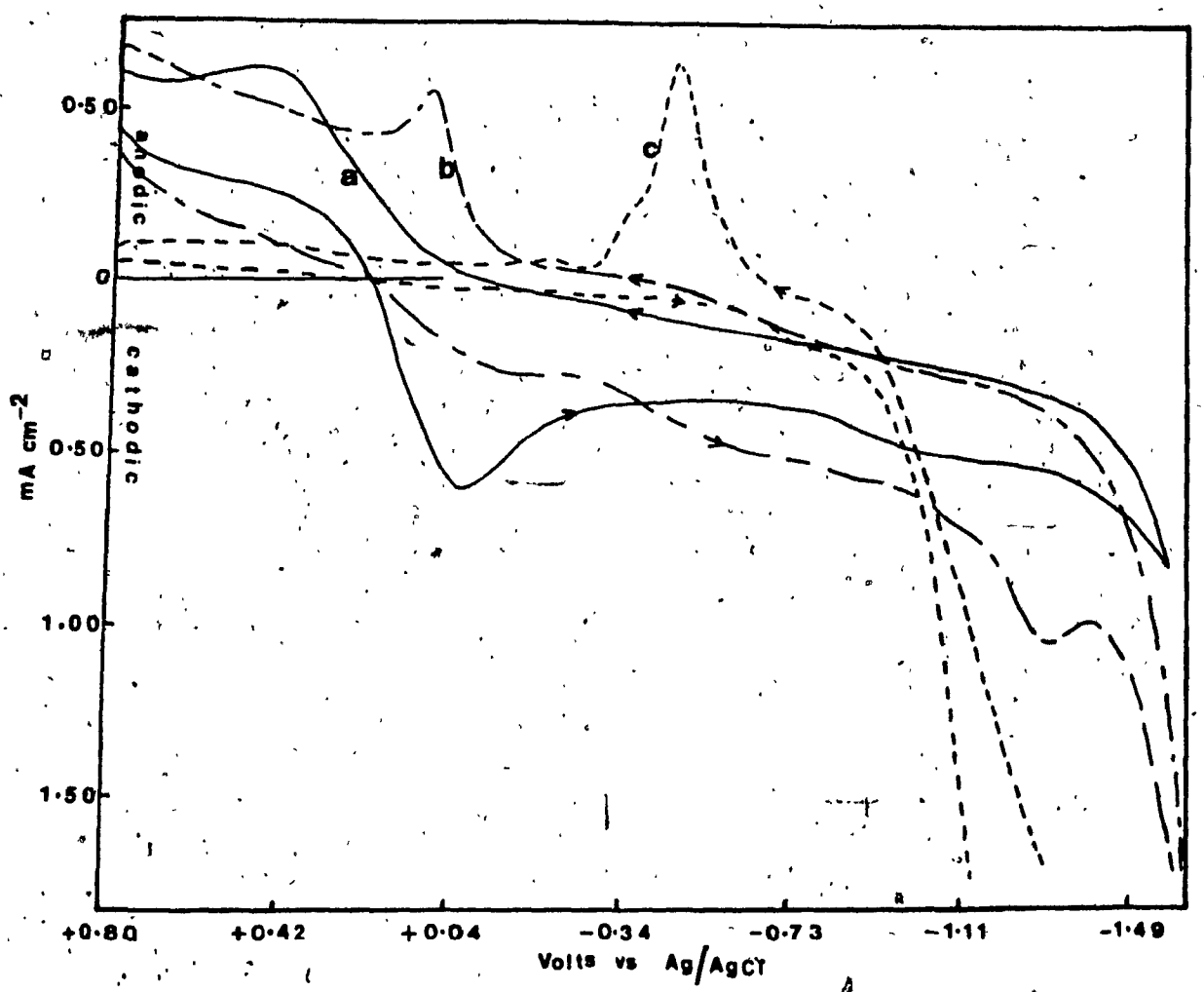

Figure 6-23. Cyclic voltammetric response for Electrode 15; SnO_2-QPVP-$Pt(mnt)_2^{2-}$ in contact with: 0.1 M KCl; (b) 0.1 M HCl before photoelectrochemical measurements; (c) 0.1 M HCl after photoelectrochemical measurements.

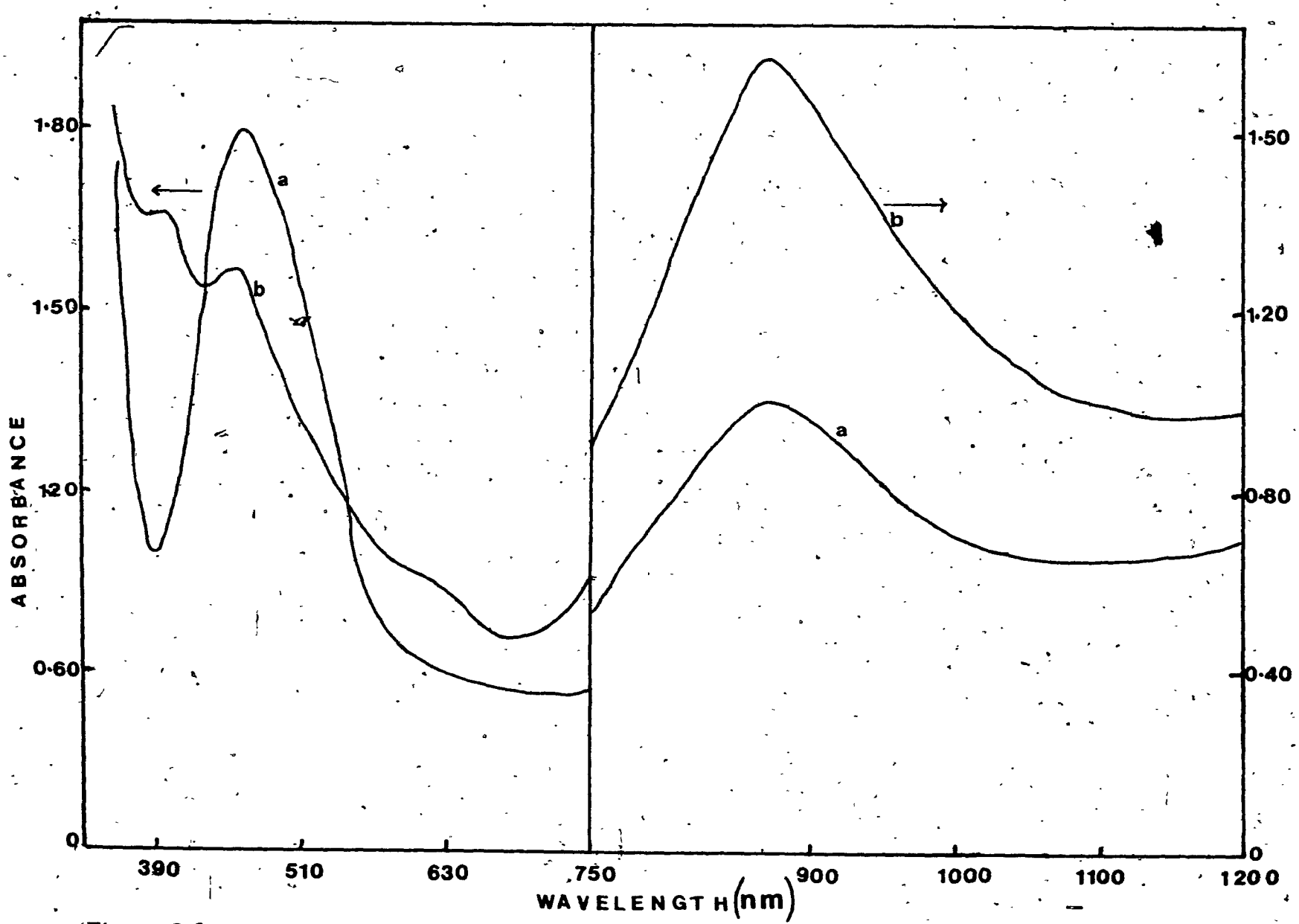

Figure 6-24. Absorption spectra for Electrode 15; SnO_2-PVP-Pt(mnt)$_2^{2-}$; (a) before photoelectrochemistry; (b) after photoelectrochemistry in contact with 0.1 M HCl electrolyte.

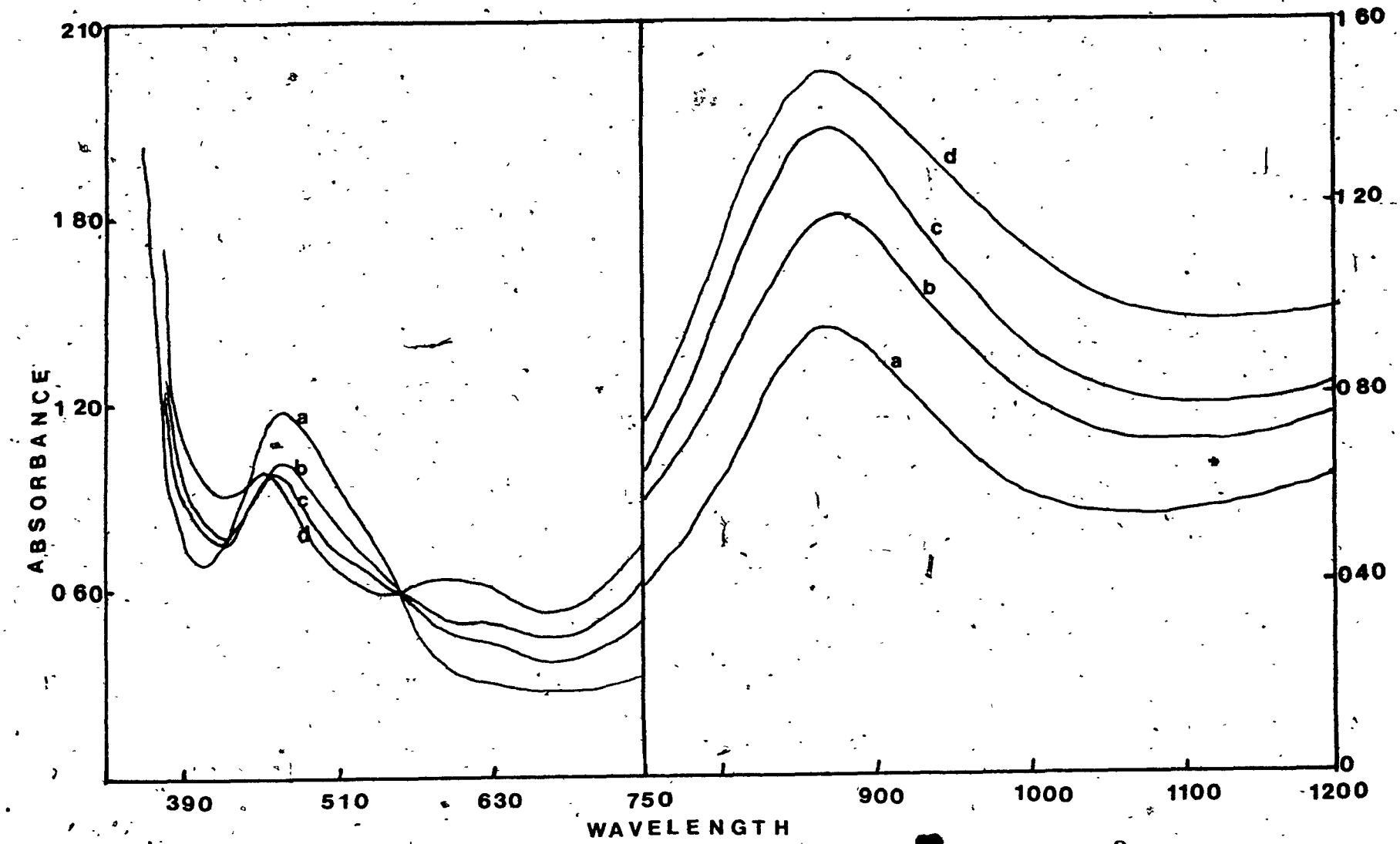

Figure 6-25. Changes in absorption spectrum of Electrode 16; SnO_2-QPVP-$Pt(mnt)_2^{2-}$ upon chemical treatment with 6.0 M HCl. (a) before treatment; (a) after treatment for 8 mins; (b) and (c) are intermediate between 0 and 8 mins.

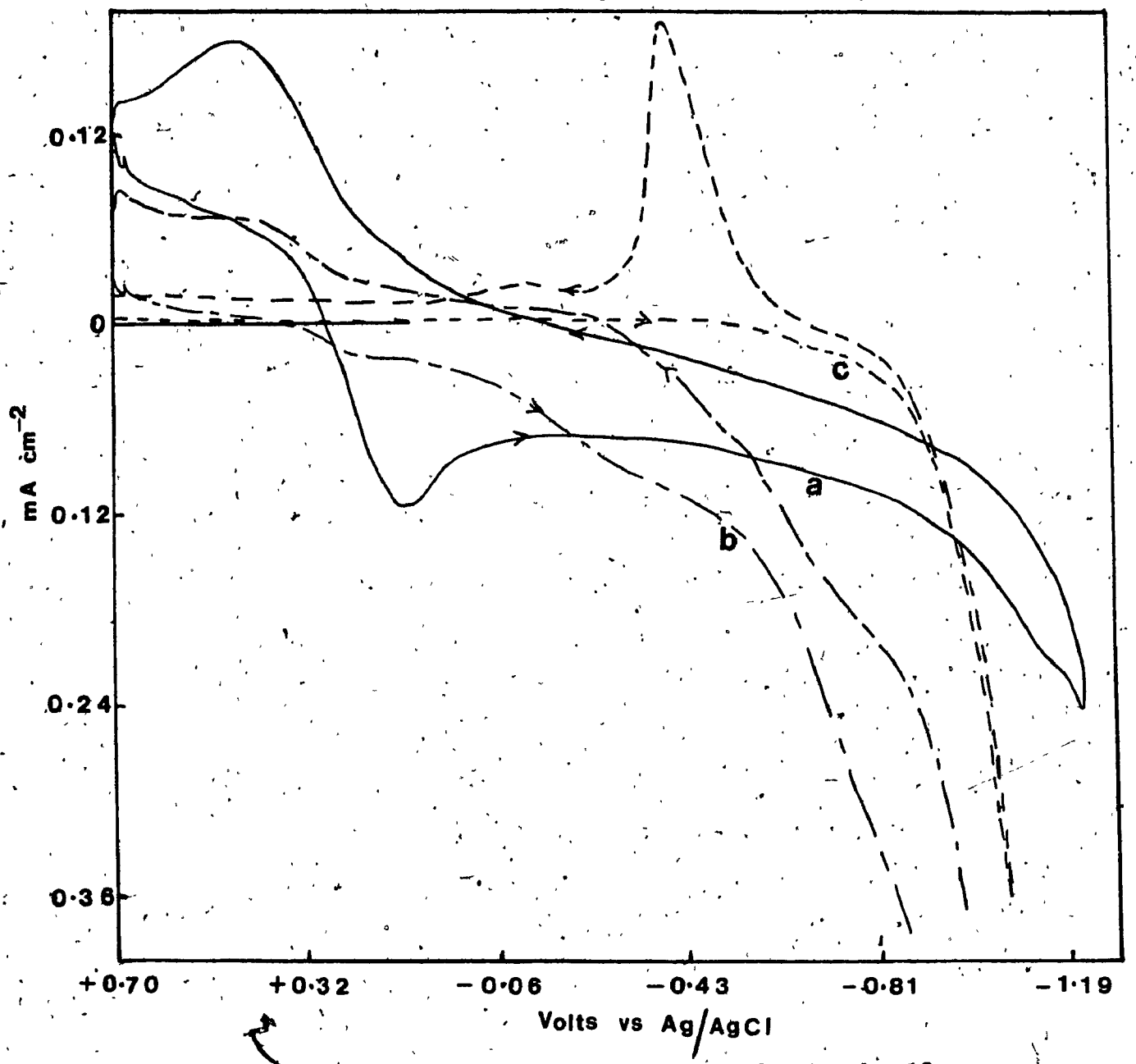

Figure 6-26. Voltammetric response of Electrode 16; SnO_2-QPVP-$Pt(mnt)_2^{2-}$ in 0.1 M KCl aqueous electrolyte; (a) before chemical treatment with 6.0 M HCl; (b) after exposure to 6.0 M HCl for 4 mins; (c) after treatment for 8 mins.

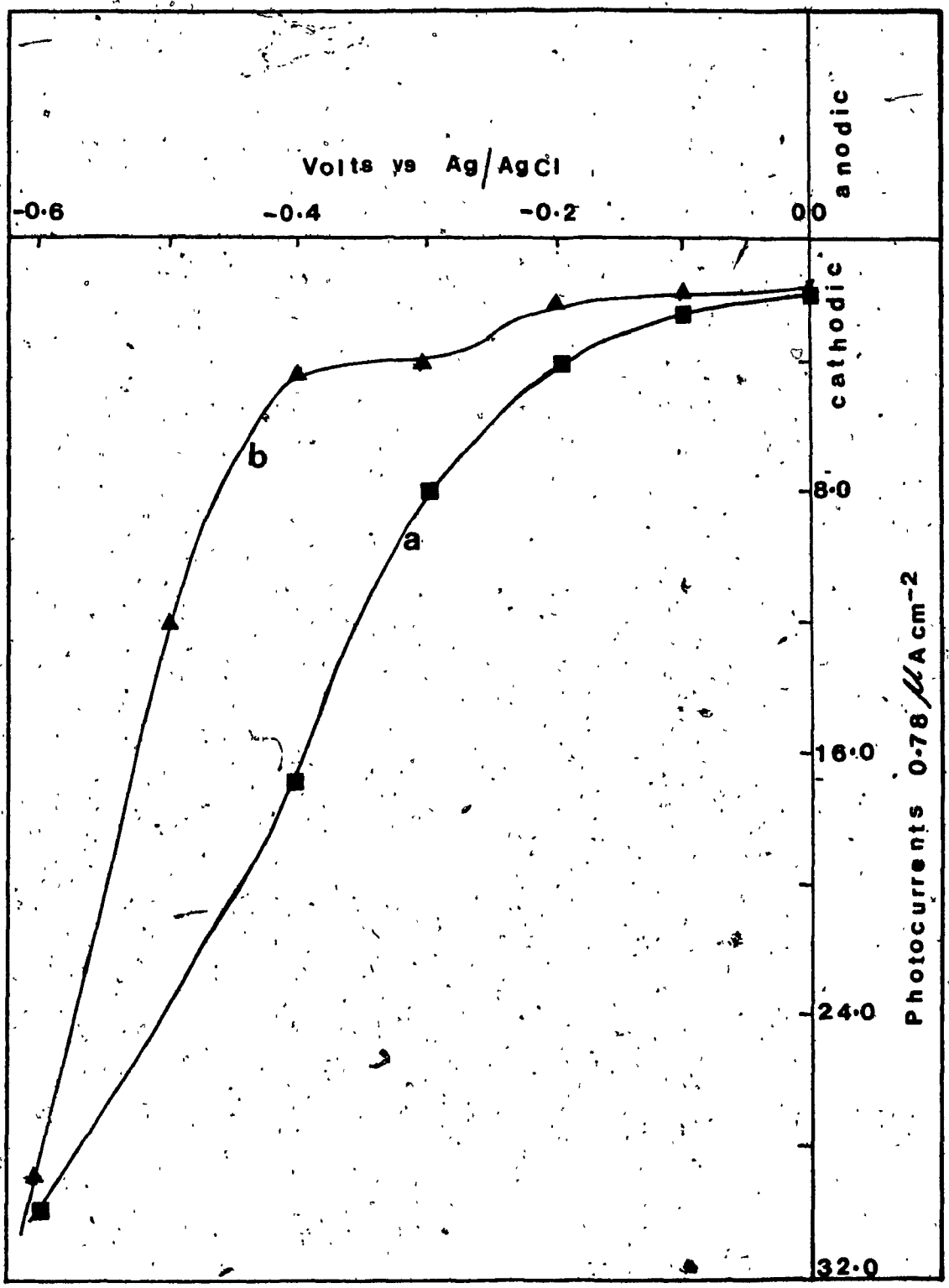

Figure 6-27. Photoelectrochemical behaviour of Electrode 16; SnO_2-QPVP-Pt(mnt)$_2^{2-}$ in 0.1 M KCl aqueous electrolyte after treatment with 6.0 M HCl. (a) first measurement; (b) second measurements.

Figure 6-28. Micrograph of SnO_2-QPVP-$Pt(mnt)_2^{2-}$ modified electrodes: (a) Before PEC; (b) After PEC.

Table 6-1

Properties of SnO_2 Modified Electrodes Used in Photoelectrochemistry.

No	Modified Electrode	Conc. of complex M cm^{-3}	Conc. of complex M cm^{-2}	Conc. of polymer M cm^{-2}	Thickness (1) m	Ratio of $\frac{[QPVP]}{[M(mnt)_2^{2-}]}$	% QPVP neutralized by $M(mnt)_2^{2-}$
8	SnO -QPVP- $Ni(mnt)_2^{2-}$	8.84×10^{-4}	2.83×10^{-7}	3.23×10^{-6}	3.2	11.41	17.51
9	SnO -QPVP- $Ni(mnt)_2^{2-}$	1.48×10^{-3}	4.90×10^{-7}	3.33×10^{-6}	3.3	6.78	29.50
10	SnO -QPVP- $Pt(mnt)_2^{2-}$	1.41×10^{-3}	4.50×10^{-7}	3.19×10^{-6}	3.2	7.08	28.24
11	SnO -QPVP- $Pt(mnt)_2^{2-}$	1.36×10^{-3}	4.49×10^{-7}	3.28×10^{-6}	3.3	7.30	27.41
12	SnO -QPVP- $Pt(mnt)_2^{2-}$	2.49×10^{-3}	7.72×10^{-7}	3.22×10^{-6}	3.1	4.16	48.02
13	SnO -QPVP- $Pt(mnt)_2^{2-}$	2.46×10^{-3}	7.86×10^{-7}	3.17×10^{-6}	3.2	4.03	49.54

Chapter 7

Results V

7.1. Photolysis of Solutions and Slurries

7.1.1 Continuous Photolysis of $Pt(mnt)_2^{2-}$ in Mixed Solvent

Continuous photolysis of $[(C_2H_5)_4N)_2Pt(mnt)_2^{2-}$ in acetonitrile containing 0.1 M $NaClO_4$ and 30% water was accomplished in a closed glass electrochemical cell. The cell was equipped for use with a conventional three electrode system including a dispersion tube for deoxygenation. The solution was thoroughly deoxygenated with prepurified nitrogen for 1 hr before the voltammogram of Figure 7-1(a) was recorded at a Pt electrode with Ag/AgCl (Sat. KCl) reference. The solution was then irradiated for 2 hrs using the same light source as was used for irradiating the modified electrodes. Voltammogram (b) of Figure 6-29 was then recorded. In this voltammogram the redox waves for the reaction $Pt(mnt)_2^{2-}/Pt(mnt)_2^{1-}$ at the Pt electrode, as was observed in voltammogram (a), completely disappeared and a new irreversible cathodic peak was seen at -0.56 V. This peak was closely followed by solvent decomposition. During the period of irradiation and in the course of recording the voltammograms the solution was not stirred.

The solution was allowed to sit still in the cell for

an additional 4 hr without illumination after which time the voltammogram of Figure 7-2 (a) was taken. The solution was then stirred by bubbling nitrogen gas then voltammogram (b) of Figure 7-2 was recorded. In voltammogram (a) no faradaic response was obtained but in (b), after stirring 6 hrs irreversible peak at -0.56 seen in Figure 7-1 (b) was apparent. No wave for the reaction $Pt(mnt)_2^{2-}/Pt(mnt)_2^{1-}$ was seen.

The content of the cell after irradiation was referred to as a "solution" but fine particles were observed and it appeared to be a suspension rather than a solution. The content of the cell was then left for another 8 hrs, fine particles settled at the bottom of the cell and were recovered. The precipitate was washed with distilled water and dried in vacuum at 50°C.

The voltammogram of these recovered particles dissolved in spectrograde acetonitrile containing 0.1 M $NaClO_4$ at Pt working electrode with a Ag/Ag^+ (0.1 M $AgNO_3$ /CH_3CN) reference is shown in Figure 7-3(a). There are two reversible reactions at +0.68 V and -0.20 V and an irreversible cathodic wave at -0.58 V. In the presence of water however, the behaviour was entirely different. When about 5% of water was present in the solution the voltammogram between +0.40 V and -1.0 V showed that the potential limit of the electrolyte is only about -0.66 V. This is shown in Figure 7-3(b). The area under the anodic peak at -0.16 V and the cathodic peak at -0.23 V

was decreased by approximately 50% compared to those in dry acetonitrile. In the voltammogram with a wider potential window between +0.80 and -1.10 V (Figure 7-3(c)) a further reduction of the area in these peaks was observed. In addition, the anodic and cathodic waves at +0.71 and +0.65 V respectively, seen in dry the acetonitrile, decreased to near disappearance. The solvent potential limit was increased beyond the -0.66 V limit observed in Figure 7-3(c). The solution was left unstirred for 4 hrs after which time a voltammogram was recorded. In this scan no faradaic response was observed only a background residual current. After stirring with nitrogen gas a voltammogram which is similar to Figure 7-2(c) was obtained.

The spectrum of the recovered particles dissolved in dry acetonitrile is shown in Figure 7-4.

The effect of irradiation of $Pt(mnt)_2^{2-}$ in the mixed solvent of acetonitrile and water on the sepctrum was also determined. A 1:4 ratio of water/acetonitrile solution of the complex was irradiated in a spectrophotometer cuvette. The curvette was rendered air tight by means of a rubber septum and after thorough deoxygenation with prepurified nitrogen it was irradiated. Figure 7-5 shows the spectrum of the solution before irradiation, curve (a), while curves (b), (c) and (d) were taken after 4, 6 and 8 hrs respectively. The low intensity band at 844 nm

increased with irradiation while the 472 nm band shifted to 450 nm.

7.2.1 Transient Spectra in the Picosecond Domain.

The complexes $Pt(mnt)_2^{2-}$, $Pt(mnt)_2^{1-}$, $Pd(mnt)_2^{2-}$ and $Ni(mnt)_2^{2-}$ were excited with the picosecond laser system described in chapter 2 using a 30 ps pulse and probed with a continuum pulse between 415 to 660 nm delayed between 20 ps and 10 ns after the excitation.

The solvent was either dry spectrgrade acetonitrile or a mixed solvent system of 30% water in acetonitrile. Water is known to have a flat baseline with no transient within the probe region. Dry acetonitrile was also examined for transient behaviour. A 20 ps delay probe produced no transient but a flat baseline. A delay time of 10 ns showed no transient absorbance but did give a narrow band fluorsecence with a maximum at 448 nm (Figure 7-6). Acetonitrile does not absorb at 335 nm but only in the far U.V. region and the fluorescence may then be induced by a simultaneous absorption of two 355 nm photons, or by impurities. No serious interference should result.

The $Ni(mnt)_2^{2-}$ and $Pd(mnt)_2^{2-}$ were examined in dry spectrograde acetonitrile, $Pt(mnt)_2^{1-}$ was examined in a 30% aqueous acetonitrile solution and $Pt(mnt)_2^{2-}$ was examined in dry acetonitrile as well as a 30% aqueous acetonitrile solution.

Neither the $Pt(mnt)_2^{1-}$ nor $Pd(mnt)_2^{2-}$ showed transient

absorbance and despite the high extinction coefficient in the 420 to 460 nm range, no ground state bleaching was observable.

Excitation of the $Ni(mnt)_2^{2-}$ in dry acetonitrile revealed both transient absorbance and ground state bleaching. Bleaching was observed at 472 nm while the transient showed a broad absorption from approximately 513 nm to the long wavelength probe limit. The absorption maximum occured near 544 nm. Both the absorption and the bleaching signals are dependent on the delay time of the probe beam. The transient absorbance decreased to the baseline as the delay time of the probe was increased to 100 ps but dispite this some of the bleaching signals was still observable. The 100 ps to 7 ns spectra were all on the baseline within the noise but the 10 ns spectrum showed a new absorbance transient. The transient absorption as well as the ground state bleaching are shown in Figure 7-7(A) and (B). These plots represent the average spectrum from 9 shots with a standard deviation of less than plus or minus .01 Δ A.

The $Pt(mnt)_2^{2-}$ complex in dry acetonitrile and in the aqueous/acetonitrile solvent system showed similar behaviour. The bleaching and transient absorbance were in the same region of the spectrum as the nickel. In dry acetonitrile as the delay time of the probe was varied ground state recovery could be seen. However, transient

absorption was practically independent of time. Figure 7-8 shows the recovery within a time delay of 500 ps to 10 ns as well as the absorbance. Between o ps and 500 ps the bleaching was found to be constant. Recovery only occured for times longer than 500 ps. In the mixed solvent system the situation is reversed. Figure 7-9 shows that the recovery of the ground state does not occur while the transient absorption decreases at later probe times. The decay of transient signals in both the nickel and the platinum complexes cannot be analysed quantatively The half-life, $\tau^{1/2}$ was however approximately estimated. For the $Ni(mnt)_2^{2-}$ in dry acetonitrile $\tau^{1/2}$ for the primary transient was estimated as 70 ps. For the $Pt(mnt)_2^{2-}$ complex $\tau^{1/2}$ for this transient was estimated from the 10 ns delay time, which is the longest delay time obtainable from the picosecond laser system. $\tau^{1/2}$ is then approximately 7 ns or greater.

7.2.2 Pulse Fluorescence Measurements

The $Ni(mnt)_2^{2-}$, $Pt(mnt)_2^{2-}$ and $Pt(mnt)_2^{1-}$ complexes were examined for fluorescence emission by the picosecond technique described in chapter 2. These complexes were tested in dry spectrograde acetonitrile and in a mixed solvent system of 40% water in acetonitrile. Additionally, samples of $Ni(mnt)_2^{2-}$ and $Pt(mnt)_2^{2-}$ in water were obtained by vigorously shaking the complex in water to obtain a "saturated solution." The emission from these

"solutions" were also recorded. Acetonitrile was examined first and a small amount of emission was observed for this solvent when excited with the 355 nm pulse. The emission probably comes from minor impurities or as mentioned in section 7.2.1 it is the result of a two photon absorption process. The emission of each sample of the complex at wavelength longer than 515 nm was monitored at two streak speeds; 26.66 ps per channel and 2.27 ps per channel. In all cases the faster streak speed showed a more intense emission but resolution of the emission band was poor. The slower streak speed showed better resolution but the emission intensity was lower. Deligent search for steady state luminescence of the $Ni(mnt)_2^{2-}$ and $Pt(mnt)_2^{2-}$ at ambient temperature bettween 500 to 800 nm using a 472 nm continuous excitation on a Perkin-Elmer MPF-44B spectrofluorometer showed no convencing evidence of emission. Additionally, since the emission of the acetonitrile may cause some interference the pulse emission data are therefore not very reliable until further studies are undertaken. The data are summarized in Table 1 in the appendix. The emission profiles are also given in Figures 1 to 9 in the appendix.

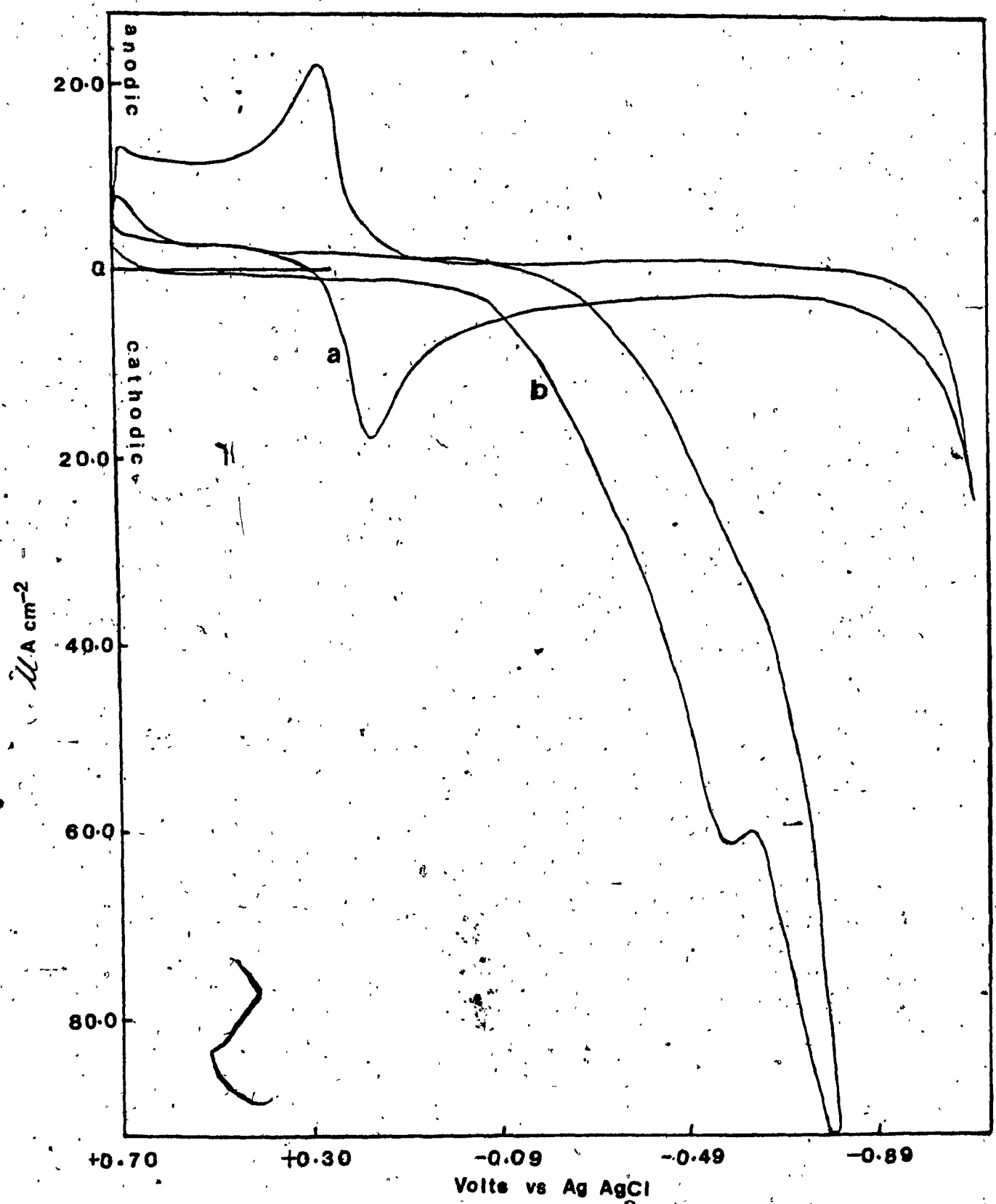

Figure 7-1. Cyclic voltammograms of Pt(mnt)$_2^{2-}$ at Pt electrode in CH_3CN containing 0.1 M $NaClO_4$ and 30% H_2O. (a) before photolysis; (b) after photolysis.

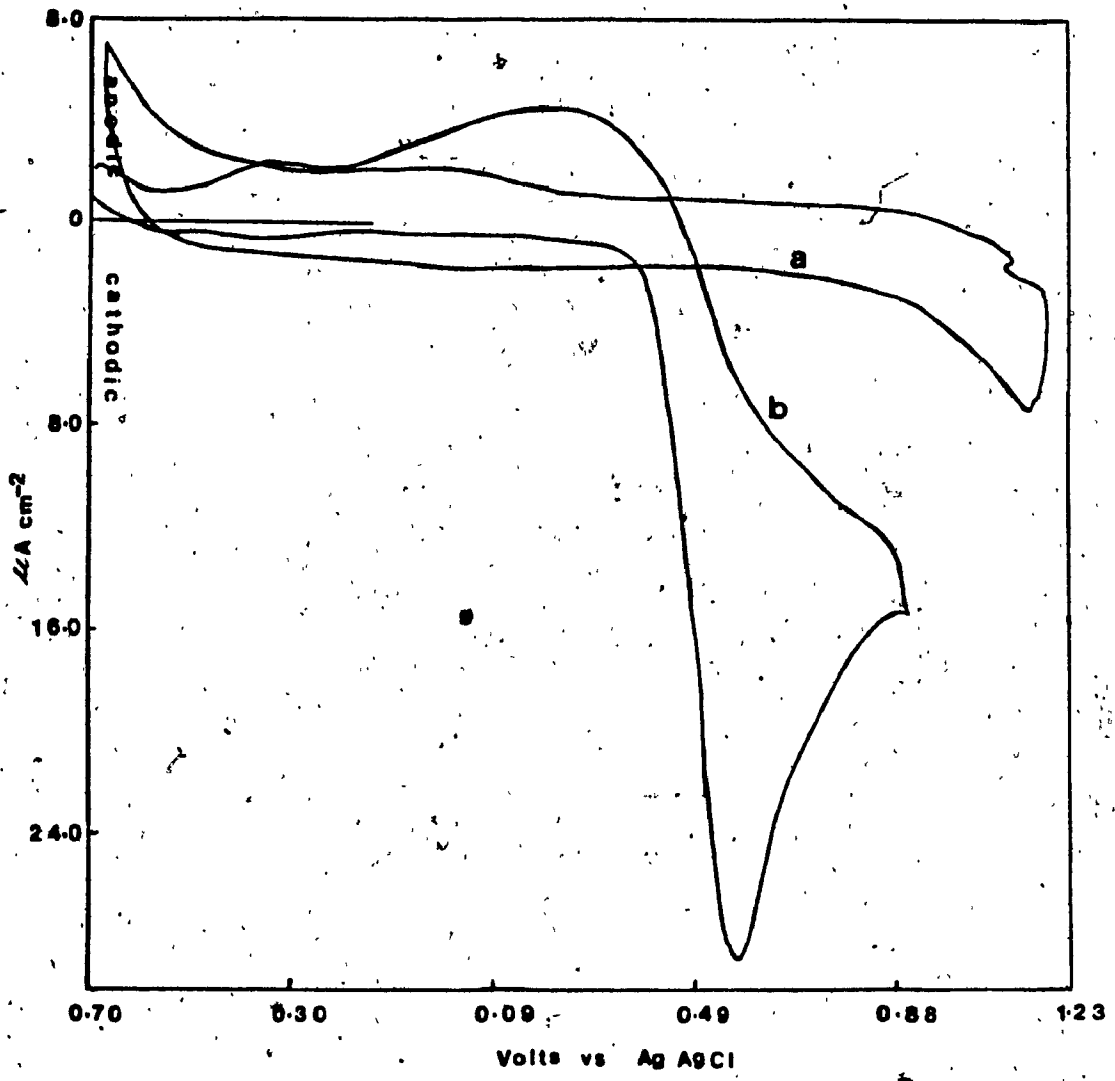

Figure 7-2. Voltammograms of $Pt(mnt)_2^{2-}$ after irradiation for 2 hrs at Pt electrode in CH_3CN containing 0.1 M $NaClO_4$ and 30% H_2O. (a) after 4 hrs without stirring; (b) after stirring.

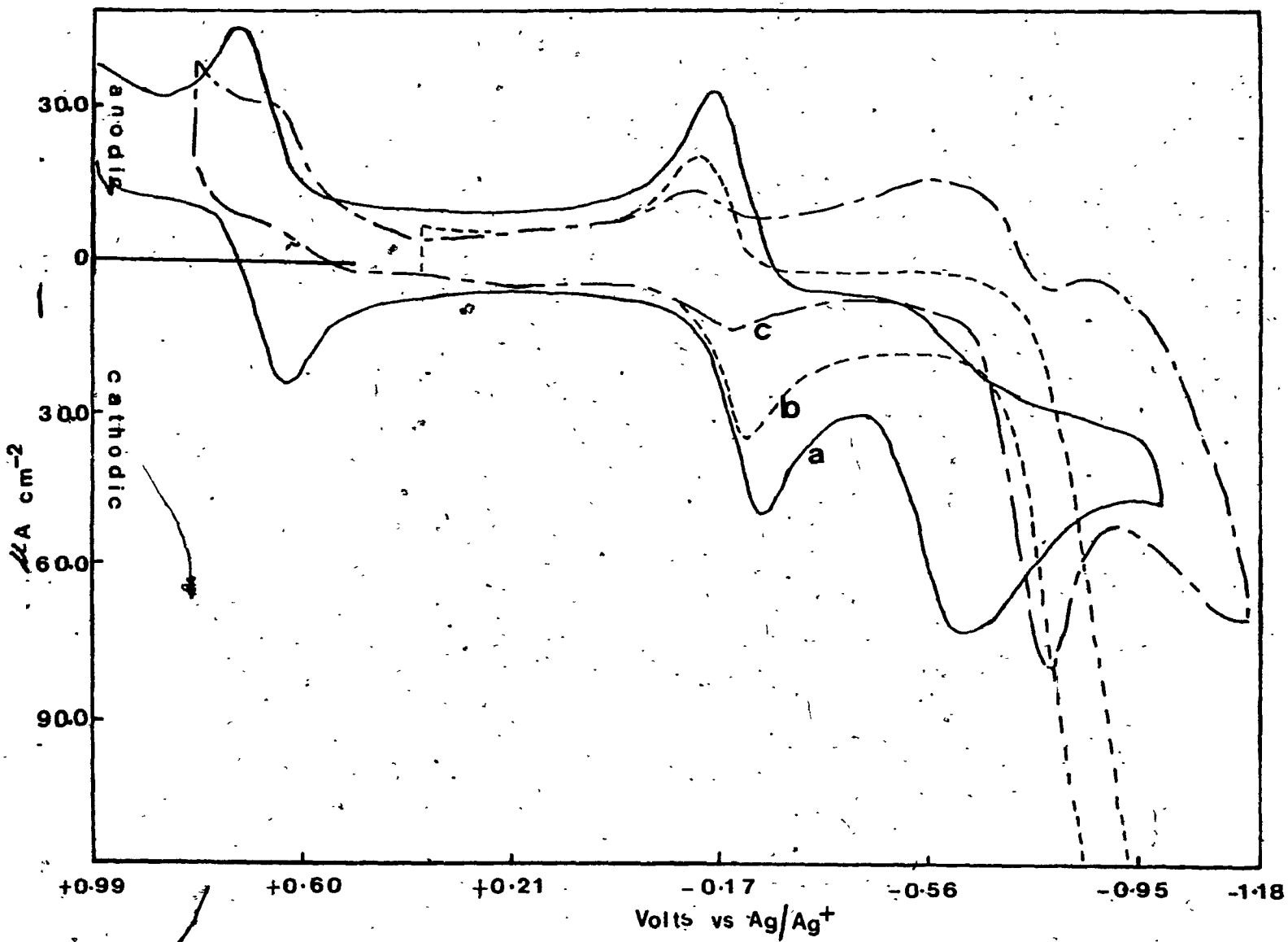

Figure 7-3. Cyclic voltammogram of precipitate (particles recovered after photolysis of $Pt(mnt)_2^{2-}$) at Pt electrode in (a) 0.1 M $NaClO_4/CH_3CN$; (b) and (c) 0.1 M $NaClO_4/CH_3CN$ containing 5% H_2O.

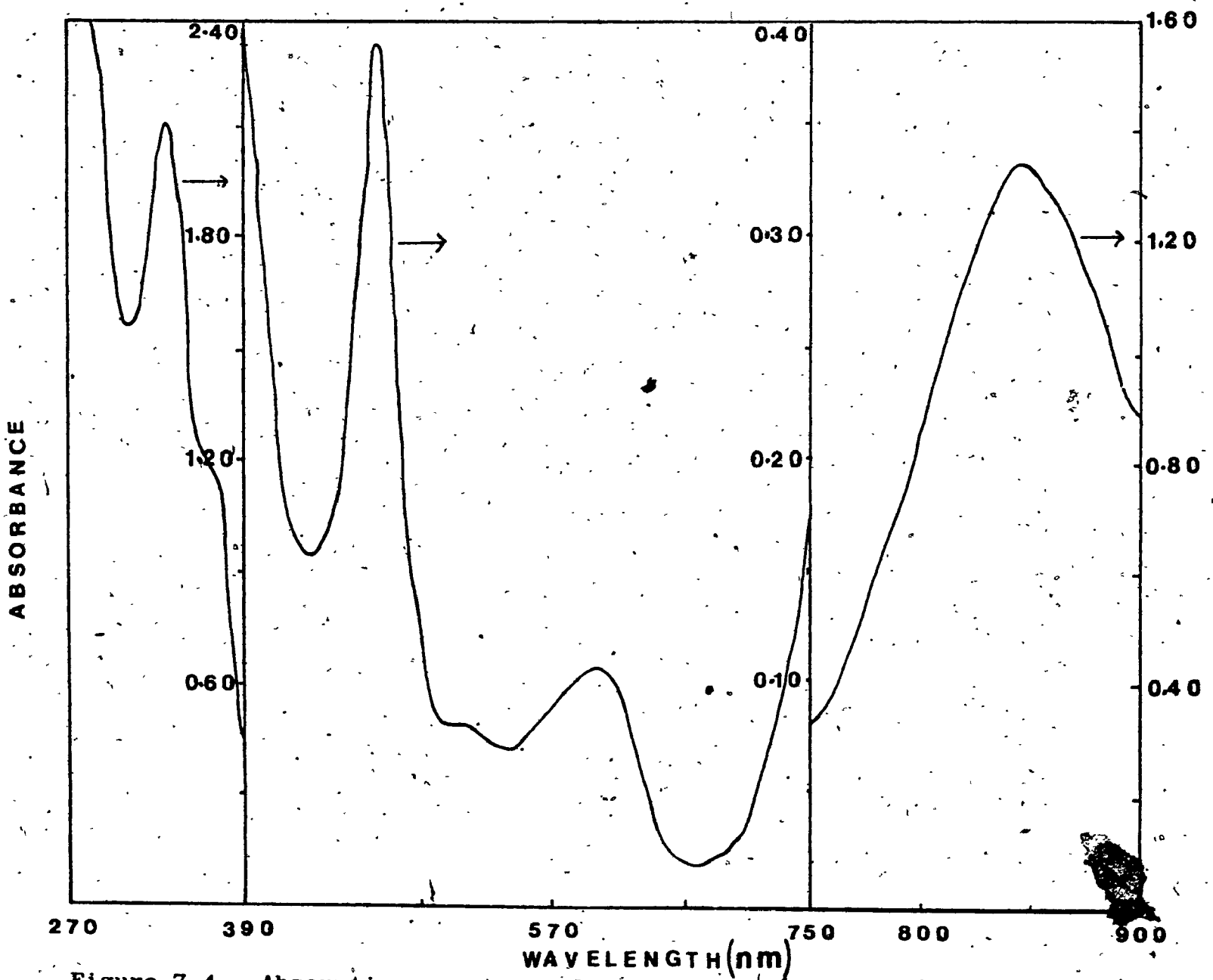

Figure 7-4. Absorption spectrum of precipitate (particles) recovered after photolysis of $Pt(mnt)_2^{2-}$ in CH_3CN

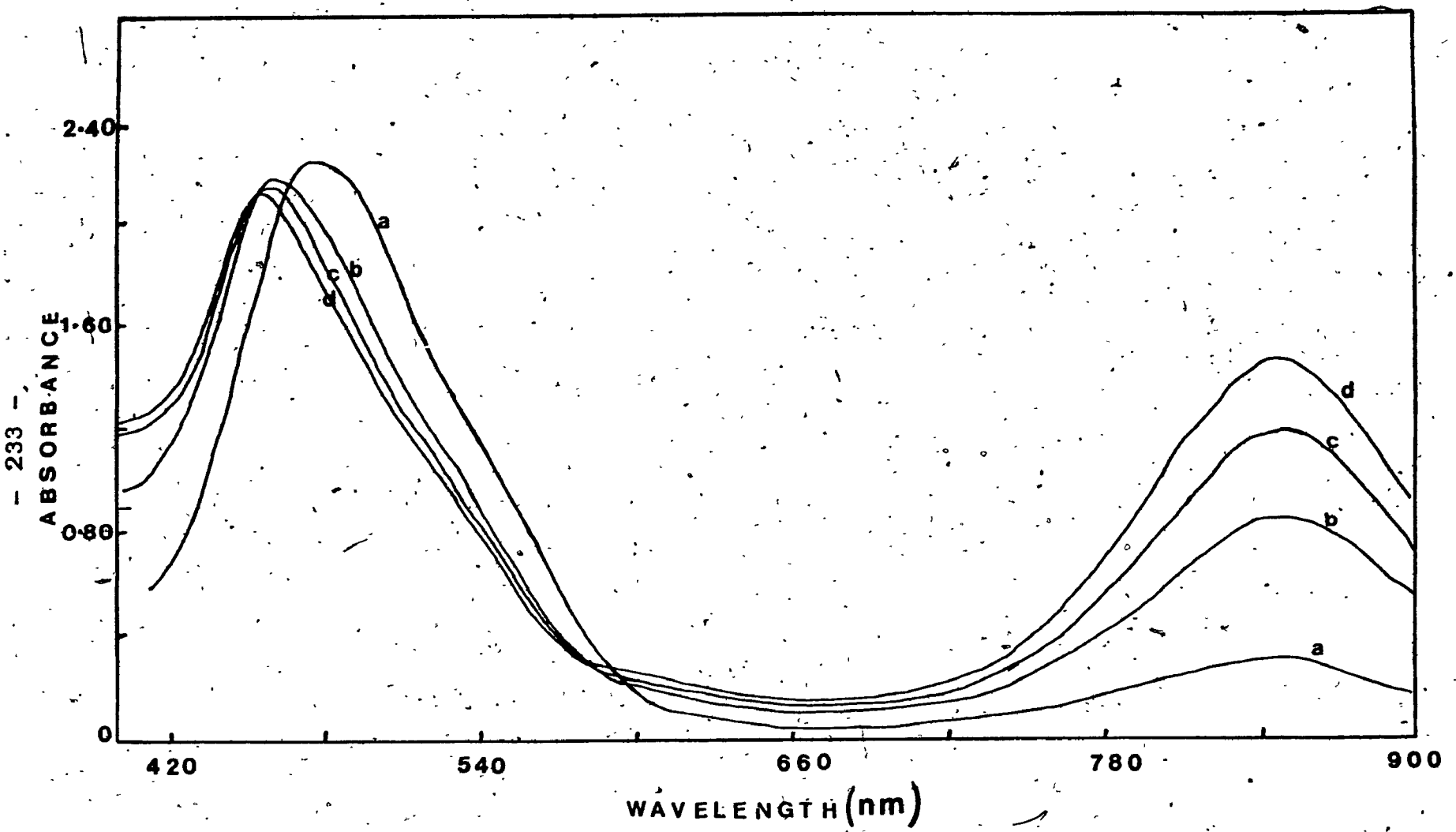

Figure 7-5 Absorption spectrum of $Pt(mnt)_2^{2-}$ in 1:4 ratio of H_2O/CH_3CN. (a) before photolysis; (b), (c) and (d) after photolysis for 4, 6 and 8 hrs, respectively.

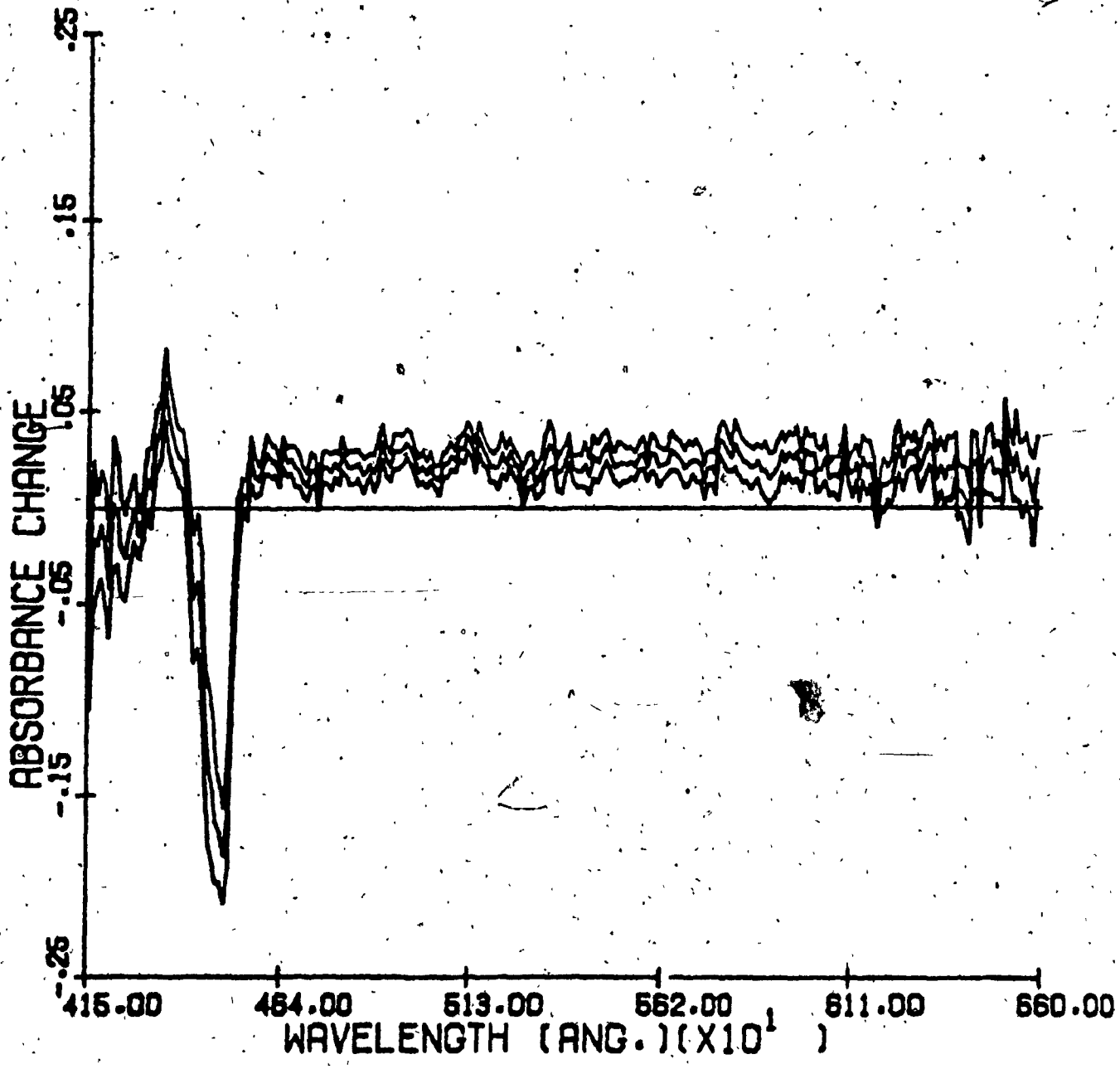

Figure 7-6. Transient behaviour of acetonitrile at pulse delay of 10 ns.

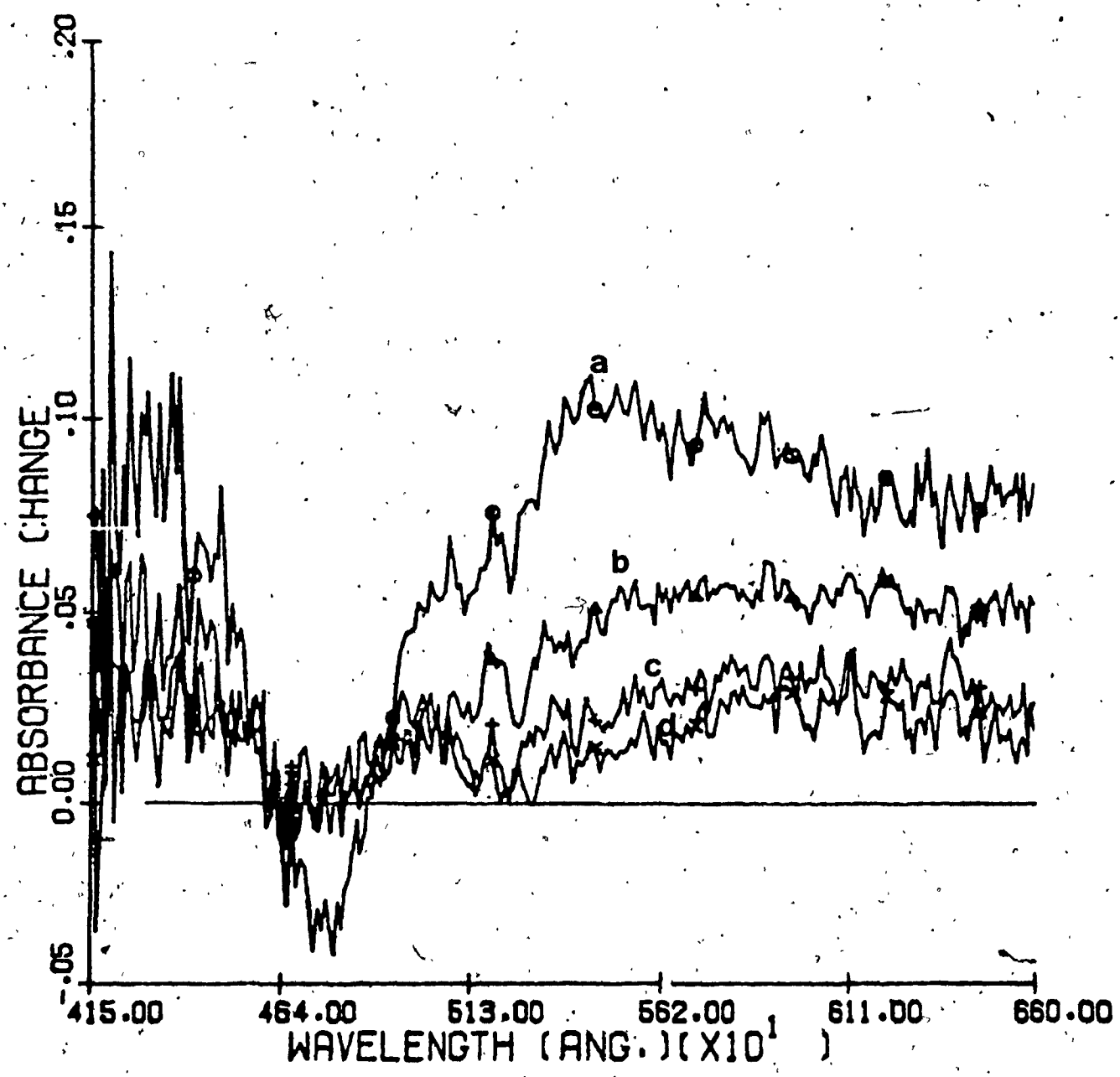

Figure 7-7 (A). Transient absorption spectrum and bleaching of $Ni(mnt)_2^{2-}$ in acetonitrile at probe pulse delay of: (a) 20 ps; (b) 50 ps; (c) 100 ps; (d) 200 ps.

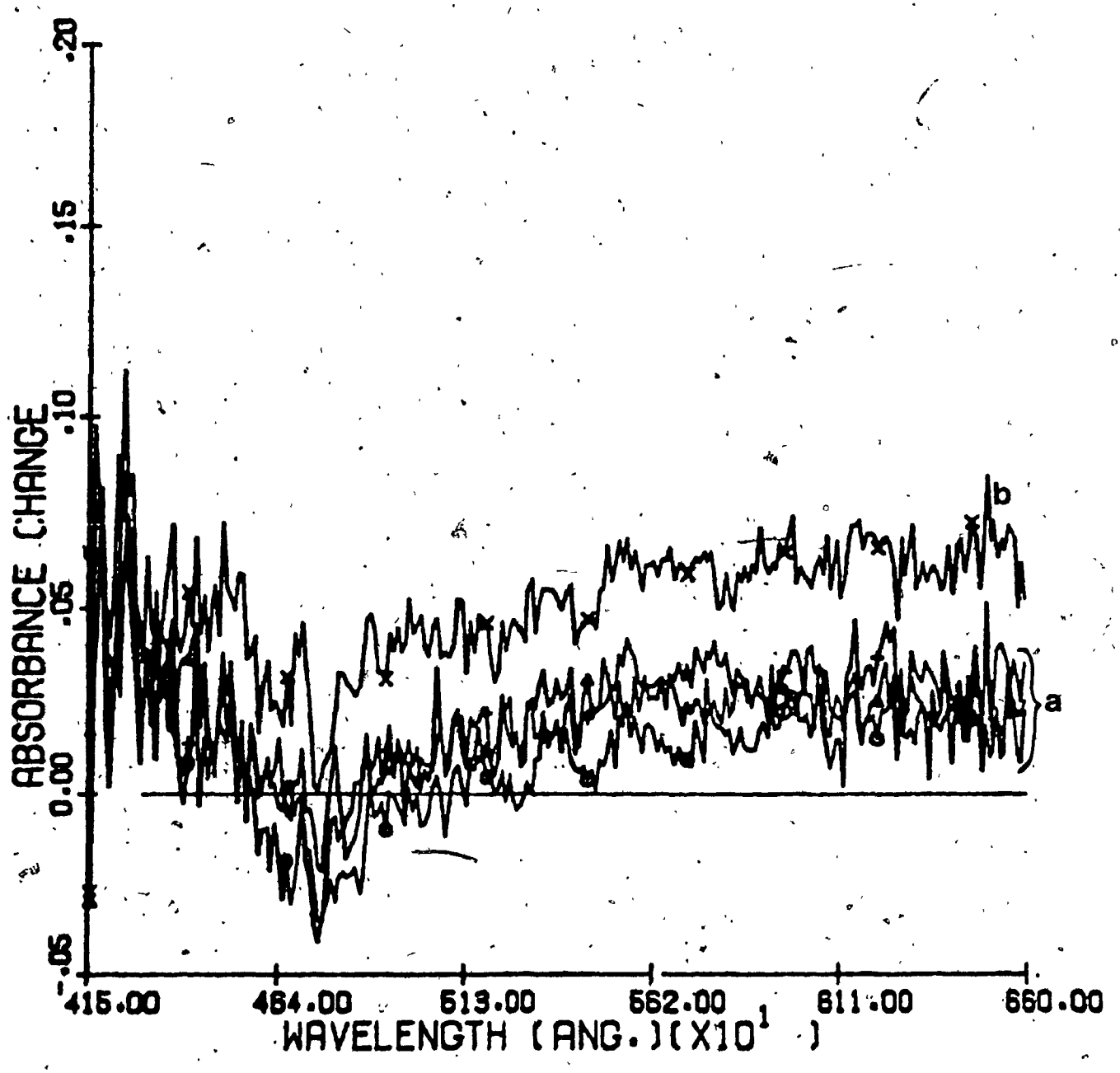

Figure 7-7 (B). Transient absorption spectrum and bleaching of $Ni(mnt)_2^{2-}$ in acetonitrile at probe pulse delay of: (a) 3 to 7 ns; (b) 10 ns.

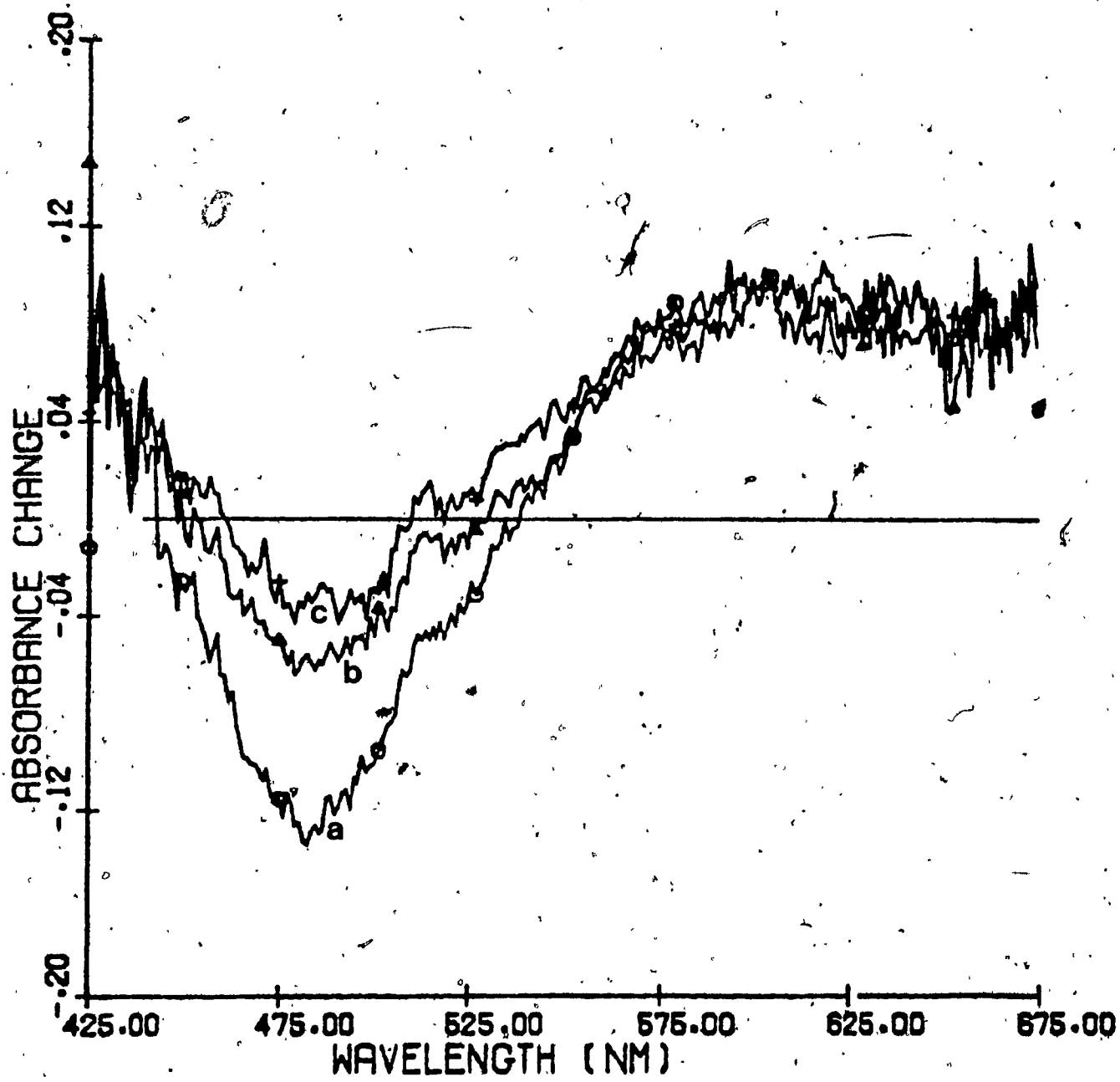

Figure 7-8. Transient absorption spectrum and bleaching of $Pt(mnt)_2^{2-}$ in dry acetonitrile at probe pulse delay of: (a) 500 ps; (b) 5 ns and (c) 10 ns.

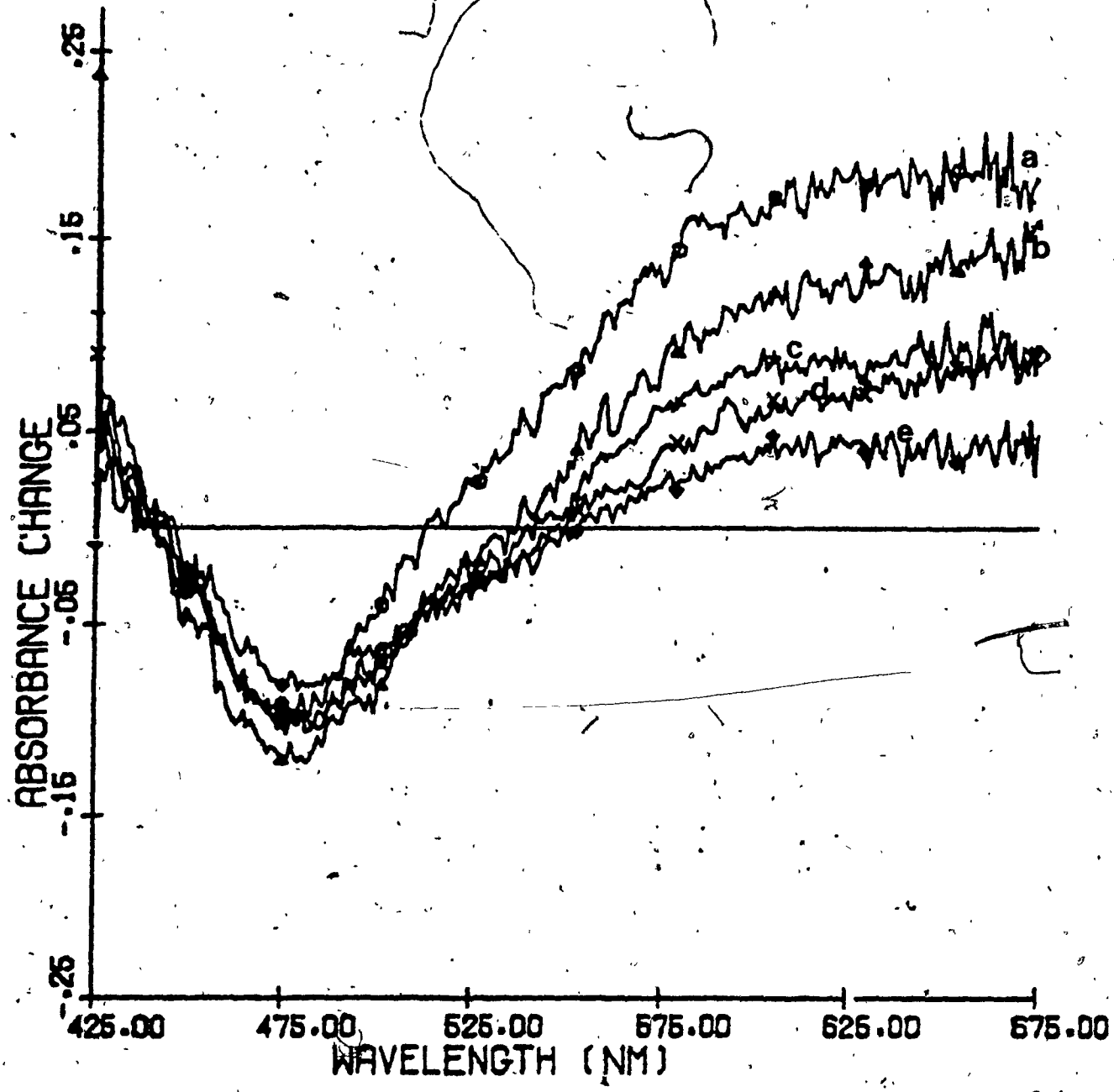

Figure 7-9 Transient absorption spectrum and bleaching of $Pt(mnt)_2^{2-}$ in mixed solvent of 30 % water in acetonitrile at probe pulse delay of: (a) 50 ps, (b) 1 ns, (c) 3 ns, (d) 5 ns and (e) 10 ns.

Chapter 8

Discussion

8.1 Homogeneous Photoelectrochemistry

8.1.1 Photoelectrochemistry of $M(mnt)_2^{2-}$; M = Ni, Pd, Pt and Cu, and $M(mnt)_2^{1-}$; M = Ni.

The homogeneous or solution photoelectrochemistry establishes two preliminary conclusions concerning the above $M(mnt)_2^{n-}$ complexes. Firstly, despite the strong absorbance of all the compounds, not all of them show photo-induced electron transfer reaction in the visible. Those that undergo photo-induced electron transfer are distinguished by the production of photocurrents. Secondly, the photocurrents that were produced are small; all were in the nano-ampere domain. These photocurrents were detected by lock-in amplification. They attained their maximum value instantaneously at zero phase angle when the light was turned on, and in the dark they immediately disappeared and returned completely to zero value. They were reproducible upon repeated illumination. The phase relation data obtained with the lock-in amplifier indicates that the photocurrents were in phase with the chopped beam. This observation contrast the earlier reports of sensitized $Fe(bpy)_3^{2+}$ currents (61) and suggests a direct reaction of short lived excited states at the transparent electrode. The magnitude of the

photocurrents are independent of the "duty cycle" of the chopper thus elimlinating the possibility that they are dominated by thermal effects. From the blank runs however, it is clear that thermal effects of light become significant in the potential region where the background currents are large. This is not unusual and is expected.

The photoelectrochemical behaviour of $Ni(mnt)_2^{2-}$, $Pd(mnt)_2^{2-}$ and $Pt(mnt)_2^{2-}$ are examined together because these complexes are simlilar; the metal ions are all in a d^8 configuration. The nickel and platinum complexes show similar behaviour. These compounds produced cathodic photocurrents in the same potential region. No photocurrents were observed for the analogous palladium complex. From the photowaves of the $Ni(mnt)_2^{2-}$ (Figure 4-1) and $Pt(mnt)_2^{2-}$ (Figure 4-5) complexes approximate photoelectrochemical "half-wave" potentials can be obtained for the excited states. For both the nickel and the platinum complexes the photocurrents approach saturation at about -0.7 V vs Ag/Ag^+(0.1 M $AgNO_3/CH_3CN$) reference. These photowaves are analogous to polarographic waves in conventional electrochemistry for which the half-wave potentials are known to be a little below the potential where the limiting current is approached. The technique adopted for determining half-wave potential in a polarographic wave, unfortunately cannot be strickly applied to these photowaves since only the the limiting current portion of the photowaves is

obtained and there is no "residual current" as in a polarographic wave. One can nevertheless assign a value of approximately -0.6 V for the half-wave potential for both, the excited state of the $Ni(mnt)_2^{2-}$ and the $Pt(mnt)_2^{2-}$ complex. This value correlates resonably well with calculations for the reduction of the excited states. The excited state redox potential cannot be obtained from the energy of the exciting photon but from the energy of the excited states and the redox potential of the ground state. For example, in the Ni case, the excitation energy for the first excited state (obtained from the electronic spectrum) is 1.45 eV (absorption at 855 nm) and the redox potential for the 2-/3- couple is -1.94 V (Table 3-3). The difference yeilds approximately -0.5 V for a predicted $^*2-/3-$ couple where the asterisk designates the excited state. The corresponding quantities for the $Pt(mnt)_2^{2-}$ complex are 2.3 eV which corresponds to an absorption at 540 nm and -3.0 V. This yields approximately -0.7 V for the $^*2-/3-$ redox reaction.

The photochemical behaviour observed in this study for the complexes, $M(mnt)_2^{2-}$; M = Ni, Pd and Pt follow the pattern of photochemistry reported by Dooley and Patterson (21) for the initiation of oxidation of halocarbon solvents. In that case the pattern was attributed to an intraligand excitation ($L \longrightarrow L\pi^*$) because of the action spectrum which shows quantum yield increases with

decreasing wavelength excitation. It was also observed that this excitation decreases bonding electron density on the ligand. In the present case the assignments based on calculation by Gray et al (8) along with the molecular orbital diagram of Figure 3-1 was used to explain the photoelectrochemical behaviour. The photoelectrochemistry of the nickel, palladium and platinum complexes depends strongly on the nature of the charge transfer transition excited by the light available. Irradiation of the ligand field bands of the $Ni(mnt)_2^{2-}$ using the 514 nm line of the argon ion laser do not result in the production of photocurrents. It is irradiated in the main visible band which corresponds to the initial population of a metal to ligand charge transfer state ($M \longrightarrow L\pi^*$) in the nickel as well as the platinum complex that produces cathodic photocurrents. For the $Pd(mnt)_2^{2-}$ complex which does not produce any photocurrent, the main visible band consists of two transition in the blue. The lower energy transition was reported at 440 nm and the higher energy transition was initially reported as a shoulder at 387 nm on the 440 nm band (8). The spectrum recorded here showed the low energy transition occuring at 440 nm but the higher energy transition shifted to a longer wavelength at 421 nm. Recent (14) low temperature absorption and Resonance Raman spectroscopic studies assigned the 440 nm band as $M \longrightarrow L\pi^*$, similar to the nickel and platinum complexes and the higher energy transition as a $L\pi \longrightarrow M$.

Therefore excitation of the palladium complex in the main visible band results in competitive absorption and initial population of a M ---> $L\pi^*$ in combination with a $L\pi$ ---> M charge transfer state. The relationship between the photoelectrochemistry and the spectroscopic assignments is obvious. Compounds in which the transition dominating the excitation is of M ---> $L\pi^*$ or more particularly xz ---> $L\pi^*$ displayed cathodic photocurrent while in situation where the transition is $L\pi$ ---> M ($L\pi$ ---> xy) no photocurrents was observed. In the Ni and Pt complexes an electron in the xz orbital is vacated and it can be suggested that the cathodic photocurrents observed reflect electron capture by this orbital. in the Pd complex, an electron from the $L\pi$ orbital is emptied and is promoted to the xy orbital where the primary excitation is M ---> $L\pi^*$ a photocurrent can arise, the reverse, $L\pi$ ---> M, seems to be ineffective. This can be discussed in terms of the MLCT state leading to the configuration (xy) $L\pi^*$ which can relax to the lowest lying ligand field (LF) state, $^3b_{1g}$ (xy) leaving a hole at the metal whereas the LMCT has poor orbital overlap for relaxation to the LF state. The energetics have suggested that the lowest state is the reactive one.

The important factor determining the magnitude of the photocurrents is the lifetime. The lifetime domain of the excited states can be estimated by considering competitive

reaction kinetics. For the nickel and platinum complexes the relevant mechanism is:

$$M(mnt)_2^{2-} \underset{k_{-1}}{\overset{k_1(h\nu)}{\rightleftharpoons}} {}^*M(mnt)_2^{2-}$$

$$^*M(mnt)_2^{2-} \xrightarrow[\text{optical electrode}]{k_2} M(mnt)_2^{3-} \qquad (18)$$

$$M(mnt)_2^{3-} \xrightarrow[\text{dark electrode}]{k_3} M(mnt)_2^{2-}$$

where M = Ni and Pt and the asterisk denotes an excited state. k_2 and k_3 represent rate constant for reduction of the excited state and reoxidation of the reduced ground state product. The latter reaction is favorable with an overpotential of up to a few hundred millivolts in the region of the tip of the photowave (see Figure 4-1 and 4-5). The overvoltage driving the k_2 process is very large in the limitating region of the photowave. The reactions of k_2 and k_3 will then make opposite contribution to the current and may lead to an under estimation of the efficiency of the photoreaction. In such a situation the actual photocurrent is the algebraic sum of the observed photocurrent and the anodic (k_3) current. Equation 19 gives the relationship:

$$i_p \text{ actual} = i_p \text{ obs (cat)} - i_{anod} \qquad (19)$$

where the cathodic current bears a negative sign (not shown) and the anodic a positive sign.

The photocurrent was found to be dependent on a

number of factors. It increases with the rate of circulation of the electrolyte containing the dissolved complex through the cell. Increasing the circulaltion rate means increasing the supply of fresh reactant to the electrode surfaceas well as removing the reaction products. This observation along with the concentration dependence (Figure 4-2) indicates that the photocurrent is governed by diffusion of the excited state to the electrode where it undergoes reaction. The linear relationship between the photocurrent and the first power of the laser intensity (Figure 4-3) suggests that the photoinduced electron transfer reaction is a result of a one photon absorption process. It also can be taken as evidence that the photocurrent is independent of the electron transfer step and it is only dependent on the excited state lifetime.

The photocurrent can be used to estimate the lifetime of the excited state. Since a limiting region is established it can be suggested that $k_2 > k_3$ in that region. The steady state equation for the excited state is:

$$d[^*M(mnt)_2^{2-}]/dt = \phi I\varepsilon[M(mnt)_2^{2-}] - k_{-1}[^*M(mnt)_2^{2-}] - k_2[^*M(mnt)_2^{2-}] \quad (20)$$

where ϕ is the quantum yeild for the formation of the reactive excited state. I is the light intensity, and is the average exinction coefficient between 450 and 570 nm.

Solving equation (20):

$$[^*M(mnt)_2^{2-}] = \phi I\varepsilon[M(mnt)_2^{2-}]/k_{-1} + k_2 \qquad (21)$$

where ϕ will be approximated as unity, I is 1.2×10^7 einsteins sec^{-1} and ε is approximately 5.6×10^3 M^{-1} cm^{-1}. Now the limiting current is given by:

$$i_1 = nFA(\text{flux of excited state to electrode}) \qquad (22)$$

where n is the number of electrons, F is the Faraday, and A is the area of the electrode. The flux of the excited state to the electrode is given by:

$$\text{Flux} = D[^*M(mnt)_2^{2-}]/\delta \qquad (23)$$

where δ is the thickness of the diffusion layer. If the diffusion layer is thicker than the distance travelled by an excited state in its lifetime, it will not contribute to the current. Thus, δ is taken as $(D\tau)^{1/2}$ where D is the conventional diffusion coefficient of approximately 1×10^{-5} cm^2sec^{-1} and τ is the excited state lifetime, $1/k_{-1}$. Collecting all terms and assuming $k_{-1} > k_2$ yields:

$$i_{1im} = nFA\,\phi I\varepsilon[M(mnt)_2^{2-}]/D^{1/2}k_{-1}^{1/2} \qquad (24)$$

The average value of k_{-1} from equation (24) for the concentration range studied is 2.5×10^8 sec^{-1} for the nickel complex. The corresponding lifetime is approximately 4 ns. For the platinum complex k_{-1} was

found to be 2.3 x 10^7 sec^{-1} and the corresponding lifetime is approximately 43 ns.

There are two major limitations on this analysis. If $\phi<1$ then k_{-1} can be less and the lifetime longer. Conversely, if there is specific adsorption of the complex at the electrode, the simple diffusional model underestimates delivery of the excited states and the lifetime may be shorter. These results merit comparison to flash photolysis indications of lowest state lifetimes.

8.1.2 Photoelectrochemistry of $Ni(mnt)_2^{1-}$ and $Cu(mnt)_2^{2-}$

The photocurrents generated by $Ni(mnt)_2^{1-}$ were in phase with the chopped radiation and can be assigned to the reaction of the excited states at the electrode. The following mechanism explains the photocurrents

$$Ni(mnt)_2^{1-} \underset{k_{-1}}{\overset{k_1(h\nu)}{\rightleftharpoons}} {}^*Ni(mnt)_2^{1-}$$

$$Ni(mnt)_2^{1-} \xrightarrow[\text{optical electrode}]{k_2} Ni(mnt)_2^{0} \qquad (25)$$

$$Ni(mnt)_2^{0} \xrightarrow[\text{dark electrode}]{k_3} Ni(mnt)_2^{1-}$$

In the above mechanism the k_2 reaction generates the photocurrent which is anodic. As mentioned before the potential window with a small background current is narrow and the wave is not defined since at about +0.5 V adsorption was noticeable. It is possible that adsorption was also occuring at lower potentials thereby connecting

the photocurrent with adsorbed $Ni(mnt)_2^{1-}$. The excitation again corresponds to a M ——>Lπ^*, (xz ——>Lπ^*) and the excited state would be similar to that of the $Ni(mnt)_2^{2-}$ species. The anodic photocurrent observed merely reflect that the excited state can either undergo oxidation or reduction depending on the reaction partner (the electrode).

The $Cu(mnt)_2^{2-}$ complex appears to be similar to the $Pd(mnt)_2^{2-}$. Firstly, no photocurrents were observed and secondly, the main visible band between 430 and 475 nm consists of two transitions. In Table 3-2 the low energy transition at 475 nm was assigned as M ——>Lπ^* (xz ——> L π^*) and the higher energy transition which appears at 430 nm was assigned as Lπ --->M (Lπ---> xy). This transition appears as a shoulder on the foot of the very intense band at 368 nm and seems to be more intense than that at 475 nm band. The competitive excitation of these two transitions in the visible probably produced too much of the unreactive state. The $Cu(mnt)_2^{2-}$ is then similar to $Pd(mnt)_2^{2-}$ except it is an odd electron system and the transitions are all doublet-doublet. The may be quite significant since no intersystem crossing (ISC) to a state system from the ground state by a spin restriction is possible.

The $Cu(mnt)_2^{3-}$ which is generated electrolytically from the $Cu(mnt)_2^{2-}$ solution is photoactive. This compound produces an anodic photocurrent which can be explained by

the following mechanism:

$$Cu(mnt)_2^{2-} \xrightarrow[\text{dark electrode}]{k_3} Cu(mnt)_2^{3-}$$

$$Cu(mnt)_2^{3-} \underset{k_{-1}}{\overset{k_1(h\nu)}{\rightleftharpoons}} {}^*Cu(mnt)_2^{3-} \qquad (29)$$

$${}^*Cu(mnt)_2^{3-} \xrightarrow[\text{optical electrode}]{k_2} Cu(mnt)_2^{2-}$$

where the k_2 reaction is the one that produces the photocurrent. The dependence of the photocurrent on concentration of $Cu(mnt)_2^{2-}$ (Figure 4-7) implies that more of the $Cu(mnt)_2^{3-}$ species is being generated at the electrode as the concentration of $Cu(mnt)_2^{2-}$ is increased. Increasing the concentration of $Cu(mnt)_2^{3-}$ produces more of the ${}^*Cu(mnt)_2^{3-}$ in solution. The linear relationship between the first power of the laser intensity and the photocurrents (Figure 4-7) suggests that the electron transfer is fast and the photocurrent is dependent on concentration of ${}^*Cu(mnt)_2^{3-}$ and the excited state lifetime. An electronic spectrum for the $Cu(mnt)_2^{3-}$ was difficult to obtain since it is not stable in air and the relation between photoactively and spectroscopic assignment cannot be analysed at present. Nevertheless certain speculations are warrented. The Cu ion in the $Cu(mnt)_2^{3-}$ species can be regarded as having a d^{10} configuration with a pair of electrons in the $3b_{1g}$ (xy) orbital. Any excitation would then promote an electron to the L π^*, the LUMO. From electrochemical measurements,

the redox reaction of $Cu(mnt)_2^{2-}/Cu(mnt)_2^{3-}$ was found to be approximately 1 V more anodic than the corresponding reaction of nickel . This means that the $3b_{1g}$ orbital is lower in energy by a corresponding value. The separation between the $3b_{1g}$ (xy) and the $L\pi^*$ would also be greater than the nickel. In this situation the reaction is from a state similar to that observed by Dooley and patterson (21)in studies following the $L \longrightarrow L\pi^*$ excitation.

8.1.3 Quenching the Excited States.

The reactions of the excited states of $Ni(mnt)_2^{2-}$ in presence of the pyridine quencher can be explained by the following mechanism:

$$Ni(mnt)_2^{2-} \underset{k_{-1}}{\overset{k_1(h\nu)}{\rightleftharpoons}} {}^*Ni(mnt)_2^{2-}$$

$${}^*Ni(mnt)_2^{2-} + Py \xrightarrow{k_q} Ni(mnt)_2^{3-} \rightarrow -Py$$

$${}^*Ni(mnt)_2^{2-} \xrightarrow{k_2} Ni(mnt)_2^{3-} \qquad (27)$$

$$Ni(mnt)_2^{2-}\text{----}Py \xrightarrow{k_4} Ni(mnt)_2^{2-} + Py$$

$$Ni(mnt)_2^{3} \xrightarrow{k_q} Ni(mnt)_2^{2-}$$

In the above mechanism the reaction of k_2 contribute to the observed photocurrents. The current observed can be given by the relationship:

$$i_{obs} = k_1[Ni(mnt)_2^{2-}]/k_{-1}[{}^*Ni(mnt)_2^{2-}] \qquad (28)$$

In the presence of the quencher the observed photocurrent

i_q is given by the relationship:

$$i_q = k_1[Ni(mnt)_2^{2-}]/[^*Ni(mnt)_2^{2-}](k_{-1} + k_q[Py]) \qquad (29)$$

The ratio of these two equations produce the Stern-Volmer relationship:

$$i_{obs}/i_q = 1 + k_q/k_{-1}[Py] \qquad (30)$$

which is the normal equation for determining the quenching rate constant for an excited state. However, quenching does not accurately follow the Stern-Volmer relationship (see Figure 4-10) and this is probably due to specific adsorption of pyridine on the electrode. Adsorption of pyridine on electrodes is known to occur and is used extensively in the study of surface enhanced Raman Spectroscopy (72,73). From the linear portion of the plot, which is at low pyridine concentration, a Stern-Volmer constant of 1.26×10^2 l M^{-1} was obtained. Using the value of 2.5×10^8 sec^{-1} for k_{-1} obtained from section 8.3.1, then the quenching rate constant k_q was estimated as 3.1×10^{10} l M sec^{-1}. It will be shown in section 8.2 that these values are in close agreement with those calculated using an approximate value of 7 ns obtained from flash photolysis experiments.

The quenching rate constant is at the diffusion controlled limit. This would suggest a dynamic process. A static mode of quenching is ruled out also because the ground state of $Ni(mnt)_2^{2-}$ was found to be inert with

respect to axial coordination or substitution with pyridine (1,2) . The quenching reaction can be regarded as a bimolecular one and the encounter between the excited state and pyridine results in an energy transfer in the excited state induced by pyridine. $Co(mnt)_2^{2-}$ in which the cobalt ion can be regarded as having a d^7 configuration, is known to form five coordinated adduct with, NO (68,69). $Co(mnt)_2^{1-}$ also forms a five coordinated species with pyridine (70,71). Emptying the metal centered orbital by electronic excitation in the $Ni(mnt)_2^{2-}$ would turn the ground state d^8 metal ion, Ni(II) into a d^7 configuration and in the presence of pi acceptor molecules such as pyridine can form a five coordinate species in the excited state.

Quenching by oxygen was not studied in detail and a quenching rate constant was not obtained. The quenching process can however be regarded as an electron transfer one. The excited state redox potentials of both $Ni(mnt)_2^{2-}$ and $Pt(mnt)_2^{2-}$ are negative with respect to the reduction of oxygen and can undergo oxidation to form superoxide. In the $Cu(mnt)_2^{3-}$ oxygen "quenches" the ground state trianion and the excited state behaviour is not observable.

8.2 Transient Spectra and Assignments.

The complexes of $Ni(mnt)_2^{2-}$, $Pd(mnt)_2^{2-}$, and $Pt(mnt)_2^{2-}$ $Pt(mnt)_2^{1-}$ were examined for transient absorption. In all cases the excitation at 355 nm corresponds to the initial population of both metal to ligand charge transfer states (MLCT) as well as a ligand to metal charge transfer states (LMCT). In the $Pd(mnt)_2^{2-}$ and the $Pt(mnt)_2^{1-}$ no excited state absorption was found in the visible nor was there any ground state bleaching despite the strong absorbance in the visible. For both, the $Ni(mnt)_2^{2-}$ and the $Pt(mnt)_2^{2-}$ excited states absorption was observed and also ground state bleaching.

In all the spectra recorded for $Ni(mnt)_2^{2-}$ (Figure 7-7(A) and (A) from a pulse delay of 20 ps to a delay of 10 ns there is a dip in the 472 nm region which corresponds to the bleaching of the ground state. This implies that some of the complex remains in an excited state beyond 10ns. Examination of the 20 ps spectrum shows a broad excited state absorption from 540 to 660 nm. The intensity of the excited state spectrum appears to be increasing in the higher energy region and it is possible that the excited state also absorbs in the region where the bleaching ocours. The non expontential decay of the transient absorbance in the 544 nm as well as the 10 ns spectrum would support the idea that the excited state absorption overlaps the bleaching region. The form of

decays of excited state absorption and bleaching indicated two excited states. One absorbs in the visible. The other, longer lived, does not but prevents complete return of the ground state spectrum. Approximate life time can be fitted by approximating half lives. Excitation of $Ni(mnt)_2^{2-}$ in dry acetonitrile by the 355 pulse can then be regarded as producing two excited state species; a primary one with a half-life of about 70 ps and a longer lived secondary one with a lifetime of the order of 7ns. The short lived species is suggested to be produced by the direct excitation and can be assigned as a singlet excited state. This excited state undergoes rapid intersystem crossing in less than a nanosecond to what is probably a triplet, the longer lived species. Figure 8-1 which is a simplified version of the M.O. diagram of Figure 3-1 illustrates the photophysical path ways. These deductions appears consistent with the photoelectrochemistry. A short lived excited state in the subnanosecond domain cannot undergo diffusion and reaction at the electrode. The triplet state with a longer lifetime is favored in the photoelectrochemical reactions. A triplet excited state of lifetime 7 ns would imply that the quenching rate constant by pyridine (section 8.1.3) is 1.8×10^{10} l M^{-1} sec^{-1}. This is comparable to the value of 3.1×10^{10} l M^{-1} sec^{-1} calculated from the 4 ns lifetime obtained from the competitive kinetics in the photoelectrochemistry where one constant, D, was assumed.

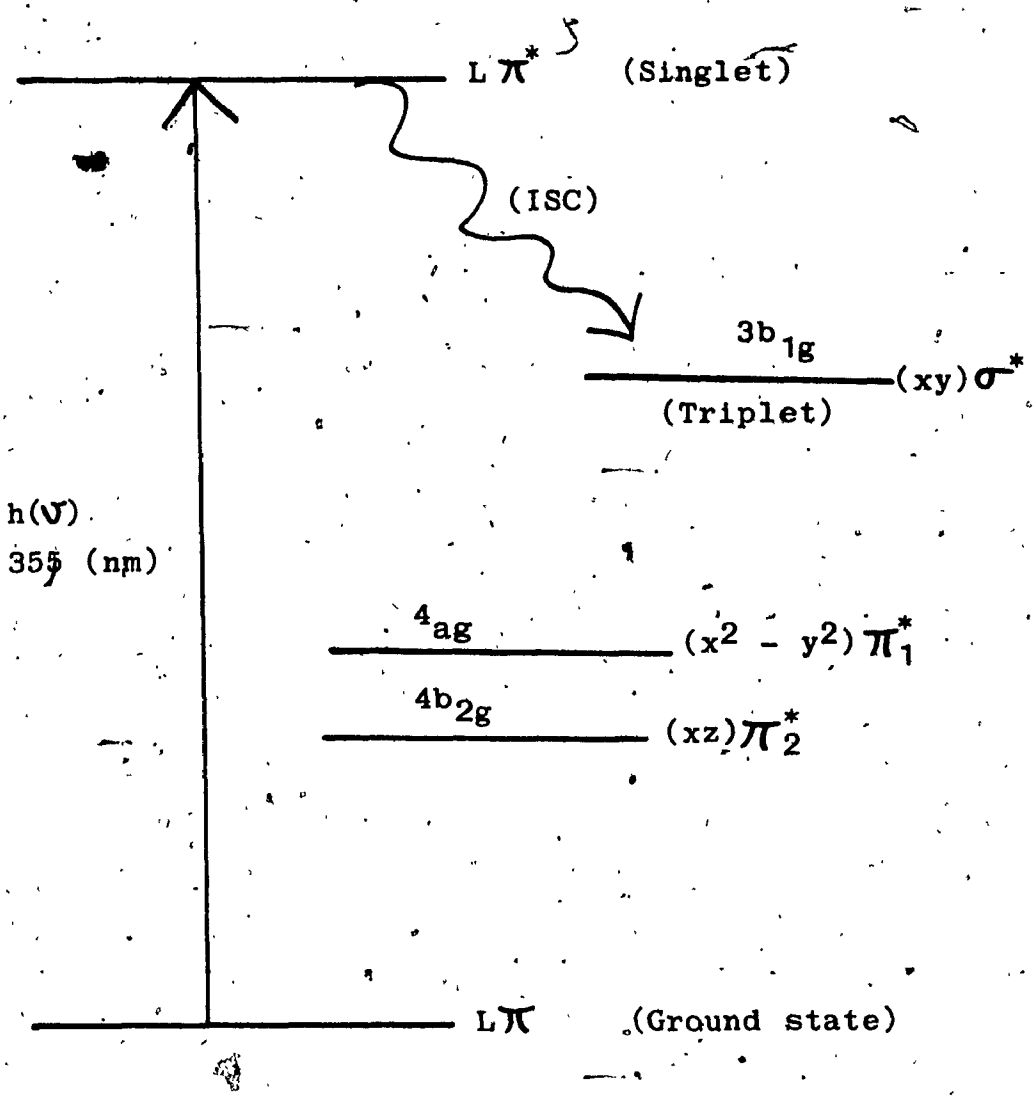

Figure 8-1. Simplified M.O. Energy scheme to illustrate the photophysical process seen upon 355 nm excitation of $Ni(mnt)_2^{2-}$.

The transient spectrum of $Pt(mnt)_2^{2-}$ in dry acetonitrile Figure 7-8 is similar to that of the nickel. The excited states absorb from 575 to 675 nm and bleaching occurs in the 472 nm region where the ground state absorbs. The bleaching however covers a wider range in the spectrum and there is also no decay of the excited state absorbance at probe times shorter than 10 ns despite more than 50% recovery of the ground state. It should be noted that 10 ns is the longest delay time that can be extracted from the laser system. On a longer time scale flash photolysis apparatus (coaxial flash lamp from phase-R-Corporation) a long lived excited state was detected with absorbance in the 630 nm region. A detail time dependence study of the transients was not accomplished at times longer than 10 ns. At first glance, the Pt results appear to parallel those for the Ni, but something more subtle is involved. The Pt results do not allow a partiton of states into an initial visible absorbing excited state and a longer lived state with a band outside the visible. The visible band is now seen as a more or less constant feature and some invisible state decaying more rapidly to the ground state. This could be explained by the shifts in the Pt spectrum to higher energy for the ligand field band if the lower state of Ni becomes visible in Pt while the visible Ni state shifts to the near U.V. This is likely but the interpretation requires that neither is primary.

One does not grow as the other decays. Both must have a short lived precursor in the upper charge transfer states. They form rapidly but decay separately. The simplest picture consistent with the interpretation of the photoelectrochemistry is that the initial $L\pi \longrightarrow L\pi^*$ state excited by 355 nm light relaxes with partitioning between the lowest LMCT state and the ligand field state at the bottom of the Jablonski diagram (Figure 8-2). The interpretation of the photoelectrochemistry required the assumption that the lowest LMCT state does not relax to the lowest excited state.

Clark et al(14) have reportedly observed fluorescence emission in their Resonance Raman studies of the $Pt(mnt)_2^{2-}$ complex at wavelength longer than 526 nm but no emission for the nickel and palladium complexes. In this study the search for steady state fluorescence or emission from the nickel as well as the platinum complexes in acetonitrile solvent was not very fruitful. Acetonitrile adds to the difficulty in detecting any significantly convincing emission since the solvent fluoresces weakly in the 380 nm region. The emission observed by Clark et al in the platinum complex is probably a consequence of the larger energy gap (separation between $xy\,\sigma^*$ and $x^2\text{--}y^2\pi^*$ levels) in the platinum complex than the nickel. This is also most likely the reason for a longer lived triplet state in the platinum.

In the mixed solvent system of water and acetonitrile

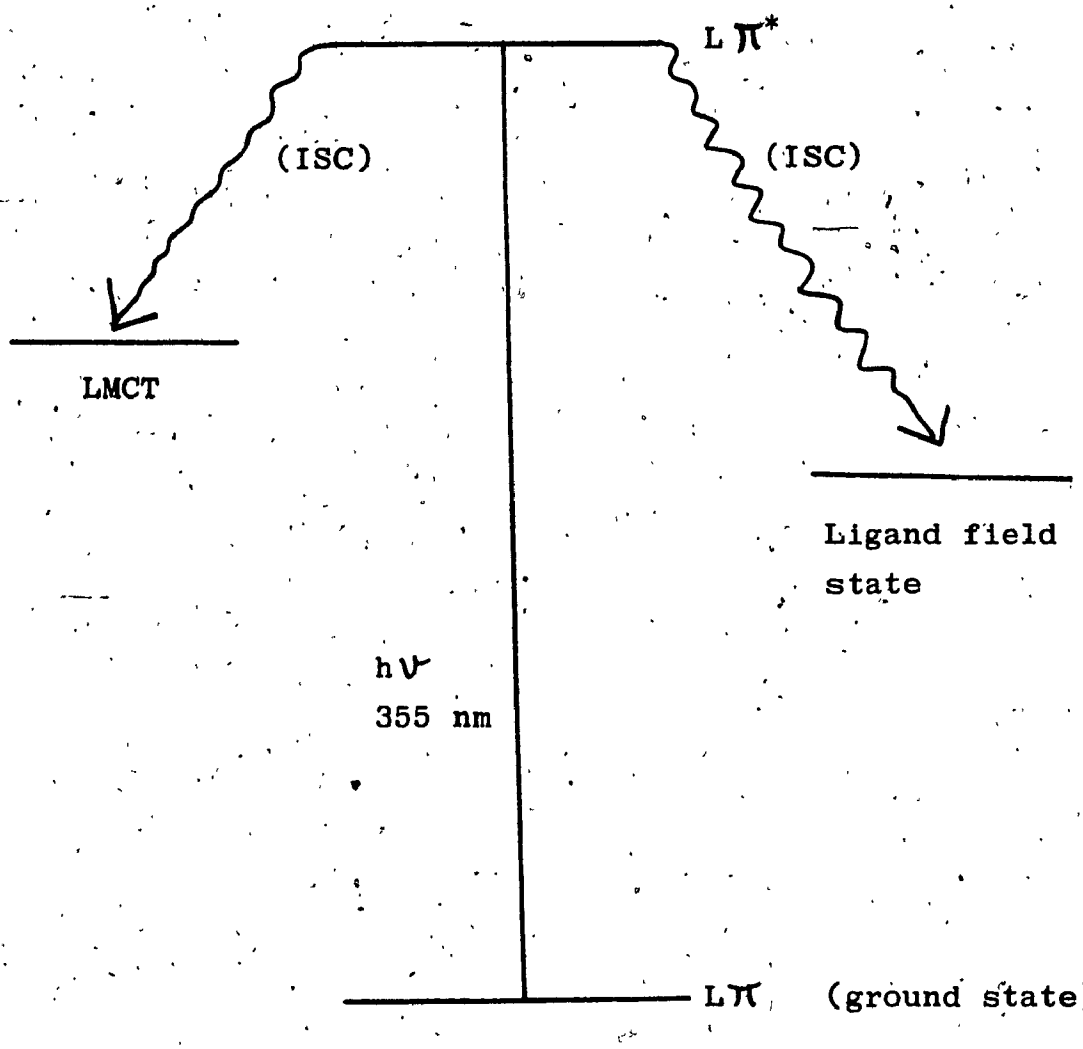

Figure 8-2. Jablonski diagram of $Pt(mnt)_2^{2-}$.

the transient spectrum of $Pt(mnt)_2^{2-}$ (see Figure 7-9) although similar in feature to that in dry acetonitrile has some important differences. Firstly, the ground state absorbance at 355 nm of the solutions used to obtain the spectra of Figures 7-8 and 7-9 are equal meaning that their concentrations are approximately the same. A comparison of the spectrum in dry acetonitrile and the spectrum in aqueous acetonitrile show a significiant difference in the behaviour of the excited states. At probe times between 20 ps and 10 ns (a 20 ps spectrum is identical to a 50 ps of Figure 7-9 there is practically no recovery of the ground state in the presence of water as indicated by the bleaching curves. Also, unlike the behaviour in dry acetonitrile, the triplet excited state absorbance is quenched in less than 10 ns. The decay of the excited state absorbance at 603 nm was found to follow first order kinetics with a rate constant of 2×10^8 sec^{-1}. It is obvious that the triplet state is being quenched by reaction with water.

8.3 Heterogeneous Photoelectrochemistry.

8.3.1 Photoelectrochemistry at SnO_2-QPVP-$Ni(mnt)_2^{2-}$ Electrode.

The photoelectrochemical behaviour of $Ni(mnt)_2^{2-}$ incorporated within the QPVP polymer on the SnO_2 electrode is similar to the homogeneous solution photoelectrochemistry. The instantaneous response of the

electrodes to irradiation and in the dark (Figure) 6-1 is exactly what was observed when the complex was irradiated in solution and the same conclusion can be drawn i.e. the excited states are reacting at the electrode. The photocurrent potential relationship of electrodes 8 and 9 (Figures 6-2 and 6-4) support this. This photowaves increase with potential and after the half-wave potential at -0.3 V vs Ag/AgCl reference, the wave tends to level. Unlike the solution photoelectrochemistry, the modified electrodes did not show any concentration dependence.

Since the photocurrent is not dependent on the amount of complex in the film it can be suggested that only the excited state within the first few layers on the SnO_2 side of the polymer may be important in the photoelectrochemistry. It should be noted that these electrodes were illuminated from the SnO_2 side. The electron transfer between the excited state and the electrode is rapid and following the electron transfer the product, $Ni(mnt)_2^{3-}$ must be oxidized to maintain the photocurrent. Hence the 3- form of the complex must be "moved" from the polymer/elecrtrode interface. This process may involve actual diffusion and replacement by the 2- form or by an electron hopping mechanism where electron exchange should occur between adjacent reduced $Ni(mnt)_2^{3-}$ and oxidized $Ni(mnt)_2^{2-}$. There is no oxidizing agent in the polymer film and if actual diffusion of

$Ni(mnt)_2^{3-}$ from the electrode surface is occuring it must either remain in the bulk film until the dark period when it can diffuse back to the electrode surface and reoxidize or migrate to the polymer/electrolyte interface and react with water. It is unlikely that the complex can diffuse throughout the polymer film faster than the chloride ions since it is a larger anion with multiple charge. Nevertheless, whether diffusion or hopping mechanism prevails, either process would require concurrent motion of chloride ions in the polymer film and exodus and uptake of chloride ions from the electrolyte. The thermal electrochemistry of the modified electrodes demonstrated that the diffusion of counterion into the polymer film is the limiting process in the electrode kinetics and it is influenced by methanol trapped in the polymer film. The apparent diffusion coefficient calculated for the photoelectrochemical process is of the order of 10^{-11} cm^2 sec^{-1} which is comparable to that obtained in the dark electrochemistry. It is then resonable to suggest that counterion diffusion may also be significantly influencing the kinetics in the photoelectrochemistry. Electron transfer may be limiting. The decrease in the peak currents for the 1-/2- redox reaction of the complex in the voltammetric wave (Figure 6-3) recorded after the photoelectrochemistry probably demonstrates this. In the photoelectrochemical measurements the reduction of $^*Ni(mnt)_2^{2-}$ to the trianion would result in the exodus of

chloride ions along with solvent (methanol), from the polymer film. The uptake of chloride ions and particularly water was demonstrated in the thermal electrochemistry to be difficult and this may also be true when the reaction is increased by irradiation. Thus the mobility of chloride ion in the film after the photoelectrochemistry would decrease and can account for the decrease in the peak currents of the voltammogram. It could also account for the decrease in the photocurrents observed in the second and subsequent attempts (see Figure 6-2(a)) in the photoelectrochemical measurements. In electrode 9, there is no decrease of the photocurrent in the second and third attempts (see Figure 6-5) but the decrease was observed after polarizing the electrode in light at -0.4 V where the excited states can undergo reduction. This is probably because there is a higher concentration of the complex in the first few layers next to the electrode and depletion of the reactant in the photoelectrochemistry takes a longer time. The spectrum of the electrodes before and after the photoelectrochemical measurements are identical, indicating that the complex has not been leached from the polymer in the photoelectrochemical reaction. It also suggests that there is no change occuring in the film during the photoelectrochemistry but that the reaction is reversible. The $Ni(mnt)_2^{3-}$ produced reacted in the dark to

produce the initial reactant. It is also possible that if $Ni(mnt)_2^{3-}$ remains in the film, the amount is so small that it may not affect a change in the spectrum.

8.3.2 Photoelectrochemistry of SnO_2-QPVP-$Pt(mnt)_2^{2-}$ Electrodes.

The photoelectrochemical behaviour of $Pt(mnt)_2^{2-}$ incorporated into the polymer film on SnO_2 electrodes does not exhibit a simple behaviour. The response of the $Pt(mnt)_2^{2-}$ modified electrodes to illumination differs significantly from that of the nickel. Unlike the modified electrodes of $Ni(mnt)_2^{2-}$ where a single photoelectrochemical redox reaction occurs under irradiation, the photocurrent profile of the $Pt(mnt)_2^{2-}$ modified electrodes suggests more than one photoinduced reaction. The prompt response in the photocurrent profile curve (Figure 6-6) suggests a reaction similar to the nickel i.e. the excited states of $Pt(mnt)_2^{2-}$ is reacting at the electrode to produce a part of the total cathodic photocurrent. The slow response in which the photocurrent is slowly increasing subsequent the prompt photocurrent represents another reaction.

The results of electrodes 10 and 11 in section 6.3.1 are analysed. On both of these electrodes the spectrum after the photoelectrochemical measurements differs. The spectrum features of electrode 16 in section 6.3.5 Figure 6-25 after it was oxidized by hydrochloric acid. Since the prompt photo-current is assigned to the reduction of

the excited states, it can be said that the slow photocurrent is a consequence of reduction of $Pt(mnt)_2^{1-}$ produced by photochemical oxidation of $Pt(mnt)_2^{2-}$. It will be shown later that this photooxidation reaction results from the excited states reacting with water. Section 8.2 already demonstrated that the excited state absorbance is quenched by water. The spectrum of the modified electrode after the photoelectrochemistry suggests that the complex has undergone a partial oxidation and tends to confirm that the excited state in the transient spectrum (Figure 7-9) is indeed quenched by an electron transfer reaction. Further evidence of such a mechanism will also be discussed later in the results of the continuous photolysis experiment. It can therefore be concluded that $Pt(mnt)_2^{2-}$ modified electrodes in contact with aqueous solution undergoes a photochemical as well as a photoelectrochemical reaction. The photochemical reaction results in oxidation of the complex and occurs at the polymer/electrolyte interface. The photoelectrochemical reaction represents an electron capture from the electrode by the excited states and occurs at the SnO_2/polymer interface.

In Figure 6-7 to 6-12 there is evidence to show that the photooxidation product affects the shape of the photowave. In Figure 6-7 measurements were commenced at 0.0 V. Within the potential range 0.0 V to -0.3 V only

the photooxidation is important. In this region the photowave (curve b) for the slow process has decreased as if it is suggesting that there is a competitive reaction between the photooxidation process and the photoelectrochemical reduction. The cathodic photocurrent observed for the slow process can be considered as representing the reduction of the photochemically generated $Pt(mnt)_2^{1-}$. In the potential region of -0.3 to -0.6 V the reduction of the excited states is also occuring and therefore reduced the amount of $Pt(mnt)_2^{2-}$ available for photooxidation. Thermodynamically the reduction of $Pt(mnt)_2^{1-}$ is favorable but the reduction of $^*Pt(mnt)_2^{2-}$ preferentially occurs because it is being generated at the SnO_2/polymer interface. The electrode was irradiated from the SnO_2 side.

Figure 6-7(a) of electrode 10 and Figure 6-11(a), of electrode 11 represent the photocurrent wave obtained in the first attempt in the photoelectrochemlical measurements. The shapes of these curves are not the same. This is because the photocurrent measurement were taken on different directions with different time scans. In Figure 6-11(a) measurements were from -0.6 V to 0.0 V, anodic direction while in Figure 6-7(a) it was from the reverse or cathodic direction. The reduction of $Pt(mnt)_2^{2-}$ would result in movement of the chloride counterions and exodus of solvent from the film. The larger current in the -0.3 to -0.6 V region and smaller current in the 0.0

to -0.3 V region in Figure 6-11(a) compare to 6-7(a) is probably a result of the effect of counterion and solvent movement. For a fresh electrode i.e. an electrode not used before, the ionic counductivity of the film is higher than one which is used for a period of time. Thus starting the measurements at -0.6 V (electrode 11, Figure 6-11(a)) resulted in a larger photocurrent in this region and as the measurement was continued to 0.0 V, the decreased in the photocurrent was found to be greater because chloride ions and solvent are continually expelled in the reduction process. When the measurements were started at 0.0 V in electrode 10, Figure 6-7(a) shows the photocurrent is larger in the 0.0 V to -0.3 V region and smaller in the -0.3 to -0.6 V region for similar reasons.

Because of the simultaneous reactions of the electrodes under irradition, the shapes of the photowaves obtained in the repeated measurements are unlike those of the $Ni(mnt)_2^{2-}$ modified electrode. This is particlarly visible for electrode 10 in Figure 6-8. The spectrum of this electrode (Figure 6-10) after the first photoelectrochemical measurements shows that there is significant oxidation of the complex. The shape then is a result of accumlulation of the $Pt(mnt)_2^{1-}$ in the film. In Figure 6-8(b), the prompt photocurrent in the -0.3 to -0.6 V region has decreased because, as mentioned before the concentration of $Pt(mnt)_2^{2-}$ is reduced. The slow

photocurrent is increasing because the amount of $Pt(mnt)_2^{1-}$ in the film has increased. The photoelectrochemical behaviour of electrode 16 in Figure 6-27 of section 6.3.5 which was preoxidized by hydrochloric acid supports this. The photocurrent is small between 0.0 to -0.4 V and increases as the electrode is poised beyond -0.4 V.

In electrode 11 (Figure 6-11 and 6-12) such behaviour is less pronounced. it was only observed after repeated measurements, (i.e. in the seventh run). The shape and magnitude of the prompt photocurrent is constant after the second attempt. This is due to the amount of $Pt(mnt)_2^{2-}$ remaining in the film at the SnO_2/polymer interface. A significant amount of the 2- species is in the film at this interface probably because the photoelectrochemical measurements were started in the potential region where there is simultaneous reduction of the excited states at the SnO_2/polymer interface and photooxidation at the polymer/electrolyte interface. The electron captured by the excited state is probably propagated through the film to reduce some of the photooxidized $Pt(mnt)_2^{1-}$. This however is limited by counter ion movement. The voltammetric response after the photoelectrochemical measurements for these electrode (Figure 6-9 and 6-13) is similar to those observed for the nickel. The peak currents for the 1-/2- redox reaction is smaller than before the photoelectrochemisty. This decrease is not only due to decrease in ionic conductivity

in the film as in the case of the nickel modified electrode but there is an additional reason. It will be shown later that the samller anodic and cathodic wave for the 1-/2- redox reaction is due to the photooxidized product, $Pt(mnt)_2^{1-}$ undergoing aggregation.

Section 6.3.2 presented the results of irradiating the electrode from the SnO_2 side (back-side) and from the solution or the front side. Electrode 12 which was irradiated from the SnO_2 side showed a prompt photocurrent due to the reduction of the excited states larger than on electrode 13 which was irradiated from the solution side. Irradiation from the SnO_2 side generates more excited states at the polymer/electrode interface and charge transfer from the electrode to the excited states is efficient. In the front side illumination layers that are further from the SnO_2 electrode are preferentially irradiated and the photoreaction at the polymer/electrolyte interface becomes more efficient. The photowaves of electrode 13 in Figure 6-18 (a) supports this. In the first attempt at the photocurrent measurements the photocurrent for the prompt reaction of the excited states is smaller than the photocurrent arising from the slow photoprocess.

In discussing the results of section 6.3.1 it was mentioned that the $Pt(mnt)_2^{1-}$ photo-produced in the polymer film of the modified electrodes is partially responsible

for the decrease in the anodic and cathodic waves for the 1-/2- redox reaction. This was investigated further in section 6.3.3 on electrode 14. The spectrum of this electrode after continuous irradiation while it was poised at -0.6 V is different from the spectrum before it was irradiated. The spectral features suggest that the complex in the film after the irradiation indicates the $Pt(mnt)_2^{1-}$ species. The spectrum was compared with those of electrode 16 in section 6.3.5 Figure 6-25. Electrode 16 contains $Pt(mnt)_2^{1-}$ in the polymer film. The voltammetric response of the electrode with the photo-produced $Pt(mnt)_2^{1-}$ in the film is different from the volatammogram recorded when $Pt(mnt)_2^{2-}$ is initially present in the polymer. Besides the drastic reduction of the peak current in 1-/2- redox waves, solvent decomposition now occurs at about -0.5 V. The evolution of gas at the electrode was observed in this potential region. At the bare Pt electrode H_2 evolves from water (aqueous electrolyte pH 5.8) at -0.79 V. It is obvious that the $Pt(mnt)_2^{1-}$ photo-produced in the film is associated with the anodic shift in the potential for decomposition of water. This was verified by the results of 6.3.4 and 6.3.5 with electrodes 15 and 16, respectively. Oxidation of $Pt(mnt)_2^{2-}$ in the polymer film of electrode 15 is enhanced when the electrode is irradiated in contact with acidic electrolyte. The spectrum (Figure 6-23) verifies the oxidation product as

$Pt(mnt)_2^{1-}$. In electrode 16, $Pt(mnt)_2^{1-}$ was produced in the film by chemical oxidation with acid and is also verified by the absorption spectra of Figure 6-25. In both of these electrodes the potential for the decomposition of water is shifted to a more anodic potential of about -0.6 V. The voltammetric responses of Figures 6-23 and 6-26 for electrodes 15 and 16 respectively was recorded as the oxidation reaction was in progress. They show that when a significant amount of the $Pt(mnt)_2^{1-}$ is in the film or when the oxidation reaction of $Pt(mnt)_2^{2-}$ in the film is completed, the decomposition of water is shifted to a more anodic potential. The photoelectrochemical behaviour of the electrode with $Pt(mnt)_2^{1-}$ in the polymer film was also altered. According to Figure 6-22 and 6-26, the $Pt(mnt)_2^{1-}$ does not produce photocurrent in the potential region of 0.0 to -0.4 V, but a large photocurrent was observed at potentials beyond -.5 V. This is the potential region where the solvent decomposition occurs. The irradiation may act as a catalyst to enhance the decomposition of water or as seen later, the reduction of aggregates of $Pt(mnt)_2^{1-}$.

In section 6.3.3, the electrode was poised at -0.6 V, where the reduction of the $Pt(mnt)_2^{2-}$ excited states occurs. At this potential the overvoltage is larger than that required for the reduction of $Pt(mnt)_2^{1-}$ to $Pt(mnt)_2^{2-}$. Despite this the monoanion still accumulates in the film.

The scanning electron micrographs of section 6.6 probably give the reason for this. The micrographs taken before photoelectrochemical measurements show the complex inside the polymer film. Those taken after the photoelectrochemistry show the complex on the surface of the polymer film. The $Pt(mnt)_2^{1-}$ which appear to form aggregates cannot diffuse through the polymer film to the electrode surface where they can be reduced. Electron transport through the film would also be difficult and limited by counterion motion. The rate of oxidation of the complex at the polymer/electrolyte interface is faster than the electron diffusion through the polymer film. This would lead to accumulation of the $Pt(mnt)_2^{1-}$ on the film and aggregation.

In the photooxidation of $Pt(mnt)_2^{2-}$ incorporated in the polymer film on the SnO_2 electrode it is not known whether the polymer is important in the reaction. Continuous photolysis of the cuvette containing $Pt(mnt)_2^{2-}$ in the mixed acetonitrile/water solvent established that the polymer is not important in the photo-oxidation. The complex was irradiated in the mixed solvent in the absence of the polymer. The change in the spectrum (see Figure 7--4) with increasing irradiation time shows an increase in absorbance of the 855 nm band and a shift of the 472 nm band to 450 nm. The absorbance at 855 nm and 450 nm are characteristic of the $Pt(mnt)_2^{1-}$. The continuous photolysis is also supportive in establishing the reaction

mechanism for the quenching of the $Pt(mnt)_2^{2-}$ excited states in the flash photolysis experiments. Since the spectrum after continuous irradiation can be assigned to $Pt(mnt)_2^{1-}$ it can be inferred that the excited states of $Pt(mnt)_2^{2-}$ is being quenched by an oxidative mechansim in which the electron acceptor is water. A plausible mechanism then is a bimolecular excited-state electron transfer to water:

$$Pt(mnt)_2^{2-} \underset{k_{-1}}{\overset{k_1(h\nu)}{\rightleftharpoons}} {}^*Pt(mnt)_2^{2-}$$

$$^*Pt(mnt)_2^{2-} + H_2O \xrightarrow{k_q} [Pt(mnt)_2^{1-} \cdots H_2O^{\cdot -}] \qquad (31)$$

$$[Pt(mnt)_2^{1-} \text{—} H_2O] \xrightarrow{k_5} Pt(mnt)_2^{1-} + {}^{\cdot}OH + H^{\cdot}$$

$$Pt(mnt)_2^{1-} \cdots H_2O] \xrightarrow{k_4} Pt(mnt)_2^{2-} + H_2O$$

The rate constant k_q for the quenching process was determined as 2×10^8 sec^{-1} from the flash photolysis studies. Although the absorption spectrum after continuous photolysis in the cuvette is characteristic of $Pt(mnt)_2^{1-}$, the voltammetric response does not support this in a simple version. The voltammogram of Figure 7-2 (b) which was recorded after 2 hr of irradiation in the electrochemical cell does not show the redox waves associated with the 1-/2- redox reaction. This reaction was observed before irradiation when $Pt(mnt)_2^{2-}$ was initially present in the solution. The fact that no faradic response was found in Figure 7-3 (a) when the

solution was allowed to sit still for 4 hr, but after stirring a huge cathodic peak is seen at -0.56 V would support the claim that the contents of the cell has become a suspension after irradiation. These observations support the explanation proposed for the micrograph taken of the film after photoelectrochemistry which is the $Pt(mnt)_2^{1-}$ forms small crystallites or aggregates after photooxidation of $Pt(mnt)_2^{2-}$. The spectrum in acetonitrile shown in Figure 7-4 of the particles recovered from the electrochemical cell after irradiation is that of $Pt(mnt)_2^{1-}$. The electrochemistry of the particles in the presence of H_2O is limited by the potential window of water. The particles recovered after irradiation in the electrochemical cell were therefore re-investigated in acetonitrile. The voltammograms of Figure 7-3 show that the electrochemical behaviour in dry acetonitrile is different from that in acetonitrile solution in which water is present. In dry acetonitrile (Figure 7-3 (a)) the reversible reactions at +0.68 V and -0.20 V versus Ag/Ag^+ (0.1 M $AgNO_3/CH_3CN$) reference can be assigned to the $Pt(mnt)_2^{0}/Pt(mnt)_2^{1-}$ and $Pt(mnt)_2^{1-}/Pt(mnt)_2^{2-}$ redox reaction respectively. These are in agreement with the solution half-wave electrochemical potentials of Table 3-3 in which $Pt(mnt)_2^{2-}$ was used as the reactant. The irreversible cathodic peak at -0.58 V can be assigned to the reduction of the aggregates. Upon addition of water

aggregation is increased and resulted in the decrease in the voltammetric wave at +0.60 V and -0.20 V (Figure 7-3 (a)). In the polymer film the reduction of the aggregates appears to be associated with the catalytic decomposition of water.

CONCLUSION

This study represents the first extensive investigation of the photochemical and photoelectrochemical behaviour of the maleonitriledithiolate complexes under visible radiation. The photocurrents obtained from the solution photoelectrochemistry are small in the nanoampere domain and appears to be limited to those cases where a M ---> L * state is available. The photocurrents were improved (larger) when the photoactive species were attached to a solid surface i.e. the modified SnO_2 electrodes. This indicates that when the lifetimes were extended these states can be used in applied photoelectrochemistry. Unfortunately, this is not possible with the type of modified electrodes used in this study since the electrode kinetics is limited by a slow counterion movement in the film. A particulate system may prove more profitable. Among those complexes investigated the Pt complex appears to be an attractive candidate as a photocatalyst for hydrogen generation from water since the excited state of this complex is oxidatively quenched by water.

References

1. J.A. McCleverty; Prog. Inorg. Chem. 10, 49 (1968).
2. R.P. Burns and C.A.Mcauliffe; Adv. in Inorg. Chem. and Radiochem. 22, 303 (1979).
3. W.E. Geiger Jr., T.E. Mines and F.C. Senftleber. Inorg. Chem. 14, 2141 (1975).
4. W.E. Geiger and F.C. Senftleber; J.Am. Chem. Soe. 97, 5018 (1975).
5. R.M. Golding, H. Lehlonen; Aust. J. Chem. 27, 2083 (1974).
6. D. Sartain and M.R. Truter; J. Chem. Soc. Chem. Commun. 382 (1966).
7. R. Eisenberg, J.A. Ebers, R.J.H. Clark and H.B. Gray; J. Am. Chem. 86, 113 (1964).
8. S.I. Shupack, E. Billing, R.J.H. Clark, R. Williams and H.B. Gray; J. Am. Chem. Soc. 86, 4594 (1964).
9. H.B. Gray, R. Williams, E. Billing and J.W. Walters; J. Am. Chem. Soc. 88, 43 (1966).
10. W.E. Mines and W.E. Geiner Jr. Inorg. Chem. 12, 1191 (1973).
11. G.N. Schrauzer; Acc. Chem. Res. 2, 72 (1969).
12. J.L. Mateinzo, O.S. Grim and W.E. Swartz; J. Am. Chem. Soc. 94, 5116 (1972).
13. J.L. Mateinzo, O.S. Grim and W.E. Swartz; J. Am.

Chem. 13, 44 (1974).

14. R.J.H. Clark and P.C. Turtle; J.C.S. Dalton Trans. 2142 (1977).

15. G.N. Schrauzer and V.P. Mayweg; J. Am. Chem. Soc. 87, 3558 (1965).

16. A.H. Maki, V. Edelstein, A. Davidson and R.H. Holms; J. Am. Chem. Soc. 86, 8645 (1964).

17. Ulricht T. Mueller - Westerhoff; Inorg. Chem. 21, 46 (1982).

18. R. Henning, W. Schlamann and H. Kisch; Agnew. Chem. 19, 645 (1980).

19. R. Battaglia, R. Henning, B. Denh - Ngoc, W. Schlamann and H. Kisch; J. Mal. Cat. 21, 239 (1983).

20. N. Zeng, J. Buckeler and H. Kish; J. Am. Chem. Soc. 107, 1459 (1985).

21. D.M. Dooley and B.M. Patterson; Inorg. Chem. 21, 4330 (1982).

22. A. Vogler and H. Kunkely; Inorg. Chem. 21, 1172 (1982).

23. M. Sharp, M. Petterson and K. Edstrom; J. Electroanal. Chem. 109, 271 (1980).

24. R.A. Simon, A.J. Ricco and M.S. Wrighton; J. Am. Chem. Soc. 104, 2031 (1982).

25. R.W. Murray; Acc. Chem. Res. 13, 135 (1980).

26. M. Flujihira, N. Ohishi and Tetsuo Osa; Nature.

268, 226 (1977).

27. R.J. Mortimer and F.C. Anson; J. Electroanal. Chem. 138, 325 (1982).

28. K. Shigehara, E. Tsuchida and F.C. Anson, J. Electroanal. Chem. 175, 291 (1984).

29. J.Q. Chambers etal; J. Electroanal Chem. 142, 277 (1982) and 161, 147 (1984).

30. F.C. Anson, K. Shigehara and N. Oyama; J. Am. Chem. Soc. 103, 552 (1981).

31. I. Rubinstein and A.J. Bard; J. Am. Chem. Soc. 102 6641 (1980).

32. P.J. Pierce and A.J. Bard; J. electroand. Chem. 114, 89 (1980).

33. Hans-Rudolf Zumbrunnen and F.C. Anson; J. Electroanal. Chem. 152, 111 (1983).

34. F. C. Anson; J. Phys. Chem. 84, 3336 (1980).

35. N. Oyama and F.C. Anson; J. Electroanal. Chem. 127 2471 (1980).

36. G.J. Samuels and T.J. Meyer; J. Am. Chem. Soc. 103, 307 (1981).

37. N. Oyama, T. Shimomura, K. Shigehara and F.C. Anson; J. Electroanal. Chem. 112, 271 (1980).

38. R.W. Murray; In Ann. Rev. Mater. Sci. 14, 145 (1984), Cd. R.A. Huggins, J.A. Giordmaine and J.B. Wachtnman, Jr. Annual Reviews Inc. California.

39. A. P. Brown and F.C. Anson; Anal. Chem. 49, 1589 (1977).

40. E. Laviron; J. Electroanal. Chem. 100, 263 (1979).

41. D.F. Smith, R.W. Murray, K. Willman and K. Kou; J. Electroanal. Chem. 95, 217 (1979).

42. E. Laviron, L. Roullion and D. Degrard; J. Electroanal. Chem. 112, 11 (1980).

43. F. B. Kaufman, A.H. Schroeder E.M. Engler, S.R. Kramer and J.O. Chambers; J. Am. Chem. Soc. 102, 483 (1980).

44. R.W. Murray, P.G. Pickup, C.R. Leidner and P. Derisevich; J. Electroanal. Chem. 164, 39 (1984).

45. H.S. White, J. Leddy and A.J. Bard; J. Am. Chem. Soc, 104, 4811 (1982)

46. K. Shigera, N.Oyama and F.C. Anson; J. Am. Chem. Soc. 103, 2552 (1981).

47. N. Oyama and F. C. Anson; J. Electroanal. Chem. 127, 640 (1980).

48. D. A. Buttry and F.C. Anson; J. Am. Chem. Soc.

49. P. Daum and R.W. Murray; J. Phys. Chem; 85, 389 (1981).

50. M.M. Nicholson; J. AM. Chem. Soc. 76, 2539 (1954).

51. G. Bhar and G. Schleiter; Ber. 190 (1957).

52. E. Billing, R. Williams, I. Bernal, J. H. Walters and H.B.Gray; Inorg. Chem. 2, 663 (1964).

53. R.E. Benson, L.R. Melby and J.F. Weiher; J. Am. Chem. Soc. 86, 4329 (1964).

54. A. Davison, N. Edelstein, R.H. Holm and H. Makai;

Inorg. Chem., 1227 (1963).

55. Auther Isreal Vogel, "Textbook of Quantitative Inorganic Analysis, including elementry instrumental analysis," 4th ed., Longmans, London and N.Y. (1978).

56. C.G. Pablo; Chem. Biomed. and Environ. Inst. 10, 197 (1980).

57. D.T. Sawyer and J.L. Roberts Jr.,"Experimental Electrochemistry for Chemist," Interscience Publishers, Inc. N.Y. (1974).

58. F.R. Meyer and G. Ronge; Angew. Chem. 52, 637 (1939).

59. C.H. Langford abd H. Kido; J. Am. Chem. Soc. 105, 1196 (1983).

60. J. Phillips, J.A. Koningstein and C.H. Langford; J. Chem. Soc. Chem. Commun. 425 (1977).

61. J. Phillips, C.H. Langford, J.A. Koningstein and R. Sassaville; J. Phys. Chem. 82, 622 (1978).

62. H. Matsuda and Y. Ayabe, Z. Elektrochem; 59 495 (1955).

63. Allen J. Bard and Larry R. Faulkner, "Electrochemical Methods Fundamentals and Apparatus," John Willey Inc. N.Y. and Toronto 1980 Chapter 6.

64. R. Raghvan and R.T. Iwamoto J. Electroanal. Chem, 92, 101 (1978).

65. R.W. Murray and J. Facci; J. Electroanal. Chem: 124, 339 (1981).

66. George Eiseman. The Molecular bases of Ion Selectivity in Macroscopic Systems, In "Mass Transfer and Kinetics of Ion Exchange, NATO ASI Series No. 71; L. Liberti and F.G. Helfferich Eds., Martinus Nighoff (1983).

67. Friedrich Helfferich, "Ion Exchange," McGraw Hill. N.Y., (1962).

68. J. Locke, J. A. McClevery, E.J. Wharton and C.J. Winscom; Chem. Commun; 677 (1966).

69. J.A. Mc Cleverty, N.M. Atherton, J. Locke, E.J. Wharton and C.J. Winscom; J. Am. Chem. Soc. 89, 6082 (1967).

70. C.H. Langford, E. Billig, S.I. Shupack and H.B. Gray; J. Am. Chem. Soc. 86, 2958 (1964).

71. E. Billing, H.B. Gray; S.I. Shupack, J.H. Walters and R. Williams; Proc. Chem. Soc. 110 (1964).

72. R.P. Van Duyne; in Chemical and Biochemical Application of Lasers, Vol.4 Chapter 4; C.B. Moore (ed.), Academic Press, New York (1978).

73. R.K. Chang and T.E. Furtak (eds.) Surface Enhanced Raman Scattering Plenum Press (1982).

APPENDIX

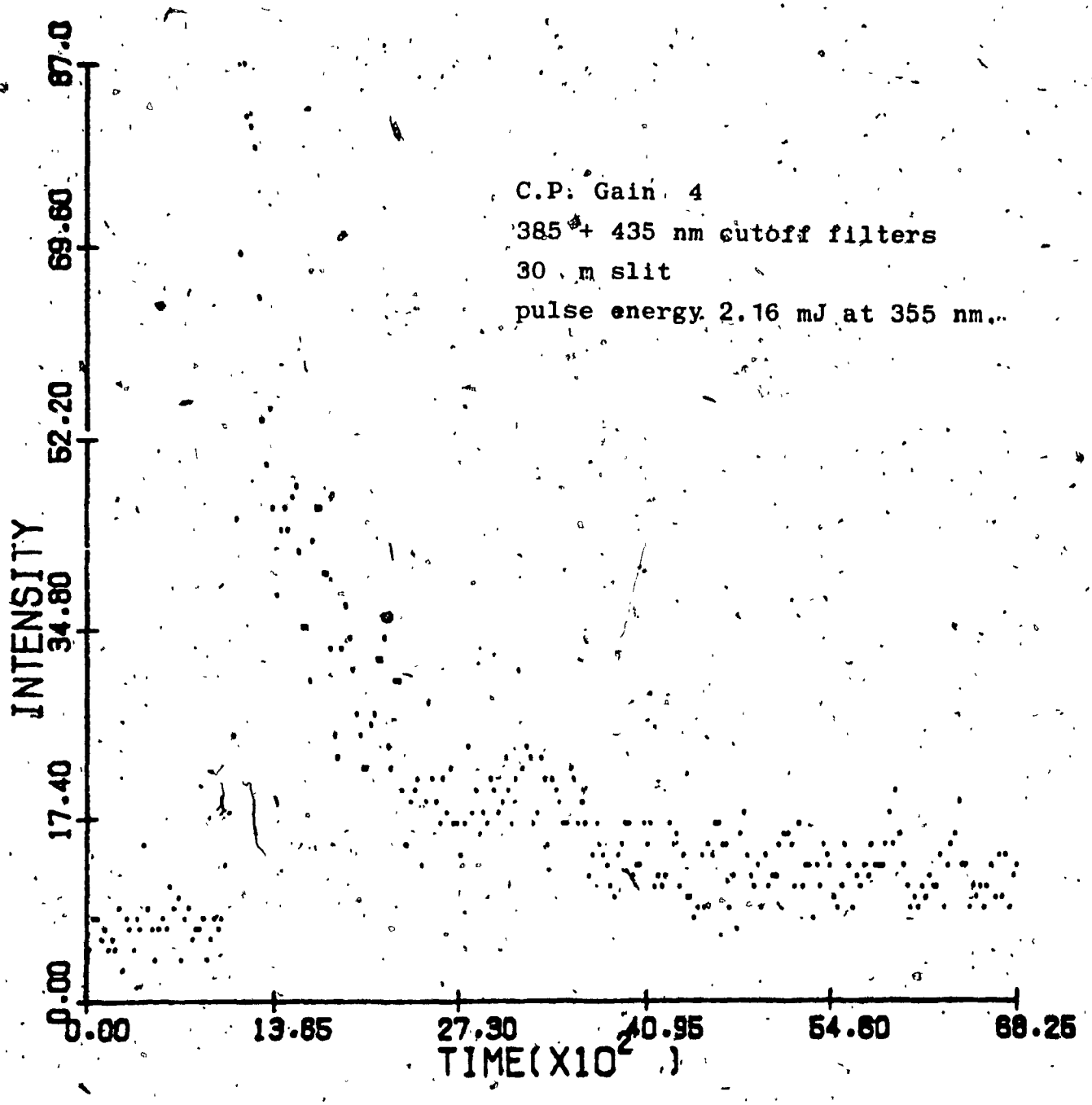

Figure 1. Emission decay of acetonitrile obtained with a single laser shot at streak speed of 26.66 ps/channel.

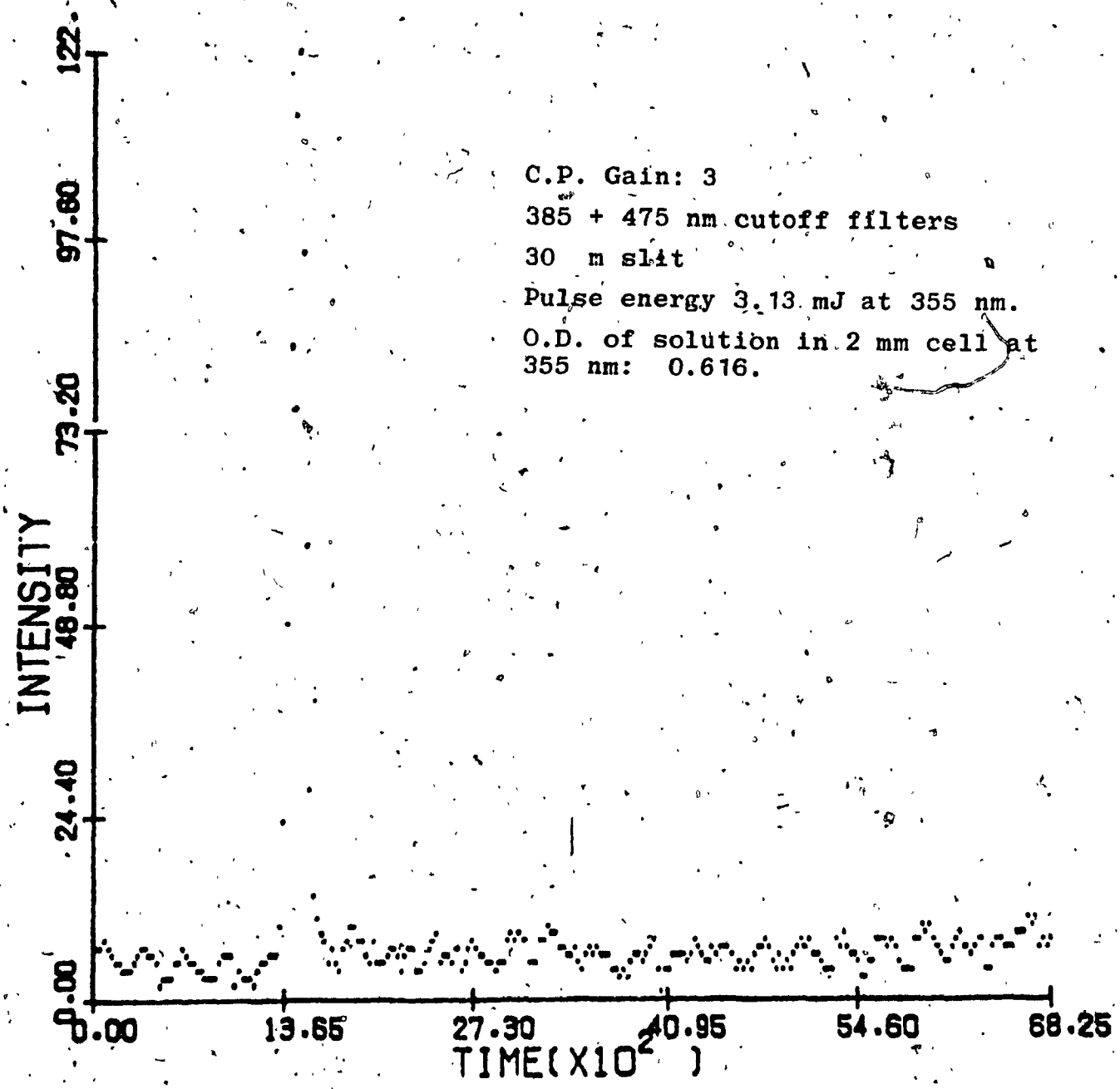

Figure 2 (a): Emission decay of $Ni(mnt)_2^{2-}$ in acetonitrile obtained with a single laser shot at streak speed of 26.66 ps/channel.

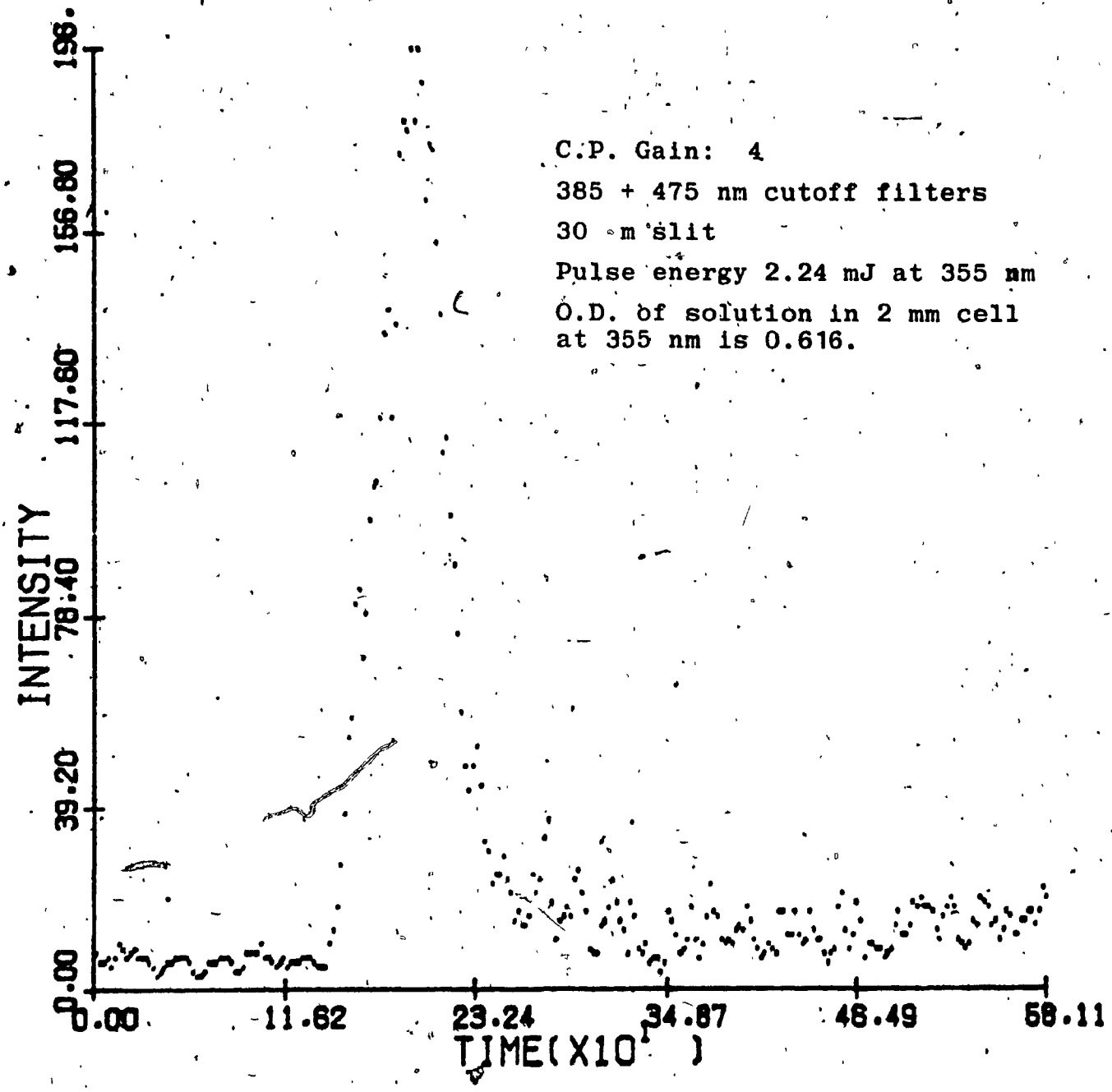

Figure 2 (b). Emission decay of $Ni(mnt)_2^{2-}$ in acetonitrile obtained with a single laser shot at streak speed 2.27 ps/channel.

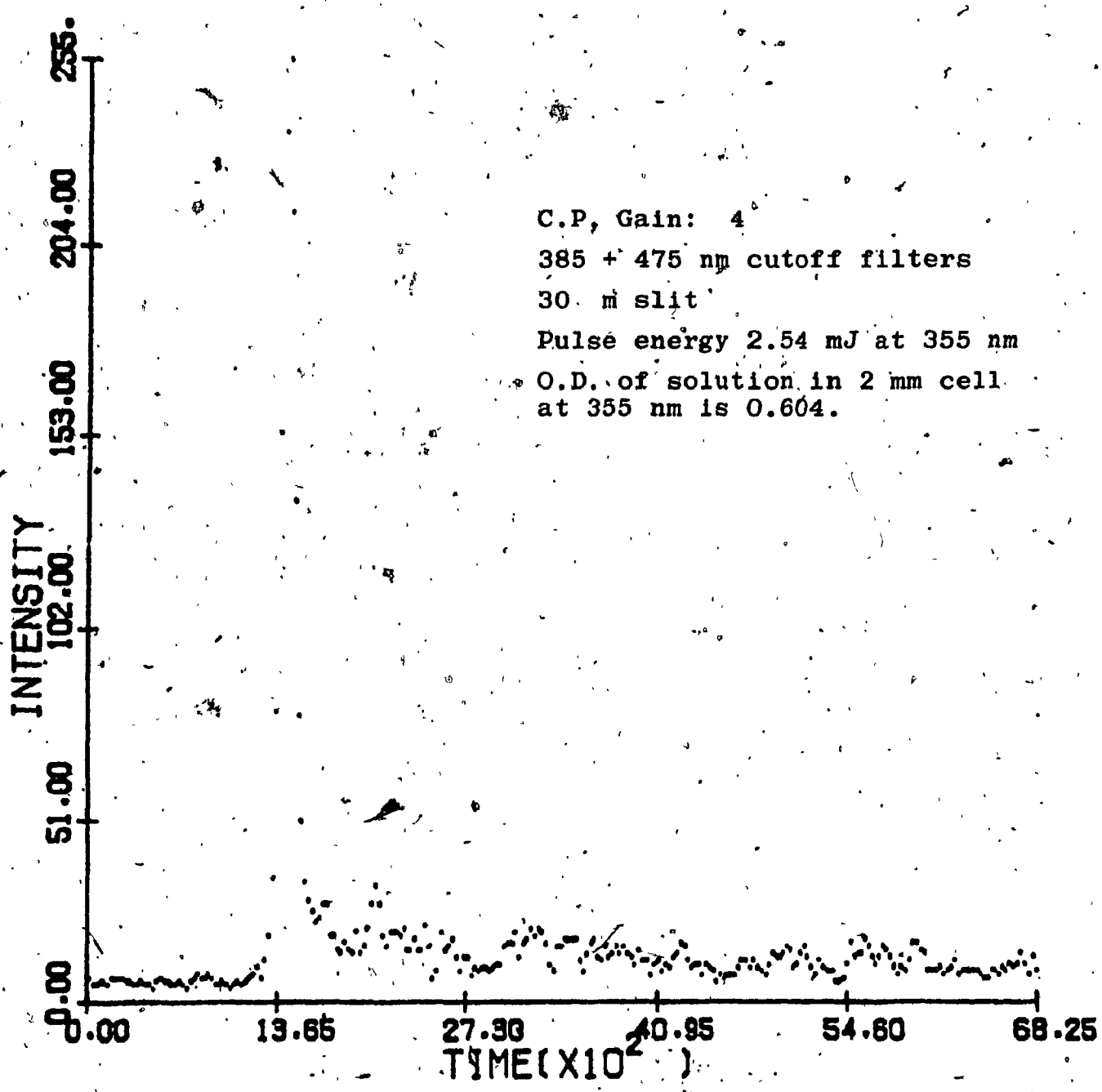

Figure 3 (a). Emission decay of $Ni(mnt)_2^{2-}$ in acetontrile/water solution obtained with a single laser shot at streak speed of 26.66 ps/channel.

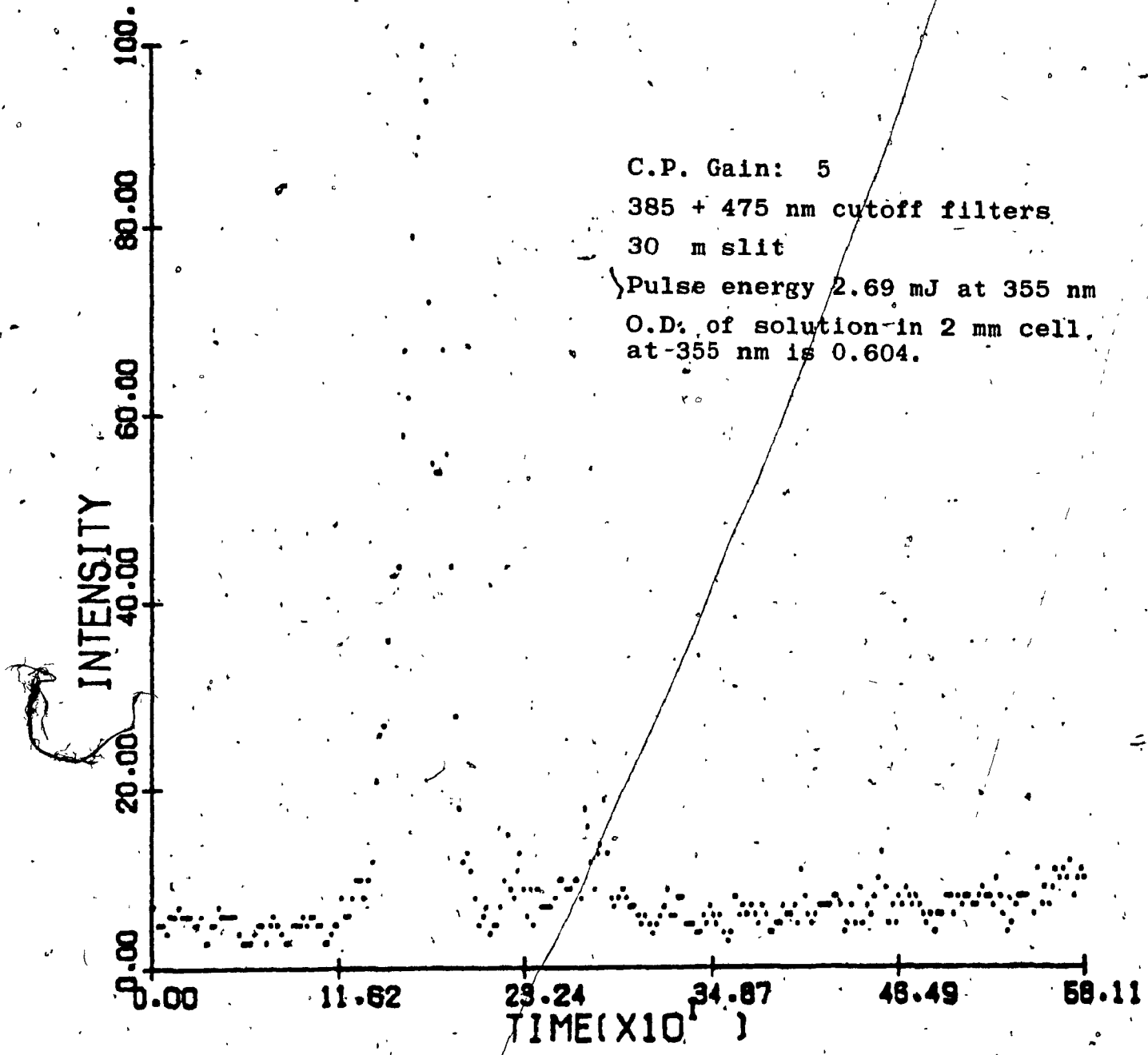

Figure 3 (b). Emission decay of $Ni(mnt)_2^{2-}$ in acetonitrile/water solution obtained with a single laser shot at streak speed of 2.27 ps/channel.

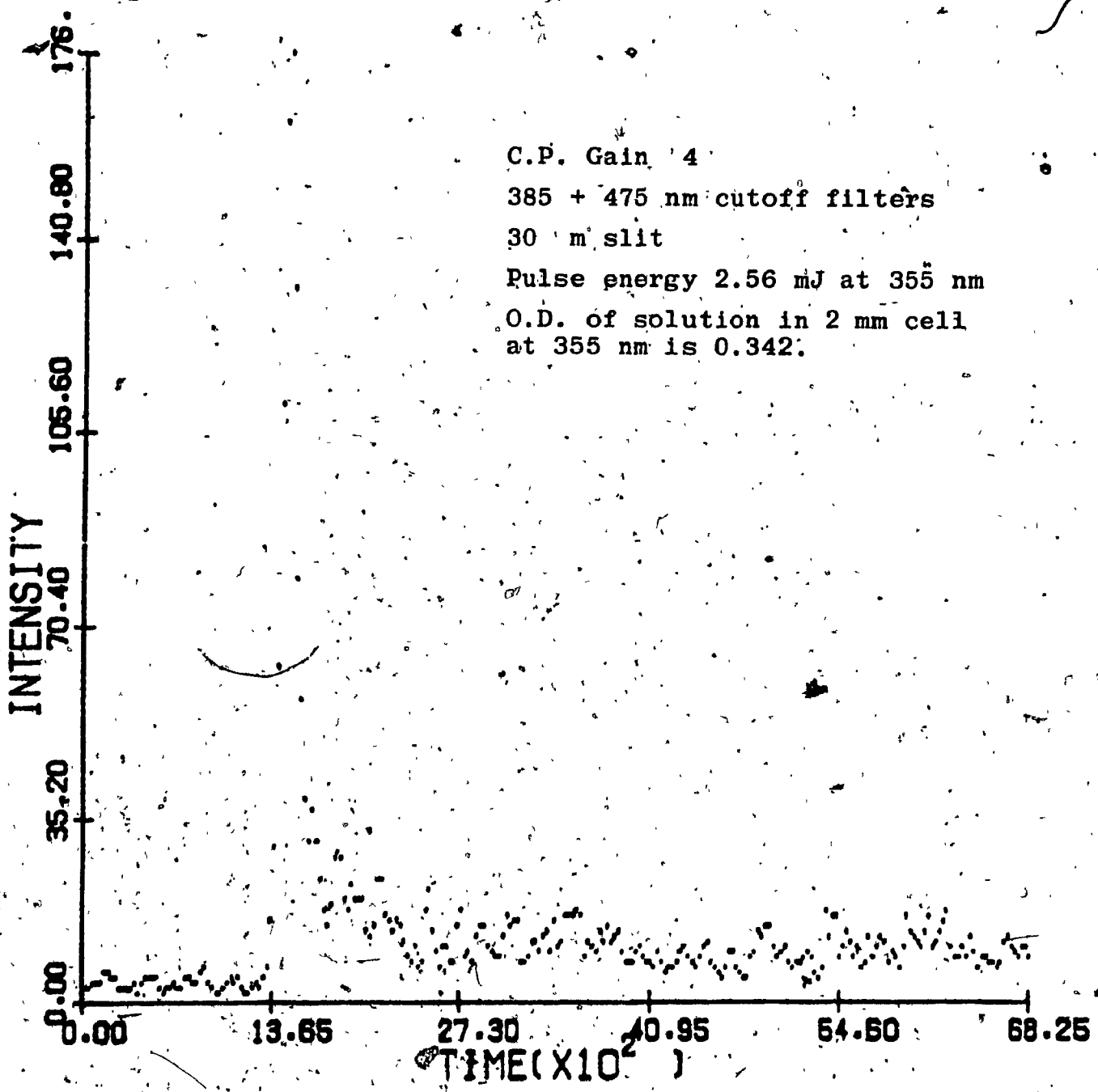

Figure 4 (a). Emission decay of $Ni(mnt)_2^{2-}$ in water obtained with a single laser shot at streak speed of 26.66 ps/channel.

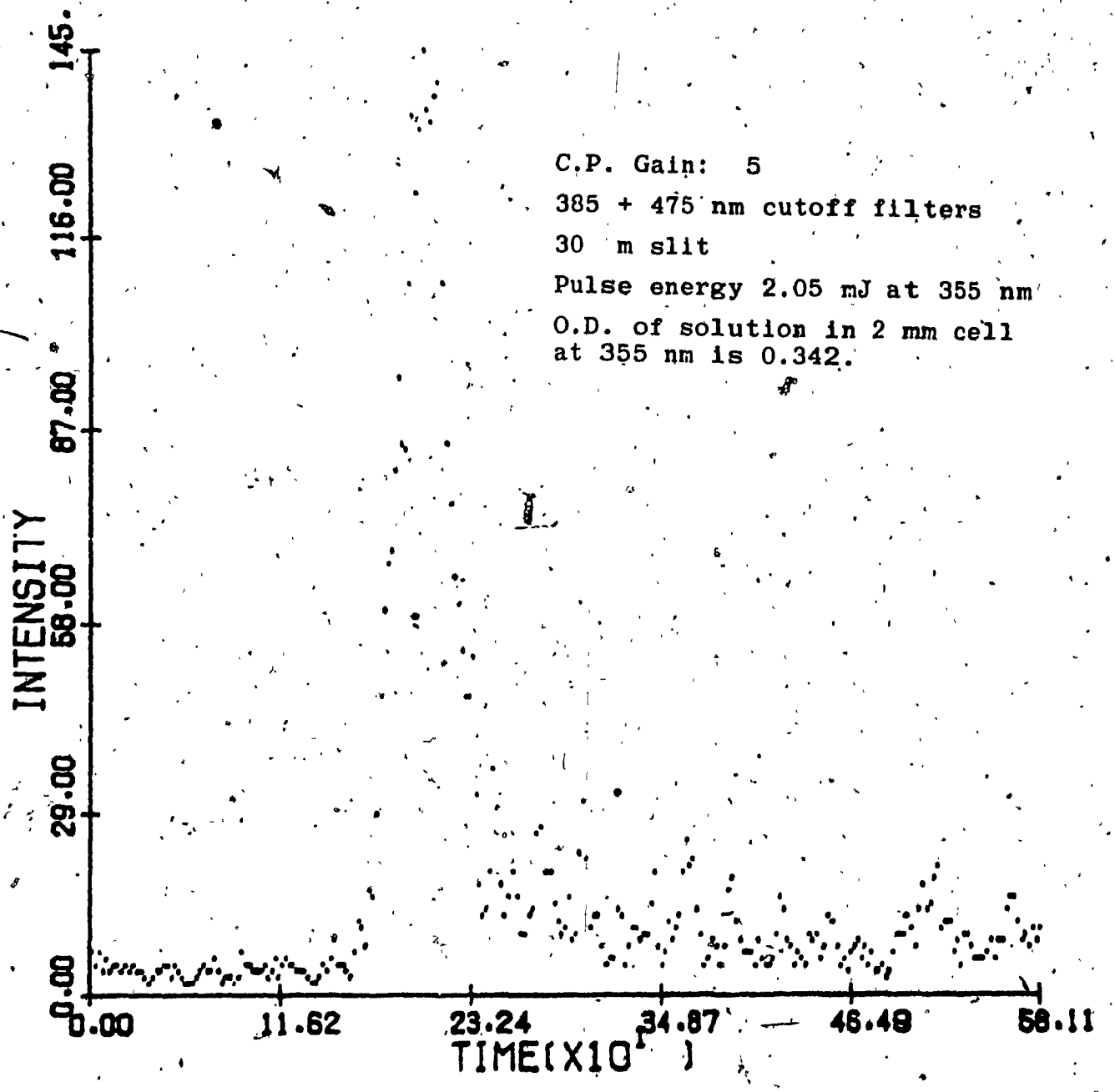

Figure 4 (b). Emission decay of $Ni(mnt)_2^{2-}$ in water obtained with a single laser shot at streak speed 2.27 ps/channel.

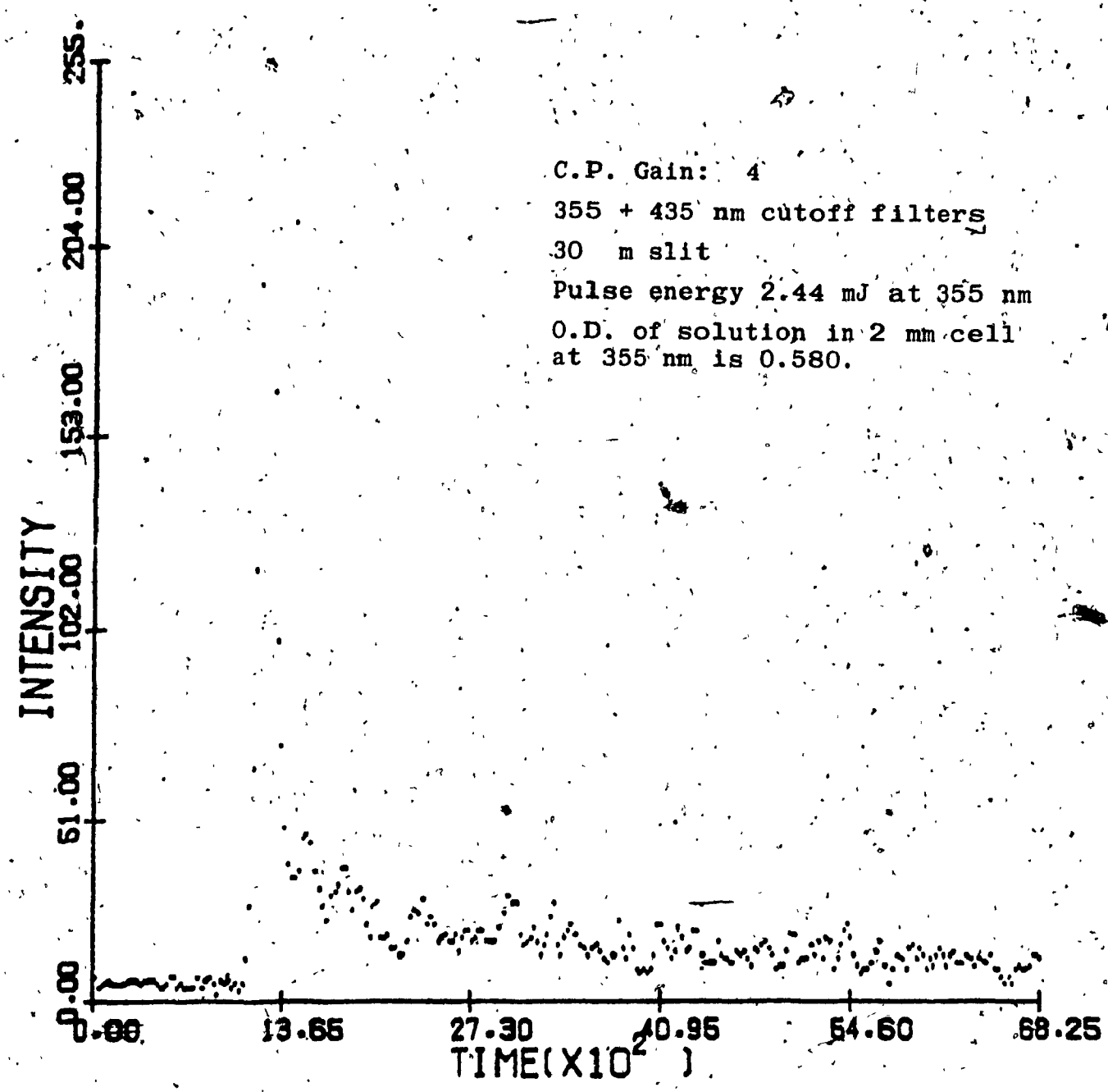

Figure 5 (a). Emission decay of $Pt(mnt)_2^{2-}$ in acetonitrile obtained with a single laser shot at streak speed of 26.66 ps/channel.

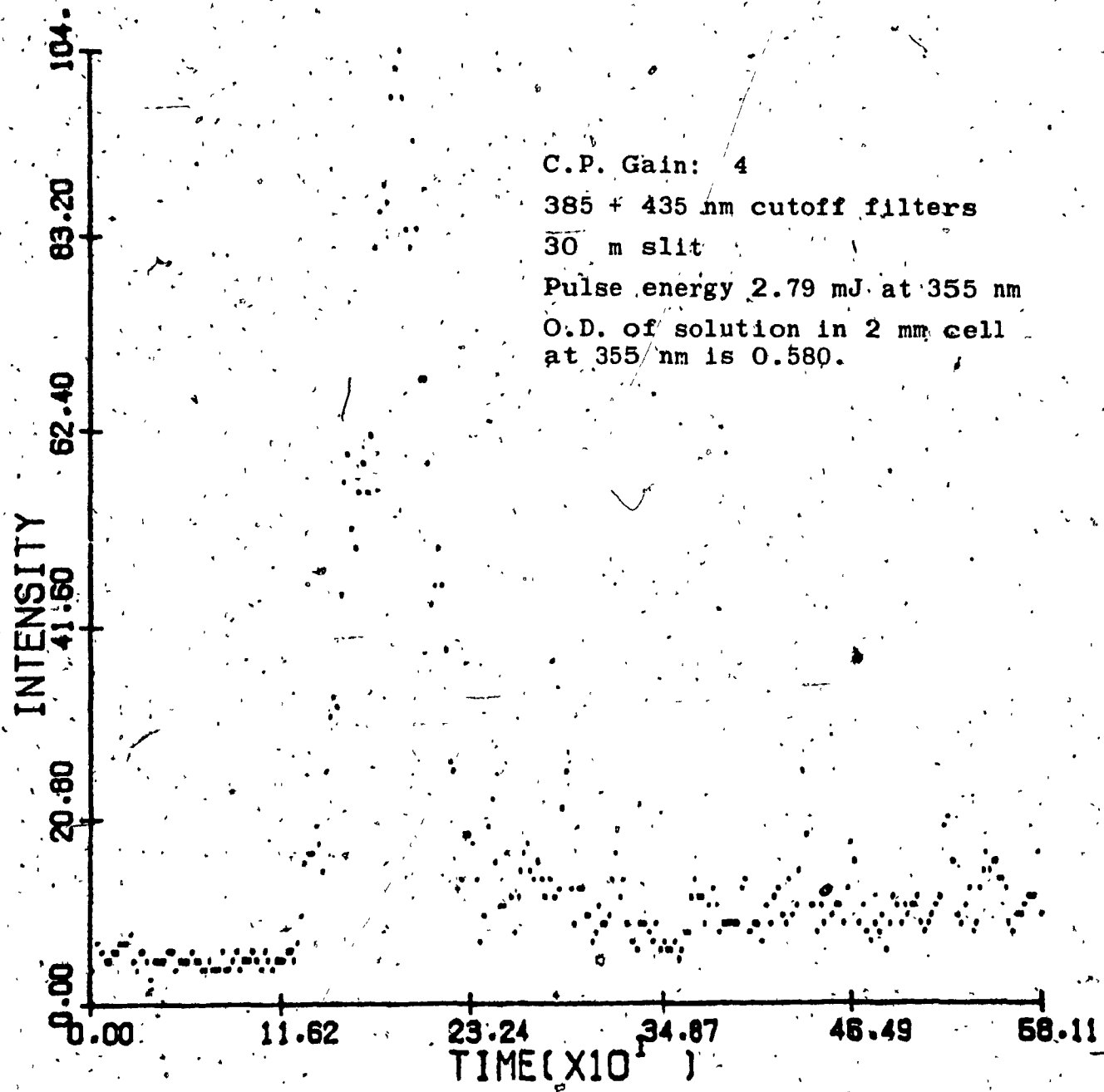

Figure 5 (b). Emission decay of $Pt(mnt)_2^{2-}$ in acetonitrile obtained with a single laser shot at streak speed of 2.27 ps/channel.

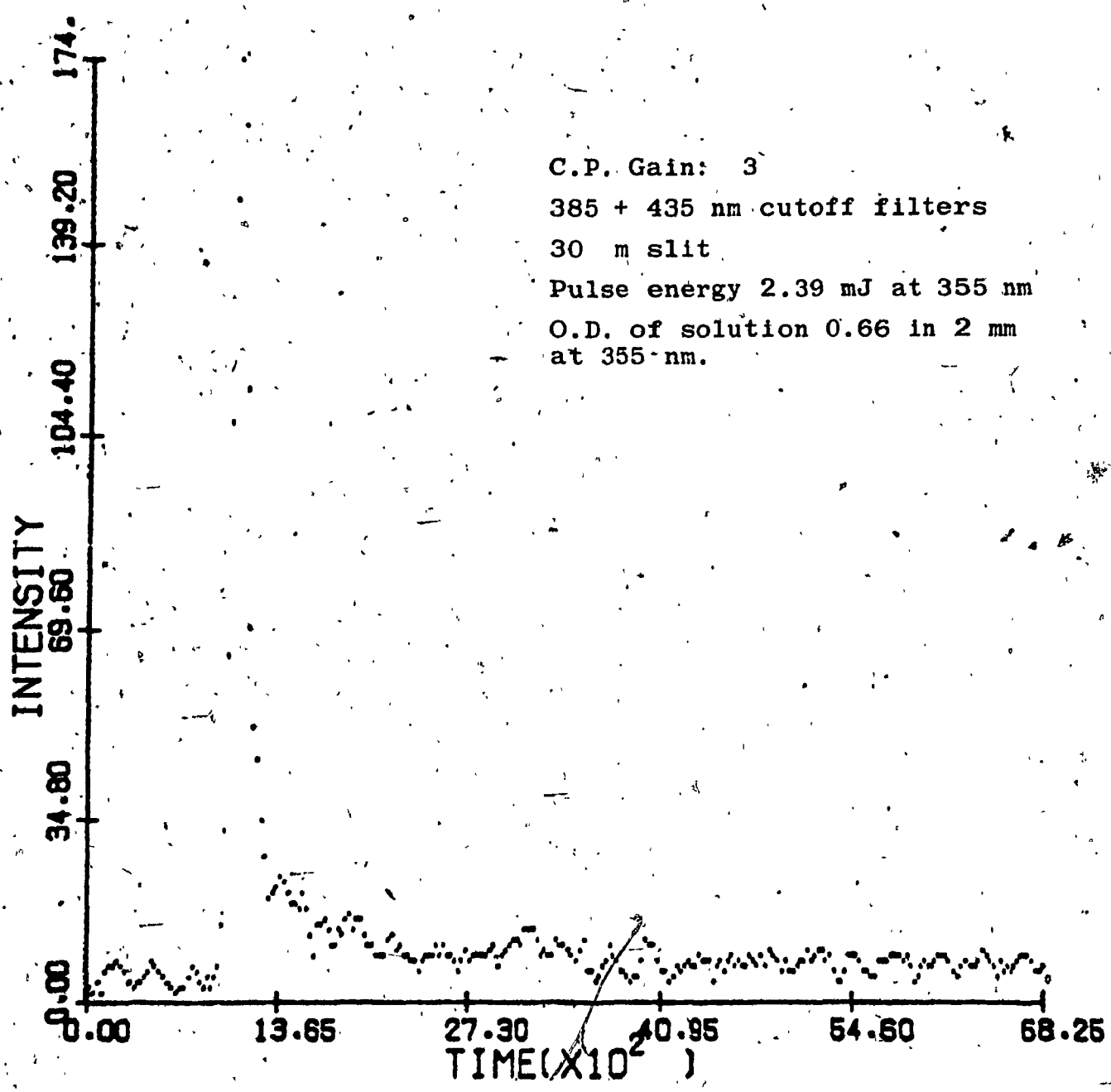

Figure 6 (a). Emission decay of $Pt(mnt)_2^{2-}$ in acetonitrile/water solution with a single laser shot at streak speed of 26.66 ps/channel.

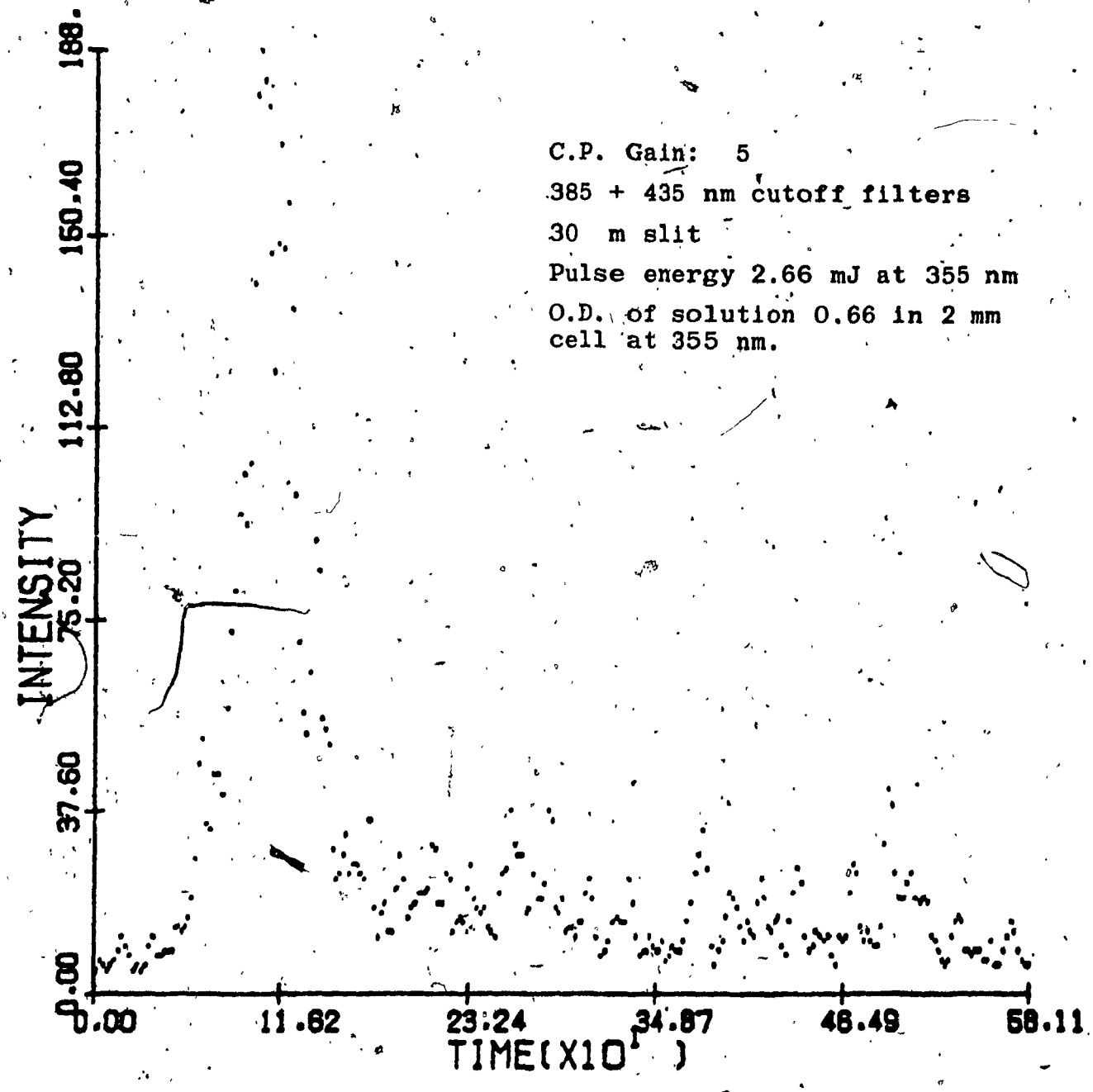

Figure 6 (b). Emission decay of $Pt(mnt)_2^{2-}$ in acetonitrile/water solution obtained with a single laser shot at streak speed of 2.77 ps/channel.

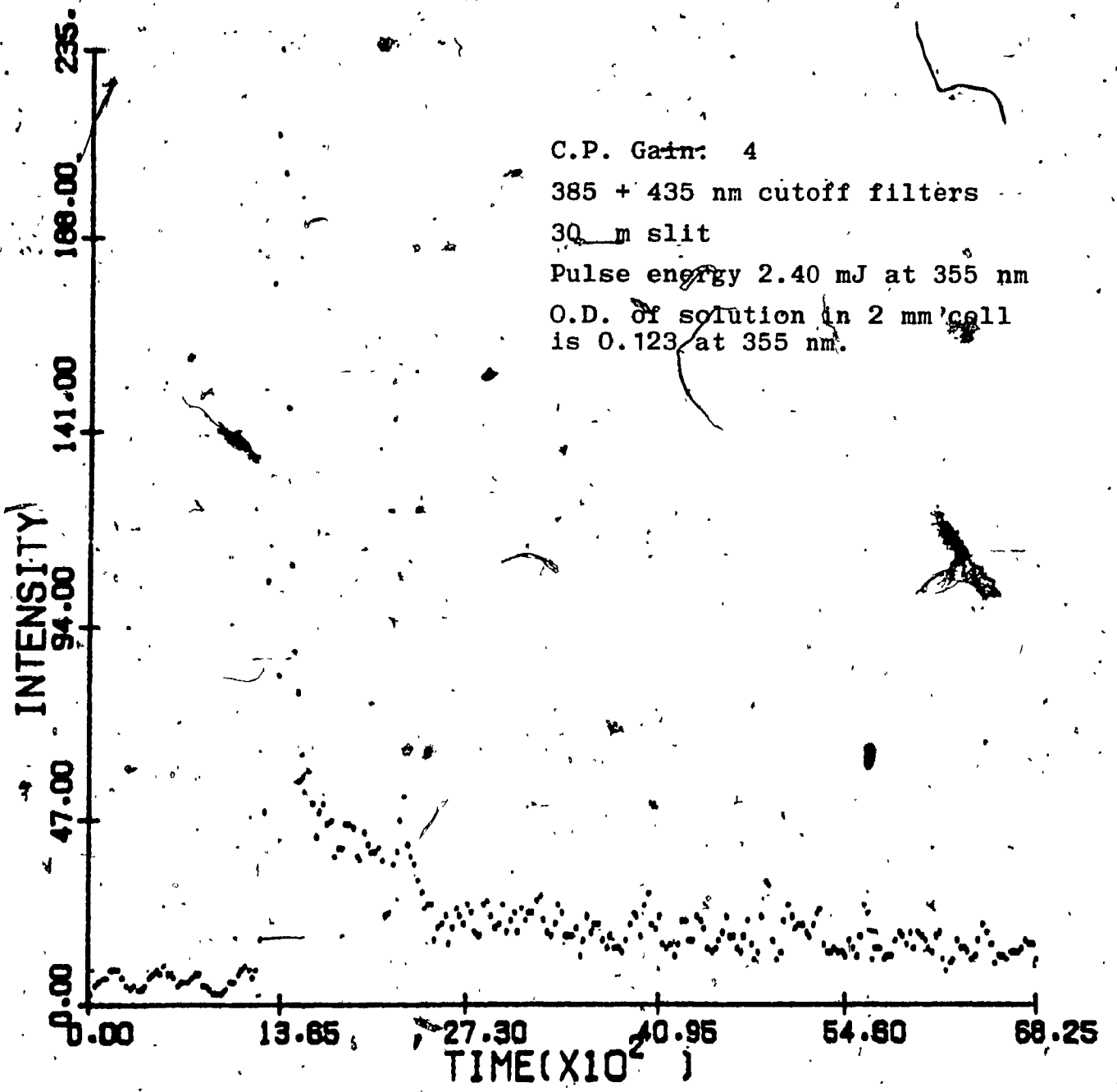

Figure 7 (a). Emission decay of $Pt(mnt)_2^{2-}$ in water obtained with a single laser shot at streak speed 26.66 ps/channel.

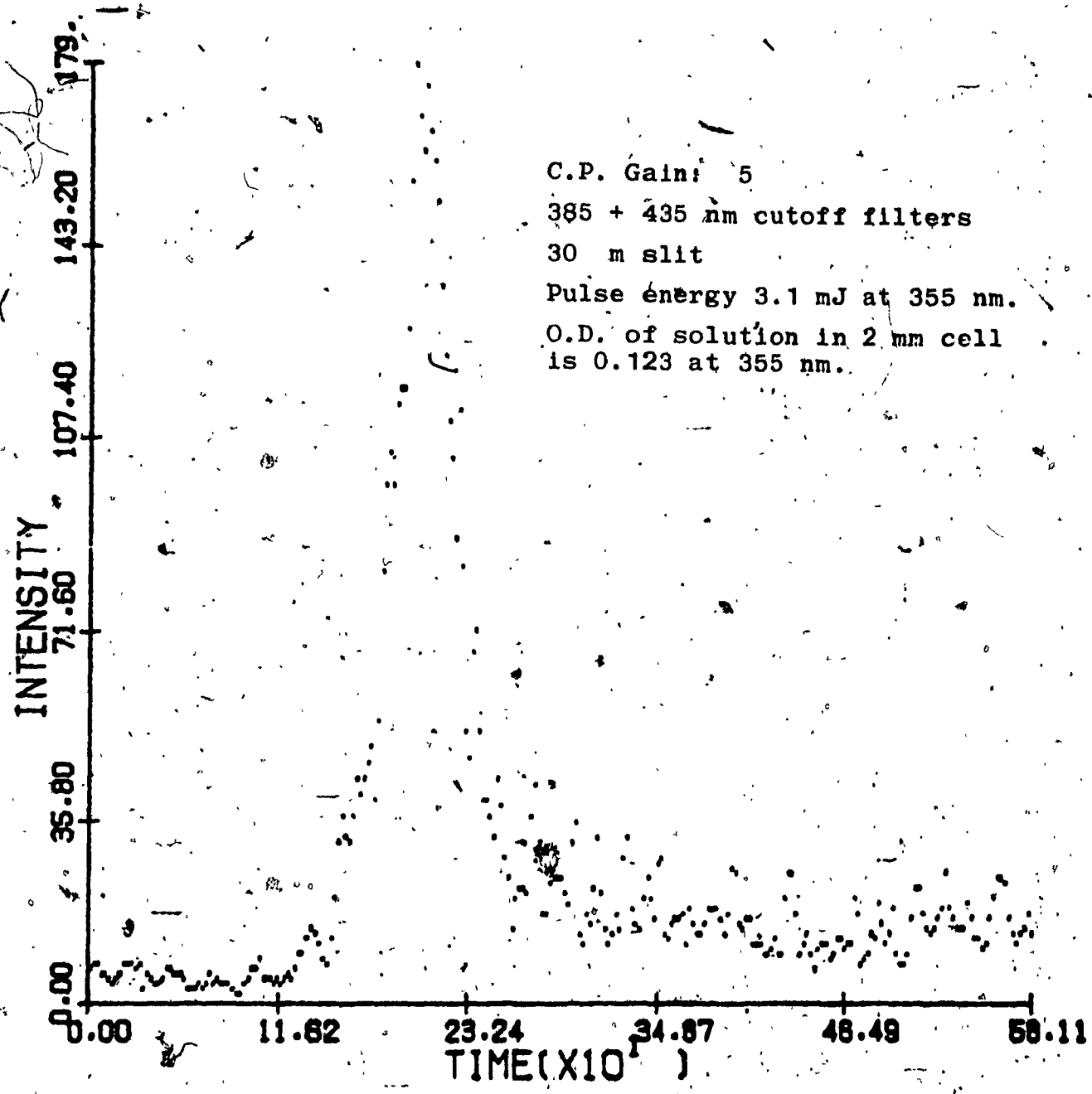

Figure 7 (b). Emission decay of $Pt(mnt)_2^{2-}$ in water obtained with a single laser shot at streak speed of 2.27 ps/channel.

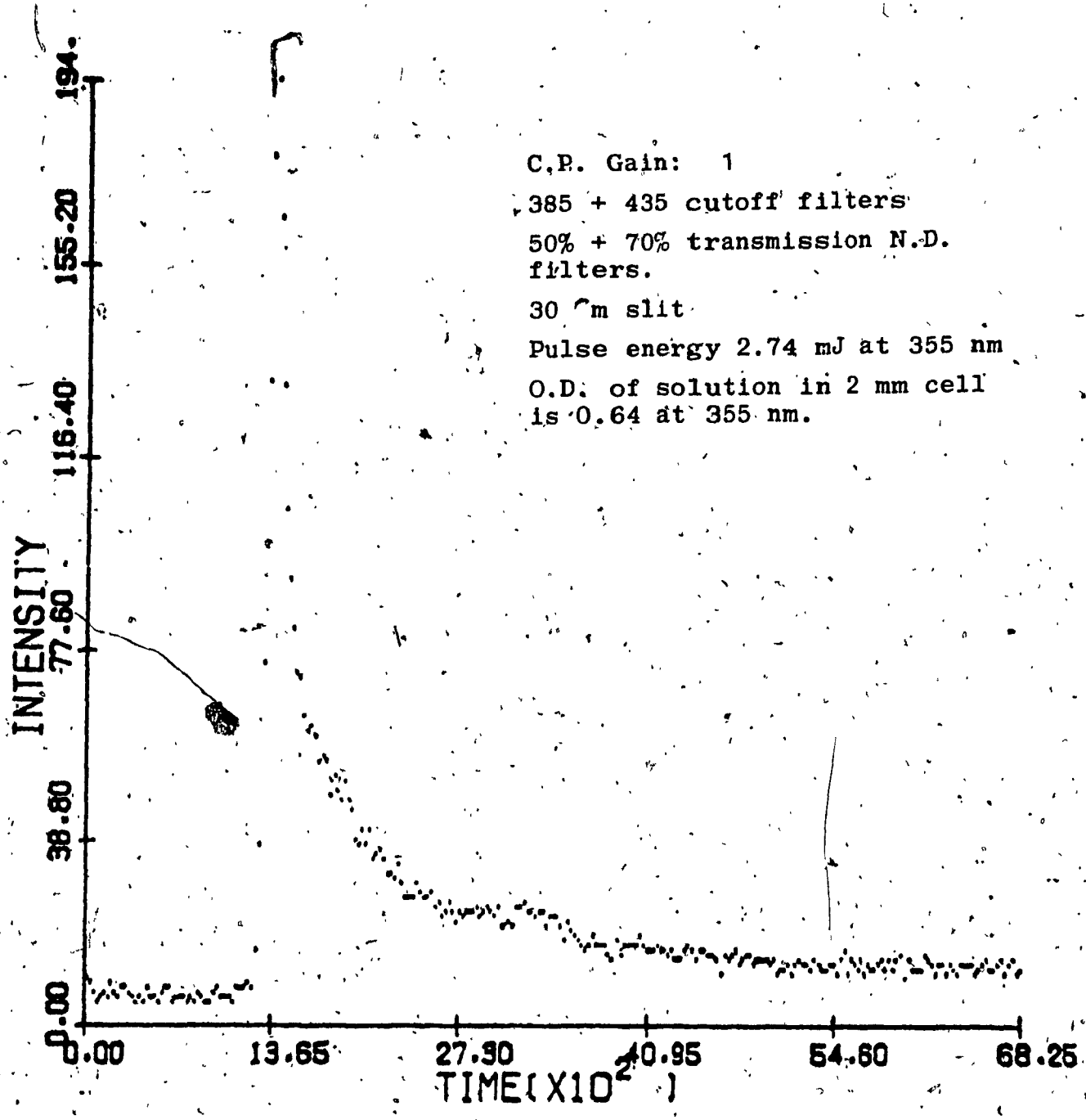

Figure 8 (a). Emission decay of $Pt(mnt)_2^{2-}$ in acetonitrile obtained with a single laser shot at streak speed 21.66 ps/channel.

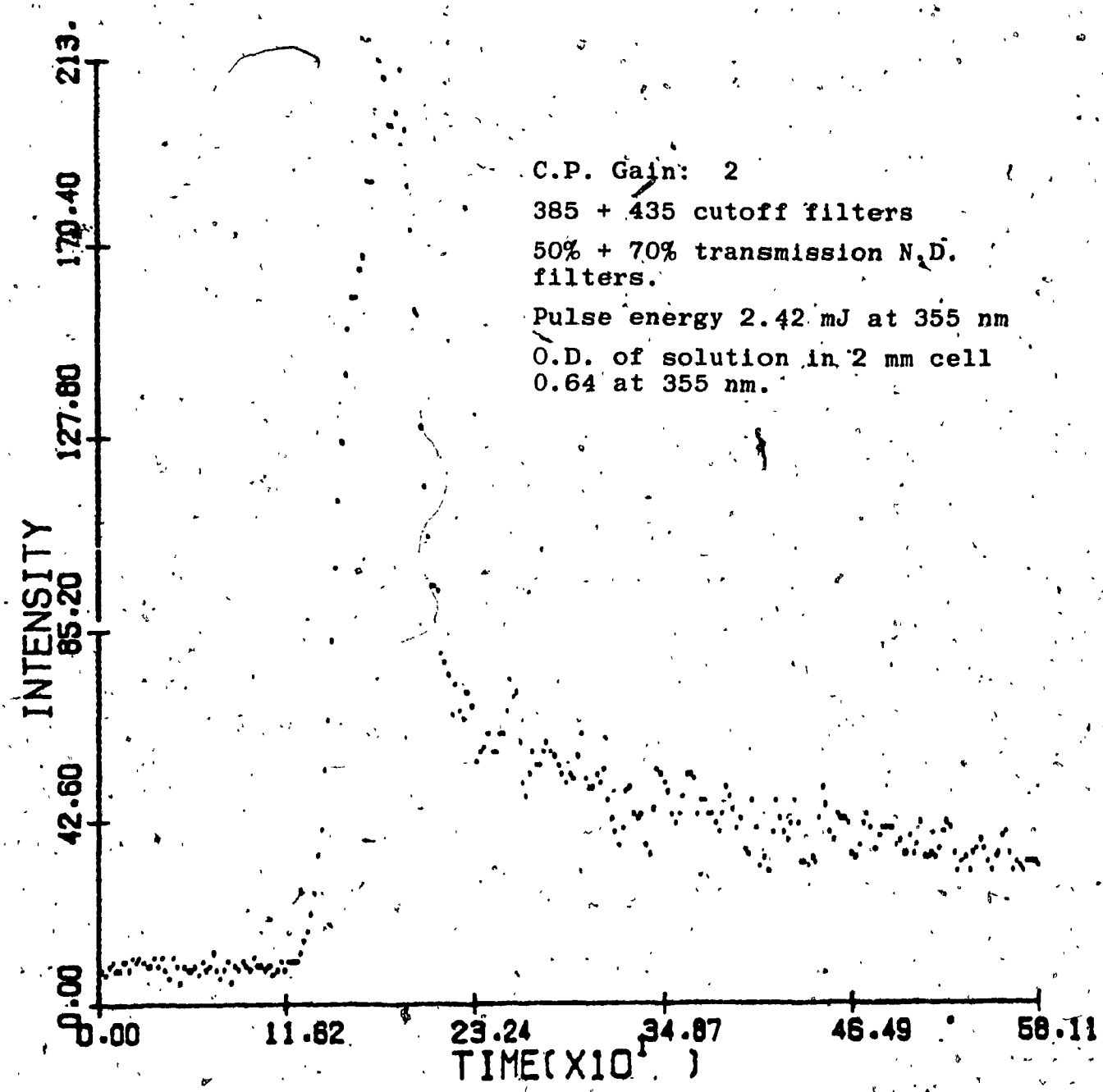

Figure 8 (b). Emission decay of $Ni(mnt)_2^{2-}$ in acetonitrile obtained with a single laser shot at streak speed of 2.27 ps/channel.

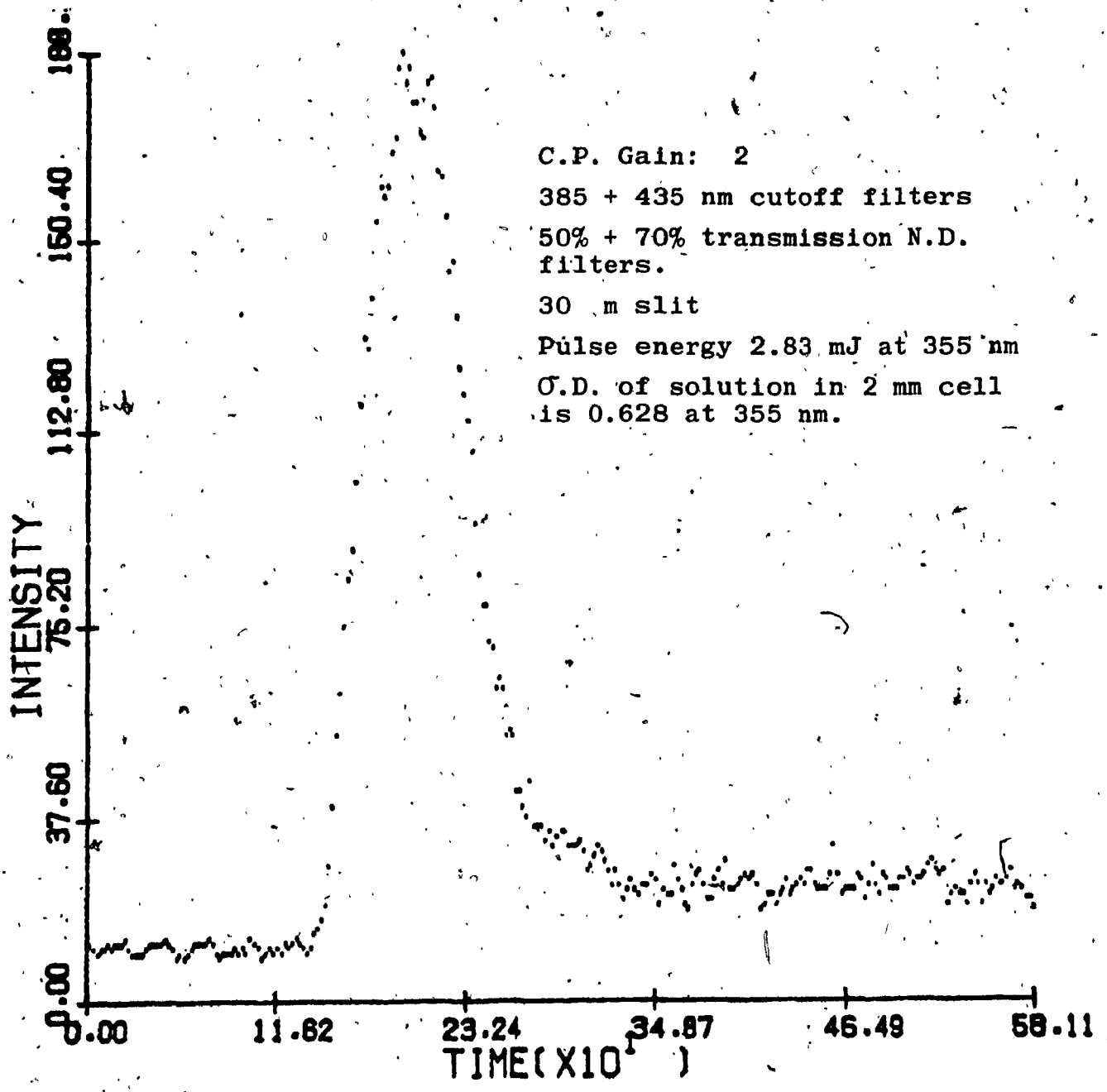

Figure 9 (a). Emission decay of $Pt(mnt)_2^{2-}$ in acetonitrile/water solution obtained with a single laser shot at streak speed of 26.66 ps/channel.

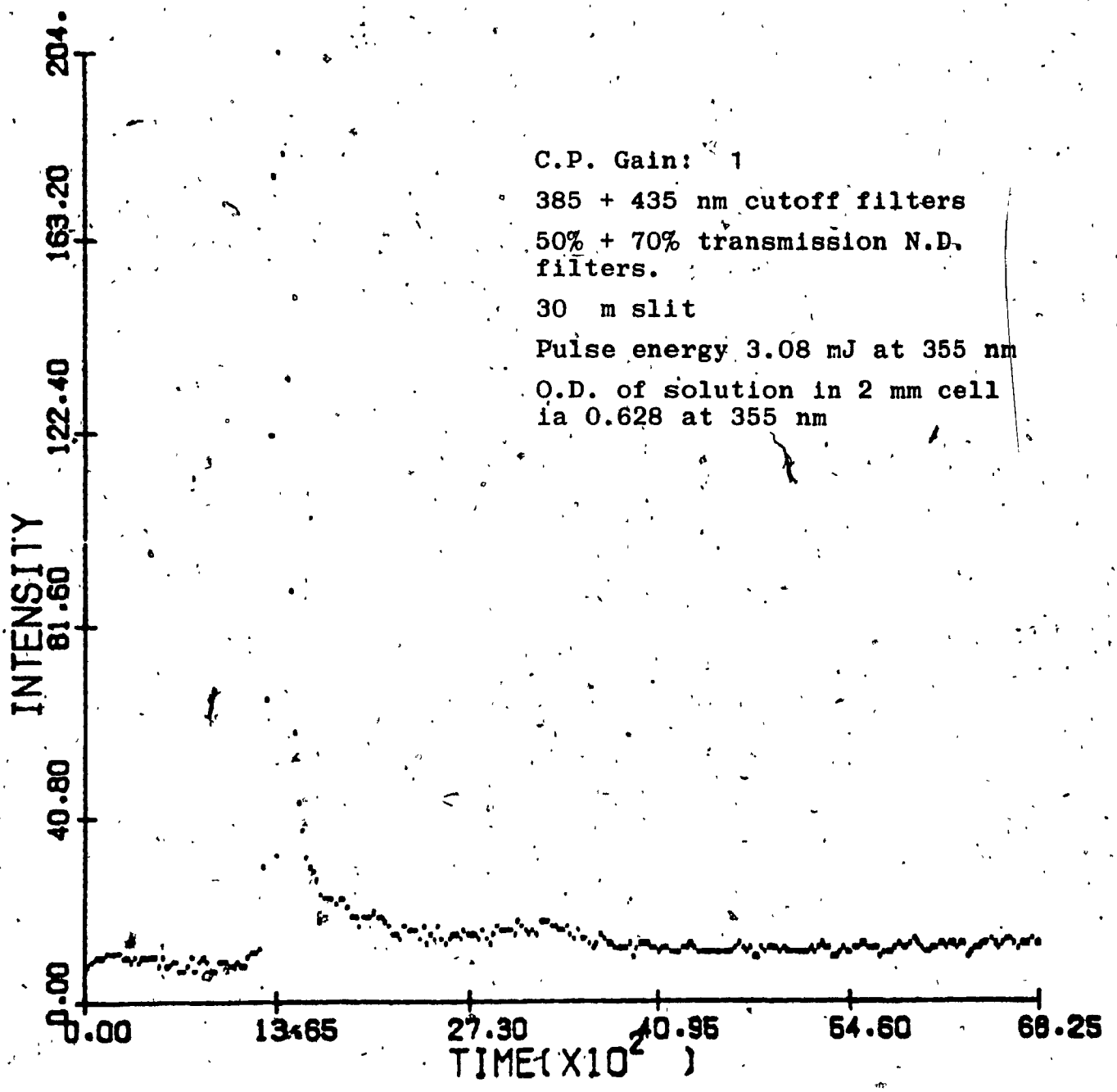

Figure 9 (b). Emission decay of $Pt(mnt)_2^{1-}$ in acetonitrile/water solution obtained with a single laser shot at streak speed of 2.27 ps/channel.

Table 1

Summary of Pulse Emission Data for $Ni(mnt)_2^{2-}$, $Pt(mnt)_2^{2-}$ and $Pt(mnt)_2^{1-}$

Complex	Solvent	Streak speed	Intensity
$Ni(mnt)_2^{2-}$	CH_3CN	26.66	408
		2.27	100
$Ni(mnt)_2^{2-}$	CH_3CN/H_2O	26.66	257
		2.27	74
$Ni(mnt)_2^{2-}$	H_2O	26.66	395
		2.27	109
$Pt(mnt)_2^{2-}$	CH_3CN	26.66	255
		2.27	104
$Pt(mnt)_2^{2-}$	CH_3CN/H_2O	26.66	547
		2.27	59
$Pt(mnt)_2^{2-}$	H_2O	26.66	1156
		2.27	325
$Pt(mnt)_2^{1-}$	CH_3CN	26.66	6162
		2.27	1128
$Pt(mnt)_2^{1-}$	CH_3CN/H_2O	26.66	5440
		2.27	836

[a] picosecond per channel

[b] all intensities were normalized to gain 4, and corrected for concentration by assuming linearity between concentration and emission